Tese de Doutorado
(PhD Dissertation)

Mecanismos envolvidos na resposta cerebral ao exercício e no papel do hipotálamo na regulação do balanço energético

(Mechanisms implicated in brain response to exercise and in the role of the hypothalamus in the regulation of energy balance)

Marcelo de Oliveira Dietrich

Volume 2

ANEXOS A: publicações do autor que não fazem parte do corpo principal desta tese, mas que foram realizados durante o período de doutoramento

Aqui estão anexados artigos e outras publicações que não foram incluídas no corpo principal desta tese, mas que foram realizados durante o período de doutoramento e estão cientificamente relacionados aos tópicos discutidos nesta tese. Além de diversos artigos de coautoria (artigos originais e de revisão), aqui também podem ser encontrados um capítulo de livro e um pôster, ambos visando educação e promoção de ciência para o público não especialista.

Anexo A-1. Megalin mediates the transport of leptin across the blood-CSF barrier

Artigo publicado no periódico *Neurobiology of Aging*.

ELSEVIER

Neurobiology of Aging 29 (2008) 902–912

NEUROBIOLOGY OF AGING

www.elsevier.com/locate/neuaging

Megalin mediates the transport of leptin across the blood-CSF barrier

Marcelo O. Dietrich [a,1], Carlos Spuch [b,1,2], Dessire Antequera [c,3], Izaskun Rodal [d,4], Justo G. de Yébenes [d,4], José Antonio Molina [e,5], Felix Bermejo [e,6], Eva Carro [c,*]

[a] *Department of Biochemistry, ICBS, University Federal do Rio Grande de Sul, Porto Alegre, RS, Brazil*
[b] *Laboratory of Molecular Neurobiology, Department of Neuroscience, Karolinska Institute, Stockholm, Sweden*
[c] *Laboratory of Neuroscience, Research Center, Hospital 12 de Octubre, Madrid, Spain*
[d] *Brain Bank for Neurological Research, University Complutense, Madrid, Spain*
[e] *Service of Neurology, Hospital 12 de Octubre, Madrid, Spain*

Received 6 September 2006; received in revised form 9 January 2007; accepted 13 January 2007
Available online 26 February 2007

Abstract

Leptin, a peptide hormone secreted by adipose tissue, exhibits a large range of central and peripheral actions. It has been proposed that the participation of leptin in diseases such as obesity is due to, at least in part, its impaired transport across the blood–brain barrier (BBB). Since, the mechanisms by which brain takes up leptin remain unclear, we set out to study how leptin may cross the BBB. We have used different immunoassays and lentiviral vectors to analyze the role of megalin in the transport of leptin in rodents and humans. We demonstrate that circulating leptin is transported into the brain by binding to megalin at the choroid plexus epithelium. Indeed, the downregulation of megalin expression in physiological and pathological situations such as aging and Alzheimer's disease was correlated with poor entry of leptin into the brain. Moreover, amyloid beta (Aβ) deposits of choroid plexus could be disturbing megalin function. The present data indicate that leptin represents a novel megalin ligand of importance in the levels and therapeutic actions of leptin into the brain.

Keywords: Megalin-LRP2; Leptin; Choroid plexus; Amyloidosis; Alzheimer's disease

1. Introduction

Obesity is an important condition in western societies affecting almost one third of the population. Obesity is not an isolated illness but rather it is typically associated with other morbid conditions such as cardiovascular diseases and dementias, including Alzheimer's disease (AD) (Lee et al., 2000; Trakas et al., 2001). Leptin peptide is thought to be involved in satiety. Indeed, leptin has been implicated in obesity, mainly because the null knockout mice (ob/ob) and the mutant leptin receptor mice (db/db) develop a severely obese phenotype (Dugail et al., 1990; Garris, 1989; Trayhurn, 1984). However, while mutations in the ob or db genes were found in only a few obese patients, serum leptin levels were significantly higher in obese individuals than in the control population (Abou Samra et al., 2005; Kinik et al., 2005; Valle et al., 2003). Thus, it has been proposed

Abbreviations: Aβ, amyloid beta; AD, Alzheimer's disease; BBB, blood–brain-barrier

* Corresponding author at: Research Center, Hospital 12 de Octubre, Avda de Cordoba s/n, 28041 Madrid, Spain. Tel.: +34 91 390 8598; fax: +34 91 390 8544.
E-mail addresses: dietrich.mo@gmail.com (M.O. Dietrich), carlos.spuch@neuro.ki.se (C. Spuch), eeara@yahoo.es (D. Antequera), anaizaskun@yahoo.es (I. Rodal), jgyebenes@yahoo.com (J.G. de Yébenes), cvillaiza@telefonica.net (J.A. Molina), fbermejop2004@yahoo.es (F. Bermejo), carroeva@yahoo.es (E. Carro).
[1] These authors contributed equally to this work.
[2] Tel.: +46 852487645; fax: +46 8339548.
[3] Tel.: +34 913908001; fax: +34 913908544.
[4] Tel.: +34 913941326/1220; fax: +34 913941329.
[5] Tel.: +34 913908293.
[6] Tel.: +34 913908098.

0197-4580/$ – see front matter © 2007 Elsevier Inc. All rights reserved.
doi:10.1016/j.neurobiolaging.2007.01.008

that leptin resistance rather than a lack of leptin might be associated with obesity. Leptin resistance can arise through many mechanisms, both in the peripheral and the central nervous system (CNS). However, at the blood–brain-barrier (BBB) leptin resistance may be particularly important, since it would impair efficient leptin delivery to the brain (Schwartz et al., 1996). Despite the potential importance of leptin transport across the BBB, very little is known about the mechanisms that underlie this process.

Megalin (or LRP2, low-density lipoprotein receptor-related protein-2) is a multi-ligand receptor that is expressed in numerous epithelia, including the choroid plexus epithelium that constitutes the barrier between the blood and the cerebrospinal fluid (CSF). Megalin is involved in the endocytic uptake of numerous ligands, including many of the known carriers of amyloid beta (Aβ) (Christensen and Birn, 2002), and as a consequence it participates in Aβ clearance (Carro et al., 2005; Deane et al., 2004; Hammad et al., 1997; Zlokovic et al., 1996). As a promiscuous receptor, megalin is also able to transcytose other growth factors such as insulin and IGF-I (Carro et al., 2005; Orlando et al., 1998). Megalin was recently shown to bind to leptin and promote its endocytosis in the proximal renal tubules of the kidney (Hama et al., 2004), raising the possibility that megalin could act as a leptin transporter at other epithelia such as the choroid plexus.

Like obesity, leptin has also been implicated in aging (Moller et al., 1998) and dementia (Fewlas et al., 2004; Power et al., 2001) and interestingly, we recently found that the expression of megalin diminishes in the choroid plexus of aged rodents (Carro et al., 2005). Here, we have examined the relationship between megalin and leptin in a rodent model of dementia/AD. We demonstrate that as in aging rodents, megalin expression in the choroid plexus is also reduced in this model, and that the diminished expression of megalin was correlated with impaired leptin uptake into the brain. Thus, in both physiological conditions such as aging and in pathological circumstances like AD, a reduction in megalin expression appears to be responsible for inducing leptin resistance at the choroid plexus.

2. Methods

2.1. Animals

Young (3–5 months) and aged (>20months) Wistar rats were used in this study. Double transgenic APP/PS1 mice (1-year-old), a cross of the Tg2576 line that overexpresses human APP695 and the mutant PS1 (M146L) mice, were used as a model of AD amyloidosis. All animals were handled and cared for in accordance with EEC guidelines.

Lentivirus vector suspensions were established at a concentration of 140 μg HIV-1 p24 protein/ml. A given volume of the vector (6 μl/rat and 2 μl/mouse) was injected into each lateral ventricle (1 mm posterior from bregma, 1.2 mm lateral and 4 mm ventral in rats, and 0.6 mm posterior from bregma, 1.1 mm lateral and 2 mm ventral in mice) using a 10-μl Hamilton syringe at a rate of 1 μl/min. CSF was collected from the animals under anesthesia from the cisterna magna. Following a period of 3 months after lentivirus injection, rats were killed and they were transcardially perfused with saline buffer or 4% paraformaldehyde in 0.1 M phosphate buffer (PB, pH 7.4) for biochemical and immunohistochemical analyses, respectively.

2.2. Human samples

This study was approved by the Ethics Committee of the Hospital '12 de Octubre', Madrid, and informed consent was obtained from all subjects prior to their participation. Three groups of human subjects were studied: (a) 16 AD patients (7 men, 9 women: mean age 70.25 ± 9.8 years) who had been clinically diagnosed by NINCDS/ADRDA criteria under the auspices of Department of Health and Human Services Task Force on Alzheimer's Disease (McKhann et al., 1984); (b) aged control group consisting of 6 men and 8 women with no neurological disease or cognitive impairment (mean age = 70.69 ± 6.7 years); and (c) a young control group consisting of 7 men and 8 women (mean age of = 38.15 ± 8.7 years). All participants undertook the Mini-Mental State Examination (MMSE) scale (Folstein et al., 1975), (average of MMSE score in AD group was 19.76 ± 1.44), the weights of each subject were recorded (AD patients: 63 ± 5.7 kg, aged control group: 70 ± 10.4 kg, and young control group: 74 ± 9 kg), and clinical examination did not reveal any cardiovascular diseases.

Lumbar CSF from all the participants was collected in a plastic tube, and immediately frozen and stored at $-80\,^{\circ}$C. Blood samples were obtained through antecubital vein puncture. The blood was centrifuged and the serum was collected, aliquoted and immediately frozen at $-80\,^{\circ}$C. All these samples were obtained at the Neurology Service of the Hospital '12 de Octubre' (Madrid, Spain).

Post mortem, the choroid plexus was removed from the frozen brains and divided in two portions. One part was solubilized in buffer containing NP-40 and then in buffers 2% containing SDS for western blotting. The other sample was used for immunohistochemical analysis. Cortical tissue was also obtained from the frozen brains and processed for biochemical analysis. These tissue samples were obtained from the Brain Bank for Neurological Research (Madrid, Spain).

2.3. Lentiviral vector

Lentiviral vectors using a four-plasmid transfection system were produced as described previously (Dull, 1988). The cDNA constructs were inserted downstream of the mouse phosphoglycerate kinase 1 (PGK) promoter in a self-inactivating HIV-1 vector containing the woodchuck

hepatitis virus posttranscriptional element (Zufferey et al., 1997). The packaging construct and the vesicular stomatitis virus G protein envelope were included in the pCMV.R-8.92, pRSV-Rev and pMD.G plasmids, respectively (Dull, 1988). The cDNA coding for the green fluorescent protein (GFP) was subcloned into the *Bam*H1/*Sal*1 site of the HIV-1-PGK transfer vector. Similarly, a cDNA encoding a portion of the two C-terminal extracellular cysteine-rich domains, the transmembrane domain and the entire cytoplasmic region of the megalin gene (Minimegalin) was subcloned into the *Bam*H1/*Sal*I site of the HIV-1-PGK transfer vector (Carro et al., 2005). To block megalin expression, a small interfering megalin RNA (siRNA) was ligated into the HIV-1 transfer vector between the *Xho*I/*Sal*I sites as described previously (Carro et al., 2005). As a control, an empty vector (no insert) was used in all experiments (void vector).

The transfer vector (13 μg), the envelope (3.75 μg) and the packaging plasmids (3.5 μg) were co-transfected with calcium phosphate in 293 T cells (5×10^6 cells/dish) cultured in Dulbecco's modified Eagle's medium (DMEM, Gibco, USA) with 10% FCS, 1% glutamine and 1% penicillin/streptomycin. The medium was changed 2 h prior to transfection and replaced after 24 h. Conditioned medium was collected 24 h latter, cleared (1000 rpm/5 min) and concentrated ≈100 fold (19,000 rpm/1.5 h). The pelleted cells were re-suspended in phosphate-buffered saline with 1% bovine serum albumin and the virus stored at −80 °C. Viral titer was determined by HIV-1 p24 ELISA (Perkin Elmer, USA).

2.4. Cell cultures

A double-chamber choroid plexus epithelial cell culture system mimicking the blood-CSF interface was used for in vitro studies, as described previously (Carro et al., 2002). Fresh DMEM containing vector particles (≈1 μg/ml) and 8 μg/ml polybrene (Sigma) was added to the cultures and replaced after 24 h. Cells were incubated for a further 24 h and thereafter, leptin (Chemicon) (1 μg/ml) was added to the lower chamber. Twenty-four hours later, the medium was collected from the upper chamber, and the leptin content was determined by immunoblotting. In other experiments, albumin (1 μg/ml), transthyretin (1 μg/ml), leptin (1 μg/ml), and $A\beta_{1–42}$ (5 μg/ml) were added to the lower chamber. $A\beta_{1–42}$ was previously dissolved in acetic acid 0.1 M, and then was dissolved in sterile distilled water. As reported by Zlokovic's lab (Zlokovic, 2004), megalin binds to $A\beta_{1–40}$ and $A\beta_{1–42}$, therefore, we decided to analyzed $A\beta_{1–42}$ interaction with megalin because we have found $A\beta_{1–42}$ accumulation in choroid plexus cells. Twenty-four hours later, upper chamber medium was collected, and content of albumin, transthyretin, and leptin was measured by immunoblotting (see below). The results are shown as the mean ± SEM and they were analyzed by one-way ANOVA followed by post-hoc Student's *t*-test to compare between groups.

2.5. Immunoassays

Western blotting and immunoprecipitation was performed as described in a previous study (Carro et al., 2002). After analysis, the western blotting membranes were reprobed with either the same antibody used for immunoprecipitation or with an antibody against unrelated proteins (PI3KP85, Calbindin) as internal standards and to normalize for protein loading. The levels of the protein under study were expressed relative to the protein loading in each lane. Densitometry measurements were made using Quantity One software (Bio-Rad).

Mouse anti-megalin (Santa Cruz), anti-p85 (Boehringer), anti-calbindin (Swant, Switzerland), anti-albumin (Bethyl, USA), anti-Dab2 (Santa Cruz), anti-pSer (Sigma), anti-Aβ clone 6F/3D (DAKO), and anti-$A\beta_{1–42}$ (Chemicon), and rabbit anti-BACE (Sigma), anti-leptin (Santa Cruz), and anti-transthyretin (Santa Cruz), were all used at a dilution between 1:500–1:1000. Secondary antibodies were either coupled to Alexa (Molecular Probes, USA) or biotinylated (Jackson Immunoresearch, USA). Leptin ELISA assays (R&D) were performed to detect endogenous rodent and recombinant human leptin. Anti-$A\beta_{1–40}$ and Anti-$A\beta_{1–42}$ ELISA assays (Sigma) and Tau ELISA assay (R&D) were performed to detect endogenous human Aβ and tau, respectively.

3. Results

3.1. Megalin mediates transport of leptin through the choroid plexus

While it is known that at least some serum leptin enters the brain by crossing the choroid plexus (Kurrimbux et al., 2004; Merino et al., 2006; Peiser et al., 2000; Tartaglia et al., 1995), the mechanisms involved remain unclear. Since megalin has been shown to bind to leptin and participate in its transport in the kidney (Hama et al., 2004), it is possible that the entrance of serum leptin into the brain could also be mediated by megalin in the choroid plexus. Thus, we immunoprecipitated megalin from rat choroid plexus epithelial cells in order to test whether megalin and leptin might interact at the blood-CSF barrier (Fig. 1A). Not only was leptin present in the material that co-precipitated with megalin, but double immunostaining showed that membrane megalin (green) and cytosolic leptin (red) co-localize in monolayers of choroid plexus epithelial cells (Fig. 1A).

Using a double-chamber culture system that mimics the blood-CSF barrier, we were able to manipulate megalin expression in epithelial cells from the choroid plexus and study leptin transport. When choroid plexus epithelial cells were cultured and infected with a lentiviral vector carrying megalin (HIV-miniMegalin), previously described (Carro et al., 2005), overexpression of megalin was accompanied by a significant increase in leptin transport and the accumulation of leptin in the upper culture chamber (Fig. 1B). In

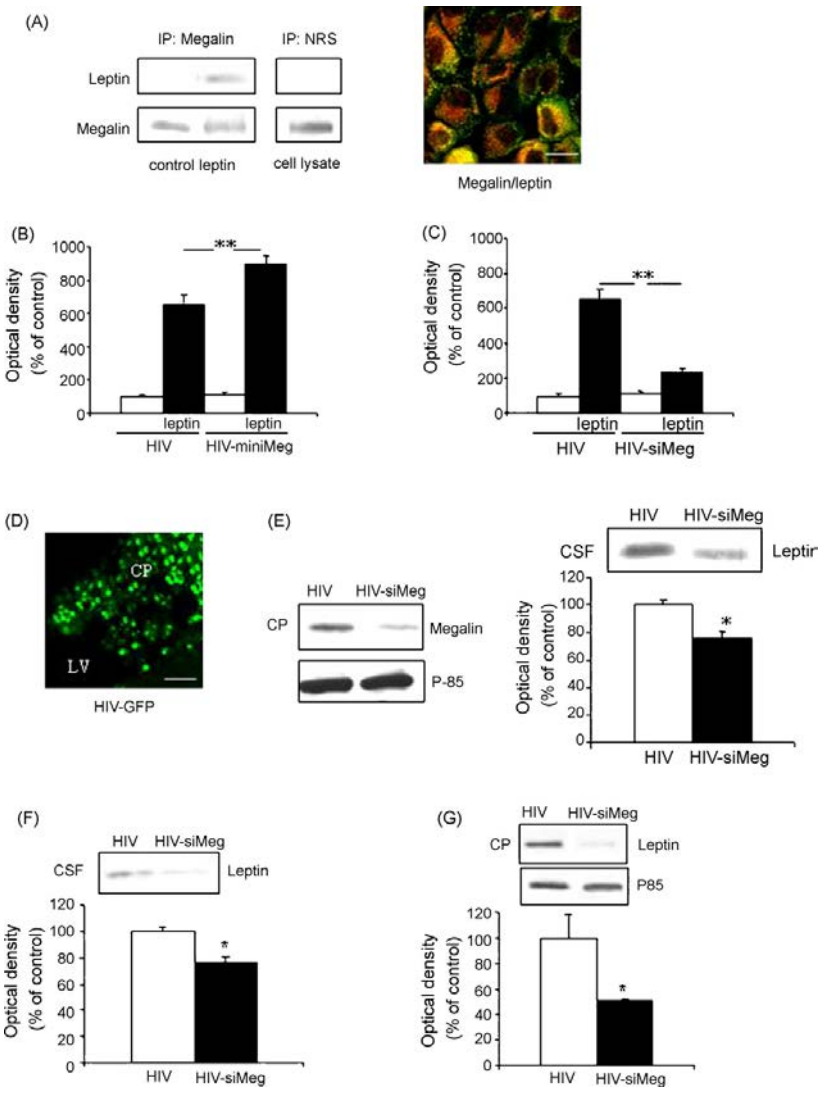

Fig. 1. Megalin mediates the transport of leptin across the choroid plexus. (A) Megalin interacts with leptin in the epithelial cells of the choroid plexus. Western Blots: immunoprecipitation of megalin from rat choroid plexus extracts probed with antibodies raised against leptin revealed the association of megalin with exogenously added leptin. No protein bands were seen in control cultures treated with vehicle. Immunoprecipitation with a non-specific serum (normal rabbit serum, NRS) demonstrated the specificity of the megalin/leptin association. Micrographs: megalin co-localizes with exogenously added leptin. Confocal image showing the merged immunostaining signals. Scale bar, 10 μm. (B) when choroid plexus cells overexpress miniMegalin (through HIV-miniMegalin infection), there is a significant increase in the amount of leptin (filled bars) translocated. Open bars without leptin administration. ($^{**}p < 0.01$ vs. HIV infected cells). (C) choroid plexus cells infected with HIV-siMegalin translocate significantly less leptin (filled bars) from the lower to the upper cell culture chamber. Open bars without leptin administration ($^{**}p < 0.01$, n = of at least 3 in all experiments). (D) photomicrograph: GFP expression in the rat choroid plexus cells 3 months after a single icv injection of HIV-GFP (CP, choroid plexus). Scale bar, 30 μm. (E) Western Blot: intraventricular HIV-siMegalin (siMeg) administration resulted in a marked decrease in the levels of megalin in the choroid plexus 3 months later when compared to HIV-injected control rats. Note that the levels of an unrelated protein, PI3Kp85, remain undisturbed following siMegalin expression in vivo, emphasizing the specificity of the RNA interference. A representative blot is shown. Significantly less exogenous leptin is translocated from the blood into the CSF in rats infected with HIV-siMegalin for 3 months via the intracarotid route. (F) CSF and choroid plexus (G) levels of endogenous leptin were significantly decreased in siMegalin rats 3 months after injection of the viral vector ($^{*}p < 0.05$ vs. HIV infected rats, $n = 6$). Representative blots and quantitative histograms are shown.

contrast, blocking the expression of megalin with an interference RNA construct in the HIV-vector (HIV-siMegalin) dramatically impaired the passage of leptin (Fig. 1C). We further examined the effects of this HIV-siMegalin in vivo where lentiviral vectors specifically infect choroid plexus cells in rats (Fig. 1D). Following siMegalin infection there was a reduction in the expression of megalin in the choroid plexus cells, blocking the transport of exogenous leptin that had been administered through the carotid artery (Fig. 1E). As a result, we examined the endogenous levels of leptin after blocking megalin expression in the choroid plexus of rats. In rats treated with HIV-siMegalin for 3 months, leptin transport into the CSF was impaired, resulting in reduced levels of leptin in the CSF (Fig. 1F) and in the choroid plexus (Fig. 1G). Here, we have infected, both in vitro and in vivo, choroid plexus cells with different controls (HIV-GFP, void vector or saline) to test any significant change on protein expression.

3.2. In vivo choroid plexus megalin expression correlates with leptin uptake

As described recently (Carro et al., 2005), aging rats have very low levels of megalin in the choroid plexus when compared to adult animals (Fig. 2A). Age related decline in megalin levels might also produce a decrease in leptin uptake. To test this hypothesis, we used western blotting and ELISA assays to determine the leptin levels in the brain and blood of aged rats. Endogenous leptin levels in the CSF (Fig. 2B) and cortex (Fig. 2C) of aged rats were diminished when compared with those in young rats, even though serum leptin levels increased with age (7.26 ± 1.22 ng/ml to 25.46 ± 4.34 ng/ml, $p < 0.05$). To assess the effects of megalin in vivo, HIV-miniMegalin was injected into the cerebral ventricles of aged rats, resulting in increased expression of megalin in the choroid plexus as described previously (Carro et al., 2005). This increase in megalin expression in the choroid plexus was accompanied by an increase in leptin levels in the CSF (Fig. 2D), which reached values similar to those observed in young rats. The amount of leptin was also significantly elevated in the cortex (Fig. 2E), an area where both the leptin receptor and megalin are expressed (Christensen and Birn, 2002; Hikita et al., 2000; Morash et al., 2003; Wicher et al., 2006; Zlokovic, 1996). The leptin resistance typically associated with aging could be related to the reduction in megalin expression. Moreover, we found that there was a significant age associated decrease in megalin expression in the choroid plexus from human brains (Fig. 2F). Likewise, CSF leptin levels were also significantly lower in the aged subjects (90 ± 7 pg/ml) when compared with younger adults (140 ± 5 pg/ml, $p < 0.05$). In contrast, the serum levels of leptin increased with age from 4.58 ± 0.93 ng/ml in the young adult subjects to 9.84 ± 2.51 ng/ml in the aged patients ($p < 0.05$). These data suggest that megalin function at the choroid plexus is required for the translocation of circulating leptin into the brain.

Table 1
CSF Aβ and tau levels in AD and healthy control subjects

	$A\beta_{1-40}$ (pg/ml)	$A\beta_{1-42}$ (pg/ml)	Tau (pg/ml)
Healthy control individuals	154.5 ± 8.5	389 ± 9	298 ± 18
AD patients	204.4 ± 44	$266 \pm 8^{*}$	$480 \pm 40^{*}$

Data are expressed as mean ± SEM. Healthy control individuals, $n = 14$. Alzheimer's disease (AD) patients, $n = 16$. $^{*}p < 0.05$.

Furthermore, transgenic APP/PS1 mice, a mouse model of AD amyloidosis, also show less megalin in the choroid plexus compared with control littermates (Fig. 3A), highlighting the importance of megalin in both physiological aging and in pathological diseases such as AD (Carro et al., 2005). We further studied if brain leptin levels could be also modified in this AD mice model, like in aging (Fig. 2C). Indeed, we found out less leptin in the cerebral cortex of APP/PS1 mice (Fig. 3B) although serum leptin levels were increased compared to controls (11.33 ± 1.98 ng/ml to 43.23 ± 7.4 ng/ml, $p < 0.05$). Altogether these results indicate that leptin levels in cerebral parenchyma depend on choroid plexus megalin expression.

To evaluate the physiological importance of the megalin-mediated transport of leptin in the choroid plexus, we analyzed the CSF from AD patients. The levels of Aβ and tau in the CSF are the most common biomarkers used in AD pathophysiology (Sunderland et al., 2003). Indeed, we found significantly lower $A\beta_{1-42}$ levels in the CSF of the AD patients studied when compared to that of controls. The vast majority of studies performed so far have reported a decreased concentration of $A\beta_{1-42}$ in CSF of patients with AD, recently reviewed by Sunderland (Sunderland et al., 2003), and our results are in agreement with these reports. However, we have found lower $A\beta_{1-40}$ levels differ from the concentration described in other studies (Lewczuk et al., 2004; Mehta et al., 2001), maybe due to other ELISA assay was used. Likewise, the accumulation of tau in the CSF was significantly higher in AD patients when compared with the controls, although no significant differences were observed in the mean $A\beta_{1-40}$ (Table 1).

In western blots, a similar reduction in the expression of megalin could be seen in the choroid plexus of patients (70.25 ± 9.8 years) in compared with healthy aged people (70.69 ± 6.7 years) (Fig. 3C), and no significant differences were observed in the levels of leptin in the their CSF (0.09 ± 0.007 ng/ml to 0.092 ± 0.002 ng/ml). However, when we compared young AD patients (55.75 ± 1.24 years) with healthy young subjects (53.25 ± 2.27 years), we found a significant difference in the accumulation of leptin in the CSF in both groups (0.134 ± 0.005 ng/ml to 0.09 ± 0.007 ng/ml, $p < 0.05$). Nevertheless, the serum leptin levels in health adult subjects and young AD patients remained unchanged (from 5.48 ± 1.45 ng/ml to 5.06 ± 1.72 ng/ml), suggesting that there is more active leptin transport across choroid plexus barrier in younger subjects. Young patients with AD underwent the same examinations described previously (methods).

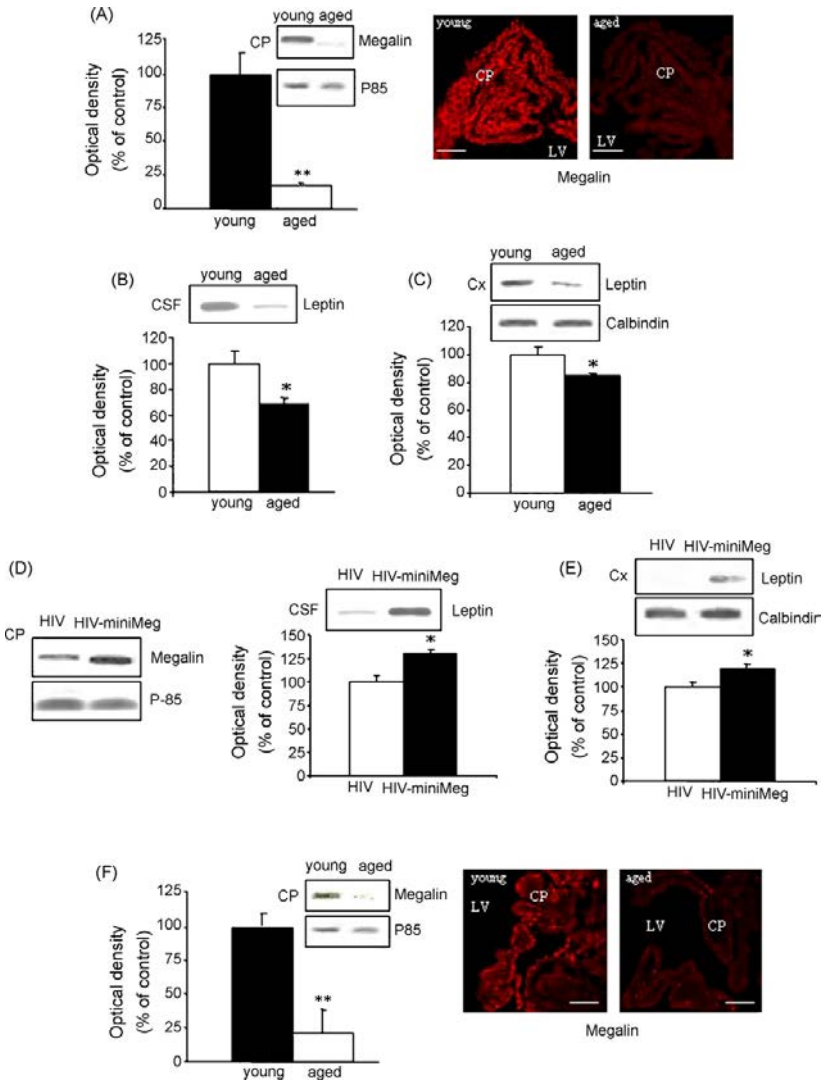

Fig. 2. Modulation of megalin and leptin expression with aging. (A) The megalin content in the choroid plexus of old rats is lower than that in young animals ($^{**}p < 0.01$ vs. young rats). Photomicrographs: young rats showed high levels of megalin immunoreactivity (red) in the choroid plexus (CP, choroid plexus; LV, lateral ventricle). Scale bar, 30 μm. (B) the amount of leptin in the CSF and cortex (Cx) (C) of aged rats was lower than in young controls. (D) Expression of HIV-miniMeg in the choroid plexus of old rats results in an increase in the expression of megalin 3 months after injection, when compared to HIV-injected control animals. In contrast, PI3Kp85 expression remains unaffected. A representative blot is shown. Injection of HIV-miniMeg into old rats resulted in an increased in leptin content of the CSF, (E) as well as an increase in leptin expression in the cerebral cortex ($^{*}p < 0.05$ vs. HIV-infected controls, $n = 5$). (F) Megalin expression is markedly reduced in the choroid plexus from aging subjects when compared with young individuals ($^{**}p < 0.01$). Photomicrographs: young subjects show high levels of megalin staining (red) in the choroid plexus (CP, choroid plexus; LV, lateral ventricle). Scale bar, 30 μm. Representative blots and quantitative histograms are shown. (For interpretation of the references to color in this figure legend, the reader is referred to the web version of this article.)

However, due to its scare sample size (only 5 subjects), this result must be confirmed increasing the number of patients, and must be consider as very preliminary data.

Based on leptin's antiamyloidogenic activity in vitro (Fewlas et al., 2004), we investigated whether these changes in leptin transport into the brain were concomitant with any alterations in CNS function. Since leptin appears to be capable of reducing β-secretase (BACE) activity in vitro, we decided to measured BACE expression in brain extracts. Both in rats treated with siMegalin, APP/PS1 mice, and AD

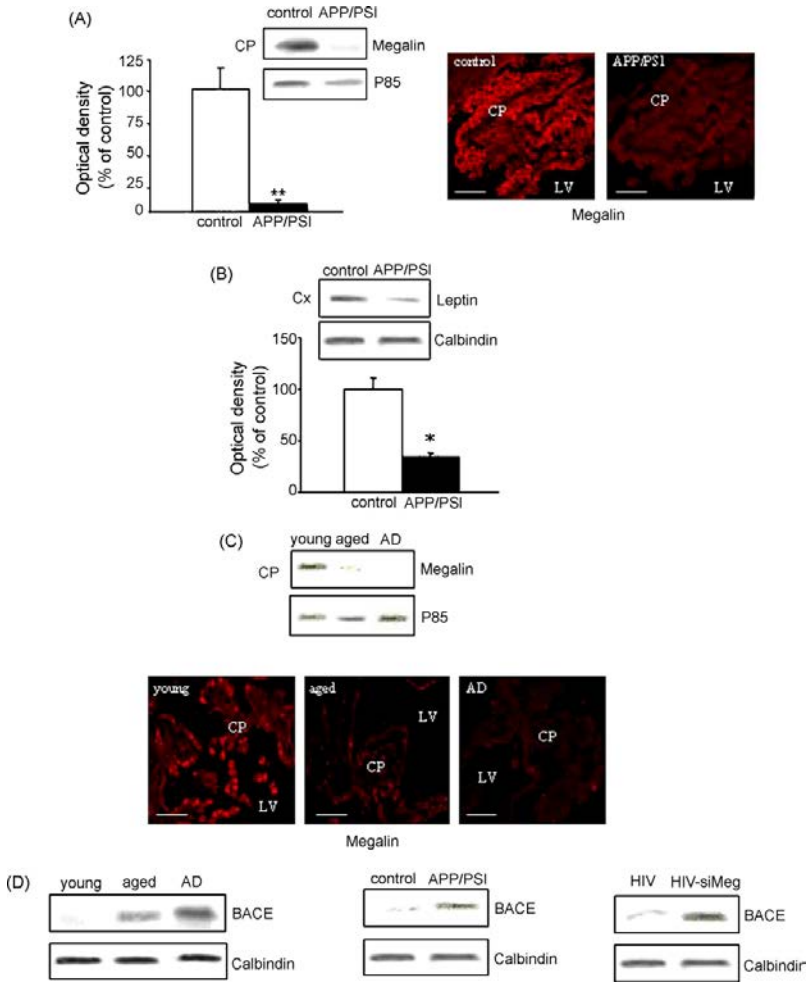

Fig. 3. Modulation of megalin and leptin expression in brain amyloidosis. (A) APP/PS1 mice show diminished megalin expression in the choroid plexus when compared to control mice ($^{**}p < 0.01$). Photomicrographs: megalin immunoreactivity (red) is abundant in the choroid plexus of control mice. Scale bar, 30 μm. (B) APP/PS1 mice have low levels of leptin in the cortex in comparison to control mice ($^{*}p < 0.05$, $n = 6$). (C) megalin expression in the choroid plexus is similar in healthy aged subjects and AD patients, but it is reduced when compared to middle-age or young individuals (Photomicrographs, megalin staining in red; CP, choroid plexus; LV, lateral ventricle. Scale bar, 30 μm). (D) BACE expression is reduced in brain cortex from AD patients, APP/PS1 mice and in siMegalin rats when compared with respective control groups. Representative blots and quantitative histograms are shown. (For interpretation of the references to color in this figure legend, the reader is referred to the web version of this article.)

patients, the low levels of brain leptin were associated with a significant increase in brain BACE expression (Fig. 3D).

3.3. Choroid plexus Aβ deposits interfere with megalin-mediated transcytosis

Immunohistochemical analysis under the light microscope revealed the presence of Aβ deposits in the choroid plexus in autopsy material from AD patients, using two different antibodies (see Methods) (Fig. 4A). The immunolabelling was observed in both the intra- and extracellular compartments, indicating that Aβ accumulation could interfere with normal choroid plexus function. Megalin-mediated transport requires internalization, and this process is regulated by phosphorylation-dephosphorylation of docking proteins such as Dab2 (Oleinikov et al., 2000). As we described previously, the dephosphorylation and uncoupling of Dab2 is accompanied by megalin internalization (Carro et al., 2005). We observed a marked increase in the phosphorylation of Dab2 in young AD patients (Fig. 4B), suggesting a reduction in

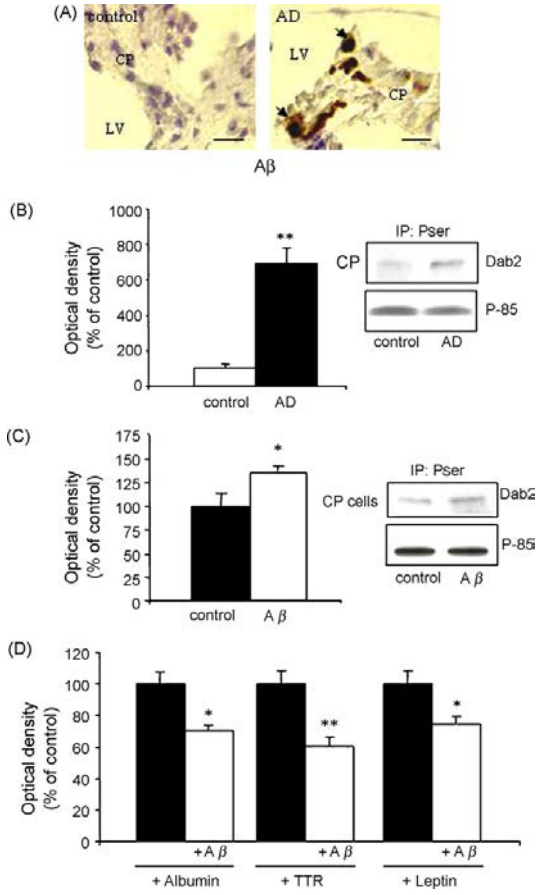

Fig. 4. Choroid plexus Aβ deposits interfere with megalin-mediated transcytosis. (A) Photomicrographs: Aβ accumulation in the choroid plexus of AD patients, as determined by antibody staining for $A\beta_{1-42}$ (CP, choroid plexus; LV, lateral ventricle, $n = 12$). Scale bar, 20 μm. (B) phosphorylation of Dab2 is dramatically increased in the choroid plexus of AD patients when compared to healthy control individuals ($^{**}p < 0.01$). (C) Administration of $A\beta_{1-42}$ to epithelial cells of the choroid plexus elevated Dab2 dephosphorylation when compared to untreated cell cultures ($^{*}p < 0.05$, $n \geq$ least 3 for all experiments). (D) $A\beta_{1-42}$ modulates in vitro transcytosis of albumin, transthyretin, and leptin through a choroid plexus monolayer. Addition of $A\beta_{1-42}$ to the upper chamber of the choroid plexus cultures together with albumin, transthyretin, and leptin induce reduction of these proteins in the lower chamber ($^{*}p < 0.05$, $^{**}p < 0.01$, $n \geq$ least 3 for all experiments). Representative blots and quantitative histograms are shown.

megalin internalization and therefore, in leptin transcytosis. Indeed, we found that when Aβ was added to choroid plexus epithelial cells in vitro, a slightly increase in the phosphorylation of Dab2 was induced (Fig. 4C). This increase in Dab2 phosphorylation was associated with a decrease in protein transport, including that of albumin, transthyretin, and leptin (Fig. 4D). Thus, these results suggest that the deposits of Aβ in the choroid plexus may impair the internalization of the protein/megalin complex across the epithelium by increasing the phosphorylation of Dab2 and thus interfering with the uptake of leptin.

4. Discussion

The mechanisms underlying leptin transport into the CNS are not only complex but there are also poorly understood. It is assumed that leptin binds to the choroid plexus (blood-CSF barrier) and to brain endothelial cells (blood–brain barrier), where high levels of the short form of leptin can be found (Banks et al., 1996; Bjorbaek et al., 1998; Golden et al., 1997; Hileman et al., 2002; Tartaglia et al., 1995). The present study reveals that megalin can also act as a receptor to transport leptin in choroid plexus epithelial cells. These observations may form the basis for establishing new therapeutic approaches for certain pathologies, as well as helping to explain previous findings regarding the neuroprotective activity of leptin after peripheral administration (Fewlas et al., 2004).

Megalin/LRP2 is a cargo receptor involved in the polarized transport of many different proteins. Its biological role has best been characterized in the renal epithelium, where it participates in blood-urine homeostasis, including leptin transport (Christensen and Birn, 2002; Hama et al., 2004). The role of megalin at the blood-CSF interface is not well understood, although previous work indicates that together with endothelial LRP1, it may be involved in Aβ clearance (Carro et al., 2005; Deane et al., 2004; Tanzi and Bertram, 2005; Zlokovic et al., 1996). In these studies it has been shown that megalin is able to transport different growth factors and hormones (Carro et al., 2005; Christensen and Birn, 2002). Hence, choroid plexus and specifically megalin receptor could represent the key site in regulating the interaction between endocrine signaling and the brain. Moreover, megalin appears to be an important transport system by which leptin could enter the brain and exert its neuroprotective effect (Dagon et al., 2005; Farr et al., 2006; Fewlas et al., 2004). Indeed, both megalin and leptin may represent two new targets for AD treatment.

We showed that leptin is bound to and transported across the choroid plexus epithelium, and the effects of blocking megalin expression with siRNA indicated that the presence of megalin is essential for properly leptin crossing into the CSF. This observation was corroborated both in vivo and in vitro, measuring leptin passage though a choroid plexus monolayer. In our hands, human recombinant leptin interact with rat megalin by similar manner than published by Hama (Hama et al., 2004) where recombinant rat leptin was used to show the ability of renal megalin to mediate the cellular binding and internalization of leptin in rats, with 3×10^2 Hz binding affinity. Then, rat megalin has demonstrated similar ability to bind rat or human (in our study) leptin. In agreement with these results, Hjalm's group published that 77% amino acid identity between human and rat megalin (Hjalm et al., 1996), therefore, their binding capacity

should be similar. Ours data were reinforced by experiments in animal models in which megalin expression was reduced. Along these lines, the diminished megalin expression led to the reduced passage of serum leptin into the CSF, despite the high circulating leptin levels in aged rats. However, when megalin was overexpressed in the choroid plexus of aged rats, via lentiviral vector infectio, CSF leptin levels were also increased. Still, an important reduction in megalin expression in the choroid plexus was also observed in a transgenic model of AD (APP/PS1 mice), coupled with low brain and high serum leptin levels. Similar results were found in human subjects corroborating the data relating to aging and AD. Taking together, these data show that leptin entry into the brain is dependent on megalin expression in the choroid plexus.

Since Aβ deposits accumulate in the choroid plexus of AD patients, it is likely that Aβ interferes with its function. As mentioned previously, one such effect could include the inhibition of protein transport, including leptin, and Aβ carriers (transthyretin, albumin). This most probably occurs by Aβ interfering with megalin translocation from the membrane to the cytosol (Carro et al., 2005; Morris et al., 2002) rather than reducing megalin expression, as seen in elderly individuals. Additionally, Aβ might block transthyretin synthesis (data not shown), which would not be surprising in view of previous studies where a reduction of transthyretin in the choroid plexus has been proposed as an added risk for AD (Chen et al., 2005; Li et al., 2000; Merched et al., 1998). This dual effect of Aβ on choroid plexus activity, megalin-mediated transcytosis and protein synthesis, may represent an important risk factor in the pathogenesis of AD, affecting Aβ/carrier complexes.

Leptin has been shown to modulate hippocampal synaptic plasticity (Harvey et al., 2006; Shanley et al., 2001) and to improve memory processing (Harvey et al., 2005; Paulus et al., 2005; Tanzi and Bertram, 2005). Thus, low levels of leptin in the brain may be involved in the cognitive deficits seen in disease states such as dementia/AD where leptin transport into the CNS is compromised. For this reason, megalin-mediated leptin uptake into the brain may also be important in AD-like pathogenesis. On the other hand, it is well documented that brain lipids are intricately involved in Aβ-related pathogenic pathways (Puglielli et al., 2001), and an important modulator of lipid homeostasis is leptin. In agreement with published data (Refolo et al., 2000), cholesterol increase Aβ production, and leptin is able to partially revert the amyloidogenic potency of cholesterol when coadministered, reducing β-secretase (BACE) activity, possibly by altering the lipid composition of membrane lipid rafts (Fewlas et al., 2004). Based on these data, we investigated whether the changes we have reported on leptin transport into the brain were concomitant with any alterations in BACE expression. Both in rats treated with siMegalin, APP/PS1 mice, and AD patients, the low uptake of brain leptin were associated with a significant increase in brain BACE expression. However, further studies will be needed to determine whether uptake of serum leptin to the brain could be a potential treatment for AD.

In summary, the findings presented here show that serum leptin enters into the brain crossing the choroid plexus barrier by binding to megalin. The levels of leptin in the CNS were directly dependent on the expression and activity of megalin in the choroid plexus epithelium, and were closely associated with accumulation of Aβ at the choroid plexus level.

Disclosure statement

There are no actual or potential conflicts of interest with other people or organizations. Source of funding was provided by the CAM (GR/SAL/0817/2004) and FIS (CP04/00179). All animals were handled and cared for in accordance with EEC guidelines (Directive 86/609/CEE). The study was performed in accordance with the principles contained in the Declaration of Helsinki as revised in 1996. Human studies were approved by the Ethics Committee of the Hospital '12 de Octubre', and informed consent was obtained from all patients prior to their participation.

Acknowledgments

We thank Dra. Sandra Perez Rial for her kind help with the human samples, and Dr. Diego Sousa, and Joaquin Piriz for their expert comments. Funding was provided by the CAM (GR/SAL/0817/2004) and FIS (CP04/00179).

References

Abou Samra, R., Baba, N.H., Torbay, N., Dib, L., El-Hajj Fuleihan, G., 2005. High plasma leptin is not associated with higher bone mineral density in insulin-resistant premenopausal obese women. J. Clin. Endocrinol. Metab. 90, 2588–2594.

Banks, W.A., Kastin, A.J., Huang, W., Jaspan, J.B., Maness, L.M., 1996. Leptin enters the brain by a saturable system independent of insulin. Peptides 17, 305–311.

Bjorbaek, C., Elmquist, J.K., Michl, P., Ahima, R.S., van Bueren, A., McCall, A.L., Flier, J.S., 1998. Expression of leptin receptor isoforms in rat brain microvessels. Endocrinol. 139, 3485–3491.

Carro, E., Trejo, J.L., Gomez-Isla, T., LeRoith, D., Torres-Aleman, I., 2002. Serum insulin-like growth factor I regulates brain amyloid-beta levels. Nat. Med. 8, 1390–1397.

Carro, E., Spuch, C., Trejo, J.L., Antequera, D., Torres-Aleman, I., 2005. Neuroprotection at the blood–brain interface: role of an Insulin-like growth factor I/megalin pathway in the choroid plexus. J. Neurosci. 25, 10884–10893.

Chen, R.L., Athauda, S.B., Kassem, N.A., Zhang, Y., Segal, M.B., Preston, J.E., 2005. Decrease of transthyretin synthesis at the blood-cerebrospinal fluid barrier of old sheep. J. Gerontol. A Biol. Sci. Med. Sci. 60, 852–858.

Christensen, E.I., Birn, H., 2002. Megalin and cubilin: multifunctional endocytic receptors. Nat. Rev. Mol. Cell Biol. 3, 256–266.

Dagon, Y., Avraham, Y., Magen, I., Gertler, A., Ben-Hur, T., Berry, E.M., 2005. Nutritional status, cognition, and survival: a new role for leptin and AMP kinase. J. Biol. Chem. 280, 42142–42148.

Deane, R., Wu, Z., Sagare, A., Davis, J., Du Yan, S., Hamm, K., Xu, F., Parisi, M., LaRue, B., Hu, H.W., Spijkers, P., Guo, H., Song, X., Lenting, P.J., Van Nostrand, W.E., Zlokovic, B.V., 2004. LRP/amyloid beta-peptide

interaction mediates differential brain efflux of Abeta isoforms. Neuron 43, 333–344.
Dugail, I., Quignard-Boulange, A., Le Liepvre, X., Lavau, M., 1990. Impairment of adipsin expression is secondary to the onset of obesity in db/db mice. J. Biol. Chem. 265, 1831–1833.
Dull, H.B., 1988. Behind the AIDS mailer. Am. J. Prev. Med. 4, 239–240.
Farr, S.A., Banks, W.A., Morley, J.E., 2006. Effects of leptin on memory processing. Peptides 27, 1420–1425.
Fewlas, D.C., Noboa, K., Pi-Sunyer, F.X., Johnston, J.M., Yan, S.D., Tezapsidis, N., 2004. Obesity-related leptin regulates Alzheimer's Abeta. FASEB J. 18, 1870–1878.
Folstein, M.F., Folstein, S.E., McHugh, P.R., 1975. Mini-mental state. A practical method for grading the cognitive state of patients for the clinician. J. Psychiatr. Res. 12, 189–198.
Garris, D.R., 1989. Morphometric analysis of obesity (ob/ob)- and diabetes (db/db)-associated hypothalamic neuronal degeneration in C57BL/KsJ mice. Brain. Res. 501, 162–170.
Golden, P.L., Maccagnan, T.J., Partridge, W.M., 1997. Human blood–brain barrier leptin receptor, Binding and endocytosis in isolated human brain microvessels. J. Clin. Invest. 99, 14–18.
Hama, H., Saito, A., Takeda, T., Tanuma, A., Xie, Y., Sato, K., Kazama, J.J., Gejyo, F., 2004. Evidence indicating that renal tubular metabolism of leptin is mediated by megalin but not by the leptin receptors. Endocrinology 145, 3935–3940.
Hammad, S.M., Ranganathan, S., Loukinova, E., Twal, W.O., Argraves, W.S., 1997. Interaction of apolipoprotein J-amyloid beta-peptide complex with low density lipoprotein receptor-related protein-2/megalin, A mechanism to prevent pathological accumulation of amyloid beta-peptide. J. Biol. Chem. 272, 18644–18649.
Harvey, J., Shanley, L.J., O'Malley, D., Irving, A.J., 2005. Leptin: a potential cognitive enhancer? Biochem. Soc. Trans. 33, 1029–1032.
Harvey, J., Solovyova, N., Irving, A., 2006. Leptin and its role in hippocampal synaptic plasticity. Prog. Lipid. Res. 45, 369–378.
Hikita, M., Bujo, H., Hirayama, S., Takahashi, K., Morisaki, N., Saito, Y., 2000. Differential regulation of leptin receptor expression by insulin and leptin in neuroblastoma cells. Biochem. Biophys. Res. Commun. 271, 703–709.
Hileman, S.M., Pierroz, D.D., Masuzaki, H., Bjorbaek, C., El-Haschimi, K., Banks, W.A., Flier, J.S., 2002. Characterizaton of short isoforms of the leptin receptor in rat cerebral microvessels and of brain uptake of leptin in mouse models of obesity. Endocrinology 143, 775–783.
Hjalm, G., Murray, E., Crumley, G., Harazim, W., Lundgren, S., Onyango, I., Ek, B., Larsson, M., Juhlin, C., Hellman, P., Davis, H., Akerstrom, G., Rask, L., Morse, B., 1996. Cloning and sequencing of human gp330, a Ca(2+)-binding receptor with potential intracellular signaling properties. Eur. J. Biochem. 1 239 (1), 132–137.
Kinik, S.T., Ozbek, N., Yucel, M., Haberal, A., Cetintas, S., 2005. Correlations among serum leptin levels, complete blood count parameters and peripheral CD34(+) cell count in prepubertal obese children. Ann. Hematol. 84, 605–608.
Kurrimbux, D., Gaffen, Z., Farrell, C.L., Martin, D., Thomas, S.A., 2004. The involvement of the blood–brain and the blood-cerebrospinal fluid barriers in the distribution of leptin into and out of the rat brain. Neuroscience 123, 527–536.
Lee, C.K., Weindruch, R., Prolla, T.A., 2000. Gene-expression profile of the ageing brain in mice. Nat. Genet. 25, 294–297.
Lewczuk, P., Esselmann, H., Otto, M., Maler, J.M., Henkel, A.W., Henkel, M.K., Eikenberg, O., Antz, C., Krause, W.R., Reulbach, U., Kornhuber, J., Wiltfang, J., 2004. Neurochemical diagnosis of Alzheimer's dementia by CSF Abeta42, Abeta42/Abeta40 ratio and total tau. Neurobiol. Ageing 25 (3), 273–281.
Li, M.D., Kane, J.K., Matta, S.G., Blaner, W.S., Sharp, B.M., 2000. Nicotine enhances the biosynthesis and secretion of transthyretin from the choroid plexus in rats: implications for beta-amyloid formation. J. Neurosci. 20, 1318–1323.
Mehta, P.D., Pirttila, T., Patrick, B.A., Barshatzky, M., Mehta, S.P., 2001. Amyloid beta protein 1-40 and 1-42 levels in matched cerebrospinal fluid and plasma from patients with Alzheimer disease. Neurosci Lett. 18 304 (1–2), 102–106.
Merched, A., Serot, J.M., Visvikis, S., Aguillon, D., Faure, G., Siest, G., 1998. Apolipoprotein E, transthyretin and actin in the CSF of Alzheimer's patients: relation with the senile plaques and cytoskeleton biochemistry. FEBS Lett. 425, 225–228.
Merino, B., Diez-Fernandez, C., Ruiz-Gayo, M., Somoza, B., 2006. Choroid plexus epithelial cells co-express the long and short form of the leptin receptor. Neurosci. Lett. 393, 269–272.
McKhann, G., Drachman, D., Folstein, M., Katzman, R., Price, D., Stadlan, E.M., 1984. Clinical diagnosis of Alzheimer's disease: report of the NINCDS-ADRDA Work Group under the auspices of Department of Health and Human Services Task Force on Alzheimer's Disease. Neurology 34, 939–944.
Moller, N., O'Brien, P., Nair, K.S., 1998. Disruption of the relationship between fat content and leptin levels with aging in humans. J. Clin. Endocrinol. Metab. 83, 931–934.
Morash, B.A., Imran, A., Wilkinson, D., Ur, E., Wilkinson, M., 2003. Leptin receptors are developmentally regulated in rat pituitary and hypothalamus. Mol. Cell Endocrinol. 210, 1–8.
Morris, S.M., Tallquist, M.D., Rock, C.O., Cooper, J.A., 2002. Dual roles for the Dab2 adaptor protein in embryonic development and kidney transport. EMBO J. 21, 1555–1564.
Oleinikov, A.V., Zhao, J., Makker, S.P., 2000. Cytosolic adaptor protein Dab2 is an intracellular ligand of endocytic receptor gp600/megalin. Biochem. J. 347, 613–621.
Orlando, R.A., Rader, K., Authier, F., Yamazaki, H., Posner, B.I., Bergeron, J.J., Farquhar, M.G., 1998. Megalin is an endocytic receptor for insulin. J. Am. Soc. Nephrol. 9, 1759–1766.
Paulus, K., Schulz, C., Lehnert, H., 2005. Central nervous effects of leptin and insulin on hippocampal leptin and insulin receptor expression following a learning task in wistar rats. Neuropsychobiology 51, 100–106.
Peiser, C., McGregor, G.P., Lang, R.E., 2000. Binding and internalization of leptin by porcine choroid plexus cells in culture. Neurosci. Lett. 283, 209–212.
Power, D.A., Noel, J., Collins, R., O¨Neill, D., 2001. Circulating leptin levels and weight loss in Alzheimer's disease patients. Dement. Geriatr. Cogn. Disord. 12, 167–170.
Puglielli, L., Konopka, G., Pack-Chung, E., Ingano, L.A., Berezovska, O., Hyman, B.T., Chang, T.Y., Tanzi, R.E., Kovacs, D.M., 2001. Acyl-coenzyme A: cholesterol acyltransferase modulates the generation of the amyloid beta-peptide. Nat. Cell Biol. 3, 905–912.
Refolo, L.M., Malester, B., LaFrancois, J., Bryant-Thomas, T., Wang, R., Tint, G.S., Sambamurti, K., Duff, K., Pappolla, M.A., 2000. Hypercholesterolemia accelerates the Alzheimer's amyloid pathology in a transgenic mouse model. Neurobiol. Dis. 7, 321–331.
Schwartz, M.W., Peskind, E., Raskind, M., Boyko, E.J., Porte Jr., D., 1996. Cerebrospinal fluid leptin levels: relationship to plasma levels and to adiposity in humans. Nat. Med. 2, 589–593.
Shanley, L.J., Irving, A.J., Harvey, J., 2001. Leptin enhances NMDA receptor function and modulates hippocampal synaptic plasticity. J. Neurosci. 21, RC186(1–6).
Sunderland, T., Linker, G., Mirza, N., Putnam, K.T., Friedman, D.L., Kimmel, L.H., Bergeson, J., Manetti, G.J., Zimmermann, M., Tang, B., Bartko, J.J., Cohen, R.M., 2003. Decreased beta-amyloid1-42 and increased tau levels in cerebrospinal fluid of patients with Alzheimer disease. JAMA 289, 2094–2103.
Tanzi, R.E., Bertram, L., 2005. Twenty years of the Alzheimer's disease amyloid hypothesis: a genetic perspective. Cell 120, 545–555.
Tartaglia, L.A., Dembski, M., Weng, X., Deng, N., Culpepper, J., Devos, R., Richards, G.J., Campfield, L.A., Clark, F.T., Deeds, J., Muir, C., Sanker, S., Moriarty, A., Moore, K.J., Smutko, J.S., Mays, G.G., Wool, E.A., Monroe, C.A., Tepper, R.I., 1995. Identification and expression cloning of a leptin receptor, Ob-R. Cell 83, 1263–1271.
Trakas, K., Oh, P.I., Singh, S., Risebrough, N., Shear, N.H., 2001. The health status of obese individuals in Canada. Int. J. Obes. Metab. Disord. 25, 662–668.

Trayhurn, P, 1984. The development of obesity in animals: the role of genetic susceptibility. Clin. Endocrinol. Metab. 13, 451–474.

Valle, M., Gascon, F., Martos, R., Bermudo, F., Ceballos, P., Suanes, A., 2003. Relationship between high plasma leptin concentrations and metabolic syndrome in obese pre-pubertal children. Int. J. Obes. Relat. Metab. Disord. 27, 13–18.

Wicher, G., Larsson, M., Svenningsen, A.F., Gyllencreutz, E., Rask, L., Aldskogius, H., 2006. Low density lipoprotein receptor-related protein-2/megalin is expressed in oligodendrocytes in the mouse spinal cord white matter. J. Neurosci. Res. 83, 864–873.

Zlokovic, B.V., 1996. Cerebrovascular transport of Alzheimer's amyloid beta and apolipoproteins J and E: possible anti-amyloidogenic role of the blood–brain barrier. Life Sci. 59, 1483–1497.

Zlokovic, B.V., 2004. Clearing amyloid through the blood–brain barrier. J. Neurochem. 89, 807–811.

Zlokovic, B.V., Martel, C.L., Matsubara, E., McComb, J.G., Zheng, G., McCluskey, R.T., Frangione, B., Ghiso, J., 1996. Glycoprotein 330/megalin: probable role in receptor-mediated transport of apolipoprotein J alone and in a complex with Alzheimer disease amyloid beta at the blood–brain and bloodcerebrospinal fluid barriers. Proc. Natl. Acad. Sci. U S A 93, 4229–4234.

Zufferey, R., Nagy, D., Mandel, R.J., Naldini, L., Trono, D., 1997. Multiply attenuated lentiviral vector achieves efficient gene delivery in vivo. Nat. Biotechnol. 15, 871–875.

Anexo A-2. STAT3 inhibition of gluconeogenesis is downregulated by SirT1.

Artigo publicado no periódico *Nature Cell Biology*.

nature cell biology

STAT3 inhibition of gluconeogenesis is downregulated by SirT1

Yongzhan Nie[1,7], Derek M. Erion[4], Zhenglong Yuan[5], Marcelo Dietrich[1], Gerald I. Shulman[4], Tamas L. Horvath[1,2,3,8] and Qian Gao[1,6,8]

The fasting-activated longevity protein sirtuin 1 (SirT1, ref. 1) promotes gluconeogenesis in part, by increasing transcription of the key gluconeogenic genes *pepck1* and *g6pase*[2,3], through deacetylating PGC-1α and FOXO1 (ref. 4). In contrast, signal transducer and activator of transcription 3 (STAT3) inhibits glucose production by suppressing expression of these genes[5,6]. It is not known whether the inhibition of gluconeogenesis by STAT3 is controlled by metabolic regulation. Here we show that STAT3 phosphorylation and function in the liver were tightly regulated by the nutritional status of an animal, through SirT1-mediated deacetylation of key STAT3 lysine sites. The importance of the SirT1–STAT3 pathway in the regulation of gluconeogenesis was verified in STAT3-deficient mice in which the dynamic regulation of gluconeogenic genes by nutritional status was disrupted. Our results reveal a new nutrient sensing pathway through which SirT1 suppresses the inhibitory effect of STAT3, while activating the stimulatory effect of PGC-1α and FOXO1 on gluconeogenesis, thus ensuring maximal activation of gluconeogenic gene transcription. The connection between acetylation and phosphorylation of STAT3 implies that STAT3 may have an important role in other cellular processes that involve SirT1.

The transcription factor STAT3 participates in various critical cellular processes[7]. In the liver, STAT3 is known to suppress expression of the transcriptional co-activator of gluconeogenesis PGC-1α and to suppress gluconeogenic genes. Ectopic expression of STAT3 in leptin receptor mutant (*lepr*$^{-/-}$) mice reduces *PGC-1α* transcription and reverses diabetes. This effect of STAT3 is abolished when Tyr 705 is mutated to a phenylalanine (Y705F; ref. 5). Other protein modifications of STAT3, such as acetylation, have recently been reported[8–10]. However, the functional significance of STAT3 acetylation remains ill-defined, and its relationship with STAT3 tyrosine phosphorylation remains unclear.

We hypothesized that STAT3 acetylation regulates physiological processes by mediating changes in the STAT3 phosphorylation status. We found that STAT3 acetylation was decreased after a 24-h fast and increased after feeding in the livers of C57BL/6J mice. STAT3 tyrosine phosphorylation directly correlated with the level of STAT3 acetylation, indicating that the reversible acetyl-modifications are functionally relevant (Fig. 1a). The observation that both acetylation and phosphorylation of STAT3 were evident in fed, but dramatically reduced in fasted, animals suggests that STAT3 acetylation and phosphorylation are actively downregulated on fasting. Overall, these observations signify that cellular metabolic status regulates STAT3 function in the liver, presumably owing to the sensitivity of the liver to the overall nutritional status of the organism[11].

SirT1 can be induced to promote gluconeogenesis[11,12] under conditions of fasting. Therefore, we asked whether SirT1 affects fed/fast-regulated STAT3 acetylation and phosphorylation. We injected the SirT1 inhibitor EX527, which has shown increased potency and specificity for SirT1 (ref. 13), into C57Bl/6J mice. EX527 increased acetylation and phosphorylation of hepatic STAT3 (Fig. 1c). These results are similar to those seen in animals treated with nicotinamide (Supplementary Information, Fig S1a), a less specific SirT1 inhibitor. EX527 also increased the acetylation of p53, a known SirT1 substrate, suggesting that a reduction of SirT1 function was achieved with EX527 treatment (Supplementary Information, Fig. S4b)[1]. In addition to EX527, we used an antisense oligionucleotide (ASO)[14,15] to knockdown hepatic SirT1 on a chronic basis. SirT1 ASO induced significant STAT3 acetylation and tyrosine phosphorylation (Fig. 1c). Together, these results support the idea that SirT1 is critically involved in hepatic STAT3 regulation.

Next, we studied the effect of nicotinamide and resveratrol (a SirT1 activator) on STAT3 acetylation and phosphorylation in an SV40-transformed mouse hepatic cell line, previously used in gluconeogenic studies[16,17]. In cells treated with nicotinamide (0.3 mM and 3 mM), the levels of STAT3 acetylation and phosphorylation increased in a dose-dependent manner and were independent of the kinase JAK2 (Fig. 1d) and class I and

Departments of [1]Comparative Medicine, [2]Obstetrics, Gynecology and Reproductive Sciences, and [3]Neurobiology, [4]Howard Hughes Medical Institute, Yale University School of Medicine, New Haven, CT 06520, USA. [5]Department of Surgery, Brown University Medical School-Rhode Island Hospital, Providence, RI 02903, USA. [6]Nanjing University School of Medicine, Jiangsu Province, 210093, China. [7]Current Address: State Key Laboratory of Cancer Biology and Xijing Hospital of Digestive Diseases, Fourth Military Medical University, Xi'an, Shaanxi, 710032, China.
[8]Correspondence should be addressed to T.L.H. or Q. G. (e-mail: tamas.horvath@yale.edu; qian.gao@yale.edu)

Received 17 November 2008; accepted 13 January 2009; published online 22 March 2009; DOI: 10.1038/ncb1857

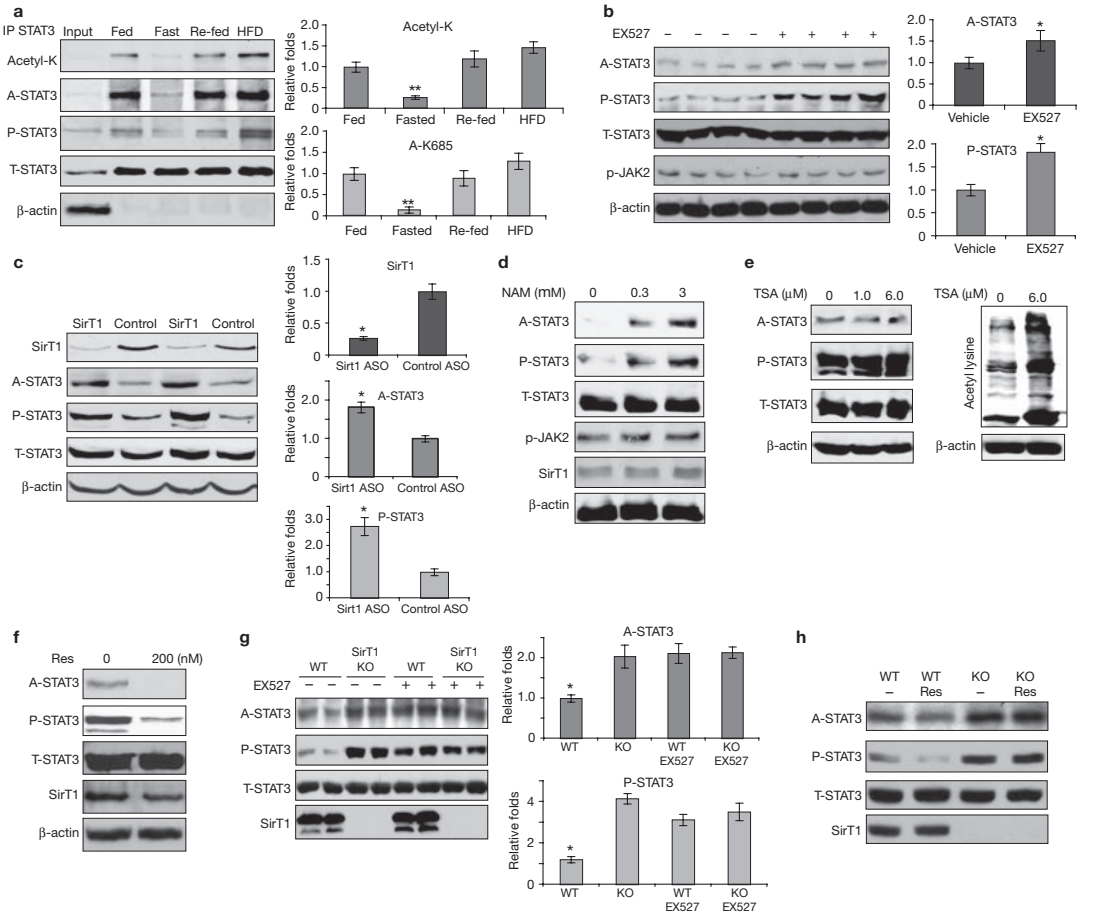

Figure 1 SirT1 is involved in regulating STAT3 acetylation. (**a**) STAT3 acetylation and phosphorylation changed in mouse livers under different nutritional conditions. Male C57Bl/6J mice were fed (normal laboratory chow), fasted (24 h), re-fed (24 h, normal laboratory chow after fasting) or fed with a high-fat diet (HFD, 48 h). The levels of STAT3 acetylation and phosphorylation in livers were determined by immunoprecipitation and/or western blot analysis. (**b**) EX527 induced acetylation and phosphorylation of STAT3. Fasted male C57Bl/6J mice were injected with EX527 (i.p. 10 mg per kg body weight) 6 h before being killed. (**c**) SirT1 ASO induced hepatic STAT3 acetylation and phosphorylation. C57Bl/6J mice were injected with ASO (i.p. 10 per kg body weight) five times in a 20-day period. (**d**–**f**) SV40-transformed mouse hepatic cells were treated with different doses of nicotinamide (NAM, **d**), trichostatin A (TSA, **e**) and resveratrol (Res, **f**). STAT3 acetylation levels were significantly increased by nicotinamide, but reduced by resveratrol. No change was observed with TSA. The significant increase of total protein acetylation shown by the pan-anti-acetylated lysine antibody indicated TSA was effective (**f**, left panel). (**g**, **h**) Decetylation of STAT3 is dependent on SirT1 *in vitro*. EX527 (10 μM for 6 h) increased STAT3 acetylation and phosphorylation in wild-type MEFs, but not in SirT1 KO MEFs (**g**). Data are mean ± s.e.m. of three repeated experiments, $n = 2$ cells. Resveratrol (100 nM for 6 h) decreased STAT3 acetylation and phosphorylation in wild-type MEFs, but not in SirT1 KO MEFs (**h**). Data are mean ± s.e.m., $n = 5$ mice * $P < 0.05$, ** $P < 0.01$ in **a**, **b** and **c**.

II HDACs (other cells were treated with trichostatin A, TSA; Fig. 1e). Conversely, resveratrol[18] (0.2 μM) reduced STAT3 acetylation and phosphorylation in the cultured hepatic cells (Fig. 1f). To determine whether deacetylation of STAT3 requires SirT1, we used SirT1 knockout (KO) and wild-type mouse embryonic fibroblasts[19] (MEFs). First, we found that levels of STAT3 acetylation and phosophrylation were constitutively higher in the SirT1 KO MEFs than in the wild-type MEFs (Fig. 1g). Second, treatment with EX527 increased levels of STAT3 acetylation and phosphorylation in wild-type MEFs, but not in SirT1 KO MEFs (Fig. 1g). Moreover, resveratrol decreased STAT3 acetylation and phosphorylation in wild-type MEFs, but not SirT1 KO MEFs (Fig. 1h). Together, these results further indicate that deacetylation of STAT3 is dependent on SirT1.

To investigate STAT3 as a SirT1 substrate, we studied the role of ectopically expressed SirT1. We found that the level of STAT3 acetylation was greatly reduced by cotransfection of human (h) SirT1, in HEK293T cells (Fig. 2a). Moreover, the introduced hSirT1 was able to potently suppress p300/CBP-induced STAT3 acetylation, suggesting that both factors affected the same set of lysine residues of STAT3 (Fig. 2a). The deacetylation of STAT3 by hSirT1 was more effective than that by HDAC1, HDAC 3 (Fig. 2a) or HDAC2 (data not shown), which were previously implicated in STAT3 deacetylation[10,20].

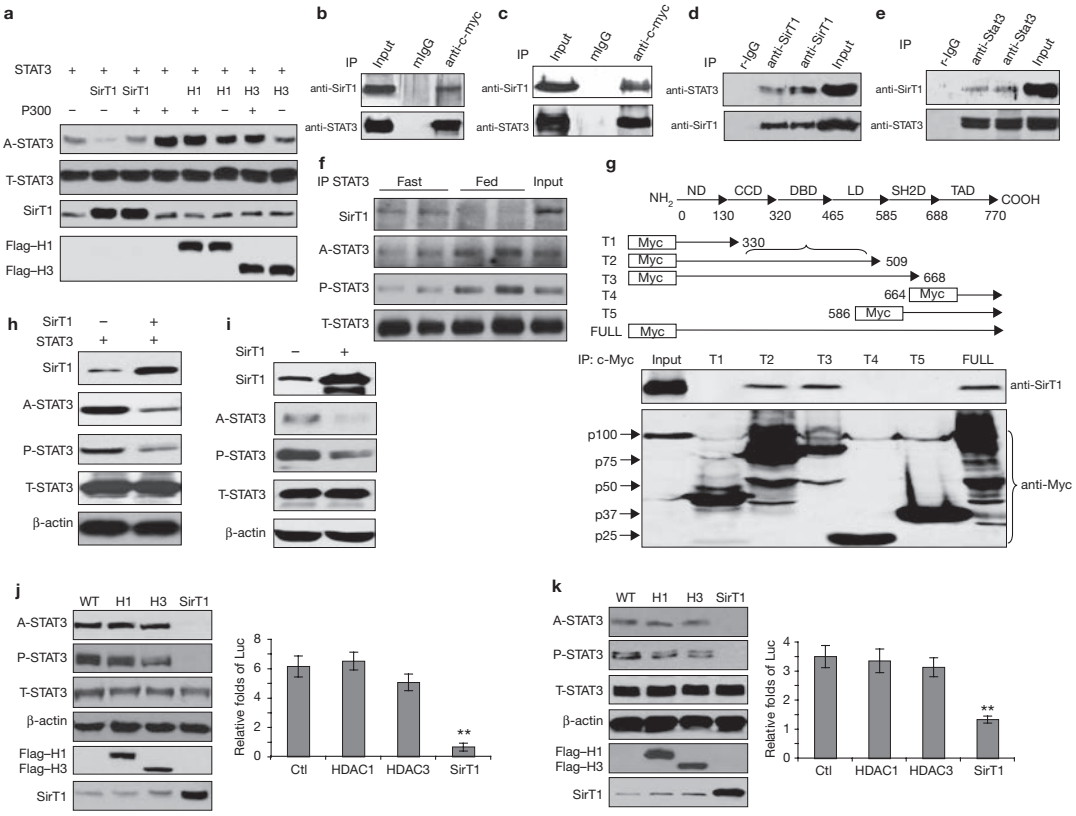

Figure 2 STAT3 phosphorylation and transactivation were downregulated by SirT1. (**a**) SirT1 deacetylates STAT3 in cultured cells. The effect of p300, SirT1 or HDACs on STAT3 acetylation was measured in transfected HEK293T cells (H1, HDCA1; H3, HDCA3). (**b**–**e**) SirT1 and STAT3 form complexes *in vitro* and *in vivo*. HEK293T cells were transfected with SirT1 and STAT3, or STAT3 alone (**b**, **c**). The physical interactions between exogenous STAT3 and exogenous (**b**) or endogenous (**c**) SirT1 were detected. In HEK293T cells, endogenous SirT1 and endogenous STAT3 were co-precipitated (**d**). STAT3 and SirT1 were co-precipitated by a STAT3 antibody in the livers of wild-type male mice ($n = 4$, **e**). (**f**) The physical interaction between STAT3 and SirT1 was enhanced in fasting livers. (**g**) Except for full-length STAT3, SirT1 was only precipitated by truncated STAT3-T2 and -T3, suggesting that both the DNA binding and the linker domains of STAT3 are involved in the interaction of STAT3 and SirT1. ND, N-terminal domain; CCD, coil-coil domain; DBD, DNA binding domain; LD, linker domain; SH2D, SH2 domain and TAD, transactivation domain. (**h**, **i**) SirT1-mediated deacetylation of STAT3 affects Y705-STAT3 phosphorylation. HEK293T cells were transfected with SirT1 and STAT3 (0.25 μg per well of each, **h**), or SirT1 alone (**i**), in 12-well-plates. (**i**) Each well was loaded with 100 μg of total protein to visually present the signals of endogenous A-STAT3 and P-STAT3. (**j**, **k**) The SirT1-mediated deacetylation of STAT3 affected STAT3 function (WT, wild-type). A2780 cells were treated with IL-6 (40 ng ml^{-1}) for 12 h. A relatively low level of the SirT1, HDAC1 and HDAC3 plasmids (0.05 μg per well) were either transfected with STAT3 (0.1 μg per well) or untreated (control). The effects on either exogenous (20 μg per well, **j**) or endogenous (60 μg per well, **k**) STAT3 acetylation and phosphorylation were determined. STAT3 transactivation activities were detected by a STAT3 specific luciferase reporter (Luc). Data are mean ± s.e.m. of three repeated experiments, ** $P < 0.01$ in **J** and **k**.

To test whether SirT1 and STAT3 formed a complex in cells, HEK293T cells were co-transfected with the wild-type genes of hSirT1 and hSTAT3. Exogenous (Fig. 2b) and endogenous (Fig. 2c) hSirT1 proteins were detected in immunoprecipitation products, suggesting that STAT3 and hSirT1 formed complexes. Next, endogenous STAT3 was co-precipitated by endogenous hSirT1 (Fig. 2d). To determine whether this physical interaction between hSirT1 and STAT3 occurs *in vivo*, we examined their association in mouse liver. SirT1 was observed in the STAT3 immunoprecipitation products, suggesting an interaction between endogenous STAT3 and SirT1 in the liver of fasted animals (Fig. 2e), and less so in the liver of fed animals (Fig. 2f).

To determine the region(s) in STAT3 responsible for SirT1 binding, a set of five c-Myc tagged STAT3 deletion mutants (T1 to T5) were generated that were designed to test each of the domains in STAT3. The DNA binding and linker domain (from amino acid 330–590) of STAT3 (ref. 21) was found to be the key region involved in the STAT3– SirT1 interaction (Fig. 2g). The various truncated STAT3s that did not contain the DNA binding and linker domain failed to form complexes with SirT1, whereas the truncated STAT3s that contained this domain pulled down SirT1 (Fig. 2g). Moreover, the latter had greatly reduced acetylation and phosphorylation on cotransfection with SirT1 (data not shown), suggesting that a direct interaction between the STAT3 DNA binding and linker domain and SirT1 is required for the enzymatic function of SiT1 on STAT3.

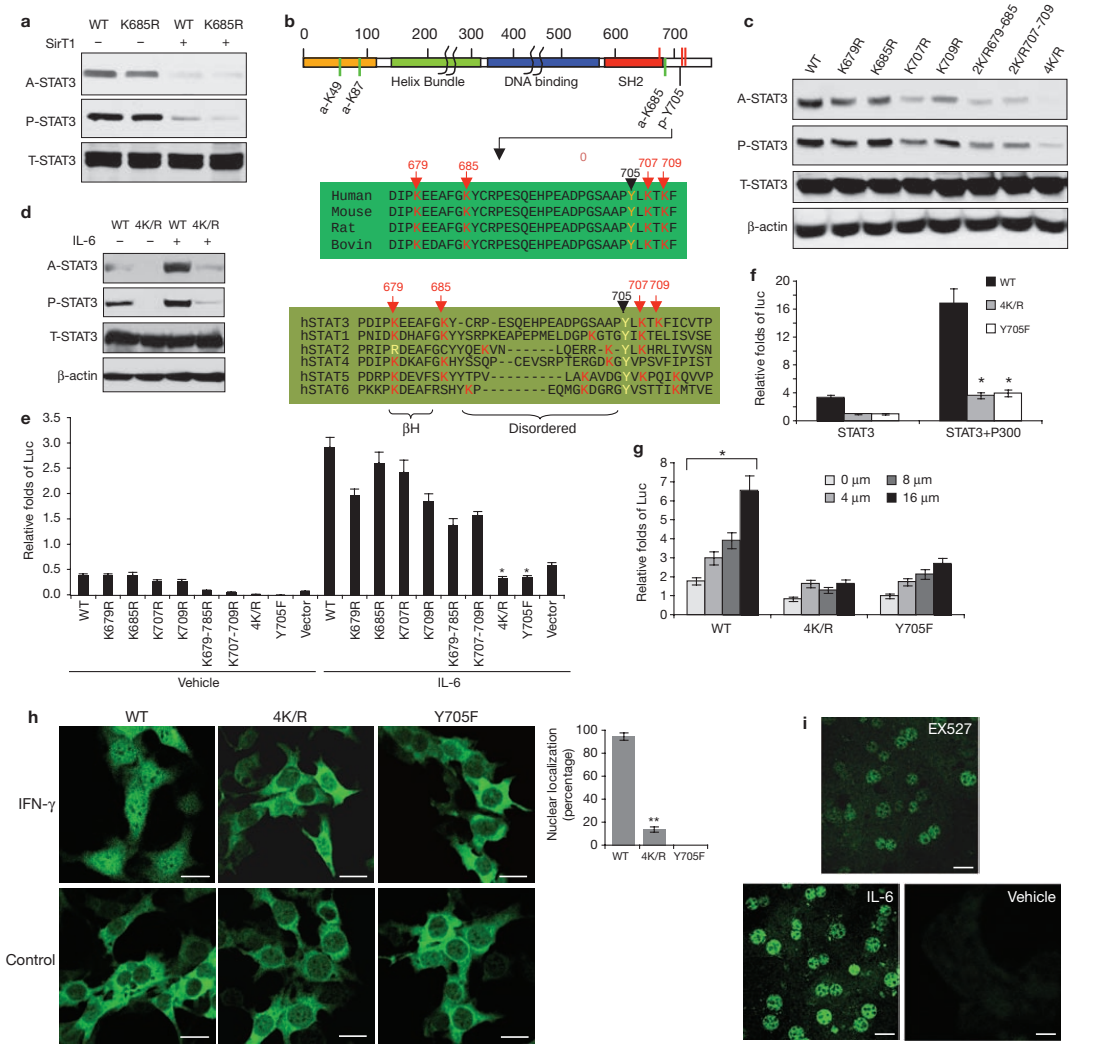

Figure 3 Critical novel acetylation sites regulate STAT3 phosphorylation and transactivation. (**a**) HEK293 cells were transfected with wild-type (WT) or K685R- STAT3 plasmids alone, or co-transfected with SirT1. STAT3 acetylation was determined. (**b**) A schematic representation of lysine acetylation sites identified in STAT3. Green lines represent the sites previously reported. Red lines represent a further three acetylation sites, identified by tandem mass spectrometry (Supplementary Information, Fig. S2b). (**c**, **d**) Mutations at four C-terminal lysine residues (4K/R) abolished STAT3 phosphorylation. A2780 cells were transfected with different K/R STAT3 mutants (**c**). Cells transfected with 4K/R or wild-type STAT3 were stimulated with 40 ng ml^{-1}) for 6 h (**d**). (**e**–**g**) The 4K/R mutation abolished STAT3 transactivation function. A2780 cells were cotransfected with different K/R-STAT3 mutants (0.15 μg), hSirT1 (0.1 μg), STAT3-dependent luciferase reporter (0.1 μg) and an internal control reporter pRL-TK plasmid (0.01 μg, **e**). Cells were treated with IL-6 (40 ng ml^{-1}) or left untreated. The transactivation function of STAT3 was assayed. The effect of p300 (0.35 μg per well, **f**) and various EX527 doses (**g**) on activating the transactivation function of wild-type or 4K/R- STAT3 were determined. (**h**, **i**) The 4K/R mutant disrupted STAT3 nuclear localization. STAT3 KO hepatoma cells were infected with retroviruses (pbabe-6Myc–STAT3 WT, Y705F and 4K/R) and stimulated with IFN-γ (50 ng ml^{-1}) for 2 h. (**i**) Primary hepatocytes were prepared from fasted animals and cultured in low nutrient media for 12 h before treatment with EX527 (10 μM) for 6 h or IL-6 (40ng ml^{-1}) for 1 h. The translocation of STAT3 was determined by immunofluorescence microscopy staining. Data are mean ± s.e.m. of three repeated experiments, * $P < 0.005$, ** $P < 0.01$ in **e**,**f** and **g**. Scale bars, 10 μm in **h**, 50 μm in **i**.

We next analysed whether the acetylation state of STAT3 affects STAT3 phosphorylation and transactivation function. After hSirT1 overexpression, the phosphorylation of exogenous (Fig. 2h) and endogenous (Fig. 2i) STAT3 was again downregulated with high efficiency. Low levels of exogenous hSirT1 DNA (0.05 μg) resulted in a reduction of exogenous and endogenous STAT3 acetylation and phosphorylation (Fig. 2j, k), whereas

transfection with HDAC1 and HDAC 3 had a limited effect (Fig. 2j, k). Consistently, an assay of STAT3-dependent luciferase reporter[10] (p4x IRF–Luc) revealed that SirT1, but not HDAC1 or HDAC3, suppressed the transactivation function of STAT3 (Fig. 2j, k). However, at increased doses of plasmid DNA, HDAC3 appreciably reduced STAT3 activity (Supplementary Information, Fig. S2a); this may contribute to downregulation of STAT3 acetylation and phosphorylation under certain conditions and in selected cells[8,20]. From these results, we conclude that SirT1 specifically and effectively deacetylated STAT3 in cultured cells and *in vivo,* and that this modification is coupled with a downregulation of STAT3 phosphorylation and transactivation.

The direct interaction between SirT1 and STAT3, and its effect on STAT3 phosphorylation and function, suggest that the state of acetylation of STAT3 may directly regulate its phosphorylation. Acetylation in a limited number of lysine residues in STAT3 was reported[8–10]; however, the coupling of acetylation and phosphorylation through these sites was not established, suggesting more lysine acetylation sites are involved. To identify these, particularly in the carboxy-terminal region, which is crucial for STAT3 phosphorylation, we initially examined acetylation in the K685R-STAT3 mutant: Lys 685 was reported to be the only acetylation site at the C terminus of STAT3 (ref. 10). We used an anti-acetyl-STAT3 antibody and, although it detected a minor reduction in acetylation, significant signal was still detected (Fig. 3a). This signal was downregulated by SirT1, suggesting that other acetylation sites exist. Three new lysine-acetylation residues, K679, 707 and 709, were identified by tandem mass spectrometry analysis (Supplementary Information, Fig. S2). These sites are evolutionally conserved among mammalian STATs, (Fig. 3b) and located either in the end β-sheet structure of the SH2 domain[21] (βH), or in the disordered signal stretch immediately after the SH2 domain. SH2 is known to specifically bind to phospho–tyrosine peptides[22,23]; therefore, it is critical to tyrosine signalling. Notably, the three new lysine residues are all in the vicinity of the Y705 of STAT3 (Fig. 3b), indicating that these sites may be pertinent to STAT3 phosphorylation[7,24].

Next, a systematic site-mutagenesis of these lysine sites of interest was performed. Mutation of all four lysine to arginine abolished the acetylation signals of STAT3 (Fig. 3c). Single or double lysine-to-arginine mutations had a limited effect on STAT3 phosphorylation, whereas changes of all four lysines to arganine (4K/R) largely abolished STAT3 phosphorylation. This effect is specific to the C-terminal acetylation sites, as mutations of the amino-terminal acetylation sites (K49/87R) did not affect the phosphorylation of STAT3 (Supplementary Information, Fig. S3a, b). These results imply that multiple lysine-acetylation sites adjacent to Y705 are vital for STAT3 phosphorylation. In contrast, the dominant-negative Y705F mutation did not affect the acetylation of STAT3 (Supplementary Information, Fig. S3c). More importantly, the 4K/R-STAT3 mutant was no longer sensitive to stimulation by IL-6 (interleukin) and IFN-γ (interferon-γ) which otherwise acetylated and phosphorylated STAT3. This suggests that the newly identified lysine acetylation sites are critical for cytokine stimulation of STAT3 (Fig. 3d).

To test whether the mutations of these acetylation sites affect STAT3 transcriptional function, STAT3-dependent luciferase reporter assays were performed in HEK293T cells and human ovarian cancer A2780 cells[25]. Consistent with the phosphorylation results, the 4K/R mutation largely abolished IL-6-induced STAT3 activation and had a dominant-negative-like effect, comparable to that of the Y705F mutation (Fig. 3e); whereas individual mutations had limited effects on STAT3 transactivation. Moreover, 4K/R-STAT3 was not capable of activating a known endogenous STAT3 target (hAGT; ref. 20) in HepG2 cells (Supplementary Information, Fig. S3d). Finally, ectopic expression of p300 (ref. 10) and treatment with EX527, which increased STAT3 acetylation and phosphorylation *in vivo*[13], failed to activate 4K/R-STAT3, whereas the same treatments increased the transactivation of wild-type STAT3 (Fig. 3f, g). These results suggest that the acetylation of the cluster of C-terminal lysine sites is up or downregulated by p300 or SirT1, respectively, and is crucial for STAT3 phosphorylation and transactivation. Next, we asked if the 4K/R mutations affect STAT3 localization, as phosphorylation is crucial for STAT3 nuclear translocation[7]. We introduced wild-type-, 4K/R- or Y705F-STAT3 into liver-STAT3 knockout (STAT3 LKO) hepatoma cells using a retrovirus (pbabe-6xcMyc–STAT3 containing wild-type-, Y705F- and 4K/R- STAT3) to test STAT3 nuclear translocation by immunofluorescence microscopy staining. Similarly to Y705F-STAT3, the mutant 4K/R-STAT3 significantly disrupted the nuclear translocation of STAT3 (Fig. 3h). This acetylation-related STAT3 localization was further supported by experiments in primary hepatocytes treated with EX527 (Fig. 3i). In addition, we found that the efficiency of 4K/R-STAT3 dimerization was greatly reduced (Supplementary Information, Fig. S3e).

If SirT1 promotes gluconeogenesis, in part through the suppression of STAT3, the knockout of STAT3 in liver should mimic the effect of SirT1 and increase gluconeogenesis independent of SirT1 activity. In normal chow fed STAT3 LKO mice, we observed a significant upregulation of *pepck1* and *g6pase*, but not of the control genes (cytochrome-*c* and *gk;* Fig. 4a–c). However, the further upregulation of *pepck1* and *g6pase* genes on fasting[26] was limited (Fig. 4a). The lack of repression of gluconeogenic gene expression after feeding, was due to the absence of STAT3 bound to the promoter region of *pepck1,* as shown by chromatin immunoprecipitation (ChIP) assay (Supplementary Information, Fig. S3f).

Next, we asked whether STAT3 is involved in the SirT1-mediated induction of hepatic gluconeogenesis. EX527 was used to inhibit SirT1 activity in STAT3 LKO mice and littermate controls after a 24-h fast. As reported previously[6], STAT3 LKO mice maintained normal glucose levels under such conditions, despite increasing gluconeogenic gene expression and plasma insulin levels (Fig. 4a, e). EX527 (i.p. 10 mg per kg body weight) reduced plasma glucose levels in fasting wild-type mice, whereas the plasma glucose levels of STAT3 LKO mice were unchanged (Fig. 4d), suggesting that STAT3 deficiency disrupted the ability of EX527 to lower fasting glucose levels independent of insulin concentration (Fig. 4e). Consistent with the reduction of plasma glucose levels in wild-type animals after EX527 treatment, the expression of the gluconeogenic genes was reduced in the livers of wild-type mice but was blunted in STAT3 LKO mice (Fig 4f). Next, we studied the effect of SirT1 knockdown on glucose homeostasis in the STAT3 LKO model. The levels of hepatic STAT3 acetylation and phosphorylation were significantly increased with SirT1 ASO in wild-type mice (Fig. 1d; Supplementary Information, Fig. S4a). Moreover, SirT1 ASO decreased hepatic gluconeogenic gene transcription (*pepck1, g6pase* and *fabpase*) in wild-type, but not STAT3 LKO, mice (data not shown).

Finally, a glucose tolerance test (Fig. 4g), a pyruvate tolerance test (Fig. 4h) and a glucagon-stimulation test (Fig. 4i) were conducted to evaluate various aspects of glucose homeostasis in wild-type and STAT3 LKO mice, with or without SirT1 knockdown. An overall reduction in glucose production was indicated in the SirT1 ASO-treated control animals. SirT1

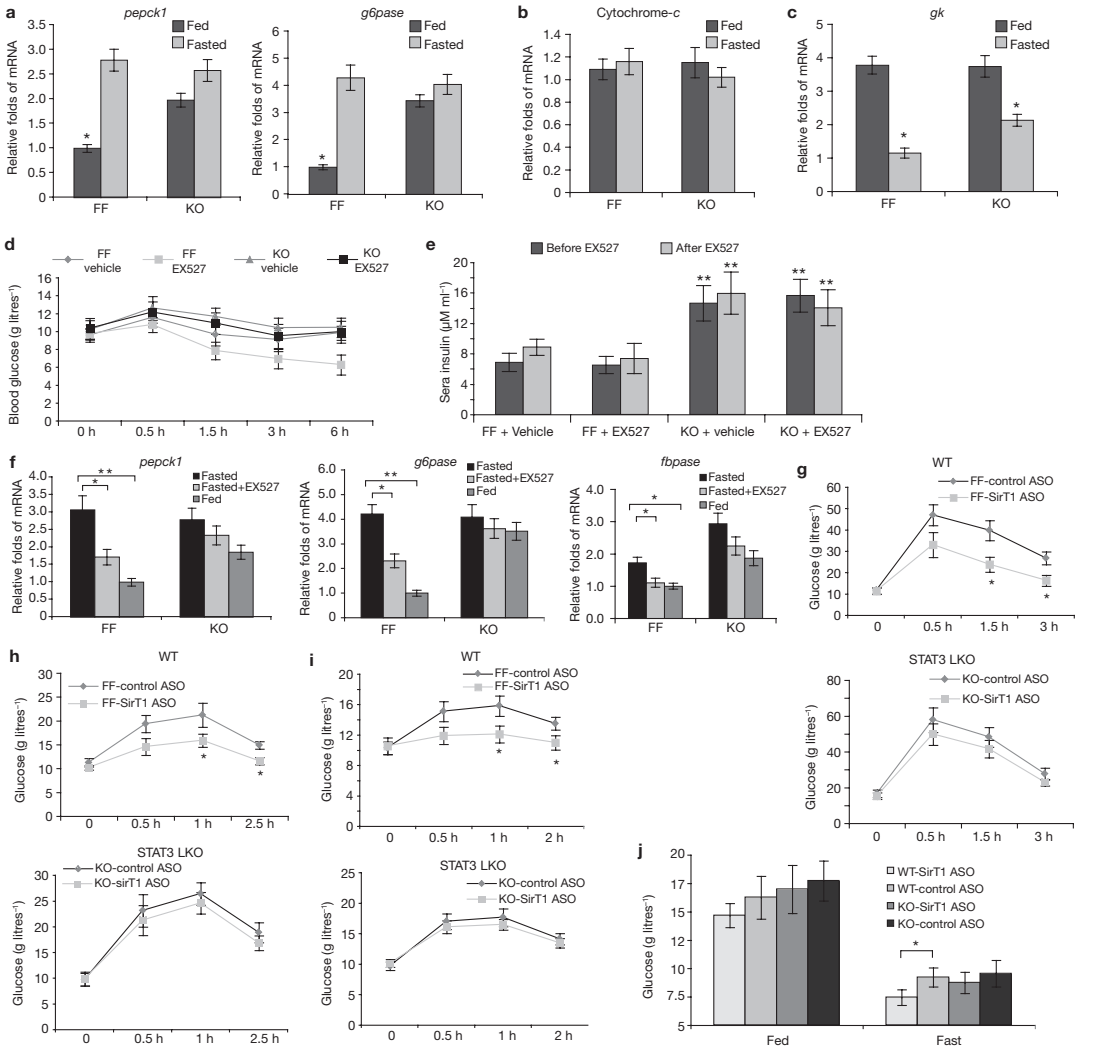

Figure 4 Liver-STAT3 deficiency disrupted fasting/SirT1 controlled gluconeogenesis. (**a**) Liver-STAT3 deficiency mimicked the effect of SirT1 in promoting gluconeogenic gene expression, independently of nutritional status and SirT1 activity. The mRNA levels of *pck1* and *g6pase* in livers were determined in fed and fasted STAT3$^{f/f}$ (FF) and STAT3 LKO (KO) mice using qrtPCR analysis (mean ± s.e.m., $n = 5$ livers). (**b**, **c**) Expression of the mitochondrial gene cytochrome-*c* as a control (**b**), and the glycolytic gene *gk* (**c**), were not altered by the absence of STAT3. Mean ± s.e.m., $^*P < 0.05$, $n = 5$ livers in **b** and **c**. (**d**) STAT3 deficiency disrupted fasting/SirT1-induced hypoglycemia. The STAT3$^{f/f}$ and STAT3 LKO mice were fasted overnight, and then injected with EX527 (i.p. 10 mg per kg body weight). Plasma glucose levels were determined at 0, 30, 90, 180 and 360 min. (**e**) The same treatment did not alter the plasma insulin levels, which were determined before and after treatment with EX527. In **d** and **e**, data are mean ± s.e.m., $n = 6$ mice, $^{**}P < 0.01$. (**f**) STAT3 deficiency in the livers disrupted fasting/SirT1 induced gluconeogenic gene expression. The transcripts of the key gluconeogenic genes *pepck1*, *g6pase* and *fbpase* in the livers were detected by qrt-PCR (mean ± s.e.m., $n = 5$ $^*P < 0.05$, $^{**}P < 0.01$). (**g**–**i**) The liver STAT3 deficiency impaired SirT1 controlled liver glucose production as assessed by a glucose tolerance test (GTT, **g**), pyruvate tolerance test (PTT, **h**) and glucagon-stimulation test (GST, Glucagon, **i**). Data are mean ± s.e.m., $n = 6$ mice in **g**–**i**. (**j**) STAT3 LKO-impaired SirT1 knockdown induced a reduction in glucose in animals on a high-fat diet. STAT3$^{f/f}$ and STAT3 LKO mice were fed a high-fat diet for two-and-a-half weeks. SirT1 ASO or control ASO was administered five times during a two week period at a dose of i.p. 10 mg per kg body weight. The levels of plasma glucose levels were measured under conditions of feeding and overnight fasting (mean ± s.e.m., $n = 7$ mice, $^*P = 0.022$).

ASO treatment of STAT3 LKO mice had little effect on the parameters measured by all three tests (Fig. 4g–i). These data led us to conclude that SirT1 promotes gluconeogenesis, in part, by suppressing the inhibitory effect of STAT3 on the expression of gluconeogenic genes. To test the effect of hepatic insulin resistance on the interaction of SirT1 with STAT3, all groups of mice were fed with a high-fat diet (Supplementary Information,

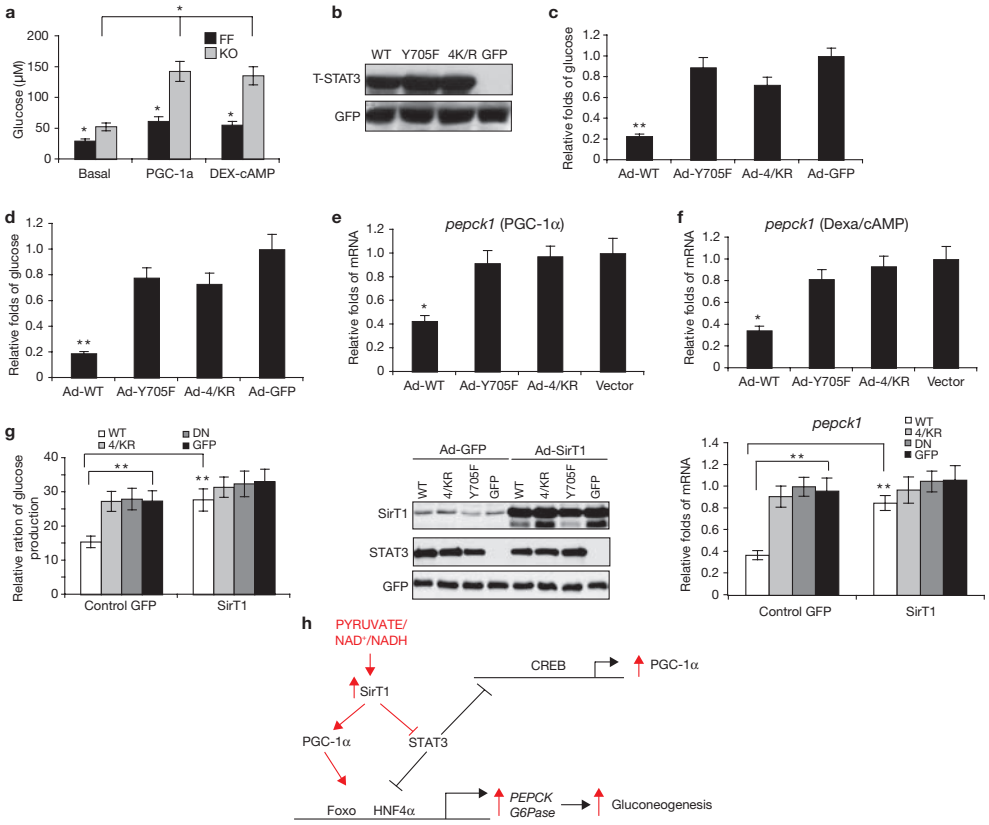

Figure 5 The 4K/R mutant STAT3 is defective in suppressing hepatic gluconeogenesis. (**a**) Basal-, PGC-1α- or dexa/cAMP-stimulated glucose production in primary hepatocytes was significantly increased in the absence of STAT3 (* $P < 0.05$; FF, $STAT3^{f/f}$; KO, STAT3 LKO). (**b**) Wild-type- (WT), 4K/R- and Y705F-STAT3 were introduced into primary hepatocytes by adenoviruses (Ad), and an equal amount of each STAT3 protein was detected. (**c**, **d**) Wild-type STAT3, but not 4K/R- or Y705F- STAT3, effectively inhibited the promotion of glucose production by either PGC-1α (**c**) or dexa/cAMP (**d**), in primary hepatocytes (** $P < 0.01$). (**e**, **f**) Similarly, the wild-type-STAT3, but not 4K/R- or Y705F-STAT3, inhibited the expression of *pepck1*, when promoted by PGC-1α (**e**) or dexa/cAMP (**f**, * $P < 0.05$). (**g**) Ectopic SirT1 disrupted the effect of wild-type-STAT3 on suppressing glucose production. STAT3 KO primary hepatocytes were co-infected by adenoviruses, with adeno-SirT1, adeno-wild-type-STAT3, mutant-STAT3 or GFP control (** $P < 0.01$). The middle panel shows the level of protein expression of SirT1 and STAT3s; the right panel shows the level *pepck1* mRNA. (**h**) A schematic representation of the nutrient sensing pathway through which SirT1 regulates hepatic gluconeogenesis by both suppressing STAT3 and activating PGC-1α /Foxo1. Data are mean ± s.e.m. of three repeated experiments in **a**–**g**.

Fig. S5a). Blood glucose levels on fasting were decreased in SirT1 ASO-treated wild-type mice, but unchanged in SirT1-ASO treated STAT3 LKO mice (Fig. 4j; Fig. S5b). This observation indicates that the loss of hepatic STAT3 is critical for SirT1 function. In addition, our results are consistent with the SirT1 LKO model[12], but differ from the SirT1 transgenic mouse model.[3,27]. However, gluconeogenic gene expression was increased in isolated primary SirT1 transgenic hepatocytes treated with cAMP and deprived of insulin treatment, suggesting that insulin-mediated inhibition of gluconeogenesis may be independent of the SirT1 pathway[3].

If the C-terminal cluster of acetylation lysine sites are crucial for STAT3 transactivation, the C-terminal 4K/R mutant should disrupt the suppressive effect of STAT3 on hepatic glucose production. First, we found that the glucose production in STAT3 LKO primary hepatocytes was increased, compared with that in wild-type cells (Fig. 5a). To further test the inhibitory effect of STAT3 on glucose production in hepatocytes, we promoted cellular glucose production in these cells, either by introducing PGC-1α or by treating cells with dexamethasone (50 nM) and 8-bromo-cAMP (2 μM; refs 2, 26). Equivalent amounts of STAT3 total proteins were detected in $STAT3^{-/-}$ cells in which wild-type STAT3, 4K/R- or Y705F-STAT3 had been re-introduced (Fig. 5b). Wild-type STAT3 suppressed hepatic glucose production (Fig. 5c, d), whereas, 4K/R- or Y705F-STAT3 had little effect. Consistent with the data on glucose production, we observed a strong reduction in expression of the gluconeogenic *pepck1* transcripts by wild-type-STAT3, but not by 4K/R-STAT3, in STAT3 LKO hepatocytes ectopically expressing PGC-1α or treated with dexamethasone/cAMP (Fig. 5e, f).

To determine whether the change in hepatic glucose production by re-introduced wild-type-STAT3 (but not 4K/R-STAT3) is mediated

by SirT1, we co-infected STAT3 LKO primary hepatocytes with both adeno-SirT1 and adeno-STAT3s (wild type, 4K/R, Y705F and GFP). Ectopic SirT1 blunted the suppression of glucose production by wild-type-STAT3; however, this effect was limited in 4K/R-STAT3- or Y705F-STAT3-expressing cells (Fig. 5g). These results further support the idea that hepatic glucose production is dependent on SirT1-mediated down-regulation of STAT3.

Our findings reveal a new molecular mechanism whereby SirT1 suppresses the inhibitory effect of STAT3 on gluconeogenesis, while activating PGC-1α and Foxo1 (ref. 4) to stimulate gluconeogenesis in the liver, in response to nutrient signals. This dual function of SirT1 has a central role in preventing concurrent activation of the two counter-mechanisms of gluconeogenesis regulation (Fig. 5h). These findings have implications for defining the basic pathways of energy homeostasis, diabetes and lifespan. □

METHODS

Animals. All the mice used in this study were on a C57BL/6J background. Twelve-week-old male wild-type mice (Jackson Laboratory) were fed *ad libitum*, fasted for 24 h, fasted and re-fed for 24 h or fed on a high-fat diet (45 Kcal% fat) for 48 h. STAT3 LKO mice were generated by crossing STAT3 $^{f/f28}$ and Alb-*Cre* transgenic mice, B6.Cg-Tg (Alb-cre) 21Mgn/J (Jackson Laboratory). Various treatments were applied depending on the experiment, including: fasting, feeding, re-feeding, feeding with a high-fat diet and administration of various chemical compounds. EX527 (6-Chloro-2, 3, 4, 9-tetrahydro-1H-carbazole-1-carboxamide; Tocris; i.p.10 mg per kg body weight) and nicotinamide (Sigma; i.p. 50 mg per kg body weight or 150 mg per kg body weight) were introduced for 6 h. Animals were killed and the liver, white adipose, muscles, kidney, heart, brain and spleen tissues were subjected to western blotting or quantitative real-time PCR (qrt-PCR) analysis. The sera were collected through tail-vein puncture at different times to test glucose, insulin and liver function (Alanine Aminotransferase, ALT; assays performed in the Yale Mouse Metabolic Phenotyping Center). All procedures were performed in accordance with the National Institutes of Health Guide for the Care and Use of Laboratory Animals, and under the approval of the Yale Medical School Animal Care and Use Committee.

SirT1 knockdown (ASO). Control and STAT3 LKO mice (2–4 months old) were divided into control ASO and SirT1 ASO groups. The mice received food *ab libitum* and were housed on a 12-h dark/light cycle. SirT1 ASO 5'-ATACCATTCTTTGGTCTAGA-3' (ASO # 384856) or control ASO (ASO# 141923; ISIS Pharmaceuticals) was administered five times during a 2–3 week period (i.p. 10 mg per kg body weight). ASO solutions were sterilized through a 0.44-μm filter before injection. The ASO targets the 3'UTR of *SirT1* mRNA and has no significant crossreactivity to other sirtuin family members. The control ASO had the same chemistry as SirT1 ASO, and had a scrambled oligonucleotide sequence. Both ASOs were prepared in normal saline.

Measurement of glucose metabolism. The glucose tolerance test (glucose 2 g per kg body weight i.p.), pyruvate tolerance test (Pyruvate 2 g per kg body weight i.p.) and glucagon-stimulation test (Glucagon 200 μg per kg body weight i.p.) were conducted to evaluate various aspects of glucose production and metabolism.

Constructs. The pcDNA3-6×Myc–mSTAT3 and its K685R mutant expression vectors were from the laboratory of Y. E. Chin[10]. pcDNA3-6×cMyc-mSTAT3 K49R, K87R, K49-87R, K679R, K685R, K707R, K709R, K685-679R, K707-709R, K679-685-707-709R and Y705F were derived from the wild-type pcDNA3-Myc–mSTAT3 vector using a site-mutagenesis kit (Stratagene). The deletion mutants of STAT3 were constructed through PCR, and the schematic map of deletions is shown in Fig. 2g. The sequences of the oligonucleotide primers are: STAT3-F, 5'-cgaattcc ATG GCT CAG TGG AAC CAG-3'; S134-R, 5'-cctcgag tca AGC TGT TGG GTG GTT GG-3'; S323-R, 5'-cctcgagtcaCAC CAC GAA GGC ACT CTT-3'; S590-R, 5'-cctcgagtcaGCT GAT GAA ACC CAT GAT G-3'; S668-R, 5'-cctcgagtcaTGG AGA CAC CAG GAT GTT G-3'; S770-R, 5'-cctcgag TCA CAT GGG GGA GGT AGC-3'; S586-F, 5'-cgaattcc ATG GGT TTC ATC AGC AAG G-3'; S664-F, 5'-cgaattccATC CTG GTG TCT CCA CTT G-3'.

Retroviruses pBaBe-6×cMyc-STAT3 (wild-type, Y705F, K49-87R and K679-685-707-709R) were subcloned from pcDNA3-xcMyc-STAT3s, by switching restriction endonuclease (*SalI*). All constructs were verified by nucleotide sequencing in Yale KECK facilities. pTOPO-hSirT1 and its inactivated form H363Y were from Wei Gu (Columbia University, New York). HA–p300 constructs were provided Tsi-Pang Yao (Duke University, Carolina). Flag–HDAC1, Flag–HDAC2 and Flag–HDAC3 constructs were originally provided by Edward Seto (H. Lee Moffitt Cancer Center and Research Institute, Florida). P4xIRF-1–Luc is a STAT3 specific Luciferase reporter. APRE–luciferase reporter[29] was a gift from David Levy (New York University School of Medicine). A PRE-TK plasmid was used as an internal control for transfection efficiency.

Cell culture, plasmid transfection, drug treatment and primary hypatocytes. A2780 cells (Sigma) were cultured in RPMI 1640 medium with 10% fetal bovine serum (FBS) supplemented with glutamine (2 mM). The SV40-immobilized mouse hepatocytes (from Domenico Accili, Columbia University, New York) were maintained in modified Eagle's medium containing 10% FBS. SirT1 KO MEFs and wild-type MEFs were gifts from Leonard Guarente (Harvard University, Massachusetts). MEFs and HEK293T cells were maintained in Dulbecco's modified Eagle's medium containing 10% fetal bovine serum. Cells were transiently transfected using LipofectAMINE 2000 (Invitrogen), according to the manufacturer's protocol. Cells were collected and washed with cold PBS for experiments and cells received one of the following treatments: (i) 200 nM Resveratrol (Sigma) for 4 h; (ii) 0.3–3 mM Nicotinamide (Sigma) for 4 h; (iii) 1–6 μM TSA (Sigma) for 6–12 h; (iv) 40 ng ml^{-1} IL-6 (Sigma) for 6–12 h; (v) 50 ng ml^{-1} IFN-γ (Sigma) for 2–6 h; (vi) 10 mM EX527 (Tocris) or (vii) 50 nM Dexamathasone (Sigma) + 2 μM 8-bromo-cAMP (Sigma).

Mouse primary hepatocytes were prepared in the Hepatocyte Isolation Core of the Yale Liver Center (Yale University School of Medicine, New Haven). Details are shown in supplementary methods.

Immunoprecipitation. Protein–protein interactions in cells were also analysed by co-immunoprecipitation. The details of these experiments have been described previously[30]. Ectopic Myc–STAT3 or SirT1 were expressed in HEK293T cells by transient transfection with PcDNA3cMyc–STAT3 or PcDNA3.1/V5-his-SirT1. The interaction of ectopic STAT3 with ectopic SirT1, or ectopic STAT3 with endogenous SirT1, was tested using an anti-c-Myc antibody. Co-IP of endogenous STAT3 and SirT1 from HEK293T cells and liver tissues was performed using an anti-STAT3 antibody (Santa Cruz). Cell pellets and mouse liver tissues were sonicated in modified IP buffer, and pre-cleaned with normal rabbit or mouse IgG-conjugated nProtein A Sepharose 4 Fast Flow beads (Amersham) for 2 h at 4 °C. The pre-cleaned lysates were then mixed with c-Myc, the anti-STAT3 antibody and normal rabbit or mouse IgG (negative control)-conjugated nProtein A Sepharose 4 Fast Flow beads. Immunoprecipitation products were separated by SDS–PAGE, and blotted using a SirT1 antibody (Millipore), and β-actin (Sigma), which was used as an internal control.

Identification of STAT3 acetylation sites by mass spectrometry. The STAT3 complexes were immunoprecipitated, separated by SDS–PAGE and stained with SYPRO Ruby (Bio-Rad). The visible bands were excised. Gel pieces were subjected to a modified in-gel trypsin digestion procedure, and the peptides were subjected to liquid chromatography-electrospray ionization-tandem mass spectrometry (LC-ESI-MS/MS) analysis (Taplin Biological Mass Spectrometry Facility). The most abundant ions were obtained, and the MS/MS spectra was directly searched against the non-redundant protein database of the National Center for Biotechnology Information with the SEQUEST database search algorithm.

ChIP assays. The ChIP Assay Kit and protocol (Upstate Biotechnology) were used. P200 (region -226 to -24 of the mouse C/EBPδ promoter containing STAT3 binding sites), was used for STAT3 positive control primers[31], see Supplementary Information, Methods for details.

Statistical analysis. Results are expressed as the mean ± s.e.m., and statistical analysis was performed by one-way or two-way ANOVA analysis of variance and Student's *t*-test. A $P < 0.05$ was considered significant.

Note: Supplementary Information is available on the Nature Cell Biology website.

ACKNOWLEDGEMENTS
We thank M. Shanabrough for her technical support and careful revision of this manuscript. Some constructs were obtained from Y. E. Chin, W. Gu, P. Yao, E. Seto and D. Levy. SirT1, PGC-1α adenovirus was a gift from P. P. Puigserver . SirT1 KO MEFs and wild-type MEFs were a gift from L. P. Guarente. Part of this work was supported by an ADA grant to Q. G. (1-08-RA-54) and NIH grants to T. L. H. (DK-08000 and DK-060711), G. I. S. (DK-40936 and DK-076169) and J.L.B. (DK-P30-34989). The preparation of primary hepatocytes was performed in the Liver Center of Yale University School of Medicine. SirT1 ASO and Control ASO were provided by ISIS Pharmaceuticals, Inc.

AUTHOR CONTRIBUTIONS
Y.N., T.L.H. and Q.G. designed, executed and analysed most of the experiments and wrote the paper. D.M.E. contributed to the execution of the SirT1-ASO animal experiments and edited the paper. Z.Y. contributed to construction of trunicated STAT3 plasmids. M.D. designed , performed and analysed the animal experiements with EX527 treatement. G.I.S. provided critical models and analysed the data of the animal experiments.

COMPETING FINANCIAL INTERESTS
The authors declare no competing financial interests.

Published online at http://www.nature.com/naturecellbiology/
Reprints and permissions information is available online at http://npg.nature.com/reprintsandpermissions/

1. Luo, J. *et al.* Negative control of p53 by Sir2α promotes cell survival under stress. *Cell* 107, 137–148 (2001).
2. Rodgers, J. T. *et al.* Nutrient control of glucose homeostasis through a complex of PGC-1α and SIRT1. *Nature* 434, 113–118 (2005).
3. Banks, A. S. *et al.* SirT1 gain of function increases energy efficiency and prevents diabetes in mice. *Cell Metab.* 8, 333–341 (2008).
4. Frescas, D., Valenti, L. & Accili, D. Nuclear trapping of the forkhead transcription factor FoxO1 via Sirt-dependent deacetylation promotes expression of glucogenetic genes. *J. Biol. Chem.* 280, 20589–20595 (2005).
5. Inoue, H. *et al.* Role of STAT-3 in regulation of hepatic gluconeogenic genes and carbohydrate metabolism *in vivo*. *Nature Med.* 10, 168–174 (2004).
6. Inoue, H. *et al.* Role of hepatic STAT3 in brain-insulin action on hepatic glucose production. *Cell Metab.* 3, 267–275 (2006).
7. Zhong, Z., Wen, Z. & Darnell, J. E. Jr Stat3: a STAT family member activated by tyrosine phosphorylation in response to epidermal growth factor and interleukin-6. *Science* 264, 95–98 (1994).
8. Ray, S., Boldogh, I. & Brasier, A. R. STAT3 NH2-terminal acetylation is activated by the hepatic acute-phase response and required for IL-6 induction of angiotensinogen. *Gastroenterology* 129, 1616–1632 (2005).
9. Wang, R., Cherukuri, P. & Luo, J. Activation of Stat3 sequence-specific DNA binding and transcription by p300/CREB-binding protein-mediated acetylation. *J. Biol. Chem.* 280, 11528–11534 (2005).
10. Yuan, Z. L., Guan, Y. J., Chatterjee, D. & Chin, Y. E. Stat3 dimerization regulated by reversible acetylation of a single lysine residue. *Science* 307, 269–273 (2005).
11. Rodgers, J. T., Lerin, C., Gerhart-Hines, Z. & Puigserver, P. Metabolic adaptations through the PGC-1α and SIRT1 pathways. *FEBS Lett.* 582, 46–53 (2008).
12. Chen, D. *et al.* Tissue-specific regulation of SIRT1 by calorie restriction. *Genes Dev.* 22, 1753–1757 (2008).
13. Solomon, J. M. *et al.* Inhibition of SIRT1 catalytic activity increases p53 acetylation but does not alter cell survival following DNA damage. *Mol. Cell. Biol.* 26, 28–38 (2006).
14. Chan, J. H., Lim, S. & Wong, W. S. Antisense oligonucleotides: from design to therapeutic application. *Clin. Exp. Pharmacol. Physiol.* 33, 533–540 (2006).
15. Savage, D. B. *et al.* Reversal of diet-induced hepatic steatosis and hepatic insulin resistance by antisense oligonucleotide inhibitors of acetyl-CoA carboxylases 1 and 2. *J. Clin. Invest.* 116, 817–824 (2006).
16. Puigserver, P. *et al.* Insulin-regulated hepatic gluconeogenesis through FOXO1-PGC-1α interaction. *Nature* 423, 550–555 (2003).
17. Nakae, J., Park, B. C. & Accili, D. Insulin stimulates phosphorylation of the forkhead transcription factor FKHR on serine 253 through a Wortmannin-sensitive pathway. *J. Biol. Chem.* 274, 15982–15985 (1999).
18. Howitz, K. T. *et al.* Small molecule activators of sirtuins extend *Saccharomyces cerevisiae* lifespan. *Nature* 425, 191–196 (2003).
19. Li, X. *et al.* SIRT1 deacetylates and positively regulates the nuclear receptor LXR. *Mol. Cell* 28, 91–106 (2007).
20. Ray, S., Lee, C., Hou, T., Boldogh, I. & Brasier, A. R. Requirement of histone deacetylase1 (HDAC1) in signal transducer and activator of transcription 3 (STAT3) nucleocytoplasmic distribution. *Nucleic Acids Res.*(2008).
21. Becker, S., Groner, B. & Muller, C. W. Three-dimensional structure of the Stat3β homodimer bound to DNA. *Nature* 394, 145–151 (1998).
22. Koch, C. A., Anderson, D., Moran, M. F., Ellis, C. & Pawson, T. SH2 and SH3 domains: elements that control interactions of cytoplasmic signaling proteins. *Science* 252, 668–674 (1991).
23. Pawson, T. & Gish, G. D. SH2 and SH3 domains: from structure to function. *Cell* 71, 359–362 (1992).
24. Minami, M. *et al.* STAT3 activation is a critical step in gp130-mediated terminal differentiation and growth arrest of a myeloid cell line. *Proc. Natl Acad. Sci. USA* 93, 3963–3966 (1996).
25. Maloney, A. *et al.* Gene and protein expression profiling of human ovarian cancer cells treated with the heat shock protein 90 inhibitor 17-allylamino-17-demethoxygeldanamycin. *Cancer Res.* 67, 3239–3253 (2007).
26. Yoon, J. C. *et al.* Control of hepatic gluconeogenesis through the transcriptional coactivator PGC-1. *Nature* 413, 131–138 (2001).

nature cell biology

DOI: 10.1038/ncb1857

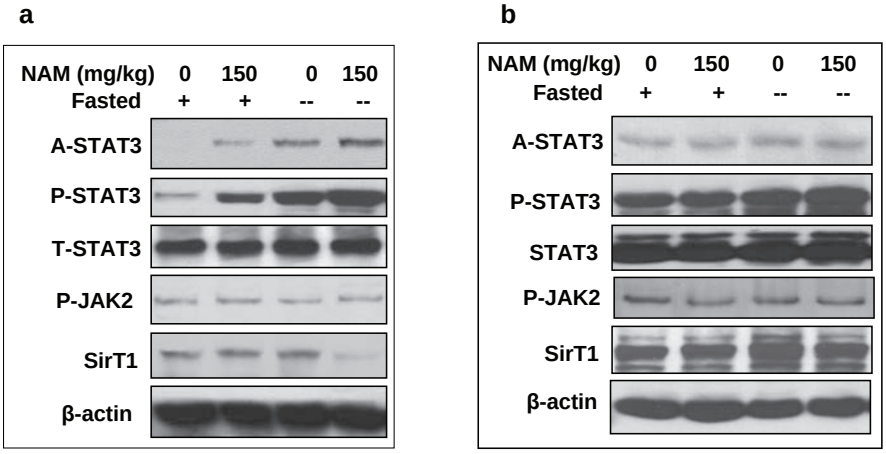

Figure S1 SirT1 inhibitor nicotinamide increased acetylation and phosphorylation of STAT3 in liver **(a)**, but not spleen **(b).** Male C57Bl/6J mice (n=5 for each group) were fed (normal chow), fasted (24 h). Mice were treated with nicotinamide at the dose of 150 mg kg^{-1} *via* i.p.

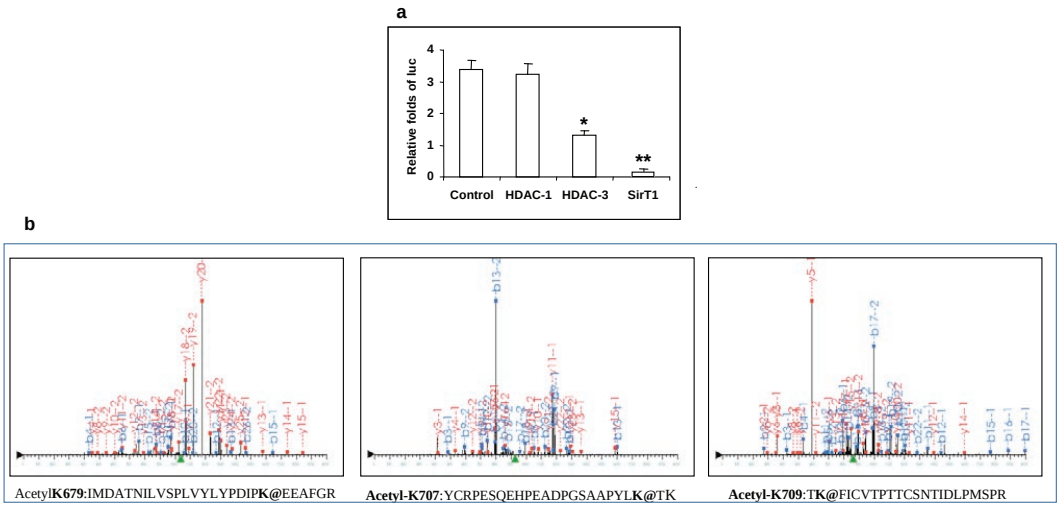

Figure S2 (a) HDAC3 at higher expression reduced the transcriptional activity STAT3. In comparison to Fig. 2j, the amount of HDAC1, HDAC3 or Sirt1 plasmids was increased from 0.05mg to 0.25mg each well (24 well-plate) in the transient cotransfection with the STAT3 specific Luciferase reporter. The result showed that the increase of HDAC3, but not HDAC1 reduced STAT3 transactivation activity. *p<0.05; **p<0.01. **(b)** Identification of three novel lysine acetylation sites in STAT3. 293T cells were cotransfected with plasmids of human P300 and cmyc-STAT3. IP products of STAT3 were subjected to a modified in-gel trypsin digestion procedure. The peptides were subjected to liquid chromatography-electrospray ionization-tandem mass spectrometry (LC-ESI-MS/MS) analysis (Taplin Biological Mass Spectrometry Facility, Harvard, Boston, MT) three acetylated peptides of STAT3 indicates the sites of acetylation, which are at K679, K707 and K709.

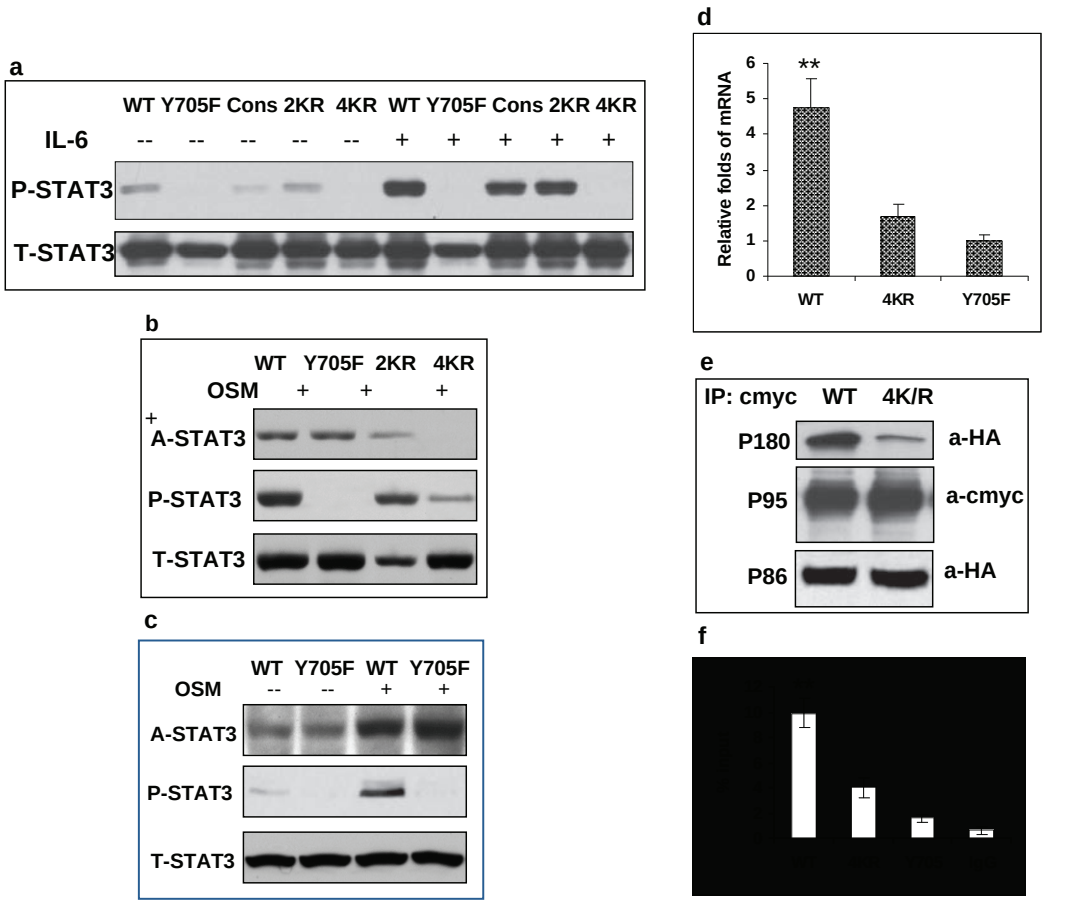

Figure S3 (a) and **(b)** K49/87R mutant (2KR) did not affect the phosphrylation of Y705 and acetylation of K685 of STAT3 in cells. **(a)** Primary hepatocytes were infected with adenovirus containing cmyc-STAT3 or its mutants. The cells were stimulated with 30ng ml^{-1} of IL-6 for 6h. (**b**) 293T cells were transfected with pcDNA3 plasmids containing cmyc-STAT3 or its mutants and stimulated with 10ng ml^{-1} OSM for 6h. **(c)** Y705F mutation did not affect STAT3 acetylation. 293T cells were transfected with pcDNA3-6myc-WT or Y705F-STAT3. Cells were stimulated with 10ng ml^{-1} OSM for 4h. **(d)** Endogenous hAGT transcripts (STAT3 target gene) were induced by WT-STAT3, but not 4K/R- or Y705F-STAT3 in HepG2 cells. HepG2 cells were transfected with STAT3 and its mutants. 12h after the transfection, IL-6 was added at 40ng ml^{-1} for 12 h. RNAs were extracted and subjected to Q-RT-PCR with strategene one step kit. **: p<0.01 hAGT, 5'-CTTCACAGAACTGGATG-3' (**f**) and 5'-GAACTCCTGGGGCTCG-3' (reverse) (product size, 241 bp). **(e)** 4K/R mutation destructed the dimerization of STAT3. 293T cells were cotransfected with either the combination of HA-WT-STAT3 and cmyc-WT-STAT3 or HA-WT-STAT3 and cmyc-4K/R-STAT3. The cell lysates were immunoprecipitated with an anti-cmyc antibody. The IP products of STAT3 were released from beads by 1.5 X loading buffer containing low levels of DTT (80mM) at 100 ºC for 90 seconds to keep the potential STAT3 dimers from dissociating. The P180 band was detected by the anti-HA antibody to reveal the dimerization of both HA-STAT3 and 6cmyc-STAT3. P95 was detected by the anti-cmyc antibody to illustrate pulled down the cmyc-STAT3s monomers. The cell lysates was directly used for Western blot analysis (the bottom panel) to detect HA-WT-STAT3 (P86) using the anti-HA antibody. **(f)** ChIP assay WT-STAT3 bound the promoter region (-3728 to -3598) of mouse pepck1, whereas the 4K/R mutant STAT3 impaired this function of STAT3. STAT3-LKO hepatocytes were reintroduced with WT-STAT3, 4K/R-STAT3, or Y705F-STAT3, respectively, by pBaBe-retrovirus and treated with IL-6 (40ng ml^{-1}, 2h) before protein-DNA cross-linking.

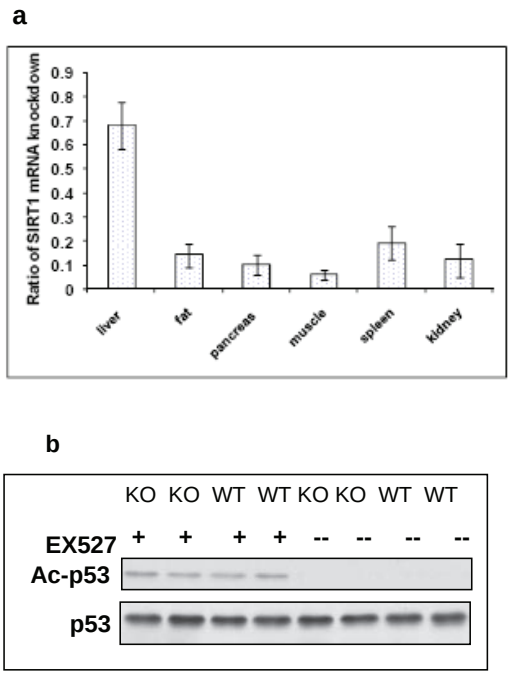

Figure S4 (a) Treatments of Nicotinamide, EX527 and ASO-Sirt1 did not affect liver function of mice. Alanine aminotransferase (ALT) is the most sensitive marker for liver cell damage. Sera were collected from animals treated with nicotinamide (150mg kg^{-1}), EX527 (10mg kg^{-1}) or ASO-Sirt1 (10mg kg^{-1} x5). **(b)** The ratios of *sirt1* mRNA knockdown in mouse different tissues. SIRT1 ASO or control ASO was administered intraperitoneally to STAT3-ff and STAT3LKO mice for 5 times with 50mg kg^{-1} within 2 weeks. RNAs were extracted and subjected to Q-RT-PCR to measure the levels of *sirt1* mRNA. Ratios of the *sirt1* mRNA knockdown = ratio of mRNA of sirt1 ASO/ Control ASO. (n=4). **(c)** Acetylated-P53 was increased by EX527 in the livers of STAT3f/f and STAT3LKO mice. Liver tissues were collected from the STAT3f/f and STAT3LKO mice (n=4) which were fasted overnight and injected with EX527 or vehicle (*i.p.* 10mg kg^{-1}). Same protocol was performed as one used in Fig.1c and Fig. 4d. The levels of Acetylated-P53 (anti-K379-P53, Cell Signaling) were measured by Western blot.

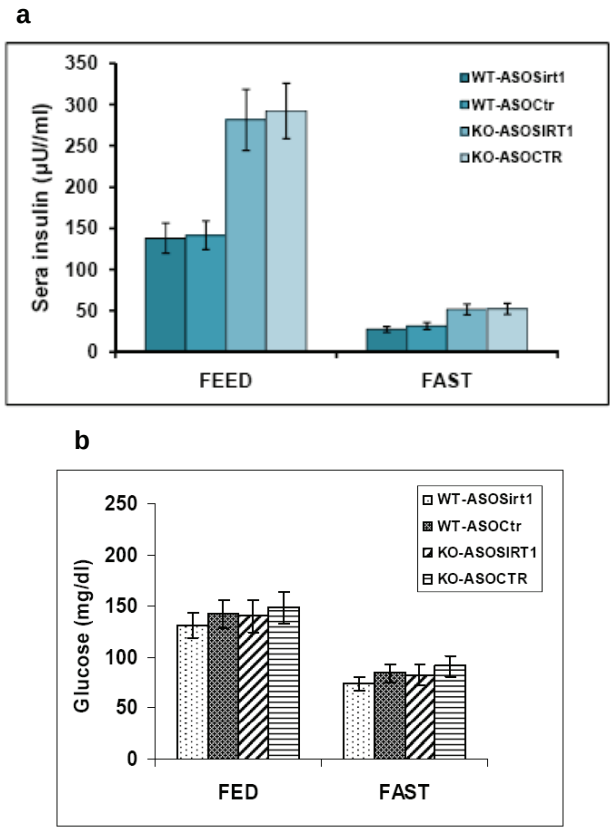

Figure S5 (a) SirT1-ASO did not affect blood insulin in mice treated with SirT1-ASO1 and fed with high fat diet. This experiment was performed at the same set as Fig. 4j. STAT3 f/f (wildtype) and STAT3 LKO mice (n=7) fed with high fat diet for 2.5 weeks days. SirT1-ASO or Control-ASO was administered intraperitoneally for 5 times at a dose of 10mg kg^{-1} within two weeks. The sera insulin was measured at feeding and overnight fasting condition. **b)** STAT3 LKO mildly impaired SirT1 knockdown induced glucose reduction in mice fed with normal chow food. This experiment was performed at the same time as Fig. 4j. STAT3 f/f (wildtype) and STAT3 LKO mice (n=7) fed with normal chow diet. SirT1-ASO or Control-ASO was administered intraperitoneally for 5 times at a dose of 10mg kg^{-1} within two weeks. The levels of plasma glucose were measured at feeding and overnight fasting condition.

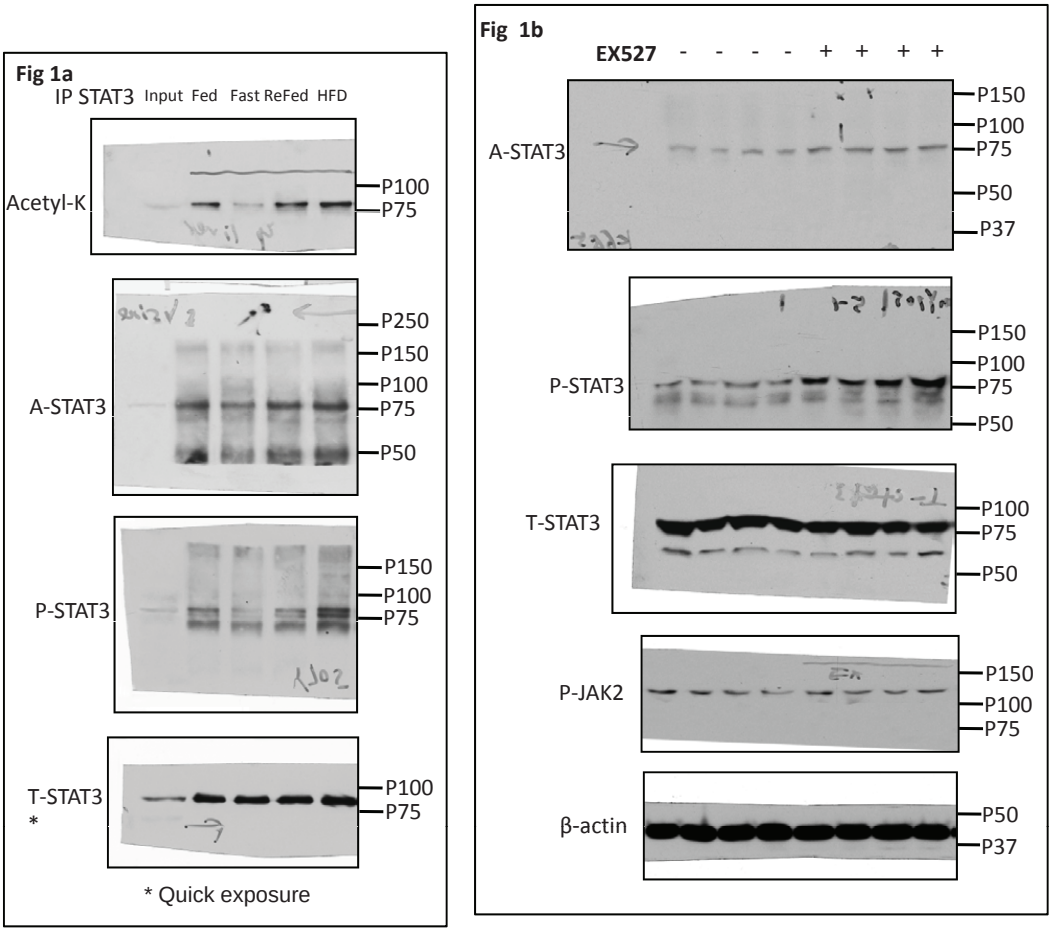

Figure S6 Full scans of western blot data

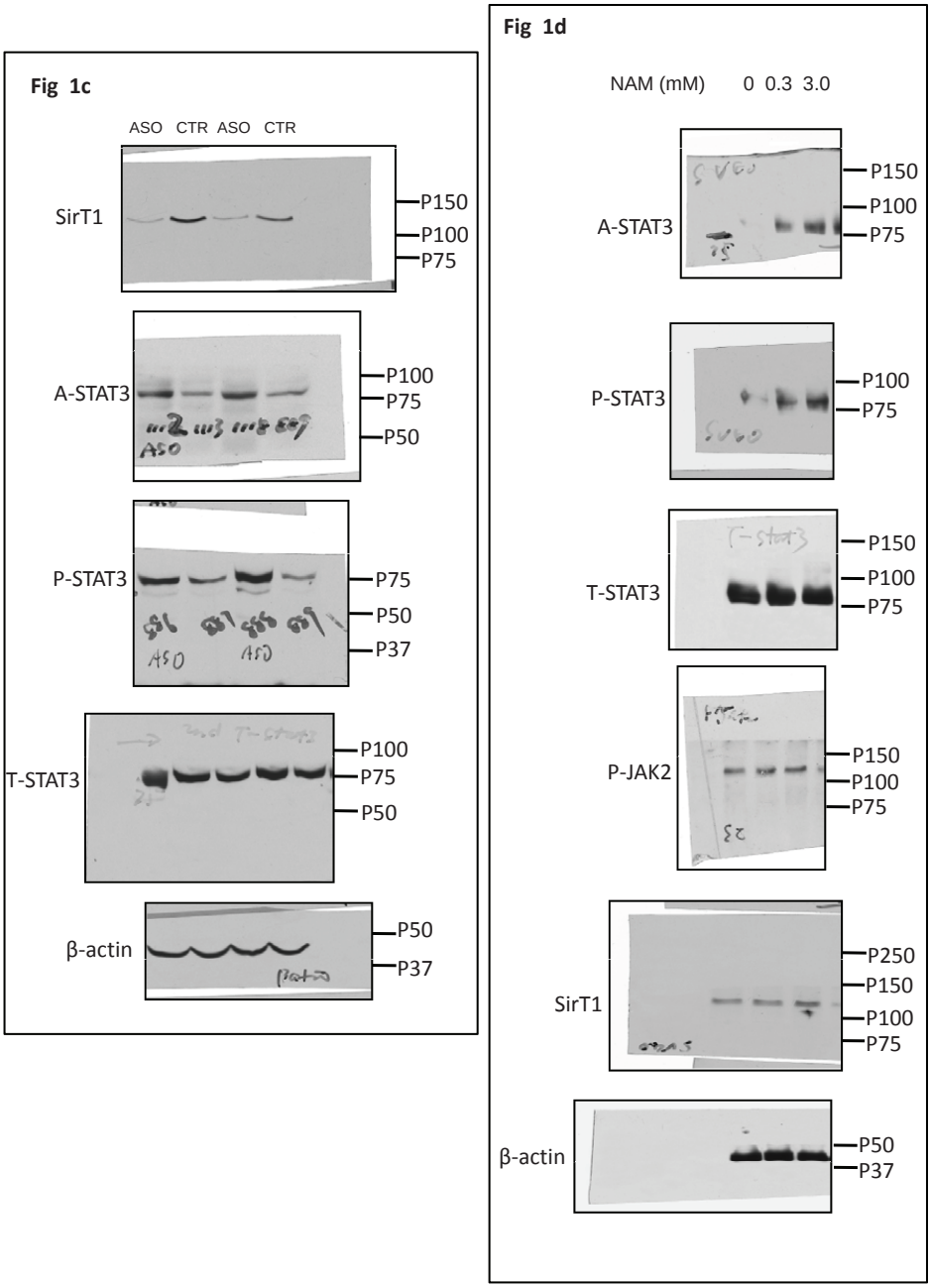

Figure S6 continued

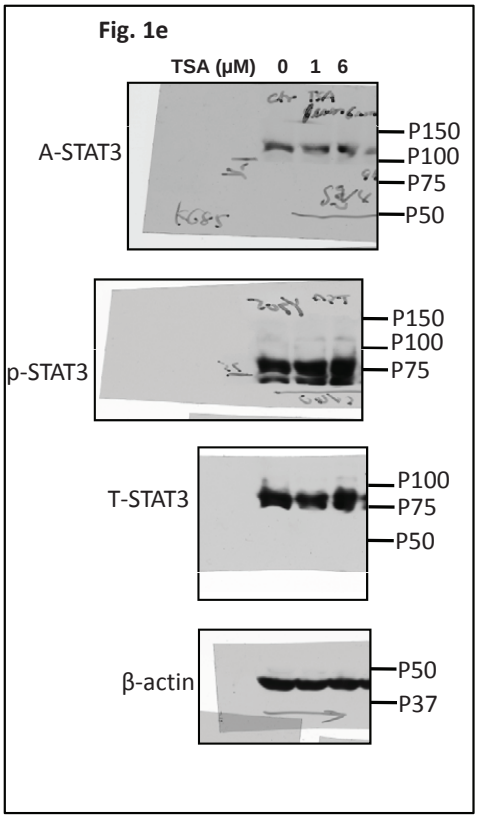

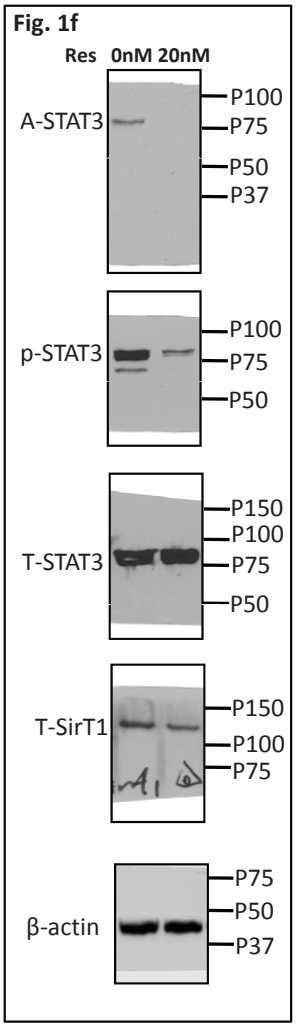

Figure S6 continued

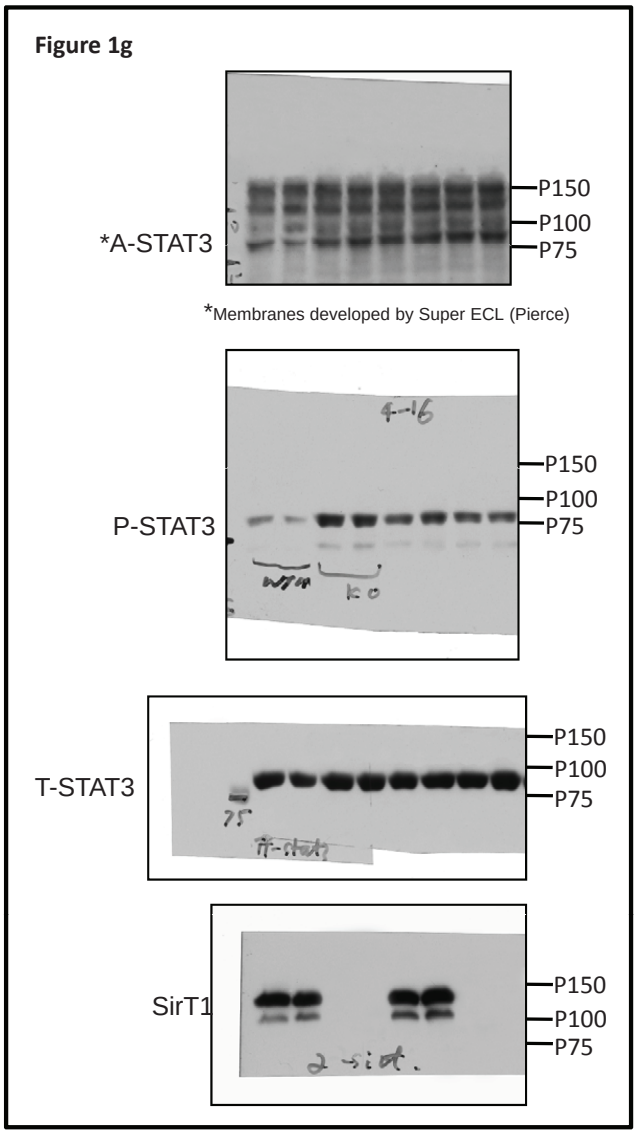

Figure S6 continued

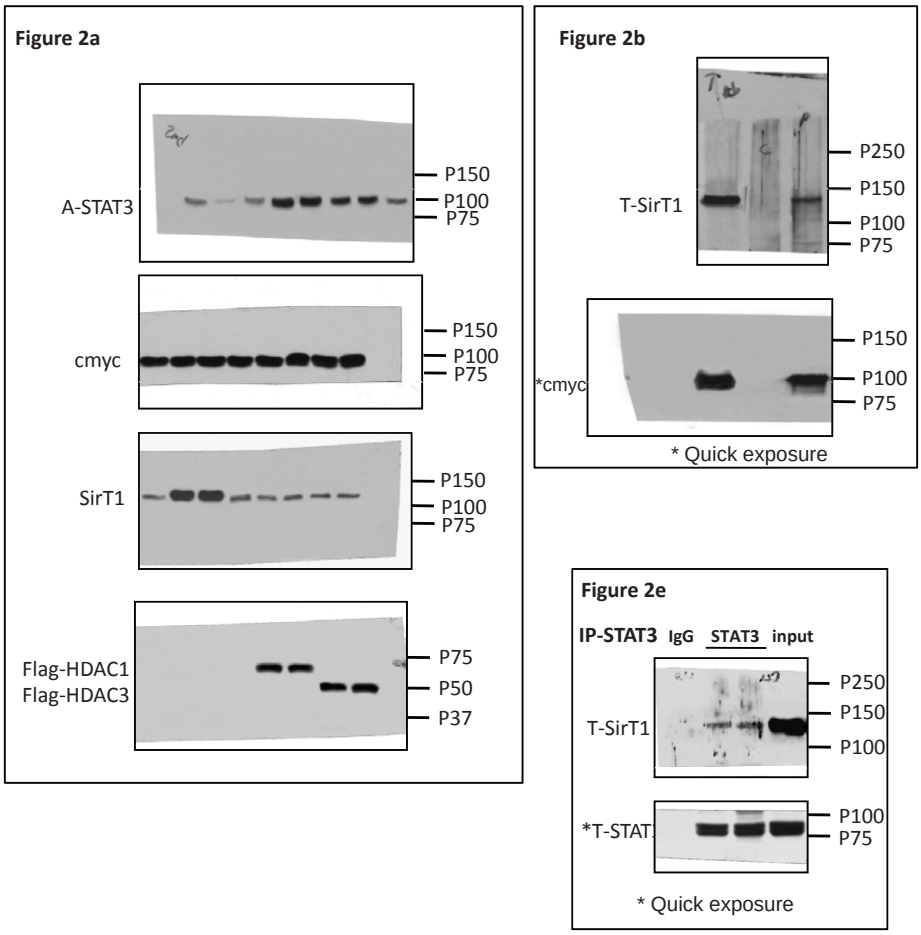

Figure S6 continued

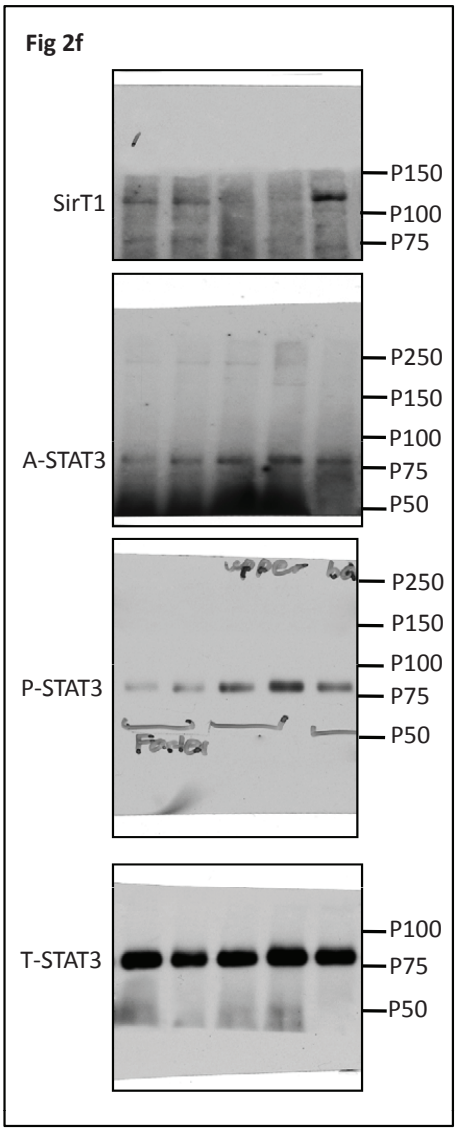

Figure S6 continued

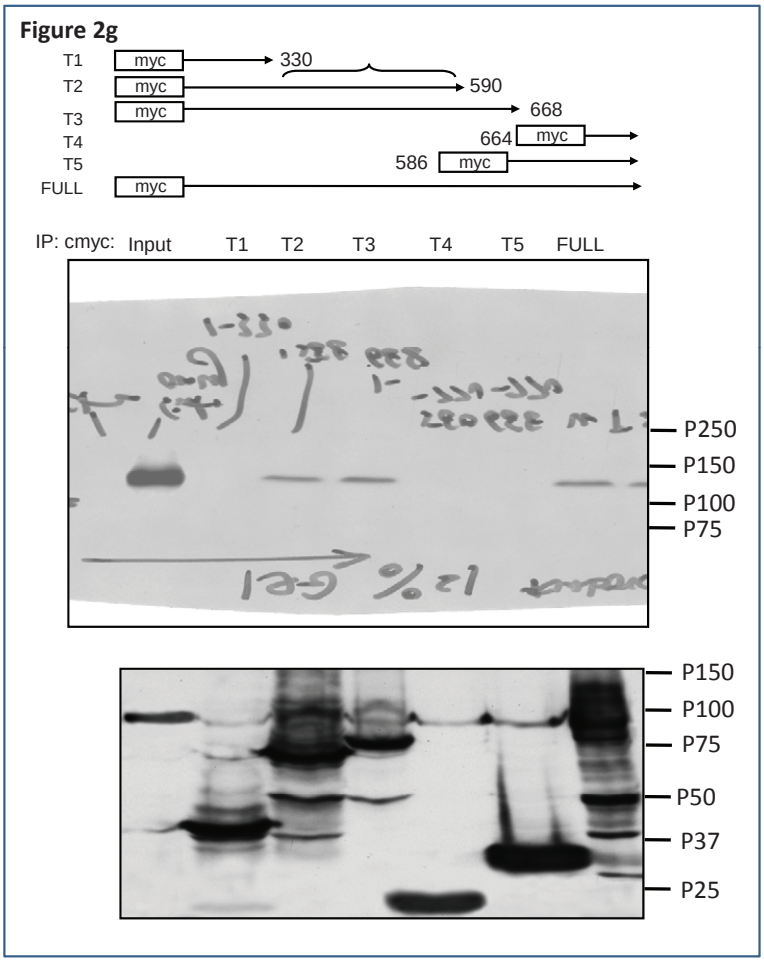

Figure S6 continued

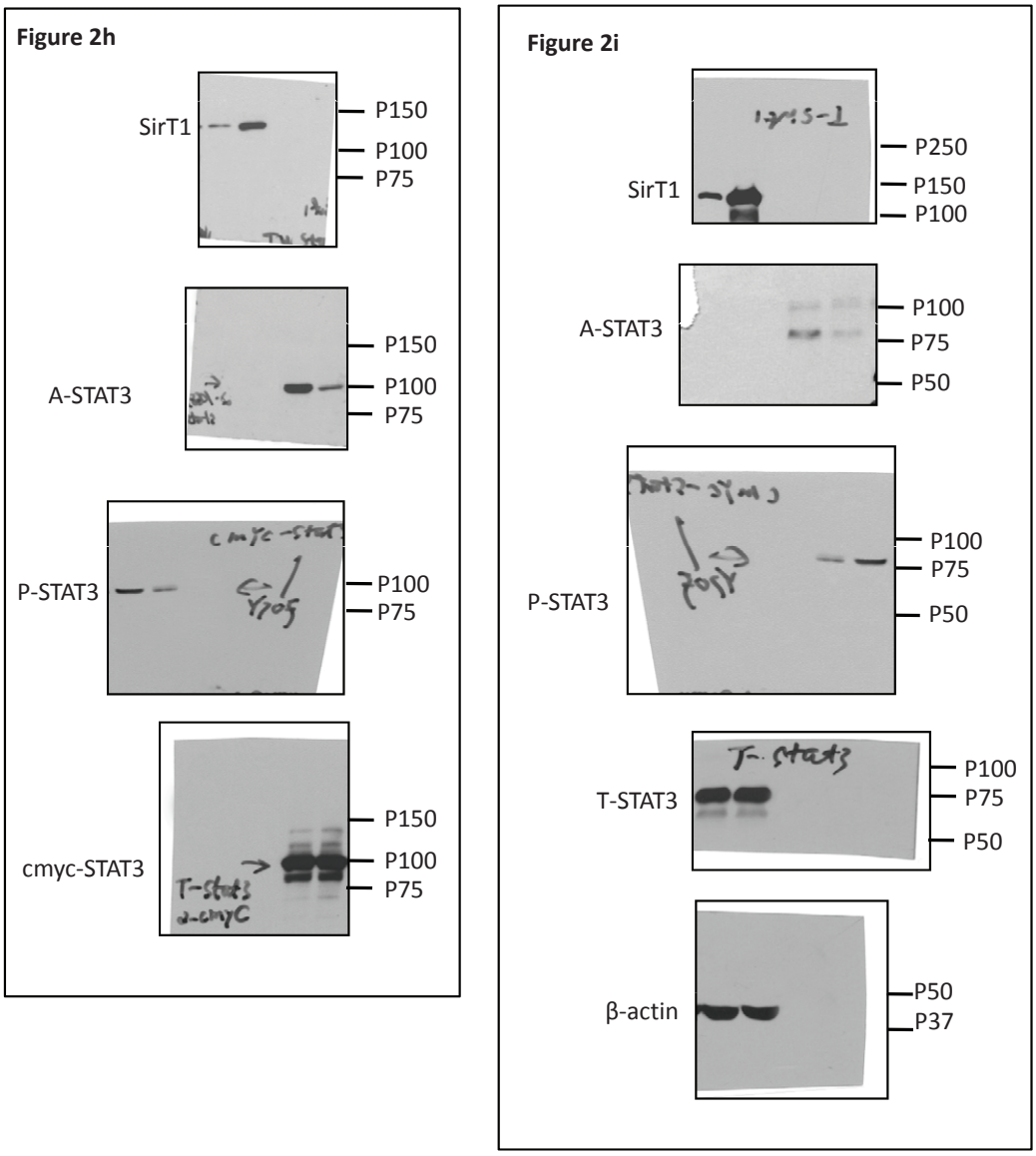

Figure S6 continued

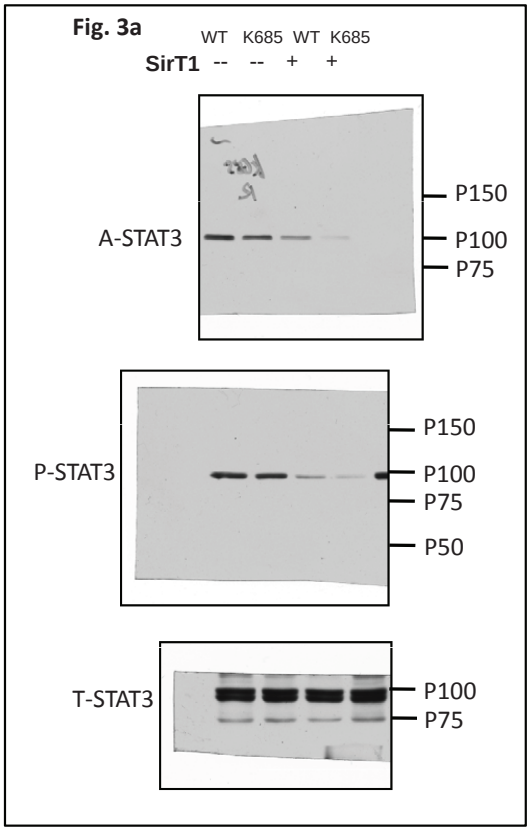

Figure S6 continued

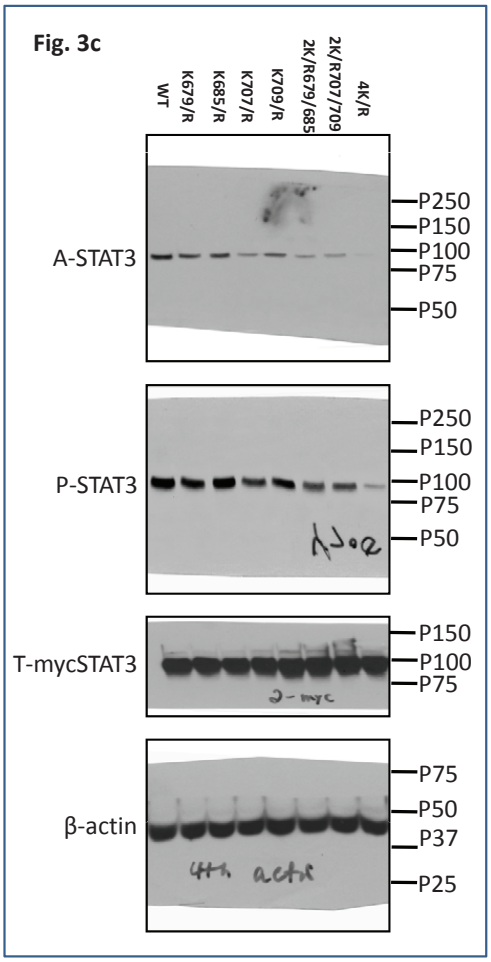

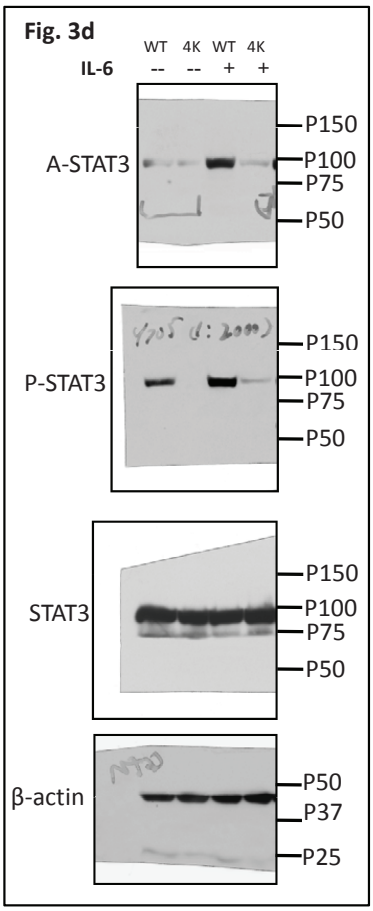

Figure S6 continued

Primer	Sequence	Annealing Temperature
F-18S	AGTCCCTGCCCTTTGTACACA	61 °C
R-18S	CGATCCGAGGGCCTCACTA	
F-tubulin	**TAGCAGAGATCACCAATGCC**	**61 °C**
R-tubulin	**GGCAGCAAGCCATGTATTTA**	
F-Cytochromsome-C	GGAGGCAAGCATAAGACTGG	61 °C
R-Cytochromsome-C	TCCATCAGGGTATCCTCTCC	
F-GK	**ACTGCGGAGATGCTCTTTGA**	**61 °C**
R-GK	**TGCCCTTGTCTATGTCTTCG**	
F-PGC1	AACAATGAGCCTGCGAACAT	61 °C
R-PGC1	CACGGCTCCATCTGTCAGT	
F-Fbpase	**GCTCTGCACCGCGATCA**	**61 °C**
R-Fbpase	**ACATTGGTTGAGCCAGCGATA**	
F-G6pase	GTGTTTGAACGTCATCTTGTG	58 °C
R-G6pase	TTAGTAGCAGGTAGAATCCAA	
F-PEPCK	**GTGGAAGGTCGAATGTGTGG**	**61 °C**
R-PEPCK	**TAAACACCCCCATCGCTAGT**	

Table S1 Primers used in Q-RT-PCR to detect the expression of gluconeogenic genes in wild type and STAT3 liver knockout mice. rRNA 18S and *tubulin* transcripts were used as internal controls in all the experiments. The primers were designed in coding regions which across introns to avoid DNA contamination. F: forward primer; R: reverse primer.

Supplementary Methods

Isolation of Primary hepatocytes. Briefly, the livers of 6-12 weeks old mice were perfused with Hanks' A then Hanks' B medium containing 0.05% collagenase (Boehringer Mannheim Biochemicals, Indianapolis, IN) and 0.8 U ml^{-1} trypsin (Sigma). During the perfusion with Hanks' B medium, the lower abdominal vena cava was intermittently occluded (15 seconds intervals) using a forceps. Livers were then excised, minced, and passed through serial nylon mesh filters, and the resultant cells were washed. The recovered cells were suspended in hepatocyte recovering medium (DMEM with 10 mg L^{-1} glucose, GIBCO), containing 10% fetal calf serum (Invitrogen), 1 ng-ml^{-1} amphotericin B (Sigma), 10 U ml^{-1} penicillin, 50 mg ml^{-1} streptomycin, 10 mg ml^{-1} gentamicin, 1 nM dexamethasone, 1 nM insulin, and plated onto collagen I (rat tail type I, BD Biosceince, Bedford, MA) coated plates or glass coverslips. Cells were incubated at 37°C for experiments.

Virus construction and infection. The STAT3 adenovirus constructs were established using AdEasy Adenoviral vector kit (Stratagene, La Jolla, CA). Briefly, various STAT3 cDNAs, including WT, Y705F, K49-87R, K697-685-707-709R etc., were cloned into the adenovirus vector, pAd-shuttle. The pShuttle-STAT3s was recombined with backbone pAdEasy-1 in BJ5183 bacteria. Adenovirus generation, amplification, and titration were done according to the guidelines of the manufacturer. PGC-1 adenovirus was a gift from Dr. Puigserver. Viral particles were purified by cesium chloride density gradient centrifugation.

Western Blot. The liver, white adipose and spleen were collected from STAT3-LKO, $STAT3^{f/f}$ and wild type C57BL/6J male mice, washed briefly with PBS and then

homogenized by sonication in RIPA lysis buffer. The homogenates were centrifuged at 4 °C at 10,000 rpm for 15 min. The supernatant was placed in a fresh tube and the protein concentration assayed by a Branford kit (Bio-Rad). Western Blots were done as previously described [37]. Rabbit Anti-phospho-(Y705)-STAT3, rabbit anti-phospho-Y1007/Y1008-JAK2, rabbit anti-JAK2, rabbit anti-Acetylated lysine, rabbit anti-acetylated 685 lysine of STAT3 antibodies were from Cell Signaling (Danvers, MA); Rabbit anti-STAT3 and mouse anti-c-myc monoclonal antibodies were from Santa Cruz (Santa Cruz, CA); rabbit anti-mouse and mouse anti-mouse monoclonal SirT1 antibody was from Upstate Biotechnology. Anti–rabbit or mouse antibodies conjugated with horseradish peroxidase (Jackson Immuno Research Labs, West Grove, PA) were used as secondary antibodies. The Western blots were visualized using chemiluminescent substrate (Pierce Chemical, Rockford, IL) The relative intensities of the signals were quantified by densitometry using image analysis software (NIH Image J).

Luciferase assays. 2-3x10^5 A2780 or 293T cells were seeded in 24-well plates in triplets (n = 3) and cotransfected with a plasmids containing STAT3 or its mutants and the luciferase reporter p4x IRF-Luc [13] or APRE−luciferase reporter by using Lipofectimane 2000 (Invitrogen). pRL-TK *Renilla* luciferase (promega, Madison, WI) reporter was used as an internal control for transfection efficiency. 24 h after transfection, cell extracts were prepared and measured for luciferase activity (Promega) using a Sirius luminometer (Berthold Technologies, Oak Ridge, TN). Protein concentrations were determined using Bio-Rad Protein Assay reagents (SmartSpectm Plus Spectrophotometer, Bio-Rad).

Chromatin Immunoprecipitation (ChIP) Assays. ChIP assays were performed using the Chromatin Immunoprecipitation (ChIP) Assay Kit and protocols (Upstate

Biotechnology, Charlottesville, VA). Briefly, 2x106 STAT3-KO-myc-WT, 4KR and Y705 cells were treated by 40 ng ml^{-1} of IL-6 for 2.5 h and then were cross-linked with 1% formaldehyde (10 min, RT), washed and pelleted by centrifugation and resuspended in 200 µl SDS lysis buffer supplemented with protease inhibitors (as described in the kit protocol). Cell lysates were sonicated to shear DNA to <0.6 kb (verified by agarose gel analysis). Sonicated lysates were centrifuged to remove debris, diluted 1:10 in dilution buffer and used for IP with desired antibodies. After immunoprecipitation, pellets were washed with 1 ml Low Salt Immune Complex Wash Buffer, High Salt Immune Complex Wash Buffer and LiCl Immune Complex Wash Buffer and TE buffer. Bead precipitates were eluted twice with fresh elution buffer (1% SDS, 0.1 M NaHCO3) and eluates were pooled and heated at 65°C for 8 h to reverse protein-DNA crosslinks. DNA was eluted into TE buffer. Q-PCR analysis (QuantiFast SYBR Green PCR kit, Qiagen, Valencia CA) was performed with 2 µl of the 70 µl DNA preparation plus the following primers: PEPCK1 (region -3728 to -3598 of the mouse PEPCK1 (NM_011044) promoter containing STAT3 binding sites), 5′- ggtttgaagtgggtgaatcc-3′ (forward primer), 5′ ggacagccagggctatacaa 3′ (reverse primer); P200 (region -226 to -24 of the mouse C/EBPδ promoter containing STAT3 binding sites, as STAT3 positive control primers), reference, 5′-GCGTGTCGGGGCCAAATCCA-3′ (forward primer), 5′TTTCTAGCCCCAGCTGACGCGC-3′ (reverse primer); P1.8k (region -1856 to -1676 of the promoter) as control, 5′-TGCTTCTATGGCATCCAG-3′ (forward primer), 5′-GAGGGGCTGTGGAATATT-3′ (reverse primer). ChIP assays performed using mouse anti-cmyc Monoclonal Antibody (sc-40, Santa Cruz), a normal mouse IgG as negative

control the blocked Protein G beads from Upstate Biotechnology. All ChIP assays were performed three times with representative results presented[38].

Anexo A-3. Nesfatin-1-Regulated Oxytocinergic Signaling in the Paraventricular Nucleus Causes Anorexia through a Leptin-Independent Melanocortin Pathway

Artigo publicado no periódico *Cell Metabolism*.

Cell Metabolism
Article

Nesfatin-1-Regulated Oxytocinergic Signaling in the Paraventricular Nucleus Causes Anorexia through a Leptin-Independent Melanocortin Pathway

Yuko Maejima,[1,9] Udval Sedbazar,[1,9] Shigetomo Suyama,[1] Daisuke Kohno,[1] Tatsushi Onaka,[2] Eisuke Takano,[1] Natsu Yoshida,[1] Masato Koike,[3] Yasuo Uchiyama,[3] Ken Fujiwara,[4] Takashi Yashiro,[4] Tamas L. Horvath,[5] Marcelo O. Dietrich,[5,6] Shigeyasu Tanaka,[7] Katsuya Dezaki,[1] Shinsuke Oh-I,[8] Koushi Hashimoto,[8] Hiroyuki Shimizu,[8] Masanori Nakata,[1] Masatomo Mori,[8] and Toshihiko Yada[1,*]

[1]Division of Integrative Physiology
[2]Division of Brain and Neurophysiology
Department of Physiology, Jichi Medical University School of Medicine, Shimotsuke, Tochigi 329-0498, Japan
[3]Department of Cell Biology and Neurosciences, Juntendo University Graduate School of Medicine, Bunkyo-ku, Tokyo 113-8421, Japan
[4]Division of Histology, Department of Anatomy, Jichi Medical University School of Medicine, Shimotsuke, Tochigi 329-0498, Japan
[5]Program on Cell and Neurobiology of Energy Metabolism, Section of Comparative Medicine, Yale University School of Medicine, New Haven, CT 06520, USA
[6]Programa de Pós-graduação em Bioquímica, Department of Biochemistry, Universidade Federal do Rio Grande do Sul, Porto Alegre RS 90035, Brazil
[7]Department of Biology, Faculty of Science, Shizuoka University, Ohya 836, Shizuoka 422-8529, Japan
[8]Department of Medicine and Molecular Science, Gunma University Graduate School of Medicine, Maebashi, Gunma 371-8511, Japan
[9]These authors contributed equally to this work
*Correspondence: tyada@jichi.ac.jp
DOI 10.1016/j.cmet.2009.09.002

SUMMARY

The hypothalamic paraventricular nucleus (PVN) functions as a center to integrate various neuronal activities for regulating feeding behavior. Nesfatin-1, a recently discovered anorectic molecule, is localized in the PVN. However, the anorectic neural pathway of nesfatin-1 remains unknown. Here we show that central injection of nesfatin-1 activates the PVN and brain stem nucleus tractus solitarius (NTS). In the PVN, nesfatin-1 targets both magnocellular and parvocellular oxytocin neurons and nesfatin-1 neurons themselves and stimulates oxytocin release. Immunoelectron micrographs reveal nesfatin-1 specifically in the secretory vesicles of PVN neurons, and immunoneutralization against endogenous nesfatin-1 suppresses oxytocin release in the PVN, suggesting paracrine/autocrine actions of nesfatin-1. Nesfatin-1-induced anorexia is abolished by an oxytocin receptor antagonist. Moreover, oxytocin terminals are closely associated with and oxytocin activates pro-opiomelanocortin neurons in the NTS. Oxytocin induces melanocortin-dependent anorexia in leptin-resistant Zucker-fatty rats. The present results reveal the nesfatin-1-operative oxytocinergic signaling in the PVN that triggers leptin-independent melanocortin-mediated anorexia.

INTRODUCTION

Obesity and obesity-based metabolic syndrome are the major risk factors for cardiovascular disease (Matsuzawa, 2006). Increasing incidence of obesity and metabolic syndrome has become a serious health problem in the world (Matsuzawa, 2006). Obesity is basically caused by excessive food intake and/or reduced energy expenditure (Schwartz et al., 2000). Food intake is regulated by the feeding-regulating centers in the hypothalamus and brain stem. Peripheral metabolic signals are sensed by the brain stem including the nucleus tractus solitarius (NTS) and by the hypothalamus including the arcuate nucleus (ARC), and the processed information is sent to the hypothalamic paraventricular nucleus (PVN). Inversely, neurons derived from the PVN also extend their information to several brain areas to determine feeding behavior. Thus, the PVN is considered an integrative center for regulation of feeding (Balthasar et al., 2005; Horvath and Bruning, 2006; Morton et al., 2006; Schwartz et al., 2000). The PVN is equipped with neurons containing classical anorectic neuropeptides, corticotropin-releasing hormone (CRH), oxytocin (Oxt), and thyrotropin-releasing hormone (TRH). However, none of these neurons has been adequately qualified to account for the pivotal anorectic function of the PVN, in clear contrast to the ARC, where the neuron subset containing orexigenic neuropeptide Y (NPY) and agouti-related peptide (AgRP) and that containing anorectic pro-opiomelanocortin (POMC) and cocaine- and amphetamine-regulated transcript (CART) well explain the feeding and metabolic functions of this nucleus (Morton et al., 2006; Schwartz et al., 2000).

Nesfatin-1 is a recently discovered anorectic peptide processed from nesfatin or nucleobindin2 (NUCB2) (Oh-I et al., 2006). Studies of injection of nesfatin-1 and NUCB2 antisense RNA in rats indicated that nesfatin-1 can serve as both pharmacologic and physiologic regulator of feeding and body weight (Oh-I et al., 2006). However, the neural pathway for the anorectic action of nesfatin-1 remains to be clarified. Nesfatin-1 is localized in the hypothalamic PVN, ARC, lateral hypothalamic area (LHA), and supraoptic nucleus (SON) and in the brain stem

NTS, the areas involved in the regulation of feeding (Oh-I et al., 2006). Moreover, starvation decreases both NUCB2 mRNA and nesfatin-1 peptide levels specifically in the PVN (Oh-I et al., 2006), and refeeding induces c-Fos expression in nesfatin-1-containing neurons in the PVN (Kohno et al., 2008). These observations suggest that the nesfatin-1 in the PVN could be implicated in the physiological regulation of food intake.

Nesfatin-1 in the PVN colocalizes most extensively with Oxt (Brailoiu et al., 2007; Foo et al., 2008; Kohno et al., 2008). To date, several functions of Oxt have been established or proposed. The PVN magnocellular Oxt neurons give rise to axons to the posterior pituitary gland and release Oxt into circulation. Peripheral Oxt stimulates uterine smooth muscle contraction and milk ejection (Kiss and Mikkelsen, 2005). Oxt is also thought to function in the central nervous system. Oxt is related to maternal nurturing and social attachment (Donaldson and Young, 2008; Neumann, 2008). Furthermore, several lines of evidence have implicated Oxt in the regulation of feeding and energy expenditure (Kublaoui et al., 2008; Leng et al., 2008). Animals deficient in Oxt gene or genes related to the differentiation of Oxt neurons show hyperphagia and obesity (Kublaoui et al., 2008; Takayanagi et al., 2008). Patients with Prader-Willi syndrome, a human genetic disorder characterized with severe obesity and hyperphagia, display reduction in Oxt neurons (Swaab et al., 1995) and plasma Oxt levels (Stock et al., 1989). Central administration of Oxt and an agonist for Oxt receptor decrease food intake (Arletti et al., 1989). Both centrally projecting parvocellular Oxt neurons of the PVN (Gimpl and Fahrenholz, 2001) and dendritic release of Oxt from magnocellular neurons (Ludwig and Leng, 2006) play a role in regulating food intake (Blevins et al., 2003; Douglas et al., 2007; Olson et al., 1991). The PVN Oxt is upregulated/depressed by feeding/fasting (Tung et al., 2008). Taken together, Oxt is considered one of the important regulators of feeding and metabolism. However, the neural pathways upstream and downstream of the PVN Oxt neurons implicated in feeding remain unclear, which hampers the full establishment of this peptide as a feeding regulator. In line with this evidence, we hypothesized that nesfatin-1 could regulate and cooperate with Oxt neurons in the PVN to evoke an anorectic signaling pathway.

It is particularly of interest to note that nesfatin-1 inhibits food intake in Zucker-fatty rats in which leptin function is impaired due to mutation of its receptor (Oh-I et al., 2006). On the other hand, the satiety effect of nesfatin-1 is blocked by an antagonist for melanocortin receptors, MC3/4R. These findings suggest that nesfatin-1 suppresses feeding via leptin-independent melanocortin signaling (Oh-I et al., 2006; Shimizu et al., 2007). However, underlying neural mechanisms absolutely remain unknown.

This study aimed to explore whether the PVN Oxt neuron is targeted by nesfatin-1 and, if so, how nesfatin-1 controls Oxt neurons in the PVN, whether the nesfatin-1 to Oxt pathway drives melanocortin signaling, and whether it can operate under leptin-resistant conditions.

RESULTS

Third Ventricle Injection of Nesfatin-1 Induces c-Fos Expression in the PVN and NTS

Third ventricle (3V) injection of nesfatin-1 induced significant expression of c-Fos in the PVN and NTS, as compared to 3V injection of vehicle in control experiments (Figures 1A–1E). In contrast, nesfatin-1 did not significantly induce c-Fos expression in the SON, LHA, ARC, dorsomedial hypothalamus (DMH), or ventromedial hypothalamus (VMH) (Figure 1E), though a rising tendency was observed in the SON, LHA, and DMH. The selective c-Fos induction in the PVN and NTS by nesfatin-1 indicates possible involvement of these nuclei in anorectic signaling for nesfatin-1. Nesfatin-1 injection through a cannula placed focally into the PVN significantly decreased cumulative food intake at 1 and 3 hr (Figure 1F). These results indicate that at least one of the primary effector sites for nesfatin-1 is the PVN, which might be connected to the NTS. This notion is supported by the fact that PVN neurons directly project to the NTS (McCann and Rogers, 1990).

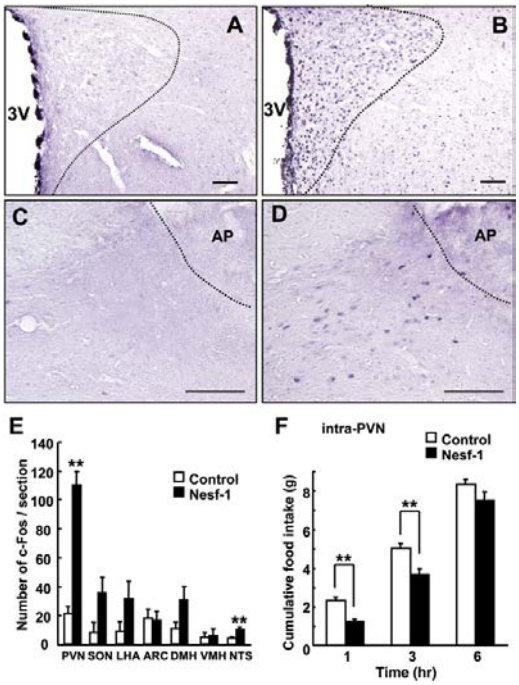

Figure 1. Third Ventricle Injection of Nesfatin-1 Induces c-Fos Expression in the PVN and NTS, and Intra-PVN Injection of Nesfatin-1 Inhibits Feeding

(A–D) c-Fos expression in the PVN (A and B) and NTS (C and D) at 2 hr after 3V injection of 5 μl vehicle as a control (A and C) or 100 pmol nesfatin-1 (Nesf-1) (B and D). Scale bars indicate 50 μm. 3V, third ventricle; AP, area postrema.

(E) Number of c-Fos IR neurons in the feeding-related areas of the hypothalamus and NTS after injection of 100 pmol Nesf-1 (filled bars) or 5 μl vehicle (open bars). n = 5 (rats) for Nesf-1 and for control.

(F) Cumulative food intake for 1, 3, and 6 hr after focal injection of 0.5 μl vehicle or Nesf-1 (50 pmol) into PVN. n = 18 for control and 15 for Nesf-1. Bars in (E) and (F) represent mean ± SE; **p < 0.01.

Nesfatin-1 Activates PVN Oxt Neurons

We next explored the target neurons of nesfatin-1 in the PVN. Double-labeling immunohistochemistry revealed that 3V injection of nesfatin-1 induced c-Fos expression in Oxt-immunoreactive

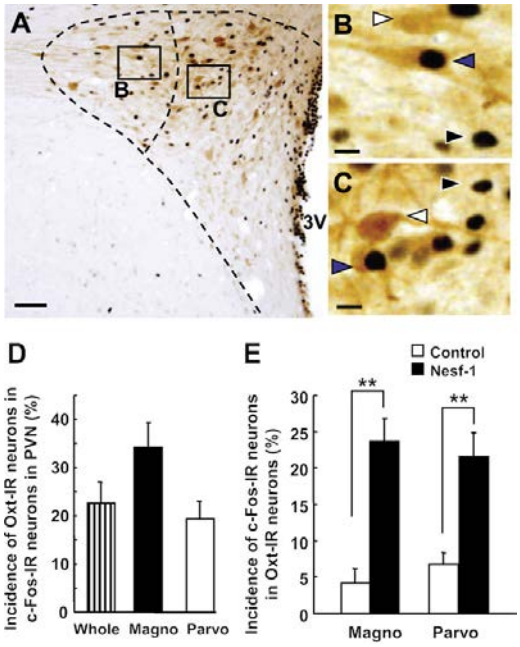

Figure 2. Nesf-1 Induces c-Fos Expression in Oxt Neurons in the PVN

(A) Double immunostaining of c-Fos and Oxt in the PVN after 3V injection of 100 pmol Nesf-1. Scale bar indicates 100 μm.

(B and C) Areas in (A) specified by squares "B" and "C" corresponding to magnocellular and parvocellular areas, respectively, are shown in an expanded scale. Black arrowheads indicate neurons IR to c-Fos only, white arrowheads indicate neurons IR to Oxt only, and blue arrowheads indicate neurons IR to c-Fos and Oxt. Scale bars indicate 10 μm.

(D) Incidence of Oxt-IR neurons among c-Fos-IR neurons in the whole, magnocellular (Magno) and parvocellular (Parvo) areas of the PVN, as expressed by percentage. Each bar represents five rats (n = 5).

(E) Incidence of c-Fos-IR neurons among Oxt-IR neurons in the PVN. n = 6 for control and 5 for Nesf-1. Bars in (D) and (E) represent means ± SE; $^{**}p < 0.01$.

(IR) neurons in the PVN, including those located in the lateral portion where magnocellular neurons are abundant (Figures 2A and 2B) and those in the medial portion where parvocellular neurons are abundant (Figures 2A and 2C). Twenty-three percent of the c-Fos-expressing neurons in the whole area of the PVN were IR to Oxt (Figure 2D), and 34% and 19% of those in the lateral and medial portions, respectively, were IR to Oxt (Figure 2D). Furthermore, the c-Fos expression in the Oxt neurons was significantly elevated by nesfatin-1 in the magnocellular and parvocellular areas of PVN to similar extents (Figure 2E). These results indicate that the PVN Oxt neuron is a major target of nesfatin-1. Nesfatin-1 also tended to increase c-Fos expression in the SON, another area where Oxt neurons are located (Figure 1E).

Nesfatin-1 Directly Targets Oxt and Nesfatin-1 Neurons in the PVN

Though nesfatin-1 influences activities of the hypothalamic neurons (Brailoiu et al., 2007; Price et al., 2008), the PVN neuron species regulated by nesfatin-1 remain to be identified. To determine direct effects of nesfatin-1 on neurochemically defined neurons of the PVN, we used a method of monitoring cytosolic Ca^{2+} concentration ($[Ca^{2+}]_i$) in isolated single neurons followed by immunocytochemical staining with specific antiserum (Yada et al., 1993; Kohno et al., 2007). Administration of nesfatin-1 at 10^{-12}, 10^{-10}, and 10^{-9} M under superfusion conditions increased $[Ca^{2+}]_i$ in single PVN neurons that were subsequently shown to be IR to Oxt (Figure 3A) and nesfatin-1 (Figure 3B). Most of the neurons that responded to nesfatin-1 were Oxt-IR neurons: 10 of 14 (71%), 8 of 10 (80%), and 7 of 10 (70%) with 10^{-12}, 10^{-10}, and 10^{-9} M nesfatin-1, respectively (Figure 3C). These results indicate that nesfatin-1 at pico to nanomolar concentrations directly activates Oxt neurons. In addition, a substantial fraction of nesfatin-1-responsive neurons were unexpectedly found to be nesfatin-1-IR neurons: 44%, 50%, and 73% with 10^{-12}, 10^{-10}, and 10^{-9} M nesfatin-1, respectively (Figure 3C), indicating that the nesfatin-1-IR neuron itself is also targeted by nesfatin-1. The peak amplitudes of $[Ca^{2+}]_i$ responses to nesfatin-1 in two neuron species were comparable, except that 10^{-9} M nesfatin-1 evoked responses with somewhat larger amplitudes in nesfatin-1-IR neurons (Figure 3D). Furthermore, nesfatin-1 increased $[Ca^{2+}]_i$ in the neurons that were IR to both Oxt and nesfatin-1 (Figure 3E). Among 18 nesfatin-1- responsive cells, six cells (33%) were IR to only Oxt (Oxt[+]/nesfatin-1[−]), two (11%) were Oxt(−)/nesfatin-1(+), five (28%) were Oxt(+)/nesfatin-1(+), and five (28%) were Oxt(−)/nesfatin-1(−) (Figure 3F). Furthermore, in Oxt neurons, repeated administration of nesfatin-1 twice increased $[Ca^{2+}]_i$ in a repetitive manner, and the $[Ca^{2+}]_i$ response to the second nesfatin-1 was inhibited by 2 μM nitrendipine, an L-type Ca^{2+} channel blocker (Figure 3G versus Figure 3H) in both the response incidence and amplitude (Figures 3I and 3J), suggesting that L-type channel-mediated Ca^{2+} influx is involved in the action of nesfatin-1 on Oxt neurons.

Nesfatin-1 Neurons Are Adjacent to Oxt Neurons or Contain Oxt in the PVN

To gain further insight into the possible relevance of nesfatin-1 activation of its own neuron, we investigated the identity of nesfatin-1 neurons in the PVN. Double-fluorescence immunohistochemistry demonstrated the presence of the neurons IR to nesfatin, Oxt, and both in the PVN (Figures 4A–4C), confirming previous reports (Brailoiu et al., 2007; Foo et al., 2008; Kohno et al., 2008): 182 of 371 (49%) Oxt-IR neurons expressed nesfatin-1, and 182 of 819 (22%) nesfatin-1-IR neurons expressed Oxt. Confocal imaging more clearly revealed a subset of neurons coexpressing both peptides and that expressing one of the peptides (Figures 4D–4F). The results suggest that some of the nesfatin-1-IR neurons activated by nesfatin-1 are Oxt neurons. In addition, some nesfatin-1-IR neurons are located in close proximity to Oxt-IR and Oxt/nesfatin-1 IR neurons (Figure 4F). This raised a possibility that nesfatin-1 could be released and act on neighboring Oxt neurons. Immunostaining on cryosections of the PVN indicated that the nesfatin-1-IR fluorescence was diffusely distributed to the cytoplasmic regions (see Figure S1 available online). Moreover, as shown in Figure 4G, immunoelectron micrographs revealed that gold particles indicating nesfatin-1 are specifically localized in the secretory vesicles around the Golgi apparatus in the perikarya of neurons in

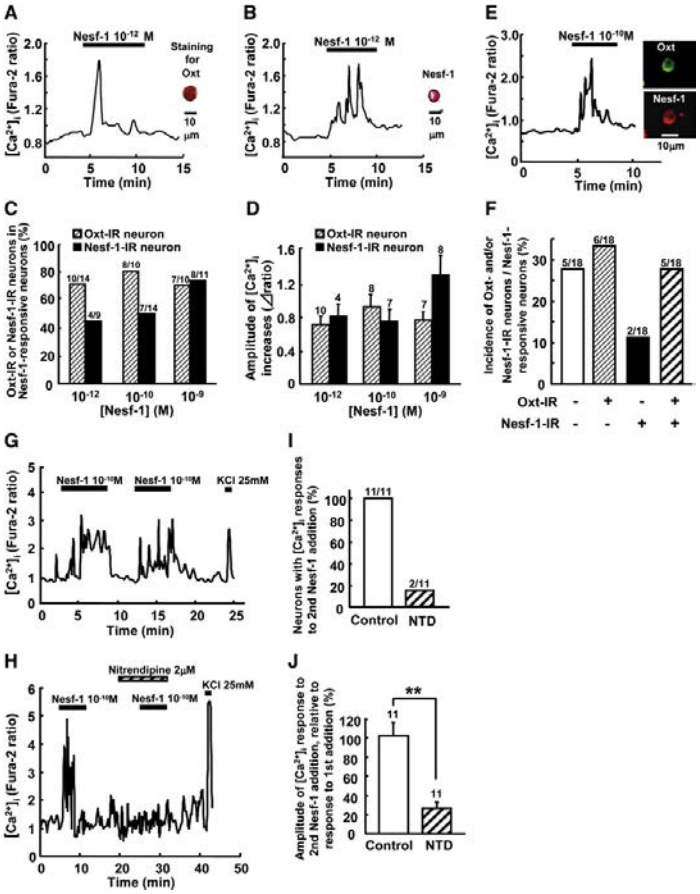

Figure 3. Nesf-1 Increases $[Ca^{2+}]_i$ in Oxt and Nesf-1 Neurons in the PVN, and $[Ca^{2+}]_i$ Increases in Oxt Neurons Are Inhibited by L-Type Ca^{2+} Channel Blocker

(A and B) Nesf-1 at 10^{-12} M increased $[Ca^{2+}]_i$ (left panel) in an isolated PVN neuron that was subsequently shown to be IR to Oxt (A) or Nesf-1 (B) (right panel). Superfusates contain 1 mM glucose. Bars above the tracings indicate the periods of administration of agents. Scale bars indicate 10 μm.

(C) Incidence of Oxt-IR and Nesf-1-IR neurons in the neurons that exhibited $[Ca^{2+}]_i$ responses to Nesf-1, expressed by percentage. Numbers above each bar indicate the number of neurons IR to each peptide over that responsive to Nesf-1.

(D) Amplitudes of $[Ca^{2+}]_i$ increases in Nesf-1-IR and Oxt-IR neurons. The number above each bar indicates the number of Nesf-1-responsive neurons.

(E) Nesf-1 at 10^{-10} M increased $[Ca^{2+}]_i$ (left panel) in an isolated PVN neuron that was subsequently shown to be IR to both Oxt and Nesf-1 (right panel).

(F) Incidence of neurons IR to Oxt, Nesf-1, Oxt+ Nesf-1, or none of them over those responded to Nesf-1. Above each bar, the numbers of specified neurons over Nesf-1-responsive neurons are indicated.

(G) Repetitive additions of Nesf-1 twice induced repeated $[Ca^{2+}]_i$ increases.

(H) Nesf-1-induced $[Ca^{2+}]_i$ increase in Oxt neurons was inhibited by an L-type Ca^{2+} channel blocker, nitrendipine (NTD) (Yoshitomi Pharmaceuticals industries; Osaka, Japan).

(I and J) Incidence (I) and amplitude (J) of $[Ca^{2+}]_i$ responses to the second Nesf-1 addition in the absence and presence of NTD in Nesf-1-responsive cells. Above each bar, the numbers of specified neurons over Nesf-1-responsive neurons are indicated in (I), and the number of Nesf-1-responsive neurons in (J). Bars in (D) and (J) represent means ± SE; $^{**}p < 0.01$.

the mouse PVN. It was confirmed in mice that nesfatin-1 also suppressed food intake (Figure S2).

Endogenous Nesfatin-1 Promotes Oxt Release in the PVN

In line with these histological observations, it was possible that nesfatin-1 in the PVN might influence Oxt neurons via a paracrine/autocrine route, dendritic release, and/or ultrashort-feedback projection, the mechanisms proposed in several brain regions including the PVN (Ludwig and Leng, 2006). PVN slices were used to examine this possibility. First, administration of exogenous nesfatin-1 at 10^{-8} M stimulated the release of Oxt from PVN slices (Figure 4H). Incubation of PVN slices with 50 mM KCl, compared to control 3 mM KCl, also increased Oxt release, and this increased Oxt release was partly and significantly suppressed by the presence of an anti-nesfatin-1 IgG (Figure 4I). The slices in 50 mM KCl solution responded to exogenous nesfatin-1 with further increase in Oxt release (Figure 4J). In addition, 50 mM KCl, nesfatin-1, and the combination failed to elevate the release of lactate dehydrogenase (LDH), a marker of cytotoxicity (Figure S3). These results indicate that slices at high K^+ are in a sound state and able to respond to additional stimulation. Collectively, our results suggest that endogenous nesfatin-1 acts on adjacent Oxt neurons to promote the release of Oxt in the PVN.

Oxt Dependence of Nesfatin-1-Induced Anorexia

Inhibition of cumulative food intake for 6 hr after 3V injection of nesfatin-1 was blocked by H4928, a selective antagonist for Oxt receptor (Figure 4K). This result indicates that nesfatin-1 suppresses feeding via stimulation of Oxt system, which may include Oxt release in the PVN and activation of the PVN Oxt neurons projecting to other brain areas.

Intra-PVN Injection of Nesfatin-1 Suppresses Feeding via Oxt Signaling to the NTS

Since 3V nesfatin-1 induced c-Fos expression selectively in the PVN and NTS (Figure 1), we examined whether the NTS is

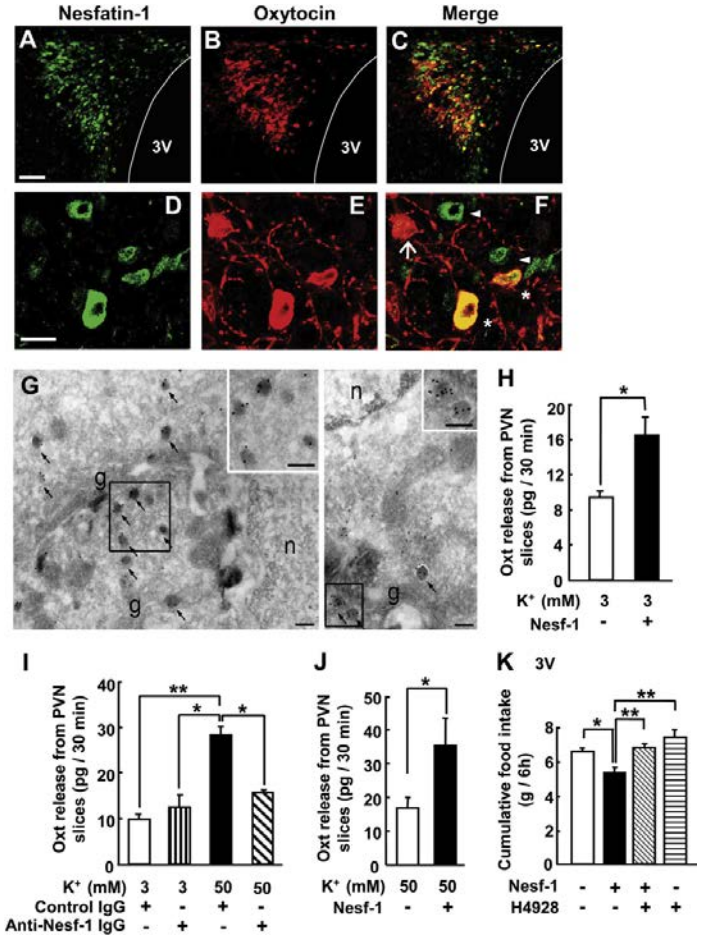

Figure 4. Nesf-1 Is Localized in Secretory Vesicles in the Neurons Located Close to Oxt Neurons in the PVN, Promotes Oxt Release, and Causes Oxt-Dependent Anorexia

(A–F) Fluorescence (A–C) and confocal (D–F) images of the PVN stained for Nesf-1 with Alexa 488 (green) (A and D), for Oxt with Alexa 594 (red) (B and E), and for both by merged images (C and F). Arrowheads indicate Nesf-1-IR neurons, arrows Oxt-IR neurons, and asterisks (*) double-IR neurons. Scale bars represent 100 μm in (A) and 20 μm in (D).

(G) Immunoelectron micrographs show that gold particles indicating Nesf-1 are specifically localized in the secretory vesicles (arrows) around the Golgi apparatus (g). Secretory granules in boxed areas are shown in insets. n, nuclei. The scale bars represent 200 nm.

(H–J) Oxt release from PVN slices following incubation for 30 min with or without 10^{-8} M Nesf-1 in control 3 mM (n = 10) (H) and 50 mM KCl solutions (n = 4–6) (J), and with Nesf-1 IgG (33 × 10^{-8} g/ml) or control IgG in 3 mM and 50 mM KCl solutions (n = 5–11) (I). Data are expressed as the amount of Oxt released per a rat.

(K) 3V injection of Nesf-1 (100 pmol) reduced food intake, and this effect was blocked by prior injection of Oxt receptor antagonist, H4928 (9 nmol) (n = 7–8). Bars in (H)–(K) represent means ± SE; *p < 0.05; **p < 0.01.

activated by the signaling from the PVN. Focal injection of nesfatin-1 into the PVN induced c-Fos expression in the NTS (Figures 5A–5C) and inhibited food intake (Figures 1F and 5D). Moreover, this inhibition of feeding was significantly counteracted by injection of Oxt receptor antagonist H4928 into fourth ventricle (4V), an area that provides an easy and effective access to the NTS (Blevins et al., 2004) (Figure 5D). These results suggest that the PVN oxytocinergic signaling to the NTS underlies the nesfatin-1-induced anorexia.

Oxt Interacts with POMC Neurons in the NTS

Nesfatin-1 decreases food intake in a melanocortin-dependent manner (Oh-I et al., 2006). Our data indicated that nesfatin-1 decreases food intake by activating Oxt neurons. Therefore, a question arises as to whether Oxt stimulates melanocortin signaling. POMC neurons form an essential element of melanocortin pathway and are exclusively localized to the NTS and ARC (Appleyard et al., 2005; Fan et al., 2004; Huo et al., 2006; Perello et al., 2007). Based on the results that nesfatin-1 induced c-Fos expression in the NTS, we examined whether Oxt could regulate POMC neurons in the NTS. Using POMC-green fluorescent protein (GFP) transgenic (Tg) mice, we performed double immunostaining for GFP and Oxt and obtained data suggesting that Oxt terminals contact to POMC neurons in the NTS (Figure 6A). Furthermore, $[Ca^{2+}]_i$ measurements in single neurons isolated from the NTS combined with immunostaining indicated that Oxt evoked $[Ca^{2+}]_i$ increases in 7 of 18 POMC-IR neurons from the NTS (39%) (Figures 6B and 6D), while it had no effect on $[Ca^{2+}]_i$ in the rest of high K^+-responsive POMC-IR neurons (Figure 6C). Conversely, 7 of 12 Oxt-responsive NTS neurons were POMC-IR neurons (58%) (Figure 6E). These results indicate that Oxt preferentially regulates POMC neurons in the NTS. The amplitude of Oxt-induced $[Ca^{2+}]_i$ increases was markedly reduced by H4928 (Figures 6F and 6G), indicating that the Oxt receptor mediates the responses. Furthermore, repeated administration of Oxt twice increased $[Ca^{2+}]_i$ in POMC neurons in a repetitive manner, and the $[Ca^{2+}]_i$ response to the second Oxt was suppressed by nitrendipine and by thapsigargin, an inhibitor of the endoplasmic reticulum (ER) Ca^{2+} pumps, in both the response incidence and amplitude (Figures S4A–S4E), suggesting that L-type channel and the ER Ca^{2+} release are involved in the action

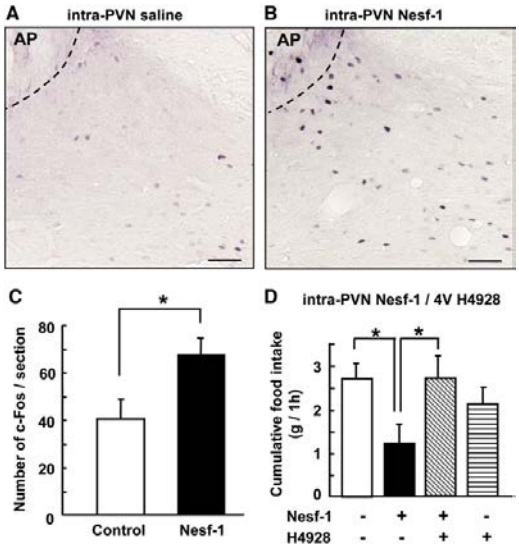

Figure 5. Intra-PVN Nesf-1 Induces c-Fos Expression in the NTS and Anorexia that Is Blocked by 4V Injection of Oxt Receptor Antagonist

(A–C) c-Fos expression in the NTS at 2 hr after intra-PVN injection of 0.5 μl vehicle (A) or Nesf-1 (50 pmol) (B), and number of c-Fos-IR neurons with vehicle (open bar) or Nesf-1 (filled bar) (C). Scale bars indicate 50 μm. n = 6 for control and 7 for Nesf-1.

(D) Intra-PVN injection of Nesf-1 (50 pmol) reduced food intake, and this effect was inhibited by prior injection of Oxt receptor antagonist, H4928, into 4V (9 nmol) (n = 6–8). Bars in (C) and (D) represent means ± SE; *$p < 0.05$.

of Oxt on POMC neurons. Furthermore, 3V injection of Oxt suppressed food intake, and this effect was counteracted by SHU9119, an antagonist for MC3/4R (Figure 6H). Thus, melanocortin-dependent property was observed consistently for Oxt-induced and nesfatin-induced anorexia (Oh-I et al., 2006). SHU9119 by itself had no effect on food intake, consistent with previous reports (Fan et al., 2004; Yosten and Samson, 2009), suggesting that signaling via MC3/4R is not significantly involved in the feeding, at least during early dark cycle, when animals are hungry.

Oxt Activates POMC Neurons and Causes Anorexia in Leptin-Resistant Zucker-Fatty Rats

Nesfatin-1 fails to affect feeding in the presence of a melanocortin antagonist, while it suppresses food intake in Zucker-fatty rats in which leptin receptor is mutated (Takaya et al., 1996), indicating the leptin-independent and melanocortin-dependent anorectic action of nesfatin-1 (Oh-I et al., 2006). If the anorectic action of nesfatin-1 is mediated by Oxt, Oxt-induced anorexia would also be expected to show similar properties. First in vitro, the effects of Oxt and leptin on $[Ca^{2+}]_i$ in single NTS neurons of Zucker-fatty and control lean rats were measured, followed by immunocytochemical identification of POMC neurons. Both Oxt and leptin induced large increases in $[Ca^{2+}]_i$ in the NTS POMC-IR neurons of lean rats (Figure 7A). In Zucker-fatty rats, leptin failed to increase $[Ca^{2+}]_i$ (Figure 7B) or increased $[Ca^{2+}]_i$ with smaller amplitudes in POMC-IR neurons, and the incidence of $[Ca^{2+}]_i$ responses to leptin was remarkably reduced: 9 of 28 (32%) in fatty versus 8 of 12 (67%) in lean rats (Figure 7C). These results show leptin resistance in the NTS POMC neurons of Zucker-fatty rats, consistent with the reports that the receptor binding and effects of leptin on signal transduction, neuropeptide expression, and feeding are reduced but not blunted in Zucker-fatty rats (Yamashita et al., 1997; da Silva et al., 1998; Dryden et al., 1999). In contrast, Oxt increased $[Ca^{2+}]_i$ in POMC-IR neurons of Zucker-fatty rats with amplitudes similar to those observed in lean rats (Figures 7A and 7B), and the incidence of $[Ca^{2+}]_i$ responses was not different between fatty (13 of 28 cells, 46%) and lean rats (5 of 12 cells, 42%) (Figure 7D). These results indicate that Oxt can activate the NTS POMC neurons even under leptin-resistant conditions. Second, in vivo, Oxt injected 3V induced marked reduction in food intake in Zucker-fatty rats, and it was counteracted by SHU9119, while this inhibitor failed to significantly alter food intake under control condition (Figure 7E). These data collectively suggest that Oxt inhibits food intake via melanocortin pathway involving NTS POMC neurons independently of leptin signaling.

DISCUSSION

In the present study, administration of nesfatin-1 into 3V induced c-Fos expression specifically in the PVN and NTS. Intra-PVN injection of nesfatin-1 suppressed food intake and induced c-Fos expression in the NTS, mimicking the effects of 3V nesfatin-1 injection. These results indicate that the PVN is an important effector site for the anorectic nesfatin-1. Furthermore, 3V nesfatin-1 induced c-Fos expression in Oxt-IR neurons in the PVN. Nesfatin-1 directly interacted with Oxt neurons isolated from the PVN and increased $[Ca^{2+}]_i$. The reduction of food intake after 3V or intra-PVN injection of nesfatin-1 was significantly attenuated by 3V or 4V injection of a selective antagonist for Oxt receptor that has widely been used (Olson et al., 1991) and shown to completely prevent anorectic action of centrally administered Oxt (Arletti et al., 1989). Furthermore, injection of Oxt suppresses food intake, and both nesfatin-1 and Oxt induce anorexia in a leptin-independent and melanocortin-dependent manner. These results confirm the proposed anorexigenic function of Oxt (Arletti et al., 1989; Douglas et al., 2007; Olson et al., 1991) and demonstrate that the anorectic action of central nesfatin-1 is mediated principally by PVN Oxt neurons, though possible additional contribution of the SON Oxt neurons cannot be excluded.

Regarding the physiological source of nesfatin-1 that activates the PVN Oxt neurons and inhibits feeding, the PVN nesfatin-1 neurons are the candidate, because their activation is regulated by fasting/refeeding (Kohno et al., 2008; Oh-I et al., 2006). In the present study, the PVN nesfatin-1-IR neurons were frequently found to be in close proximity to both Oxt-IR and nesfatin-1-IR neurons in the PVN (Figures 4A–4F). Immunoelectron micrographs revealed that nesfatin-1 is specifically localized in the secretory vesicles of the PVN neurons (Figures 4G). Moreover, slice experiments indicated that the endogenous nesfatin-1 promotes Oxt release in the PVN (Figure 4I). Furthermore, $[Ca^{2+}]_i$ measurements in single PVN neurons demonstrated

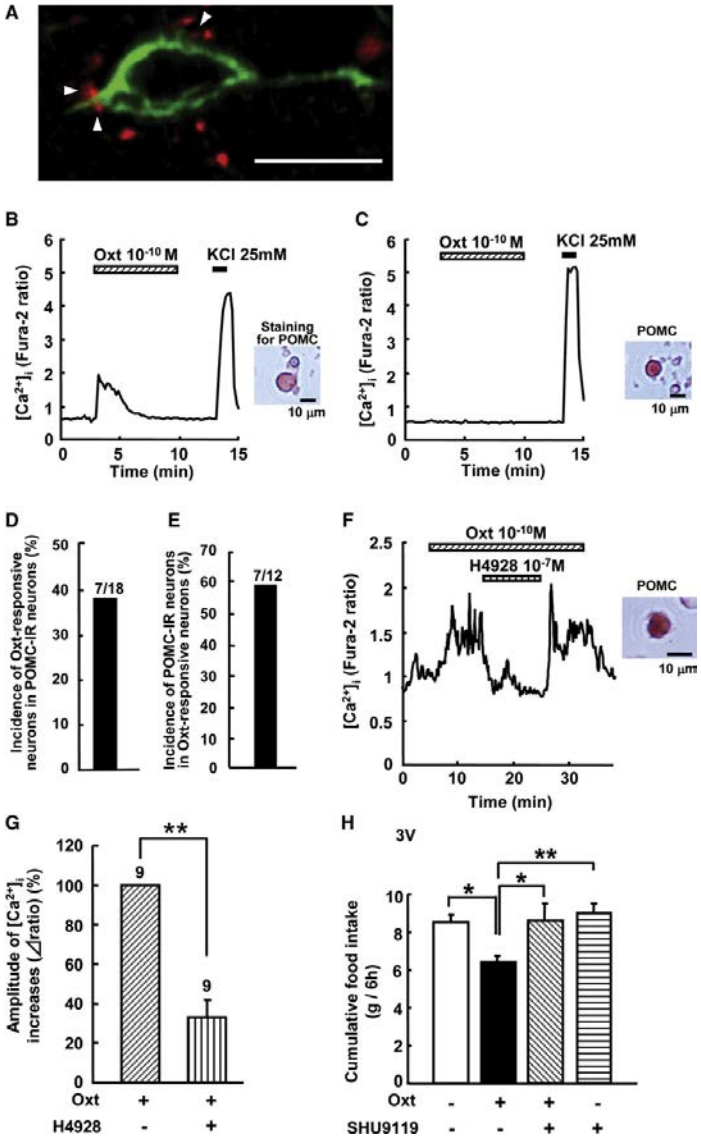

Figure 6. Oxt Neuron Terminals Contact to NTS POMC Neurons, and Oxt Evokes $[Ca^{2+}]_i$ Increases in NTS POMC Neurons and Melanocortin-Dependent Anorexia

(A) Confocal images of double immunofluorescence for POMC with Alexa 488 (green) and for Oxt with Alexa 594 (red) in the NTS prepared from POMC GFP-Tg mice. Oxt-IR terminals contact to POMC-GFP-IR neuron (arrow heads). Scale bar indicates 10 μm.

(B and C) Oxt at 10^{-10} M increased $[Ca^{2+}]_i$ in an isolated NTS neuron that was subsequently shown to be IR to POMC (B), while it had no effect on $[Ca^{2+}]_i$ in another POMC-IR NTS neuron (C).

(D) Incidence of Oxt-responsive neurons among POMC-IR neurons, expressed by percentage.

(E) Incidence of POMC-IR neurons among Oxt-responsive neurons, expressed by percentage. Numbers above each bar in (D) and (E) indicate the number of neurons specified.

(F) Oxt at 10^{-10} M increased $[Ca^{2+}]_i$, and the $[Ca^{2+}]_i$ increase was inhibited by Oxt receptor antagonist H4928 in a reversible manner.

(G) Amplitude of $[Ca^{2+}]_i$ response to Oxt in the presence of H4928 is expressed relatively to that in the control by percentage. n = 9 (neurons).

(H) 3V injection of Oxt (4 nmol) reduced food intake, and this effect was inhibited by prior injection of MC3/4R antagonist, SHU9119 (500 pmol) (n = 7–9). Bars in (G) and (H) represent means ± SE; *$p < 0.05$; **$p < 0.01$. In (B), (C), and (F), superfusates contain 1 mM glucose.

that nesfatin-1 directly interacted with Oxt-IR and nesfatin-1-IR neurons to increase $[Ca^{2+}]_i$ (Figure 3). These results suggest that nesfatin-1 is released and activates neighboring Oxt neurons in the PVN in a paracrine/autocrine manner (Ludwig and Leng, 2006) and/or via an ultrashort-feedback route (Cowley et al., 2001). Alternatively, histological studies have shown the projections from different brain areas to the PVN (Csaki et al., 2000; Sawchenko et al., 1988). Therefore, under in vivo situations, nesfatin-1-containing neurons in several brain regions, including NTS, ARC, and LHA, may send projections to the PVN to regulate Oxt neurons. Our study has identified nesfatin-1 as the upstream regulator of the PVN Oxt neurons implicated in regulation of feeding (Figure S5). Another notable finding is that of the nesfatin-1 activation of its own neuron, which might reflect the nesfatin-1-mediated autoamplification system in the PVN.

It was previously shown that the anorectic effect of central nesfatin-1 is blocked by SHU9119, a melanocortin antagonist (Oh-I et al., 2006). In the present study, the anorectic effect of central nesfatin-1 was blocked by an antagonist for Oxt receptor, and Oxt-induced anorexia was antagonized by SHU9119. These results indicate that the neural information conveyed via nesfatin-1-Oxt axis is linked to the melanocortin pathway. POMC neurons, the essential component of melanocortin pathway, are located exclusively in the brain stem NTS and hypothalamic ARC (Fan et al., 2004; Li et al., 2007; Valassi et al., 2008), where receptors or binding sites for Oxt are expressed (Gimpl and Fahrenholz, 2001; Martins et al., 2005; Quiñones-Jenab et al., 1997). A tight link between the PVN Oxt neurons and the brain stem NTS has been documented: the PVN parvocellular Oxt neurons densely innervate

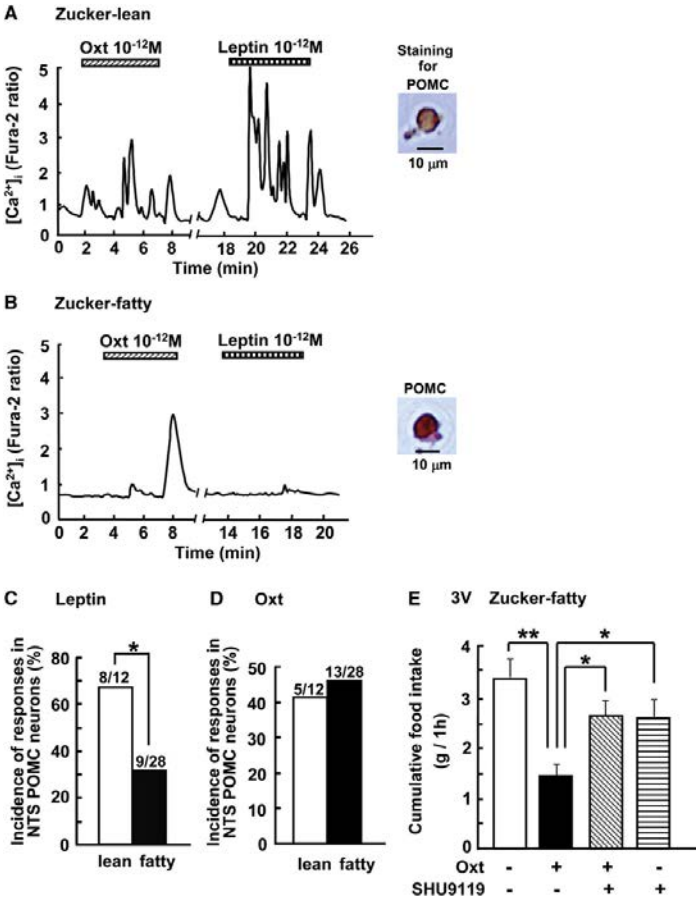

Figure 7. Oxt Induces $[Ca^{2+}]_i$ Increases in NTS POMC Neurons and Melanocortin-Dependent Anorexia in Leptin-Resistant Zucker-Fatty Rats

(A) Leptin and Oxt at 10^{-12} M increased $[Ca^{2+}]_i$ (left panel) in an isolated NTS neuron of Zucker-lean rats, and this neuron was subsequently shown to be IR to POMC (right panel).

(B) Oxt induced a large increase while leptin induced a little increase in $[Ca^{2+}]_i$ (left panel) in an isolated NTS neuron of Zucker-fatty rats that was subsequently shown to be IR to POMC. In (A) and (B), superfusates contain 1 mM glucose.

(C and D) Incidence of $[Ca^{2+}]_i$ responses to leptin (C) and Oxt (D) in NTS POMC neurons in Zucker-lean (open bar) and Zucker-fatty (filled bar) rats, expressed by percentage. Numbers above each bar indicate the numbers of neurons that responded to peptide over POMC-IR neurons.

(E) 3V injection of Oxt (4 nmol) induced anorexia that was attenuated by prior injection of SHU9119 (500 pmol) in Zucker-fatty rats (n = 9–10). Bars represent means ± SE; *p < 0.05; **p < 0.01.

the NTS (Blevins et al., 2004; Rinaman, 1998; Sabatier, 2006; McCann and Rogers, 1990), and oxytocinergic fibers in the NTS originate solely from the PVN neurons, as demonstrated by a retrograde transport of cholera toxin (Rinaman, 1998). In the present study, 3V injection of nesfatin-1 induced c-Fos expression in the medial PVN region that contains the parvocellular Oxt neurons projecting to the NTS. Intra-PVN injection of nesfatin-1 induced c-Fos expression in the NTS and evoked anorexia that was significantly blocked by injection of an Oxt receptor antagonist into 4V, the area that possesses an easy access to the NTS. These data collectively suggest that the nesfatin-1-regulated Oxt neuron of the PVN is functionally, as well as anatomically, linked to the NTS.

The Oxt injection (Arletti et al., 1989) and stimulation of melanocortin system in the brain stem (Adan, 2006) share a common property of inhibiting food consumption by reducing meal size. The current immunohistochemical study using POMC GFP-Tg mice suggested that Oxt terminals contacted to the NTS POMC neurons. Moreover, Oxt directly interacted with and increased $[Ca^{2+}]_i$ in a substantial fraction (39%) of NTS POMC neurons, and POMC neurons constituted a major population (58%) of the NTS Oxt-responsive neurons. Collectively, it is suggested that the NTS POMC neuron is the target for the PVN Oxt neurons, though ARC POMC neurons could additionally be involved. The PVN to NTS neural circuit most likely underlies the Oxt- and melanocortin-dependent anorectic action of nesfatin-1. By now, it has been known that a particular subpopulation of the NTS neurons receive dense Oxt, but not CRH, axon innervations from the PVN (Blevins et al., 2003). However, the upstream regulator of this PVN Oxt to NTS circuit has remained unclear. Our study reveals nesfatin-1 as the upstream regulator of the PVN Oxt-NTS POMC route, whereas the downstream effector site for this route remains to be clarified.

It has been proposed that melanocortin signaling has both leptin-dependent and -independent components (Shimizu et al., 2007). It is well established that POMC neurons in the ARC are regulated by leptin. In contrast, it is in controversy whether POMC neurons in the NTS are insensitive (Huo et al., 2006; Perello et al., 2007) or sensitive (Ellacott et al., 2006; Morton et al., 2006) to leptin. In our study, POMC neurons isolated from the NTS of normal rats responded to leptin with increases in $[Ca^{2+}]_i$, clearly demonstrating that the NTS POMC neurons are sensitive to leptin. Moreover, in Zucker-fatty rats in which the leptin receptor is mutated at one amino acid (Glu269Pro mutation), leptin-induced $[Ca^{2+}]_i$ increases in the NTS POMC neurons were markedly attenuated, in accordance with previous reports of reduced, but not blunted, effects of leptin (Yamashita et al., 1997; da Silva et al., 1998; Dryden et al., 1999), whereas

Oxt-induced $[Ca^{2+}]_i$ increases were intact (Figures 7C and 7D). Thus, Oxt can fully activate the NTS POMC neurons under leptin-resistant conditions. Furthermore, Oxt inhibited feeding in Zucker-fatty rats in a melanocortin-dependent manner (Figure 7E). Thus, the leptin-independent property is now commonly observed for nesfatin-1-induced anorexia (Oh-I et al., 2006) and for Oxt-induced anorexia and $[Ca^{2+}]_i$ increases in NTS POMC neurons. A recent report has shown that PVN Oxt is upregulated by leptin (Tung et al., 2008). It is therefore possible that the activity of the PVN Oxt is attenuated under conditions of leptin resistance and restored by nesfatin-1. We propose that the neural circuit of the nesfatin-1-operated PVN Oxt neurons that signal to the NTS POMC neurons represents an important component of the leptin-independent melanocortin pathway, which has been postulated but mechanistically unsolved (Shimizu et al., 2007).

In conclusion, we propose an anorectic pathway operated by the PVN and associated areas (Figure S5). Centrally administered nesfatin-1 and feeding activate nesfatin-1 and Oxt neurons in the PVN. The nesfatin-1 neurons, once activated, stimulate Oxt neurons in the PVN. These processes drive oxytocinergic signaling to the NTS POMC neuron, as at least one of the targets, thereby causing melanocortin-dependent anorexia. This PVN Oxt neuronal pathway operated by nesfatin-1 and relayed to NTS POMC neurons can function independently of leptin signaling and may provide a therapeutic target for treatment of leptin-resistant obese humans showing hyperphagia. This study also identifies nesfatin-1 as the upstream regulator and melanocortin pathway as the downstream effector of the PVN Oxt neurons, which uncovers the neural pathway for anorexigenic Oxt and thereby greatly substantiates the proposed status of Oxt as a feeding regulator. This study provides Oxt with a general function throughout the life beyond its established roles in the female-specific physiology and maternal nurturing during perinatal and postnatal periods.

EXPERIMENTAL PROCEDURES

Animal Care

Male Wistar rats (200–250 g, Japan SLC, Japan), Zucker-fatty (370–400 g), and Zucker-lean rats (260–290 g) (Clea, Osaka, Japan) were housed on 12 hr dark/light cycle (19:30 lights off) and given standard food CE-2 and water ad libitum. The animal protocols for this study were approved by the Jichi Medical University Institute of Animal Care and Use Committee.

Cannulation, Injection, and Analysis

A 26-gauge guide cannula was placed stereotaxically into 3V (2.5 mm caudal to the bregma in the midline and 8 mm below the surface of the skull), 4V (12.3 mm caudal to the bregma in the midline and 7.4 mm below the surface of the skull), or PVN (1.8 mm caudal to the bregma in the midline, 0.5 mm lateral, and 7.0 mm below the surface of the skull). The injector needle extended 1.2 mm and 0.7 mm below the guide cannula for 3V and intra-PVN injection, respectively, but not for 4V injection. Rats were allowed to recover from the operation for 10 days while they were habituated to handling.

On the day of experiments, food was removed from cages at 15:00. At 19:00, rats received an injection of antagonist, when combined, prior to the injection of nesfatin-1 or Oxt at 19:30. Then food was returned to cages, and cumulative food intake for the following 1, 3, and 6 hr was measured. The agents dissolved in vehicle (sterile saline; 0.9% NaCl) were injected as described below: Oxt receptor antagonist, H4928 ([d$(CH_2)_5^1$, Tyr(Me)^2, Orn^8]-Oxt) (Bachem, Budendorf, Switzerland), 9 nmol/5 μl into 3V or 4V; nesfatin-1 (Yanaihara Institute Co., Shizuoka, Japan), 100 pmol/5 μl into 3V or 50 pmol/0.5 μl into PVN; Oxt (Peptides Institute Inc., Osaka, Japan), 4 nmol/5 μl into 3V; SHU9119 (Phoenix Pharmaceuticals Inc., CA), 500 pmol/5 μl into 3V.

Measurements of c-Fos Expression

Animals were deprived of food at 15:00 and injected with 100 pmol nesfatin-1 (n = 5) or 5 μl saline (n = 5) into 3V or 50 pmol nesfatin-1 (n = 7) or 0.5 μl saline (n = 6) into the PVN at 19:30–20:00. Two hours after injection, rats were transcardially perfused, as described previously (Kohno et al., 2007). Coronal sections at 200 μm interval between −0.92 and −3.3 mm and between −13.3 and −14.3 mm from the bregma were processed for c-Fos and Oxt immunoreactivity as previously reported (Kohno et al., 2008). Anti c-Fos antisera Ab-5 (Calbiochem, CA, dilution 1:40,000) and c-52 (Santa Cruz, CA, 1:5,000) were used for immunohistochemistry post-intra-PVN and -intracerebroventricular (i.c.v) injection of nesfatin-1, respectively. Anti-Oxt antibody (Chemicon, Temecula, CA, 1:5,000) was used for Oxt staining. The number of c-Fos-positive cells per a section was counted for PVN, SON, LHA, ARC, DMH, and VMH between −0.92 and −3.3 or for NTS between −13.3 and −14.3 mm. Three to five sections were averaged for PVN, SON, DMH, VMH, and NTS and six to eight sections for LHA. The magnocellular and parvocellular subdivisions of the PVN were determined by the rat brain map (Paxinos and Watson, 1998).

Immunofluorescence for Nesfatin-1 and Oxt

Double immunofluorescence for nesfatin-1 and Oxt was performed as reported (Kohno et al., 2008). Briefly, sections were incubated with rabbit anti-nesfatin-1 antibody, Ab24 (Oh-I et al., 2006) (1:1,000), or mouse anti-Oxt monoclonal antibody (MAB5296; Chemicon, 1:600) and then with goat Alexa 488 anti-rabbit or Alexa 594 anti-mouse IgG (Molecular Probes, Carlsbad, CA; 1:500). Images were acquired with Olympus BX50 and Olympus Fluoreview FV300-TO confocal laser-scanning microscope.

Immunofluorescence for Oxt and POMC-GFP

Mice expressing GFP under the transcriptional control of POMC genomic sequence (Pinto et al., 2004) were from a mixed background, predominantly C57BL/6 (BW; 22–29 g). Mice were perfused with 4% paraformaldehyde (PFA) in 0.1 M PB containing 15% picric acid. Coronal sections (40 μm) between −7.32 and −7.92 mm from the bregma were incubated with rabbit anti-GFP antiserum (A11122, Molecular Probes, 1:4000) and mouse anti-Oxt monoclonal antibody (1:5000) overnight at 4°C, and then with species-specific Alexa 488 and 594 antibodies for 40 min. Confocal fluorescence images were acquired with Olympus FV1000 confocal laser-scanning microscope.

Measurements of Oxt Release

The PVN area located at −0.92 to −2.12 mm from the bregma was dissected, from which three 400 μm thickness slices were prepared using a vibrating microtome in the buffer composed of (in mM) 229 mannitol, 3 KCl, 26 $NaHCO_3$, 1 H_3PO_4, 0.5 $CaCl_2$, 7 $MgCl_2$, 7 glucose, and 1 kynurate at pH 7.4 with 95% O_2 and 5% CO_2 mixed gas. Six slices from two rats composed one sample.

The slices were first incubated at RT for 1 hr in artificial cerebrospinal fluid (aCSF) composed of 126 NaCl, 3 KCl, 26 $NaHCO_3$, 1 H_3PO_4, 2 $CaCl_2$, 1 $MgSO_4$, and 7 glucose at pH 7.4 with 95% O_2 and 5% CO_2 mixed gas, and then for 30 min at 36°C in 200 μl aCSF under 3 mM and 50 mM K^+ conditions supplemented either with 10^{-8} M nesfatin-1 or with 0.1% anti-nesfatin-1 IgG. KCl substituted for equimolar NaCl in 50 mM K^+ conditions. Oxt in the supernatant was determined by radioimmunoassay (RIA) with specific anti-Oxt antiserum (Higuchi et al., 1985) and [I-125]-labeled Oxt (Perkin Elmer, MA), as described previously (Onaka and Yagi, 1990). Intra- and interassay variations were within 3.6% and 10%, respectively. Oxt RIA kit (Phoenix) was used for experiments with IgG.

Immunoelectron Micrograph

Ultrathin cryosections were prepared as reported elsewhere (Koike et al., 2000; Mori et al., 2008). Briefly, adult male C57BL/6J mice (n = 4) were deeply anesthetized with pentobarbital (25 mg/kg, i.p.) and fixed by cardiac perfusion using 4% PFA buffered with 0.1 M PB (pH 7.2). Brain tissues containing PVN were excised from the mice, further immersed in the same fixative at 4°C for 2 hr, and embedded in 12% gelatin in 0.1 M PB (pH 7.2). Small blocks were rotated in 2.3 M sucrose in PB overnight at 4°C and quickly plunged into liquid nitrogen. Sections approximately 60 nm thick were cut with a Leica UC6/FC6

ultramicrotome and picked up with a 1:1 mixture of 2% methylcellulose and 2.3 M sucrose. The sections were reacted for 1 hr at RT with rabbit anti-nesfatin-1 antiserum (1:10) and then for 1 hr at RT with goat anti-rabbit IgG conjugated with 10 nm colloidal gold particles (GE Healthcare) and examined with a Hitachi H-7100 electron microscope. For control experiments, ultrathin sections were reacted only with the gold particle-conjugated secondary antibody.

Preparation of Single Neurons

Single neurons were prepared from the PVN and NTS as reported elsewhere (Kohno et al., 2007), except that the entire PVN or the portion of NTS at the level of the area postrema (AP) were punched out and that we used 1 mM glucose-containing Krebs-Ringer bicarbonate buffer solution (KRB) composed of (in mM) 129 NaCl, 5.0 $NaHCO_3$, 4.7 KCl, 1.2 KH_2PO_4, 2.0 $CaCl_2$, 1.2 $MgSO_4$, and 10.0 HEPES at pH 7.4.

Measurement of $[Ca^{2+}]_i$, Criteria for Responses, and Subsequent Immunocytochemistry in Single Neurons

We used the method for analyzing species-specified single cells (Yada et al., 1993), which is composed of ratiometric fura-2-$[Ca^{2+}]_i$ imaging and subsequent immunostaining as reported elsewhere (Kohno et al., 2007). Criteria for $[Ca^{2+}]_i$ responses and their inhibition followed previous report (Kohno et al., 2007). In addition, we excluded the cells with gradual elevation of basal $[Ca^{2+}]_i$, large spontaneous fluctuations of $[Ca^{2+}]_i$, and insufficient recovery to the baseline upon washing out agents. Post-$[Ca^{2+}]_i$ immunostaining was performed with rabbit antiserum against Oxt (Chemicon, 1:5000), nesfatin-1 (1:5000), or POMC (Tanaka and Kurosumi, 1992) (1:2000) and, for double immunocytochemistry, with mouse anti-Oxt monoclonal antibody and rabbit anti-nesfatin-1 antiserum (1:5000) followed by species-specific Alexa 488 and 594 antibodies.

Statistical Analysis

One-way ANOVA followed by Bonferroni multiple range tests was used to compare multiple test groups and unpaired Student's t tests for two groups. Incidence of responses was analyzed by χ^2 test.

SUPPLEMENTAL DATA

Supplemental Data include Supplemental Experimental Procedures, five figures, and Supplemental References and can be found with this article online at http://www.cell.com/cell-metabolism/supplemental/S1550-4131(09)00267-8.

ACKNOWLEDGMENTS

We thank Drs. Motoshi Kikuchi and Kotaro Horiguchi at Jichi Medical University for technical assistance. This work was supported by Grant-in-Aid for Scientific Research (B) (18390065, 20390061) from the Japan Society for the Promotion of Science (JSPS) and a grant from the Smoking Research Foundation to T. Yada, Grant-in-Aid for Young Scientists (B) (20790633) from JSPS and Jichi Medical University Young Investigator Award to Y.M., and a National Institutes of Health (NIH) grant (DK-060711) to T.L.H.

Received: March 8, 2009
Revised: July 7, 2009
Accepted: September 15, 2009
Published: November 3, 2009

REFERENCES

Adan, R.A. (2006). The MC4 receptor and control of appetite. Br. J. Pharmacol. *149*, 815–827.

Appleyard, S.M., Bailey, T.W., Doyle, M.W., Jin, Y.H., Smart, J.L., Low, M.J., and Andresen, M.C. (2005). Proopiomelanocortin neurons in nucleus tractus solitarius are activated by visceral afferents: regulation by cholecystokinin and opioids. J. Neurosci. *25*, 3578–3585.

Arletti, R., Benelli, A., and Bertolini, A. (1989). Influence of oxytocin on feeding behavior in the rat. Peptides *10*, 89–93.

Balthasar, L., Dalgaard, T., Lee, C.E., Yu, J., Funahashi, H., Williams, T., Ferreira, M., Tang, V., McGovern, R.A., Kenny, C.D., et al. (2005). Divergence of melanocortin pathways in the control of food intake and energy expenditure. Cell *123*, 493–505.

Blevins, J.E., Eakin, T.J., Murphy, J.A., Schwartz, M.W., and Baskin, D.G. (2003). Oxytocin innervation of caudal brainstem nuclei activated by cholecystokinin. Brain Res. *993*, 30–41.

Blevins, J.E., Schwartz, M.W., and Baskin, D.G. (2004). Evidence that paraventricular nucleus oxytocin neurons link hypothalamic leptin action to caudal brain stem nuclei controlling meal size. Am. J. Physiol. Regul. Integr. Comp. Physiol. *287*, R87–R96.

Brailoiu, G.C., Dun, S.L., Brailoiu, E., Inan, S., Yang, J., Chang, J.K., and Dun, N.J. (2007). Nesfatin-1: distribution and interaction with a G protein-coupled receptor in the rat brain. Endocrinology *148*, 5088–5094.

Cowley, M.A., Smart, J.L., Rubinstein, M., Cerdan, M.G., Diano, S., Horvath, T.L., Cone, R.D., and Low, M.J. (2001). Leptin activates anorexigenic POMC neurons through a neural network in the arcuate nucleus. Nature *411*, 480–484.

Csaki, A.M., Kocsis, K., Halasz, B., and Kiss, J. (2000). Localization of glutamatergic/aspartatergic neurons projecting to the hypothalamic paraventricular nucleus studied by retrograde transport of [3H] D-aspartate autoradiography. Neuroscience *101*, 637–655.

da Silva, B.A., Bjørbaek, C., Uotani, S., and Flier, J.S. (1998). Functional properties of leptin receptor isoforms containing the gln→pro extracellular domain mutation of the fatty rat. Endocrinology *139*, 3681–3690.

Donaldson, Z.R., and Young, L.J. (2008). Oxytocin, vasopressin, and the neurogenetics of sociality. Science *322*, 900–904.

Douglas, A.J., Johnstone, L.E., and Leng, G. (2007). Neuroendocrine mechanisms of change in food intake during pregnancy: a potential role for brain oxytocin. Physiol. Behav. *91*, 352–365.

Dryden, S., King, P., Pickavance, L., Doyle, P., and Williams, G. (1999). Divergent effects of intracerebroventricular and peripheral leptin administration of feeding and hypothalamic neuropeptide Y in lean and obese (*fa/fa*) Zucker rats. Clin. Sci. *96*, 307–312.

Ellacott, K.L., Halatchev, I.G., and Cone, R.D. (2006). Characterization of leptin-responsive neurons in the caudal brainstem. Endocrinology *147*, 3190–3195.

Fan, W., Ellacott, K.L., Halatchev, I.G., Takahashi, K., Yu, P., and Cone, R.D. (2004). Cholecystokinin-mediated suppression of feeding involves the brainstem melanocortin system. Nat. Neurosci. *7*, 335–336.

Foo, K.S., Brismar, H., and Broberger, C. (2008). Distribution and neuropeptide coexistence of nucleobindin-2 mRNA/nesfatin-like immunoreactivity in the rat CNS. Neuroscience *156*, 563–579.

Gimpl, G., and Fahrenholz, F. (2001). The oxytocin receptor system: structure, function, and regulation. Physiol. Rev. *81*, 629–683.

Higuchi, T., Honda, K., Fukuoka, T., Negoro, H., and Wakabayashi, K. (1985). Release of oxytocin during suckling and parturition in the rat. J. Endocrinol. *105*, 339–346.

Horvath, T.L., and Bruning, J.C. (2006). Development programming of the hypothalamus: a matter of fat. Nat. Med. *12*, 52–53.

Huo, L., Grill, H.J., and Bjørbæk, C. (2006). Divergent regulation of proopiomelanocortin neurons by leptin in the nucleus of the solitary tract and in the arcuate hypothalamic nucleus. Diabetes *55*, 567–573.

Kiss, A., and Mikkelsen, J.D. (2005). Oxytocin-anatomy and functional assignments: a minireview. Endocr. Regul. *39*, 97–105.

Kohno, D., Nakata, M., Maekawa, F., Fujiwara, K., Maejima, Y., Kuramochi, M., Shimazaki, T., Okano, H., Onaka, T., and Yada, T. (2007). Leptin suppresses ghrelin-induced activation of neuropeptide Y neurons in the arcuate nucleus via phosphatidylinositol 3-kinase- and phosphodiesterase 3-mediated pathway. Endocrinology *148*, 2251–2263.

Kohno, D., Nakata, M., Maejima, Y., Shimizu, H., Sedbazar, U., Yoshida, N., Dezaki, K., Onaka, T., Mori, M., and Yada, T. (2008). Nesfatin-1 neurons in paraventricular and supraoptic nuclei of the rat hypothalamus coexpress oxytocin and vasopressin and are activated by refeeding. Endocrinology *149*, 1295–1301.

Koike, M., Nakanishi, H., Saftig, P., Ezaki, J., Isahara, K., Ohsawa, Y., Schulz-Schaeffer, W., Watanabe, T., Waguri, S., Kametaka, S., et al. (2000). Cathepsin D deficiency induces lysosomal storage with ceroid lipofuscin in mouse CNS neurons. J. Neurosci. *20*, 6898–6906.

Kublaoui, B.M., Gemelli, T., Tolson, P.K., Wang, Y., and Zinn, A.R. (2008). Oxytocin deficiency mediates hyperphagic obesity of Sim1 haploinsufficient mice. Mol. Endocrinol. *22*, 1732–1734.

Leng, G., Onaka, T., Caquineau, C., Sabatier, N., Tobin, V.A., and Takayanagi, Y. (2008). Oxytocin and appetite. Prog. Brain Res. *170*, 137–150.

Li, G., Zhang, Y., Rodrigues, E., Zheng, D., Matheny, M., Cheng, K.Y., and Scarpace, P.J. (2007). Melanocortin activation of nucleus of the solitary tract avoids anorectic tachyphylaxis and induces prolonged weight loss. Am. J. Physiol. Endocrinol. Metab. *293*, E252–258.

Ludwig, M., and Leng, G. (2006). Dendritic peptide release and peptide-dependent behaviors. Nat. Rev. Neurosci. *7*, 126–136.

Martins, A.S., Crescenzi, A., Stern, J.E., Bordin, S., and Michelini, L.C. (2005). Hypertension and exercise training differentially affect oxytocin and oxytocin receptor expression in the brain. Hypertension *46*, 1004–1009.

Matsuzawa, Y. (2006). Therapy insight: adipocytokines in metabolic syndrome and related cardiovascular disease. Nat. Clin. Pract. Cardiovasc. Med. *3*, 35–42.

McCann, M.J., and Rogers, R.C. (1990). Oxytocin excites gastric-related neurones in rat dorsal vagal complex. J. Physiol. *428*, 95–108.

Mori, Y., Koike, M., Moriishi, E., Kawabata, A., Tang, H., Oyaizu, H., Uchiyama, Y., and Yamanishi, K. (2008). Human herpesvirus-6 induces MVB formation and virus egress occurs by an exosomal release pathway. Traffic *9*, 1728–1742.

Morton, G.J., Cummings, D.E., Baskin, D.G., Barsh, G.S., and Schwartz, M.W. (2006). Central nervous system control of food intake and body weight. Nature *443*, 289–295.

Neumann, I.D. (2008). Brain oxytocin: a key regulator of emotional and social behaviors in both females and males. J. Neuroendocrinol. *20*, 858–865.

Oh-I, S., Shimizu, H., Satoh, T., Okada, S., Adachi, S., Inoue, K., Eguchi, H., Yamamoto, M., Imaki, T., Hashimoto, K., et al. (2006). Identification of nesfatin-1 as a satiety molecule in the hypothalamus. Nature *443*, 709–712.

Olson, B.R., Drutarosky, M.D., Stricker, E.M., and Verbalis, J.G. (1991). Brain oxytocin receptor antagonism blunts the effects of anorexigenic treatments in rats: evidence for central oxytocin inhibition of food intake. Endocrinology *129*, 785–791.

Onaka, T., and Yagi, K. (1990). Differencial effects of naloxone on neuroendocrine responses to fear-related emotional stress. Exp. Brain Res. *81*, 53–58.

Paxinos, G., and Watson, C. (1998). The Rat Brain in Stereotaxic Coordinates, Fourth Edition (New York: Academic Press).

Perello, M., Stuart, R.C., and Nillni, E.A. (2007). Differential effects of fasting and leptin on proopiomelanocortin peptides in the arcuate nucleus and in the nucleus of the solitary tract. Am. J. Physiol. Endocrinol. Metab. *292*, E1348–E1357.

Pinto, S., Roseberry, A.G., Liu, H., Diano, S., Shanabrough, M., Cai, X., Friedman, J.M., and Horvath, T.L. (2004). Rapid rewiring of arcuate nucleus feeding circuits by leptin. Science *304*, 110–115.

Price, C.J., Hoyda, T.D., Samson, W.K., and Ferguson, A.V. (2008). Nesfatin-1 influences the excitability of paraventricular nucleus neurones. J. Neuroendocrinol. *20*, 245–250.

Quiñones-Jenab, V., Jenab, S., Ogawa, S., Adan, R.A.M., Burbach, J.P.H., and Pfaff, D.W. (1997). Effects of estrogen on oxytocin receptor messenger ribonucleic acid expression in the uterus, pituitary, and forebrain of the female rat. Neuroendocrinology *65*, 9–17.

Rinaman, L. (1998). Oxytocinergic inputs to the nucleus of the solitary tract and dorsal motor nucleus of the vagus in neonatal rats. J. Comp. Neurol. *399*, 101–109.

Sabatier, N. (2006). α-melanocyte-stimulating hormone and oxytocin: a peptide signaling cascade in the hypothalamus. J. Neuroendocrinol. *18*, 703–710.

Sawchenko, P.E., Benoit, R., and Brown, M.R. (1988). Somatostatin 28-immunoreactive inputs to the paraventricular and supraoptic nuclei: principal origin from non-aminergic neurons in the nucleus of the solitary tract. J. Chem. Neuroanat. *1*, 81–94.

Schwartz, M.W., Woods, S.C., Porte, D., Jr., Seeley, R.J., and Baskin, D.G. (2000). Central nervous system control of food intake. Nature *404*, 661–671.

Shimizu, H., Inoue, K., and Mori, M. (2007). The leptin-dependent and -independent melanocortin signaling system: regulation of feeding and energy expenditure. J. Endocrinol. *193*, 1–9.

Stock, S., Granstrom, L., Backman, L., Matthiesen, A.S., and Uvnas-Moberg, K. (1989). Elevated plasma levels of oxytocin in obese subjects before and after gastric banding. Int. J. Obes. *13*, 213–222.

Swaab, D.F., Purba, J.S., and Hofman, M.A. (1995). Alterations in the hypothalamic paraventricular nucleus and its oxytocin neurons (putative satiety cell) in Prader-Willi syndrome: a study of five cases. J. Clin. Endocrinol. Metab. *80*, 573–579.

Takaya, K., Ogawa, Y., Isse, N., Okazaki, T., Satoh, N., Masuzaki, H., Mori, K., Tamura, N., Hosoda, K., and Nakao, K. (1996). Molecular cloning of rat leptin receptor isoform complementary DNAs-identification of a missense mutation in Zucker fatty (*fa/fa*) rats. Biochem. Biophys. Res. Commun. *225*, 75–83.

Takayanagi, Y., Kasahara, Y., Onaka, T., Takahashi, N., Kawada, T., and Nishimori, K. (2008). Oxytocin receptor-deficient mice developed late-onset obesity. Neuroreport *19*, 951–955.

Tanaka, S., and Kurosumi, K.A. (1992). Certain step of proteolytic processing of proopiomelanocortin occurs during the transition between two distinct stages of secretory granule maturation in rat anterior pituitary corticotrophs. Endocrinology *131*, 779–786.

Tung, Y.C., Ma, M., Piper, S., Coll, A., O'Rahilly, S., and Yeo, G.S.H. (2008). Novel leptin-regulated genes revealed by transcriptional profiling of the hypothalamic paraventricular nucleus. J. Neurosci. *19*, 12419–12426.

Valassi, E., Scacchi, M., and Cavagnini, F. (2008). Neuroendocrine control of food intake. Nutr. Metab. Cardiovasc. Dis. *18*, 158–168.

Yada, T., Vigh, S., and Arimura, A. (1993). Pituitary adenylate cyclase activating polypeptide (PACAP) increases cytosolic free Ca^{2+} concentration in folliculostellate cells and somatotropes of rat pituitary. Peptides *14*, 235–239.

Yamashita, T., Murakami, T., Iida, M., Kuwajima, M., and Shima, K. (1997). Leptin receptor of Zucker-fatty rat performs reduced signal transduction. Diabetes *46*, 1077–1080.

Yosten, G.L., and Samson, W.K. (2009). Nesfatin-1 exerts cardiovascular actions in brain: possible interaction with the central melanocortin system. Am. J. Physiol. Regul. Integr. Comp. Physiol. *297*, R330–R336.

Cell Metabolism, Volume *10*

Supplemental Data

Nesfatin-1-Regulated Oxytocinergic Signaling in the Paraventricular Nucleus Causes Anorexia through a Leptin-Independent Melanocortin Pathway

Yuko Maejima, Udval Sedbazar, Shigetomo Suyama, Daisuke Kohno, Tatsushi Onaka, Eisuke Takano, Natsu Yoshida, Masato Koike, Yasuo Uchiyama, Ken Fujiwara, Takashi Yashiro, Tamas L. Horvath, Marcelo O. Dietrich, Shigeyasu Tanaka, Katsuya Dezaki, Shinsuke Oh-I, Koushi Hashimoto, Hiroyuki Shimizu, Masanori Nakata, Masatomo Mori, and Toshihiko Yada

SUPPLEMENTAL EXPERIMENTAL PROCEDURES

Immunostaining for nesfatin-1 (Nesf-1)

Following perfusion with 4% paraformaldehyde (PFA), the rat brains were removed, postfixed in 4% PFA for overnight, and soaked in 30% sucrose in PB for 48 h. Sections of 8 μm thickness were cut by cryostat (CM3000; Leica Inc., Buffalo, NY), rinsed in PBS, and blocked with 2% normal goat serum for 30 min at room temperature (RT). They were incubated with rabbit anti-Nesf-1 antibody (Oh-I et al., 2006) (1:5,000) for overnight at 4°C, followed by incubation with Alexa 488 goat anti-rabbit IgG for 30 min at RT. Slices were mounted on slides and coverslipped with Vectashield hard set mounting medium (Vector Laboratories, Burlingame, CA). Confocal fluorescence images were acquired with Olympus FV1000 laser microscope. Brightness and contrast were adjusted using Adobe Photoshop (Adobe, San Jose, CA).

3V injection and measurements of food intake in mice

For icv injection in mice, a guide cannula (type; OM205-113, diameter; 0.2 mm; Unique

medical, Tokyo, Japan) was placed stereotaxically into 3V, at 1.5 mm caudal to the bregma in the midline and 5 mm below the surface of the skull. Mice were allowed to recover from the operation for 10 days while they were habituated to handling. On the day of experiment, food was removed from individual cage at 17:30. Mouse Nesf-1 (100 pmol/1 μl) (n = 9) or vehicle (1 μl sterile saline, 0.9% NaCl) (n = 6) was injected into 3V at 19:30, the onset of the dark cycle, and cumulative food intake for the following 1, 2, 4, 6 and 18 h was measured.

Measurements of LDH release from the PVN slices

The lactate dehydrogenase (LDH) released from the rat PVN slices during incubation at 36°C for 0.5 h under basal conditions (3 mM K^+) and those with 50 mM K^+ and/or 10^{-8} M Nesf-1 was measured by Cytotoxity Detection Kit (LDH) (Roche Diagnostics, Indianapolis, IN). The values are expressed as relative values to the positive control, in which the LDH released from the slices treated with protein kinase was normalized to "1".

Figure S1. Confocal image of immunofluorescence for Nesf-1 in the PVN

Nesf-1-IR fluorescence was diffusely distributed and localized preferentially to the cytoplasmic regions that appear to correspond to the secretory granules and membrane bound Golgi structures. Scale bar indicates 10 μm.

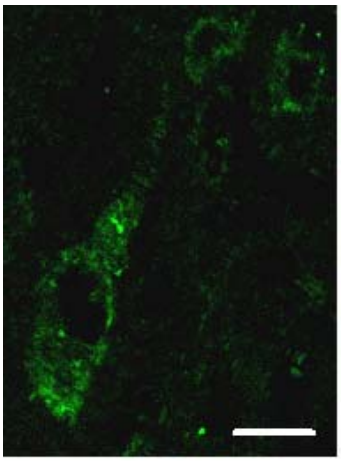

Figure S2. Nesf-1 suppresses food intake in mice

Mouse Nesf-1 (Shimizu et al. 2009) injected into 3V (100 pmol/1 μl) at 19:30 suppressed cumulative food intake at 2, 4, 6, and 18 h after injection. Bars represent means ± SE. **P < 0.01.

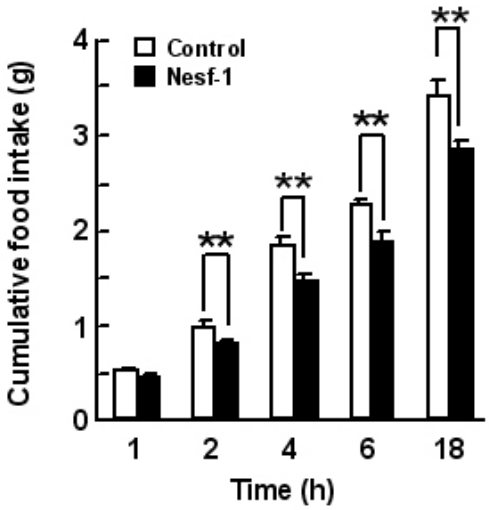

Figure S3. Neither high K^+ nor Nesf-1 influences LDH release from PVN slices

LDH release from PVN slices during incubation at 36°C for 0.5 h under basal conditions (3 mM K^+) and those with 50 mM K^+ and/or 10^{-8} M Nesf-1. The values are expressed as relative values to the positive control, in which the slices were treated with protein kinase. There was no significant difference in LDH release between control and 3 test groups. Bars represent means ± SE.

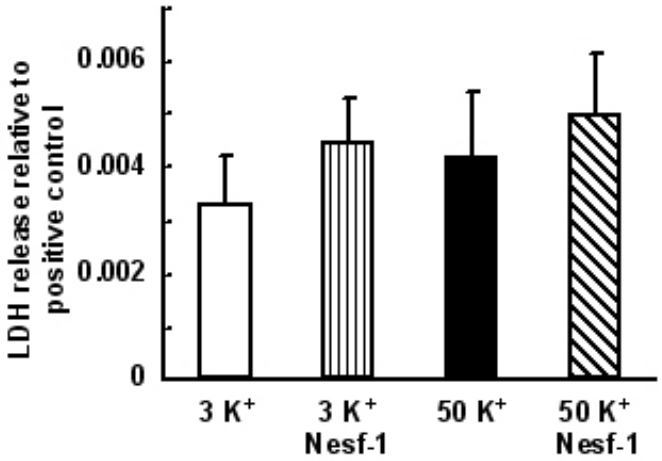

Figure S4. Oxt-induced $[Ca^{2+}]_i$ increases are suppressed by inhibitors of L-type Ca^{2+} channels and endoplasmic reticulum (ER) Ca^{2+} pumps in the NTS neurons

(A) Repetitive addition of Oxt at 10^{-10}M twice induced repeated $[Ca^{2+}]_i$ increases. **(B** and **C)** Oxt-induced $[Ca^{2+}]_i$ increases were suppressed by 2 μM nitrendipine (NTD), a blocker of L-type Ca^{2+} channels (B)**,** and by 0.5 μM thapsigargin (Tg), an inhibitor of ER Ca^{2+} pumps (C). **(D)** Incidence of $[Ca^{2+}]_i$ responses to the 2nd addition of Oxt in Oxt-responsive neurons under control and test conditions, expressed by percentage. The numbers above each bar indicate the number of neurons that responded over that examined. **(E)** The amplitude of Oxt-induced $[Ca^{2+}]_i$ increases under control conditions and those with NTD or Tg. The number above each bar indicates the number of neurons examined. Bars represent means ± SE. **P < 0.01.

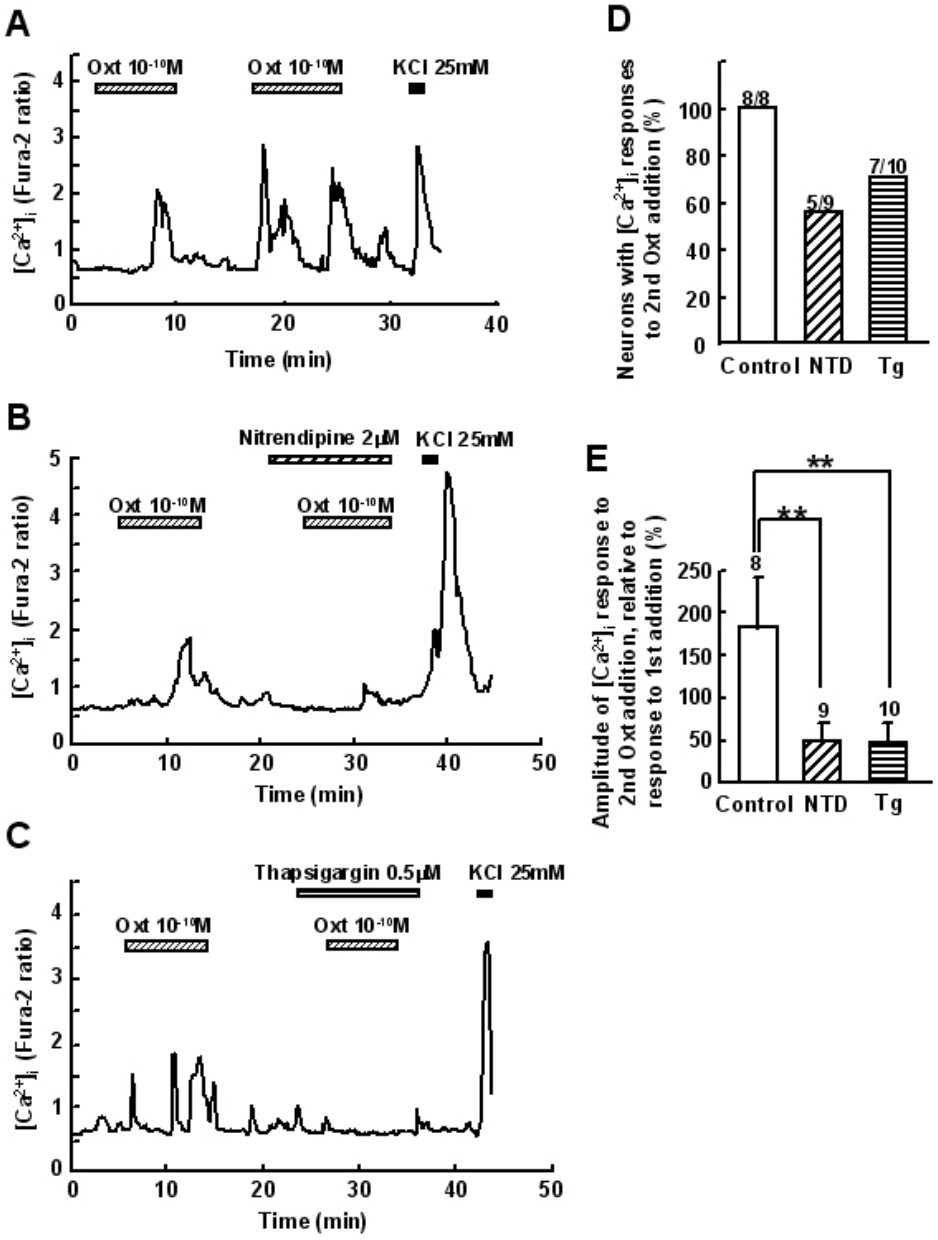
A
Oxt 10-10M
Oxt 10-10M
KCl 25mM
[Ca2+]i (Fura-2 ratio)
Time (min)
B
Nitrendipine 2μM
KCl 25mM
Oxt 10-10M
Oxt 10-10M
[Ca2+]i (Fura-2 ratio)
Time (min)
C
Thapsigargin 0.5μM
KCl 25mM
Oxt 10-10M
Oxt 10-10M
[Ca2+]i (Fura-2 ratio)
Time (min)
D
Neurons with [Ca2+]i responses to 2nd Oxt addition (%)
8/8
5/9
7/10
Control
NTD
Tg
E
Amplitude of [Ca2+]i response to 2nd Oxt addition, relative to response to 1st addition (%)
**
**
8
9
10
Control
NTD
Tg

Figure S5. A model for nesfatin-1-operative PVN oxytocinergic pathway relayed to NTS POMC neurons, causing melanocortin-dependent satiety

In this hypothetical model, central Nesf-1 or food intake activates Oxt and Nesf-1 neurons in the PVN. In the PVN, endogenous Nesf-1 serves as a paracrine/autocrine or local neuronal stimulator of Oxt neurons. The PVN oxytocinergic signaling to the NTS activates POMC neurons, inducing melanocortin-dependent anorexia. Dotted line indicates that POMC neurons lead to anorexia via a pathway that remains to be elucidated.

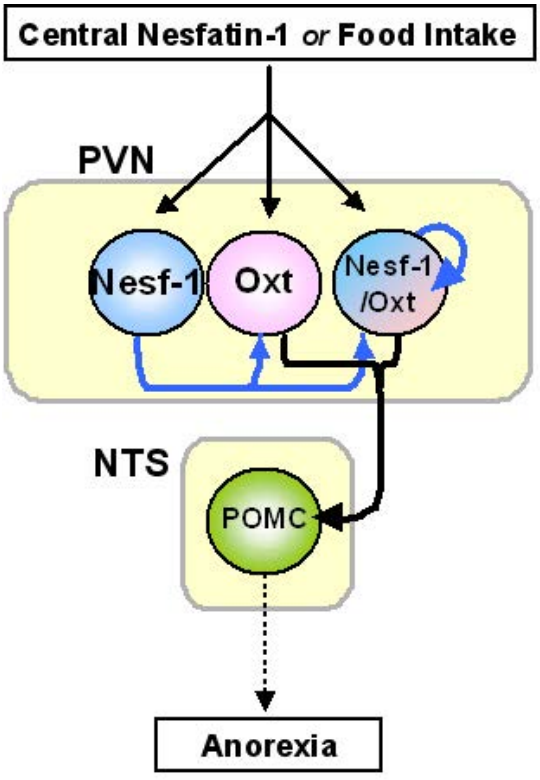

SUPPLEMENTAL REFERENCES

Shimizu, H., Oh-I, S., Hashimoto, K., Nakata, M., Yamamoto, S., Yoshida, N., Eguchi, H., Kato, I., Inoue, K., Satoh, T., et al. (2009). Peripheral administration of nesfatin-1 reduces food intake in mice: the leptin-independent mechanism. Endocrinology *150*, 662-671.

Anexo A-4. Peroxisome proliferation–associated control of reactive oxygen species sets melanocortin tone and feeding in diet-induced obesity

Artigo publicado no periódico *Nature Medicine*.

nature medicine

Peroxisome proliferation–associated control of reactive oxygen species sets melanocortin tone and feeding in diet-induced obesity

Sabrina Diano[1–4], Zhong-Wu Liu[1,3], Jin Kwon Jeong[1,2], Marcelo O Dietrich[1,3,5], Hai-Bin Ruan[1,3], Esther Kim[6,7], Shigetomo Suyama[1,3], Kaitlin Kelly[1,2], Erika Gyengesi[1,2], Jack L Arbiser[8], Denise D Belsham[9], David A Sarruf[10,11], Michael W Schwartz[10,11], Anton M Bennett[1,3,12], Marya Shanabrough[1,3], Charles V Mobbs[5], Xiaoyong Yang[1,3], Xiao-Bing Gao[1–3] & Tamas L Horvath[1–4]

Previous studies have proposed roles for hypothalamic reactive oxygen species (ROS) in the modulation of circuit activity of the melanocortin system[1,2]. Here we show that suppression of ROS diminishes pro-opiomelanocortin (POMC) cell activation and promotes the activity of neuropeptide Y (NPY)- and agouti-related peptide (AgRP)-co-producing (NPY/AgRP) neurons and feeding, whereas ROS-activates POMC neurons and reduces feeding. The levels of ROS in POMC neurons were positively correlated with those of leptin in lean and *ob/ob* mice, a relationship that was diminished in diet-induced obese (DIO) mice. High-fat feeding resulted in proliferation of peroxisomes and elevated peroxisome proliferator–activated receptor γ (PPAR-γ) mRNA levels within the hypothalamus. The proliferation of peroxisomes in POMC neurons induced by the PPAR-γ agonist rosiglitazone decreased ROS levels and increased food intake in lean mice on high-fat diet. Conversely, the suppression of peroxisome proliferation by the PPAR antagonist GW9662 increased ROS concentrations and c-fos expression in POMC neurons. Also, it reversed high-fat feeding–triggered elevated NPY/AgRP and low POMC neuronal firing, and resulted in decreased feeding of DIO mice. Finally, central administration of ROS alone increased c-fos and phosphorylated signal transducer and activator of transcription 3 (pStat3) expression in POMC neurons and reduced feeding of DIO mice. These observations unmask a previously unknown hypothalamic cellular process associated with peroxisomes and ROS in the central regulation of energy metabolism in states of leptin resistance.

Much has been learned about the control of feeding behavior mediated by the hypothalamus and its impact on the melanocortin system[3–6]. One remaining enigma is the neurobiological basis of leptin resistance; that is, the inability of high leptin levels to promote decreased feeding and body weight in states of obesity[7]. Many have argued that leptin resistance is the consequence of impaired activation of anorexigenic POMC neurons by elevated leptin levels during obesity and that this mechanism involves altered intracellular signaling cascades, including activation of Socs3 (ref. 8). However, there is no conclusive neurobiological proof for impaired synaptic transmission in the melanocortin system in diet-induced obese mice and rats[9,10]. Indeed, several neurobiological correlates of the melanocortin system do not show a clear leptin resistance[9,11]. Thus, the underlying cause for the impaired correlation between elevated leptin levels, POMC neuronal activity and feeding during diet-induced obesity remains elusive.

We have observed that central scavenging of ROS is permissive of AgRP neuronal firing and promotion of feeding, whereas activity of POMC neurons and satiety is associated with increased intracellular ROS levels[1,2]. These observations on circuit function regulated by ROS[1,2], together with the reported effect of hypothalamic ROS in glucose and lipid sensing[12,13], made us explore whether regulation of ROS has a role in the development of impaired melanocortin tone in diet-induced obesity.

First, we analyzed the effect of a ROS scavenger on POMC neuronal activation and feeding in wild-type mice (**Fig. 1**). We observed that intracerebroventricular (i.c.v.) administration of the ROS scavenger honokiol[14] resulted in significantly elevated (67.00% ± 8.02 s.e.m. versus 14.33% ± 6.29 s.e.m.; $P < 0.01$) c-fos expression in NPY/AgRP

[1]Program in Integrative Cell Signaling and Neurobiology of Metabolism, Yale University School of Medicine, New Haven, Connecticut, USA. [2]Department of Obstetrics and Gynecology, Yale University School of Medicine, New Haven, Connecticut, USA. [3]Section of Comparative Medicine, Yale University School of Medicine, New Haven, Connecticut, USA. [4]Department of Neurobiology, Yale University School of Medicine, New Haven, Connecticut, USA. [5]Department of Biochemistry, Universidade Federal do Rio Grande do Sul, Porto Alegre, Brazil. [6]Department of Neuroscience, Friedman Brain Institute, Mount Sinai School of Medicine, New York, New York, USA. [7]Department of Geriatrics, Friedman Brain Institute, Mount Sinai School of Medicine, New York, New York, USA. [8]Department of Dermatology, Emory University School of Medicine, Winship Cancer Institute, Atlanta VA Medical Center, Atlanta, Georgia, USA. [9]Department of Physiology, University of Toronto and Division of Cellular and Molecular Biology, Toronto General Hospital Research Institute, University Health Network, Toronto, Ontario, Canada. [10]Diabetes and Obesity Center of Excellence, University of Washington, Seattle, Washington, USA. [11]Department of Medicine, University of Washington, Seattle, Washington, USA. [12]Department of Pharmacology, Yale University School of Medicine, New Haven, Connecticut, USA. Correspondence should be addressed to S.D. (sabrina.diano@yale.edu) or T.L.H. (tamas.horvath@yale.edu).

Received 28 March; accepted 15 June; published online 28 August 2011; corrected after print 16 September 2011; doi:10.1038/nm.2421

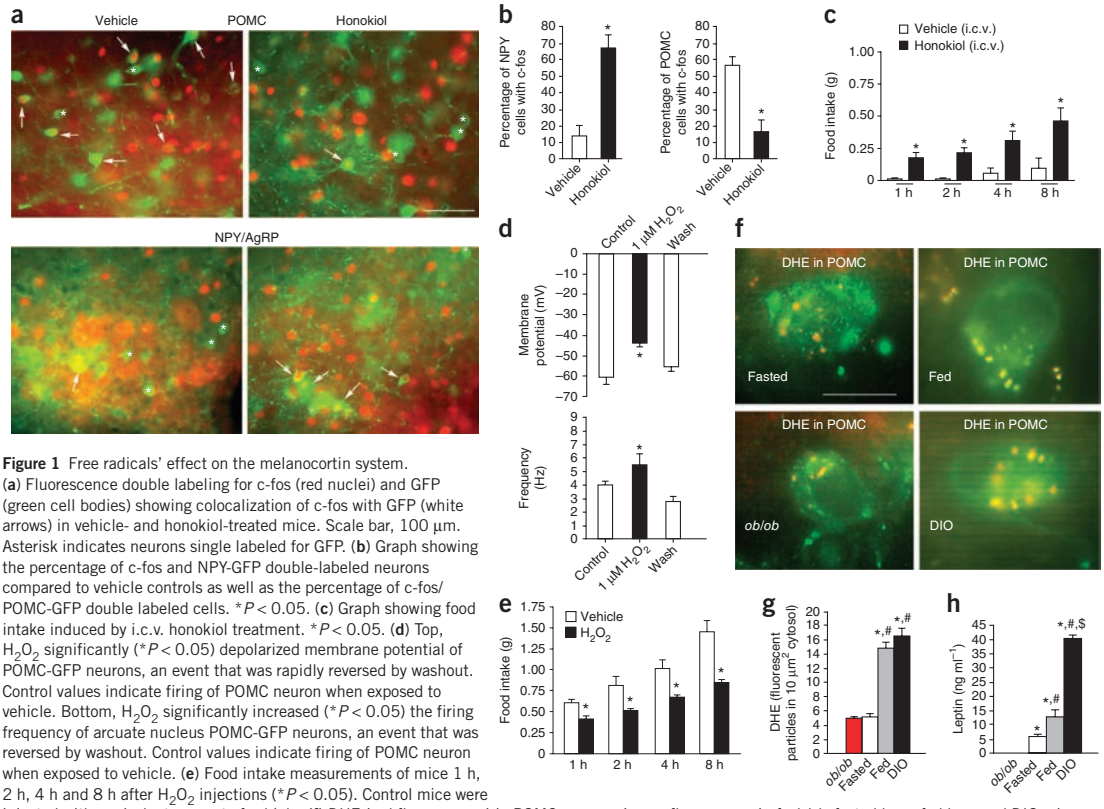

Figure 1 Free radicals' effect on the melanocortin system. (**a**) Fluorescence double labeling for c-fos (red nuclei) and GFP (green cell bodies) showing colocalization of c-fos with GFP (white arrows) in vehicle- and honokiol-treated mice. Scale bar, 100 μm. Asterisk indicates neurons single labeled for GFP. (**b**) Graph showing the percentage of c-fos and NPY-GFP double-labeled neurons compared to vehicle controls as well as the percentage of c-fos/POMC-GFP double labeled cells. $^*P < 0.05$. (**c**) Graph showing food intake induced by i.c.v. honokiol treatment. $^*P < 0.05$. (**d**) Top, H_2O_2 significantly ($^*P < 0.05$) depolarized membrane potential of POMC-GFP neurons, an event that was rapidly reversed by washout. Control values indicate firing of POMC neuron when exposed to vehicle. Bottom, H_2O_2 significantly increased ($^*P < 0.05$) the firing frequency of arcuate nucleus POMC-GFP neurons, an event that was reversed by washout. Control values indicate firing of POMC neuron when exposed to vehicle. (**e**) Food intake measurements of mice 1 h, 2 h, 4 h and 8 h after H_2O_2 injections ($^*P < 0.05$). Control mice were injected with equivalent amount of vehicle. (**f**) DHE (red fluorescence) in POMC neurons (green fluorescence) of *ob/ob*, fasted lean, fed lean and DIO mice. (**g**) Quantification of DHE in POMC neurons indicated the highest level of ROS production in POMC neurons of DIO and fed lean mice compared to fasted lean and *ob/ob* mice. $^*P < 0.05$ compared to *ob/ob* values. $\#P < 0.05$ compared to fasted lean values. There was no significant difference between fed and DIO values. (**h**) Leptin was not detectable in *ob/ob* mice. Leptin levels were significantly higher in fed mice compared to fasted values ($\#P < 0.05$). DIO mice had leptin levels that were significantly higher compared to those in fed ($\$P < 0.05$) and fasted ($\#P < 0.05$) mice. $^*P < 0.05$ compared to *ob/ob* values. Data are expressed as the mean ± s.e.m. $n = 6$ for each experimental group.

neurons and significantly lower (16.54% ± 7.33 s.e.m. versus 57.01% ± 4.85 s.e.m., $P < 0.01$) c-fos expression in POMC neurons compared to vehicle-treated controls (**Fig. 1a**,**b**). The same treatment caused elevated food intake during the light cycle compared to vehicle controls (1 h: 0.17 ± 0.05 g versus 0.01 ± 0.01 g; 2 h: 0.21 ± 0.04 g versus 0.01 ± 0.01 g; 4 h: 0.31 ± 0.08 g versus 0.06 ± 0.04 g; 8 h: 0.46 ± 0.11 g versus 0.1 ± 0.08 g; $P < 0.05$, all values mean ± s.e.m.) (**Fig. 1c**). These observations are in line with our earlier findings[1], and they reveal that suppression of ROS inhibits POMC neuronal activity, as assessed by c-fos expression.

Next, we tested the effect of promotion of ROS generation on POMC neuronal activity *ex vivo* and feeding behavior *in vivo*. We conducted patch-clamp whole-cell electrophysiological recordings in slice preparations from POMC-GFP mice (mice that express tau-topaz green fluorescent protein under the transcriptional control of POMC genomic sequence by the use of a bacterial artificial chromosome (BAC)) with and without H_2O_2 application. 1 μM H_2O_2 depolarized POMC neurons (**Fig. 1d**) and increased the firing rate of these cells (**Fig. 1d**). In line with these neurobiological effects in the arcuate nucleus, i.c.v. injection of 5 μM H_2O_2 in 2 μl caused significantly less feeding ($P < 0.01$) of mice after an overnight fast compared to vehicle-injected controls (**Fig. 1e**). This effect of H_2O_2 on promotion of decreased feeding is in line with the effect of ROS in glucose sensing and experimental hypertriglyceridemia[12,13]. Taken together, these observations provide evidence that ROS can be an acute regulator of POMC neuronal activity and that exogenous ROS administered to the brain can promote satiety in lean mice.

We next analyzed ROS levels in POMC cells using dihydroethidium (DHE; a substrate for fluorimetric detection of peroxidase as a readout for ROS) from mice with normal metabolism (fed and fasted wild-type mice) and from mice with impaired POMC neuronal activity (*ob/ob* and diet-induced obese (DIO) mice). We found the lowest level of DHE fluorescent particles in POMC neurons of *ob/ob* mice (4.96 ± 0.23 (s.e.m.) fluorescent particles per 10 μm^2 of cytosol) and wild-type mice that, following a previously reported protocol[10], were fasted overnight (5.16 ± 0.48 (s.e.m.) fluorescent particles per 10 μm^2 of cytosol) (**Fig. 1f**,**g**). In contrast, 48 h of leptin treatment[10] of *ob/ob* mice resulted in elevated DHE expression in POMC neurons compared to PBS-treated controls (16.25 ± 1.15 versus 7.5 ± 1.32 fluorescent particles in 10 μm^2 cytosol; $P < 0.05$, means ± s.e.m.). DHE fluorescent levels were significantly ($P < 0.001$) higher in fed wild-type animals (14.79 ± 0.83 (s.e.m.) fluorescent particles in 10 μm^2 cytosol)

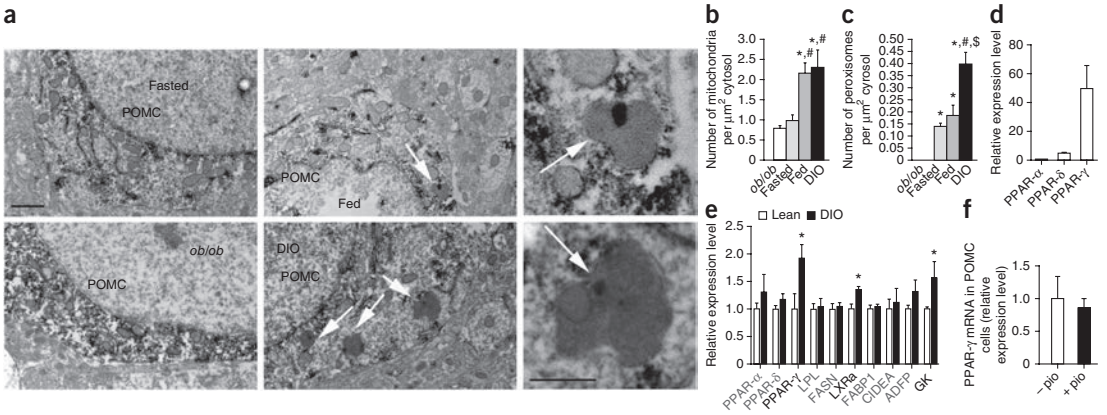

Figure 2 Peroxisome proliferation in POMC neurons. (**a**) Electron micrographs showing a representative section of POMC-GFP perykarya in the arcuate nucleus from fasted lean (top left), *ob/ob* (bottom left), fed lean (top middle) and DIO (bottom middle) mice. White arrows on the middle images point to peroxisomes. The top and bottom right images are high-power magnifications of peroxisomes from the fed lean and DIO images, respectively. Top left scale bar, 1 µm for left and middle columns. Bottom right scale bar, 500 nm for right column. (**b**) Mitochondria number in POMC neurons of fed and DIO mice compared to fasted and *ob/ob* values. $^{*}P < 0.05$ compared to *ob/ob* values. $^{\#}P < 0.05$ compared to fasted values. (**c**) Graph showing the number of peroxisomes in POMC neurons in DIO, fed, fasted and *ob/ob* mice, $^{*}P < 0.05$ compared to *ob/ob* values. $^{\#}P < 0.05$ compared to fasted values. $\$P < 0.05$ compared to fed values. (**d**) PCR analyses of PPAR-α, PPAR-δ and PPAR-γ mRNA. (**e**) Real-time PCR analyses of PPAR-α, PPAR-δ and PPAR-γ and of various other gene transcripts related to PPAR signaling and cellular metabolism in DIO hypothalamus relative to lean control values. LPL, lipoprotein lipase; FASN, fatty acid synthase; LXRa, liver X receptor α; FABP1, fatty acid binding protein 1; CIDEA, cell death–inducing DFFA-like effector a; GK, glucokinase. Results are shown as mean ± s.e.m. The comparison of different groups was carried out using two-tailed unpaired Student's *t* test. $^{*}P < 0.05$. (**f**) PPAR-γ mRNA expression in the POMC neuronal cell line mHypoA-2/28 with and without pioglitazone treatment (pio). (**g**) mRNA expression of the PPAR-γ target Gpd1 in the POMC-expressing hypothalamic cell line after pioglitazone treatment. (**h**) mRNA expression of the PPAR-γ target Fabp4 in the AgRP-expressing hypothalamic cell line after pioglitazone treatment. (**i**) mRNA expression of the PPAR-γ target (ADFP in the AgRP-expressing hypothalamic cell line after pio treatment. (**j**) Real-time PCR analyses of PPAR-α, PPAR-δ and PPAR-γ and of various other gene transcripts related to PPAR signaling and cellular metabolism in *ob/ob* hypothalamus relative to wild-type controls. Results are shown as mean ± s.e.m. $n = 6$ for each experimental group. The comparison of different groups was carried out using two-tailed unpaired Student's *t* test. $^{*}P < 0.05$.

and in DIO mice (16.61 ± 0.98 (s.e.m.) fluorescent particles in 10 µm^2 cytosol) (**Fig. 1f**,**g**) compared to fasted wild-type and untreated *ob/ob* values. However, there was no statistically significant difference in POMC DHE levels between fed and DIO mice (**Fig. 1f**,**g**). The lack of difference in POMC ROS levels between fed (lean) and DIO mice was associated with almost threefold higher levels of circulating leptin in DIO mice compared to lean fed mice (**Fig. 1h**). Thus, although there is a positive correlation between circulating leptin levels and ROS levels in POMC neurons of fasted and *ob/ob* mice, in DIO mice substantially higher levels of circulating leptin resulted in no proportional increase in ROS levels in POMC neurons (**Fig. 1g**,**h**).

The dissociation of elevated leptin levels from increased POMC ROS content in DIO mice could involve multiple mechanisms, including a putative role for mitochondrial uncoupling protein 2 (UCP2)[1,15]. We noted the presence of peroxisomes in POMC neurons. Peroxisomes are intracellular organelles involved with non–ATP-generating lipid beta oxidation and control of ROS[16]. We evaluated the number of mitochondria and peroxisomes in POMC neurons of *ob/ob*, fasted lean, fed lean and DIO mice. We found the lowest number of mitochondria (0.8 ± 0.06 (s.e.m.) mitochondria per 1 µm^2 cytosol) and peroxisomes (0 peroxisomes per 1 µm^2 cytosol) in the cytosol of POMC in *ob/ob* mice (**Fig. 2a**–**c**). Lean fed mice had higher mitochondrial numbers (2.19 ± 0.27 (s.e.m.)) compared to fasted (0.98 ± 0.13 (s.e.m.)) and *ob/ob* mice (**Fig. 2b**), but peroxisome numbers were not different in fed (0.18 ± 0.04 (s.e.m.)) and fasted mice (0.14 ± 0.01 (s.e.m.)) (**Fig. 2c**). Whereas mitochondria numbers were not different in POMC neurons of DIO mice (2.3 ± 0.42 (s.e.m.)) from those in fed mice (**Fig. 2b**), peroxisome counts were almost threefold higher in POMC neurons of DIO mice (0.39 ± 0.04 (s.e.m.)) compared to the values of lean fed mice (**Fig. 2c**). Through analysis of 50 POMC neurons (ten cells analyzed per mouse; $n = 5$)[17], peroxisomes were not found in POMC neurons of *db/db* mice (**Supplementary Fig. 1**). We also analyzed peroxisome number in NPY/AgRP neurons. We found that peroxisome number was significantly higher in AgRP neurons of DIO mice compared to lean mice (**Supplementary Fig. 2**). Taken together, these observations suggest that peroxisomes may render melanocortin neurons less active in DIO mice, decreasing the ability of elevated leptin to promote POMC neuronal activity and satiety.

In mice, proliferation of peroxisomes is governed, in part, by nuclear receptors, such as PPAR-γ (ref. 18). PPAR-γ has been associated with brain inflammation, gliosis[19] and ROS control[20], mechanisms that are characteristic of the arcuate nucleus of DIO mice (present study and refs. 9,21). Additionally, in mice, PPAR-γ has been detected in the brain[22] and in neurons of the arcuate nucleus[23]. We analyzed

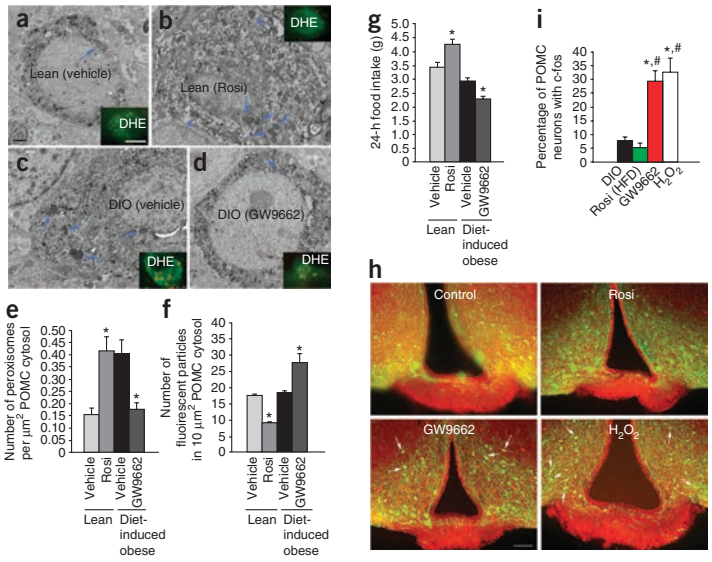

Figure 3 Peroxisome proliferation in POMC neurons is associated with altered feeding. (**a**–**d**) Electron micrographs with fluorescence insets of POMC neurons from lean vehicle-treated (top left), lean rosiglitazone-treated (top right), DIO vehicle-treated (bottom left) and DIO GW9662-treated (bottom right) mice. On the electron micrographs, blue arrows point to peroxisomes. On the fluorescence insets, red labeling indicates DHE in green POMC-GFP neurons. Electron micrograph scale bar, 1 μm; inset scale bar, 10 μm. (**e**) Graph showing peroxisome number in POMC neurons of lean mice on high-fat diet after rosiglitazone treatment and in DIO mice treated with GW9662, $^{*}P < 0.05$. (**f**) DHE levels in lean mice treated with rosiglitazone and in DIO mice treated with GW9662, $^{*}P < 0.05$. (**g**) Daily food intake measurements of lean mice after rosiglitazone treatment and of DIO mice after GW9662 administration compared to vehicle treated controls. $^{*}P < 0.05$. (**h**) Double immunofluorescence labeling for c-fos (red) and POMC (green) from control DIO (top left), rosigliatzone-treated (top right), GW9662-treated (bottom left) and H_2O_2-treated (bottom right) high-fat diet–fed mice. Scale bar, 100 μm. (**i**) Bar graphs showing the percentage of c-fos–immunolabeled POMC neurons in the different experimental groups. $^{*}P < 0.05$ compared to DIO control values; $^{\#}P < 0.05$ compared to rosiglitazone-treated mice. Data are expressed as the mean ± s.e.m. $n = 6$ for each experimental group.

transcript levels in the hypothalamus of PPAR-α, PPAR-δ and PPAR-γ and some of their putative target genes. PPAR-γ mRNA expression was several fold higher in the hypothalamus compared to PPAR-α or PPAR-δ mRNA in normal-weight wild-type mice (**Fig. 2d**). In DIO mice, hypothalamic transcripts of PPAR-γ but not PPAR-α or PPAR-δ were upregulated compared to lean controls (**Fig. 2e**). DIO hypothalamus also showed elevated liver X receptor α and glucokinase transcript levels (**Fig. 2e**). This constellation of transcript inductions in DIO mice is in line with increased carbohydrate and lipid metabolism in the hypothalamus in response to high-fat feeding and with processes uncovered in the liver[24].

Next, we analyzed PPAR-γ transcript levels in POMC and AgRP neuronal cell lines[25]. PPAR-γ transcripts were identified in both neuronal cultures (**Fig. 2f** for POMC cultures; data not shown for AgRP cultures). Treatment of the cultures with 10 μM of the PPAR-γ agonist pioglitazone for 24 h resulted in elevated mRNA expression of the PPAR-γ target[26] glycerol-3-phosphate dehydrogenase 1 (Gpd1) in POMC neurons (**Fig. 2g**) and expression of mRNA encoding fatty acid binding protein 4 (Fabp4) and adipose differentiation-related protein (ADFP or adipophilin) in AgRP neurons (**Fig. 2h**,**i**). Thus, high-fat feeding–inducible hypothalamic PPAR-γ is expressed in key neurons of the melanocortin system, and it can be activated by selective agonists.

In *ob/ob* hypothalamus, it was PPAR-δ mRNA that was elevated, together with transcripts classically characteristic of preadipocytes such as cell-death–inducing DNA fragmentation factor α–like effector A (CIDEA)[27] and ADFP (**Fig. 2j**)[28]. Thus, obesity in *ob/ob* mice has differential cellular pressure on hypothalamic neurons compared to DIO mice.

Next, we tested whether chemical agonists and antagonists of PPAR-γ[29] may affect peroxisome number, ROS levels and feeding in lean and DIO mice. We analyzed lean and DIO mice on high-fat diet, because previous studies[30], as well as the present study (data not shown), revealed no effect of PPAR-γ agonists or antagonists on feeding of mice on normal chow. We injected lean mice after 5 d on high-fat diet with the PPAR-γ agonist rosiglitazone i.c.v. twice a day for 7 d and DIO mice with 0.5 μg of the PPAR-γ antagonist GW9662 twice a day for 7 d. We i.c.v. injected control mice for both groups (lean mice and DIO mice on high-fat diet) with equivalent volume of the diluent (DMSO in saline). In similar cohorts of mice, we injected DHE in the last day of the treatment to analyze ROS levels in POMC neurons. Seven-day i.c.v. rosiglitazone treatment of lean mice resulted in significantly elevated peroxisome numbers in POMC neurons compared to controls (rosiglitazone: 0.41 ± 0.05 versus vehicle 0.15 ± 0.02; $P < 0.05$, means ± s.e.m.), which was accompanied by decreased appearance of ROS in these neurons (rosiglitazone: 9.03 ± 0.26; vehicle 17.55 ± 0.4; $P < 0.05$, means ± s.e.m.) and increased daily food intake (4.28 ± 0.14 g versus 3.43 ± 0.18 g; $P < 0.05$, means ± s.e.m.) (**Fig. 3a**–**g**). In contrast, 7-d treatment of DIO mice with GW9662 resulted in lower numbers of peroxisomes in POMC neurons compared to controls (GW9662: 0.17 ± 0.02; vehicle: 0.4 ± 0.05; $P < 0.05$, means ± s.e.m.), with elevated DHE levels (GW9662: 27.45 ± 2.92 fluorescent particles in 10 μm^2 POMC cytosol; vehicle: 18.31 ± 0.66 fluorescent particles in 10 μm^2 POMC cytosol; $P < 0.05$, means ± s.e.m.) and lower daily food intake (GW9662: 2.29 ± 0.1 g; vehicle: 2.92 ± 0.11 g; $P < 0.05$, means ± s.e.m.) (**Fig. 3a**–**g**). These observations are consistent with two recent reports showing that interference with neuronal PPAR-γ signaling has no detectable phenotype on standard chow but attenuates DIO[31,32].

To further test the relationship between PPAR-γ and peroxisomes, we analyzed the expression of a key peroxisomal enzyme, catalase, in hypothalami of neuron-specific PPAR-γ–knockout mice[31] and wild-type littermates. After 2 weeks on high-fat diet, wild-type mice showed a significantly higher number of catalase-immunopositive arcuate nucleus cells compared to PPAR-γ–knockout mice (51.75 ± 5.75 cells per 0.0025 mm^3 of arcuate nucleus versus 12.75 ± 3.75 cells per 0.0025 mm^3 of arcuate nucleus; $P < 0.05$; **Supplemental Fig. 3**). These data corroborate a role for PPAR-γ in peroxisome proliferation in the hypothalamus.

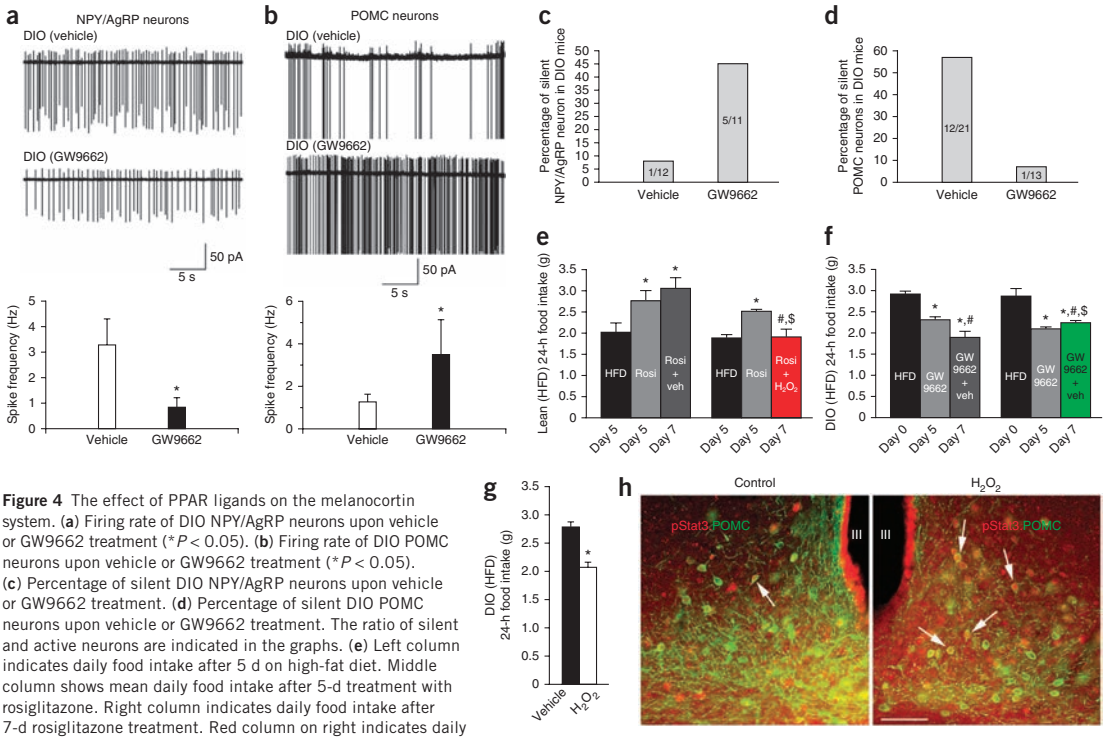

Figure 4 The effect of PPAR ligands on the melanocortin system. (**a**) Firing rate of DIO NPY/AgRP neurons upon vehicle or GW9662 treatment (*$P < 0.05$). (**b**) Firing rate of DIO POMC neurons upon vehicle or GW9662 treatment (*$P < 0.05$). (**c**) Percentage of silent DIO NPY/AgRP neurons upon vehicle or GW9662 treatment. (**d**) Percentage of silent DIO POMC neurons upon vehicle or GW9662 treatment. The ratio of silent and active neurons are indicated in the graphs. (**e**) Left column indicates daily food intake after 5 d on high-fat diet. Middle column shows mean daily food intake after 5-d treatment with rosiglitazone. Right column indicates daily food intake after 7-d rosiglitazone treatment. Red column on right indicates daily food intake of mice with 7-d rosiglitazone treatment with H_2O_2 in the last 2 d of the 7-d treatment. *$P < 0.05$ relative to values before rosiglitazone treatment. $^{\#}P < 0.05$ between daily food intake values after 5-d treatment with rosiglitazone. $^{\$}P < 0.05$ between 7-d treatment values. (**f**) Left column indicates daily food intake at the beginning of GW9662 treatment (day 0). Middle column shows mean food intake after 5-d treatment with GW9662. Right column indicates daily food intake after 7-d GW9662 treatment. Green column on right indicates daily food intake of mice with 7-d GW9662 treatment with honokiol in the last 2 d of the 7-d treatment. *$P < 0.05$ relative to values before GW9662 treatment. $^{\#}P < 0.05$ between daily food intake values after 5-d treatment with GW9662. $^{\$}P < 0.05$ between 7-d treatment values. (**g**) Two-day i.c.v. H_2O_2 treatment alone resulted in significantly (*$P < 0.05$) decreased daily food intake of DIO mice compared to vehicle-treated controls. (**h**) Photomicrographs of pStat3 (red) and POMC (green) double-immunolabeled hypothalamic sections from leptin-treated DIO mice concurrently treated with vehicle or H_2O_2 after peripheral leptin injections. $P < 0.05$ for H_2O_2-treated mice compared to vehicle-treated controls. Arrows indicate pStat3 labeled nuclei. Arrows indicate pStat3 and POMC co-labeled cells. Scale bar, 100 μm. Data are expressed as the mean ± s.e.m. $n = 6$ for each experimental group.

To test whether interference with PPAR-γ activity affects neurobiological correlates of feeding regulation, first we analyzed c-fos expression in POMC neurons of vehicle-, rosiglitazone- and GW9662-treated female mice on high-fat diet. Although rosiglitazone did not affect the number of c-fos–expressing POMC neurons, GW9662 treatment resulted in a significant ($P < 0.05$) induction of c-fos in melanocortin cells compared to DIO control values (**Fig. 3h**,**i** and **Supplementary Fig. 4**).

Because GW9662 induced c-fos expression in POMC neurons, and because peroxisome number and PPAR-γ signaling were induced also in NPY neurons, we next analyzed electric activity of NPY/AgRP and POMC neurons in NPY-GFP and POMC-GFP DIO mice with or without GW9662 treatment. The firing rates of NPY/AgRP and POMC neurons were measured on slices taken at 10:00 a.m. from GW9662- or vehicle-treated DIO mice. This time of day represents relative satiety with high POMC and low NPY/AgRP neuronal firing of standard-chow–fed mice[14,32]. In contrast to standard-chow–fed mice, in vehicle-treated DIO mice, analysis of action potential frequency at 10:00 a.m. revealed high NPY/AgRP neuronal firing and low POMC firing (**Fig. 4a**,**b**). The level of NPY/AgRP neuronal firing in fed DIO mice was not dissimilar from the firing frequency recorded in these neurons during fasting[33]. The low degree of firing of POMC neurons at the time of relative satiety in DIO mice is consistent with the measured lower α-melanocyte–stimulating hormone release by hypothalamic explants of DIO mice[15]. Of note, i.c.v. GW9662 treatment significantly ($P < 0.05$) reversed this DIO-induced firing alteration of the melanocortin system, whereby NPY/AgRP neurons reduced their firing rate and POMC neurons increased action potential generation (**Fig. 4a**,**b**). In DIO mice, very few NPY/AgRP neurons were silent, but this number was elevated after GW9662 treatment (**Fig. 4c**). In contrast, whereas more then half of the POMC neurons were silent (not firing at all) in vehicle-treated DIO mice, this population was smaller after GW9662 treatment (**Fig. 4d**). Thus, GW9662 reversed firing of both NPY/AgRP and POMC neurons in DIO mice to resemble the firing rates of these cells in lean mice at a time of satiety on normal chow[15,33].

ROS abundance was elevated by GW9662 treatment and readily enhanced POMC neuronal firing (**Fig. 1**). To test whether ROS may

be a mediator of the effects of PPAR-γ, we next analyzed the effect of rosiglitazone and GW9662 in mice on high-fat diet with and without i.c.v. H_2O_2 and honokiol administration, respectively. We found that changes in feeding of high-fat–fed mice induced by 7-d treatment with rosiglitazone or GW9662 were diminished by co-administration of H_2O_2 or honokiol, respectively, between days 5 and 7 (**Fig. 4e**,**f**). Thus, alteration of PPAR-γ signaling may exert its effect on hypothalamic regulation of feeding via ROS. To further test this notion, we analyzed the effect of GW9662 and rosiglitazone in UCP2-knockout mice, which have endogenously elevated hypothalamic ROS levels[1]. We found no significant effect of either GW9662 or rosiglitazone on feeding of these mice (**Supplementary Fig. 5**). The lack of effect of rosiglitazone in UCP- knockout mice is in line with an inhibitory effect of ROS on rosiglitazone. GW9662 may not have been effective because there were very few peroxisomes in POMC neurons of UCP2-knockout mice (**Supplementary Fig. 5**).

To test whether ROS alone could reverse POMC function, we injected H_2O_2 i.c.v. in DIO mice. We found that i.c.v. H_2O_2 resulted in elevated c-fos expression in POMC neurons (**Fig. 3h**,**i** and **Supplementary Fig. 4d**), decreased feeding (**Fig. 4g**) and elevated pStat3 expression in response to peripheral leptin injection compared to controls (**Fig. 4h**). We found that 3% of POMC neurons (3 out of 100 POMC perikarya from five mice) contained pStat3, whereas in H_2O_2-treated DIO mice, 18% of POMC cells (18 out of 100 POMC perikarya from five mice) were immunolabeled for pStat3. These observations suggest that whereas ROS enhances leptin sensitivity in DIO mice, the effects of ROS on feeding may be downstream from leptin signaling, a notion consistent with the electric actions of H_2O_2 on POMC neurons (**Fig. 1**). How other intracellular controllers of ROS interact to set metabolically and functionally relevant cellular ROS levels will need further studies.

This study has established that ROS is an acute activator of POMC neuronal firing and that, in lean mice, hypothalamic ROS is positively correlated with circulating leptin level. ROS levels are controlled in hypothalamic POMC neurons of DIO mice in association with peroxisome proliferation. This previously unrecognized metabolically regulated intracellular mechanism can be regulated by PPAR-γ activity, which itself is under nutritional control in the hypothalamus. Peroxisome proliferation in the hypothalamus is consistent with the origin of peroxisomes from the endoplasmic reticulum under increased metabolic pressure[34,35], as endoplasmic reticulum stress has been identified as a contributor to DIO-related leptin resistance[36]. Our results argue for endogenous ROS control during diet-induced obesity as a potential cause of functional leptin resistance, manifested by lower POMC and elevated NPY/AgRP neuronal firing. In light of the deleterious effects of sustained elevated ROS levels[37], our study gives support to the notion that promotion of sustained satiety through the brain in states of diet-induced obesity may increase degenerative processes[2].

METHODS

Methods and any associated references are available in the online version of the paper at http://www.nature.com/naturemedicine/.

Note: Supplementary information is available on the Nature Medicine website.

ACKNOWLEDGMENTS

We thank J.M. Olefsky, Department of Medicine, University of California–San Diego, for generating and providing brain-specific PPAR-γ–knockout mice and B.B. Lowell, Beth Israel Deaconess Medical Center, for providing breeding pairs of UCP2-knockout mice. This work was supported by US National Institutes of Health (NIH) grants DK084065 (S.D.) and DK080000 and OD006850 (T.L.H.) and by American Diabetes Association grant 7-08-MN-25 (T.L.H.). This work was also supported by NIH grants DK089098 (X.Y.), DK072033 (C.V.M.) DK090320 and DK052989 (M.W.S.) and AR47901and P30 AR42687 (J.L.A.).

AUTHOR CONTRIBUTIONS

S.D. and T.L.H. developed the conceptual framework of the study, designed the experiments, conducted studies, analyzed data and wrote the paper. Z.-W.L., J.K.J., M.O.D., H.-B.R., E.K., S.S., K.K., E.G., D.A.S. and M.S. conducted experiments. J.L.A. initiated studies with honokiol and provided reagents. C.V.M. designed and supervised *in vitro* cell signaling studies. M.W.S. designed studies on PPAR-γ–knockout mice. D.D.B. provided POMC and AgRP cell cultures and helped design experiments. A.M.B. provided reagents and advised on signaling aspects of the work. X.Y. and X.-B.G. supervised experiments and analyzed data.

COMPETING FINANCIAL INTERESTS

The authors declare no competing financial interests.

Published at http://www.nature.com/naturemedicine/.
Reprints and permissions information is available at http://www.nature.com/reprints/index.html.

1. Andrews, Z.B. *et al.* UCP2 mediates ghrelin's action on NPY/AgRP neurons by lowering free radicals. *Nature* **454**, 846–851 (2008).
2. Horvath, T.L., Andrews, Z.B. & Diano, S. Fuel utilization by hypothalamic neurons: roles for ros. *Trends Endocrinol. Metab.* **20**, 78–87 (2009).
3. Gropp, E. *et al.* Agouti-related peptide–expressing neurons are mandatory for feeding. *Nat. Neurosci.* **8**, 1289–1291 (2005).
4. Luquet, S., Perez, F., Hnasko, T. & Palmiter, R. NPY/AgRP neurons are essential for feeding in adult mice but can be ablated in neonates. *Science* **310**, 683–685 (2005).
5. Cone, R.D. Studies on the physiological functions of the melanocortin system. *Endocr. Rev.* **27**, 736–749 (2006).
6. Gao, Q. & Horvath, T.L. Neurobiology of feeding and energy expenditure. *Annu. Rev. Neurosci.* **30**, 367–398 (2007).
7. Halaas, J.L. *et al.* Physiological response to long-term peripheral and central leptin infusion in lean and obese mice. *Proc. Natl. Acad. Sci. USA* **94**, 8878–8883 (1997).
8. Bjørbaek, C., Elmquist, J.K., Frantz, J.D., Shoelson, S.E. & Flier, J.S. Identification of SOCS-3 as a potential mediator of central leptin resistance. *Mol. Cell* **1**, 619–625 (1998).
9. Horvath, T.L. *et al.* Synaptic input organization of the melanocortin system predicts diet-induced hypothalamic reactive gliosis and obesity. *Proc. Natl. Acad. Sci. USA* **107**, 14875–14880 (2010).
10. Pinto, S. *et al.* Rapid re-wiring of arcuate nucleus feeding circuits by leptin. *Science* **304**, 110–115 (2004).
11. Pal, R. & Sahu, A. Leptin signaling in the hypothalamus during chronic central leptin infusion. *Endocrinology* **144**, 3789–3798 (2003).
12. Leloup, C. *et al.* Mitochondrial reactive oxygen species are required for hypothalamic glucose sensing. *Diabetes* **55**, 2084–2090 (2006).
13. Benani, A. *et al.* Role for mitochondrial reactive oxygen species in brain lipid sensing: redox regulation of food intake. *Diabetes* **56**, 152–160 (2007).
14. Dikalov, S., Losik, T. & Arbiser, J.L. Honokiol is a potent scavenger of superoxide and peroxyl radicals. *Biochem. Pharmacol.* **76**, 589–596 (2008).
15. Parton, L.E. *et al.* Glucose sensing by POMC neurons regulates glucose homeostasis and is impaired in obesity. *Nature* **449**, 228–232 (2007).
16. Schrader, M. & Fahimi, H.D. Peroxisomes and oxidative stress. *Biochim. Biophys. Acta* **1763**, 1755–1766 (2006).
17. Gao, Q. *et al.* Anorexigenic estradiol mimics leptin's effect on re-wiring of melanocortin cells and Stat3 signaling in obese animals. *Nat. Med.* **13**, 89–94 (2007).
18. Green, S. PPAR: a mediator of peroxisome proliferator action. *Mutat. Res.* **333**, 101–109 (1995).
19. Bernardo, A. & Minghetti, L. PPAR-γ agonists as regulators of microglial activation and brain inflammation. *Curr. Pharm. Des.* **12**, 93–109 (2006).
20. Yu, X. *et al.* Activation of cerebral peroxisome proliferator–activated receptors γ exerts neuroprotection by inhibiting oxidative stress following pilocarpine-induced status epilepticus. *Brain Res.* **1200**, 146–158 (2008).
21. Thaler, J.P. & Schwartz, M.W. Minireview: Inflammation and obesity pathogenesis: the hypothalamus heats up. *Endocrinology* **151**, 4109–4115 (2010).
22. Cullingford, T.E. *et al.* Distribution of mRNAs encoding the peroxisome proliferator–activated receptor α, β, and γ and the retinoid X receptor α, β, and γ in rat central nervous system. *J. Neurochem.* **70**, 1366–1375 (1998).
23. Sarruf, D.A. *et al.* Expression of peroxisome proliferator-activated receptor-γ in key neuronal subsets regulating glucose metabolism and energy homeostasis. *Endocrinology* **150**, 707–712 (2009).
24. Kim, T.H. *et al.* Interrelationship between liver X receptor α, sterol regulatory element-binding protein-1c, peroxisome proliferator-activated receptor γ, and small heterodimer partner in the transcriptional regulation of glucokinase gene expression in liver. *J. Biol. Chem.* **284**, 15071–15083 (2009).

25. Belsham, D.D. *et al.* Ciliary neurotrophic factor recruitment of glucagon-like peptide-1 mediates neurogenesis, allowing immortalization of adult murine hypothalamic neurons. *FASEB J.* **23**, 4256–4265 (2009).
26. Poplawski, M.M. *et al.* Hypothalamic responses to fasting indicate metabolic reprogramming away from glycolysis toward lipid oxidation. *Endocrinology* **151**, 5206–5217 (2010).
27. Puri, V. *et al.* Cidea is associated with lipid droplets and insulin sensitivity in humans. *Proc. Natl. Acad. Sci. USA* **105**, 7833–7838 (2008).
28. Heid, H.W. *et al.* Adipophilin is a specific marker of lipid accumulation in diverse cell types and diseases. *Cell Tissue Res.* **294**, 309–321 (1998).
29. Kouidhi, S. *et al.* Peroxisome proliferator–activated receptor-γ (PPAR-γ) modulates hypothalamic Trh regulation *in vivo*. *Mol. Cell. Endocrinol.* **317**, 44–52 (2010).
30. Festuccia, W.T. *et al.* Peroxisome proliferator–activated receptor-γ–mediated positive energy balance in the rat is associated with reduced sympathetic drive to adipose tissues and thyroid status. *Endocrinology* **149**, 2121–2130 (2008).
31. Lu, M. *et al.* Brain PPAR-γ promotes obesity and is required for the insulin-sensitizing effect of thiazolidinediones. *Nat. Med.* **17**, 618–622 (2011).
32. Ryan, K.K. *et al.* A role for central nervous system PPAR-γ in the regulation of energy balance. *Nat. Med.* **17**, 623–626 (2011).
33. Takahashi, K.A. & Cone, R.D. Fasting induces a large, leptin-dependent increase in the intrinsic action potential frequency of orexigenic arcuate nucleus neuropeptide Y/Agouti-related protein neurons. *Endocrinology* **2005**, 1043–1047 (2005).
34. Hoepfner, D. *et al.* Contribution of the endoplasmic reticulum to peroxisome formation. *Cell* **122**, 85–95 (2005).
35. Tabak, H.F. *et al.* Formation of peroxisomes: present and past. *Biochim. Biophys. Acta* **1763**, 1647–1654 (2006).
36. Ozcan, L. *et al.* Endoplasmic reticulum stress plays a central role in development of leptin resistance. *Cell Metab.* **9**, 35–51 (2009).
37. Finkel, T. & Holbrook, N.J. Oxidants, oxidative stress and the biology of ageing. *Nature* **408**, 239–247 (2000).

ONLINE METHODS

Mice and diet. All procedures described below have been approved by the Institutional Animal Care and Use Committee of Yale University. Mice were kept under standard laboratory conditions with free access to food and water. All experiments described below were conducted on either NPY-GFP, POMC-GFP, UCP2-knockout or *ob*/*ob* male and female mice on a C57BL/6 background[1,10]. Regular diet: Purina Lab Chow #5001 (Ralston Purina). High-fat diet: Rodent Chow #D12451 (Research Diets). High-fat diet was fed for 12 weeks starting at 6 weeks of age. Daily food intake was assessed in individually housed mice.

Lateral ventricle canullation. A sterile guide cannula 9 mm in length was implanted into the lateral brain ventricle (0.3 mm posterior and 1 mm lateral relative to bregma and 3 mm below the surface of the skull). The position of the cannula was verified at the end of the experiments by dye administration before the mice were killed.

Honokiol or its vehicle was administered i.c.v. at 9:00 a.m., and food intake was measured for the subsequent 8 s. We injected a 2-µl stock solution of 37.6 mM honokiol (Wako Chemical Company) dissolved in 100 µl ethanol that was further dissolved in 1 ml of intralipid [14].

We injected 5 µM H_2O_2 in 2 µl saline i.c.v. into lean mice. Saline was used as vehicle. Rebound feeding after a 16-h fast was analyzed. The same dose of H_2O_2 (and vehicle) was also injected i.c.v. to DIO female mice (n = 6) three times, the injections 8 h apart. Daily food intake was measured before and after the treatment. In a subset of these mice, we injected intraperitoneally 3 µg per g body weight recombinant leptin dissolved in PBS. Mice were killed 45 minutes later and processed for pStat3 (Cell Signaling Technology) and POMC immunolabeling.

PPAR-γ agonist (rosiglitazone; Cayman Chemical Company) and antagonist GW9662 (2-chloro-5-nitrobenzanilide; Cayman Chemical Company) and dissolved in DMSO in saline (1:3 ratio). We injected 0.5 mg of rosiglitazone or GW9662 in 2 µl of vehicle i.c.v. twice daily (9:00 a.m. and 6:00 p.m.) for 7 d.

A subset of females (n = 6), after the fifth day of rosiglitazone treatment, received H_2O_2 (5 µM H_2O_2 in 2 µl) or saline i.c.v. in association with rosiglitazone treatment at days 6 and 7. In another subset of females (n = 6), after the fifth day of GW9662 treatment, honokiol or its vehicle was also administered in association with the GW9662 treatments at days 6 and 7. Daily food intake was monitored and analyzed at days 5 and 7 in all groups.

c-fos staining in NPY and POMC neurons. NPY-GFP or POMC-GFP and mice were treated with honokiol or vehicle and rapidly perfused 1 h later. c-fos immunofluorescence staining was carried out as described previously[17].

Electrophysiology. Whole-cell recording was made in POMC-GFP neurons in the arcuate nucleus of the hypothalamus as described previously[24]. For firin=rate analysis in older DIO mice, we used extracellular recordings from GFP=labeled NPY or POMC cells.

Dihydroethidium. ROS levels in identified POMC-GFP neurons were measured by injecting DHE (Invitrogen) as described previously[1].

Leptin treatment of *ob*/*ob* mice. Alzet 2002 mini-osmotic pumps (Alza) were implanted subcutaneously into 8-week-old obese transgenic mice under anesthesia[10]. Pumps were filled with either PBS (control) or 420 ng μl^{-1} leptin (Amgen). Pumps were incubated the night before at 37 °C in sterile 0.9% NaCl. Mice and food were weighed daily at midday. Mice were killed at 48 h after implantation and 3 h after DHE injections.

Measurement of leptin. Blood levels of leptin were measured by ELISA using a commercially available Leptin Elisa Kit (Millipore).

Mitochondria and peroxisome counts. Mice were perfused, and their brains were processed for GFP immunolabeling for electron microscopic examination as described previously[1].

Cell culture. The POMC- and AgRP-expressing hypothalamic neuronal cell lines were cultured as previously described[25]. The culture medium contained 0.5 mM glucose with or without exposure to 10 µM pioglitazone (Sigma) for 24 h.

Real-time PCR. RNA from hypothalamus or cultures was isolated with the RNeasy Micro Kit (Qiagen) and reverse transcribed to cDNA using MultiScribe Reverse Transcriptase (Applied Biosystems). Quantitative PCR was performed with SYBR Green I Master or Probe Master (Applied Biosystems) using the LightCycler 480 Real-time PCR system (Roche).

PPAR-γ neuron-specific knockout mice. Mice with neuron-specific PPAR-γ knockout generated in the laboratory of J.M. Olefsky as described recently[31]. Sections from 14-week-old mice with or without 2 weeks on high-fat diet were processed for catalase immunocytochemistry.

Statistical analyses. All data are expressed as the mean ± s.e.m. The means between two groups were analysed by Student's t test and between more than two groups and two genotypes by two-way analysis of variance followed by Bonferroni *post hoc* tests unless otherwise stated. Significance was taken at $P < 0.05$.

doi:10.1038/nm.2421

Corrigendum: Peroxisome proliferation–associated control of reactive oxygen species sets melanocortin tone and feeding in diet-induced obesity

Sabrina Diano, Zhong-Wu Liu, Jin Kwon Jeong, Marcelo O Dietrich, Hai-Bin Ruan, Esther Kim, Shigetomo Suyama, Kaitlin Kelly, Erika Gyengesi, Jack L Arbiser, Denise D Belsham, David A Sarruf, Michael W Schwartz, Anton M Bennett, Marya Shanabrough, Charles V Mobbs, Xiaoyong Yang, Xiao-Bing Gao & Tamas L Horvath

***Nat. Med.* 17, 1121–1127 (2011); published online 28 August 2011; corrected after print 16 September 2011**

In the version of this article initially published, the top electrophysiological trace of Figure 4a was inadvertently repeated as the bottom electrophysiological trace of Figure 4b. The scientific conclusions of the paper were not affected by the error. The error has been corrected in the HTML and PDF versions of the article.

Supplementary Figure 1

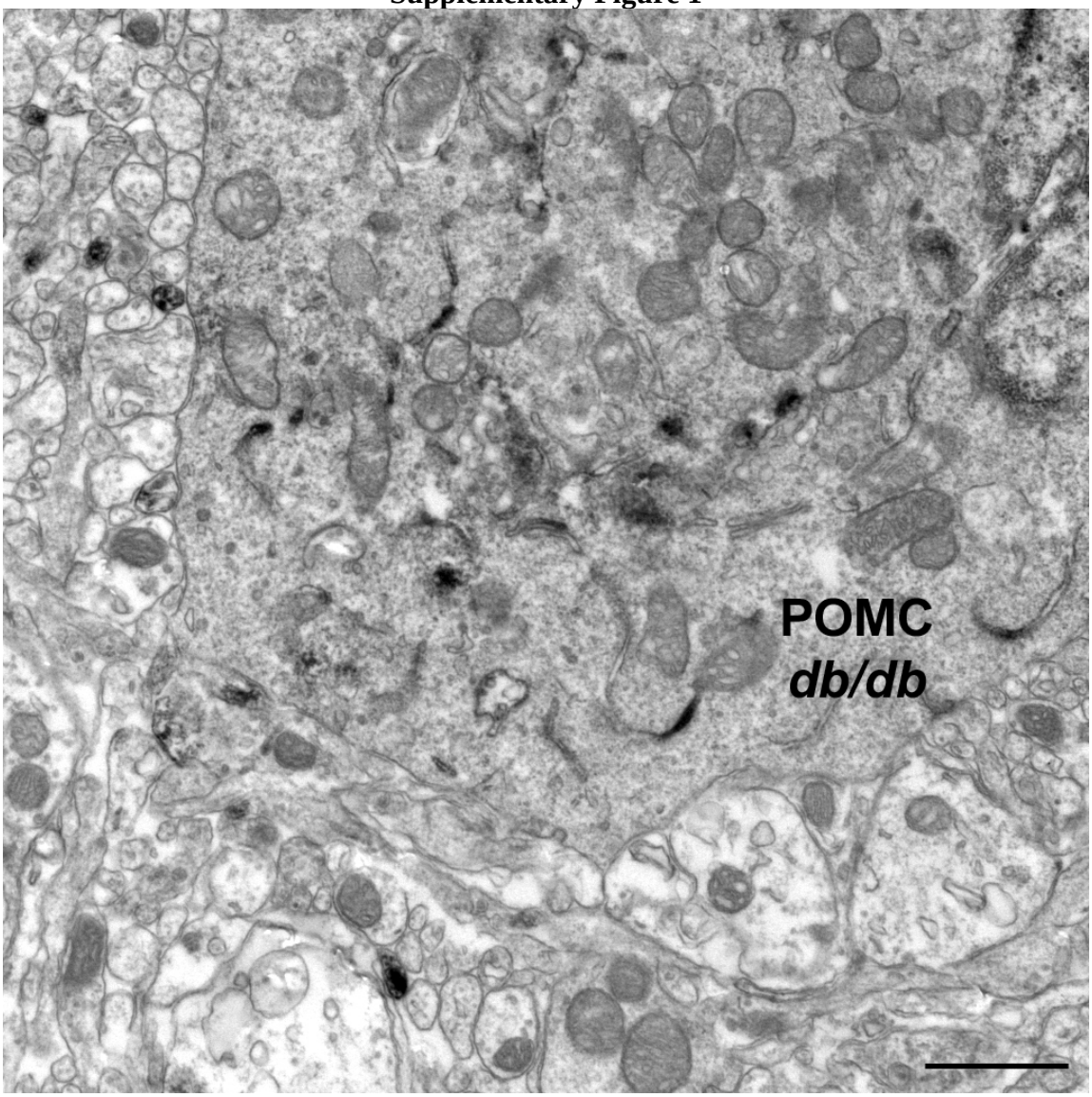

Supplementary Fig. 1

Electron micrograph of a POMC perikarion from a *db/db* mouse. Note the lack of peroxisome presence in this cell. Bar scale represents 1 μm.

Supplementary Figure 2

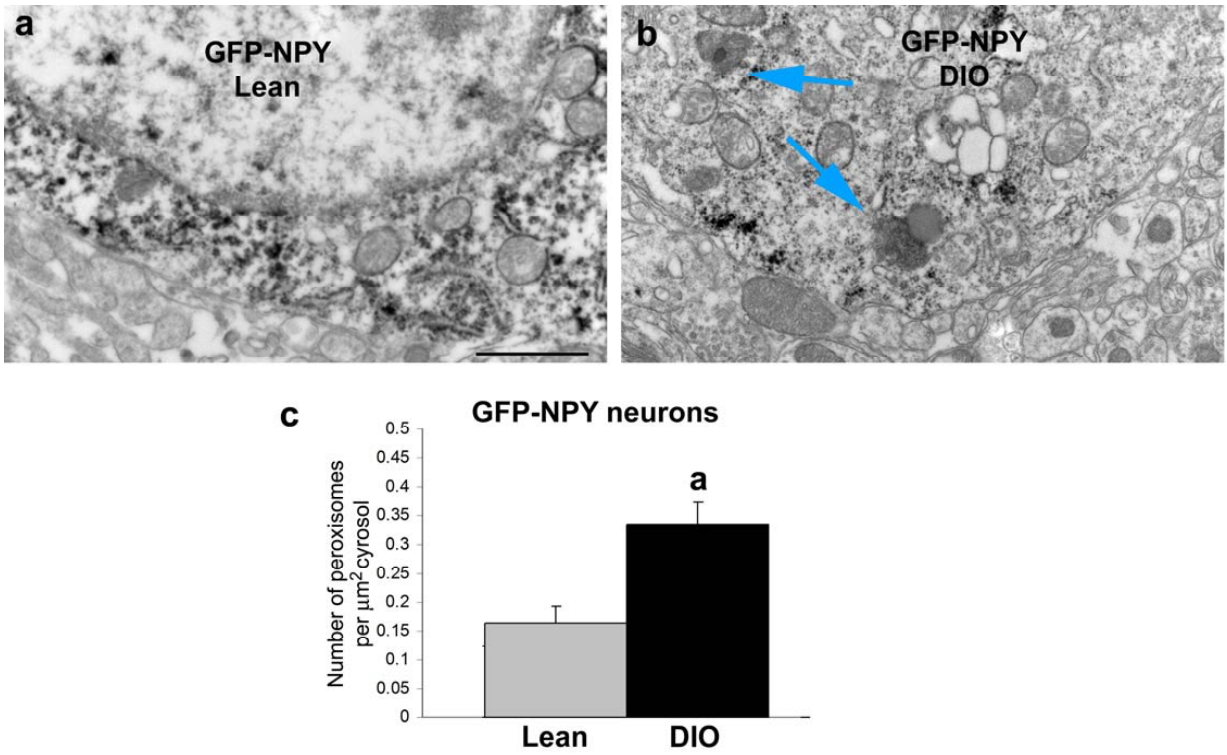

Supplementary Fig. 2

a, b: electron micrograps of NPY-GFP perikarya from a lean (**a**) and a DIO animal (**b**). Peroxisomes (blue arrows on **b**) are readily visible in DIO NPY neurons. Bar scale on a represent 1 µm for panels **a** and **b**.

c: Quantification of peroxisome number showed significantly higher number of peroxisomes in arcuate NPY neurons of DIO mice compared to lean controls. * indicate $p<0.05$.

Supplementary Figure 3

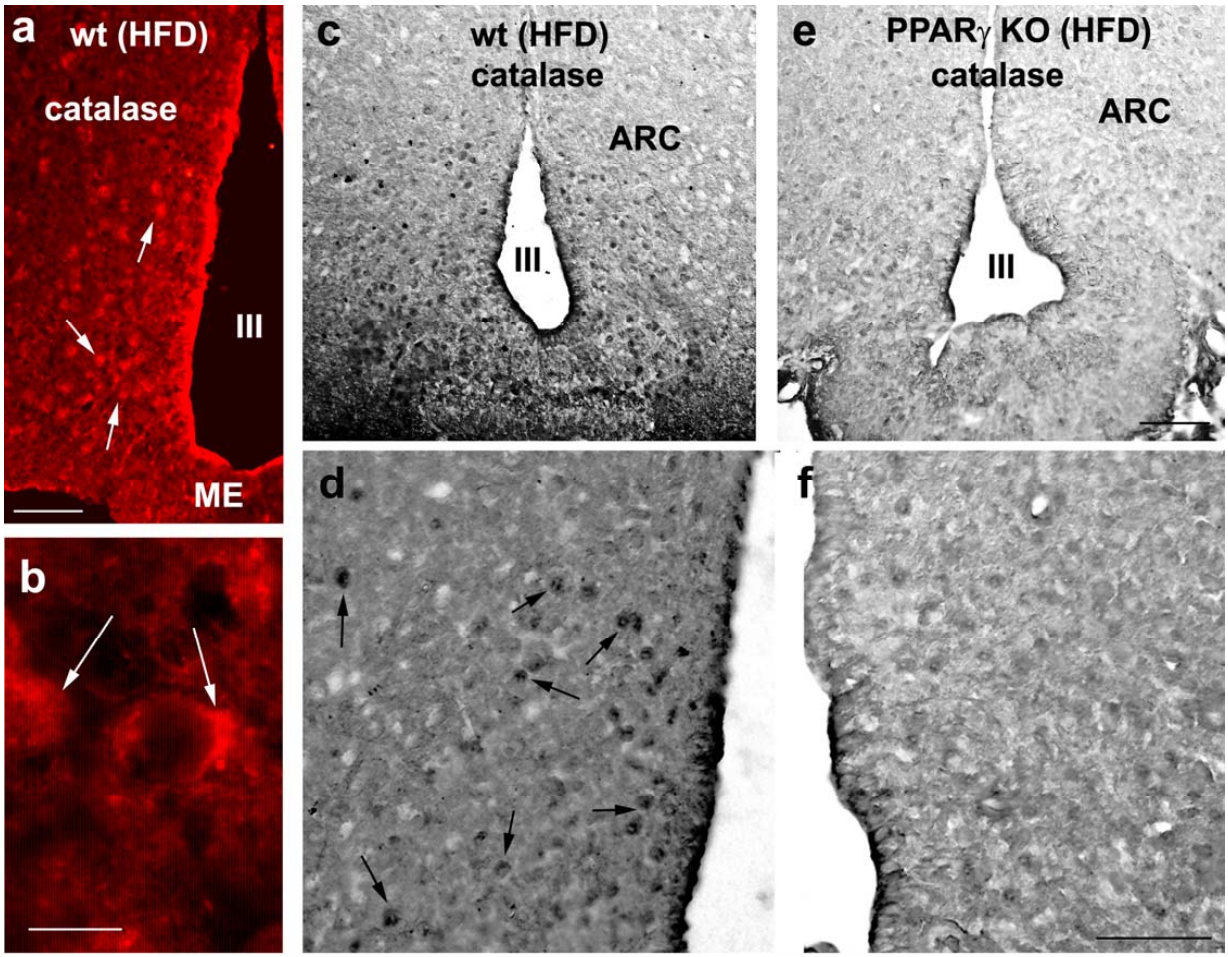

Supplementary Fig. 3

a,b: immunofluorescence labeling for catalase revealed labeled cells in the hypothalamus of wild type animals on high fat diet. Arrows point to labeld cells. On **b**, the subcellular labeling of catalase indicate punctuate cytoplasmic labeling. Bar scale on **a** indicates 100 μm. Bar scale on **b** indicate 10 μm.

c-f: Immunolabeleing with avidin-biotin peroxidase revelaes numerous catalase immunoporitive cells of the arcuate nucleus of wild type mice on high fat diet (**c** and **d**), while catalase immunolabeleing was substantially lower in the arcuate nucleus of neuron-specifc PPARγ knockout mice (**e** and **f**). Bar scales on **e** represents 100 μm for panels **c** and **e**, and, on **f**, it represents 100 μm for panels **d** and **f**.

Supplementary Figure 4

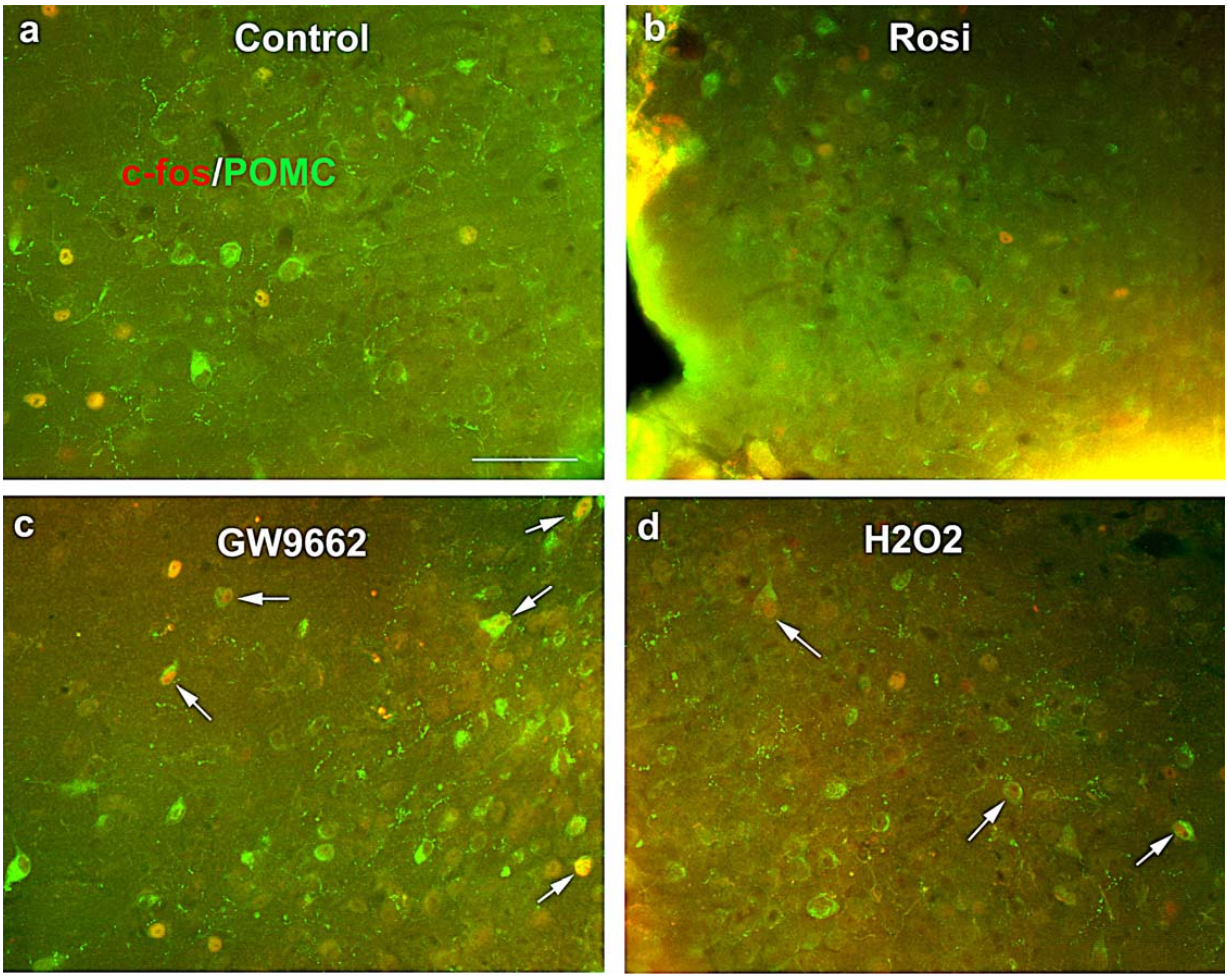

Supplementary Fig. 4

a-d: double immunofluorescence labeling for c-fos (red) and POMC (green) from control DIO (**a**), rosigliatzone-treated (**b**), GW9662-treated (**c**) and H2O2-treated (**d**) high fat-fed animals. Bar scale on **a** represents 100 μm for panels **a-d**.

Supplementary Figure 5

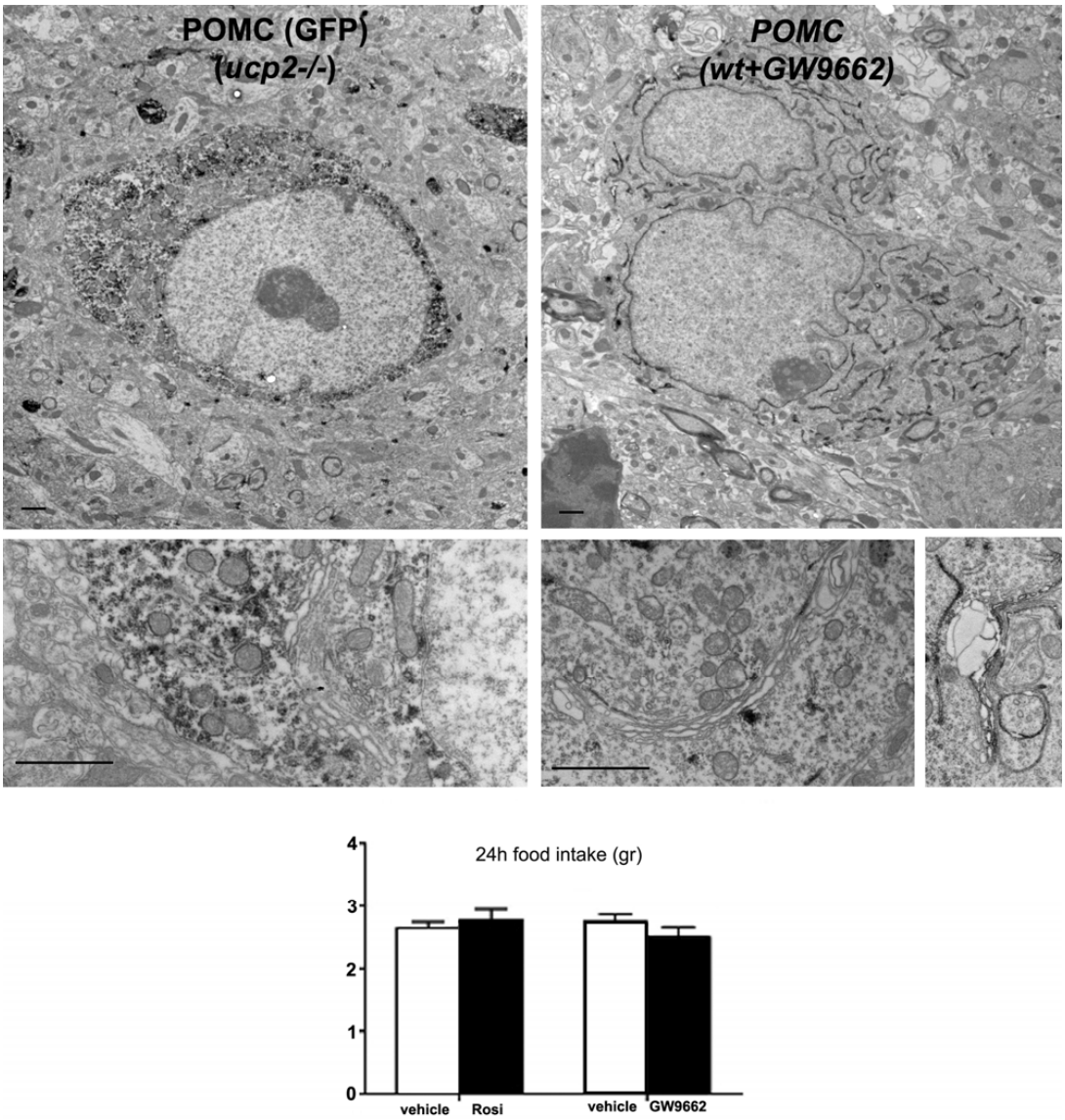

Supplementary Fig. 5

Electron migrographs showing a POMC neuron (GFP-POMC) from a UCP2 knockout mouse (left panels) and from a DIO mouse (immunolabaled for POMC) treated with GW9662 (right panels). Note the similarity in cell integrity, abundance of endoplasmic reticulum (lower panels) and low incidence of peroxisomes. Lower right panel shows an endoplasmic reticulum with lipid accumulation. Peroxisomes would bud off the endoplasmic reticulum in response to lipid overload. Bar scales indicate 1 μm. Bar graphs show that neirher rosiglitazone nor GW9662 affected feeding in UCP2 knockout mice. Bar graphs show lack of effect of either rosiglitazone or GW9662 on daily food intake of UCP2 knockout mice.

Anexo A-5. Wired for Hunger: The Brain and Obesity and Anorexia Nervosa: A Mortal Clash between Reward and Hunger. Cerebrum 2010. Dana Foundation.

Capítulo publicado no livro intitulado *Cerebrum* 2010 (Dana Foundation).
Este livro tem como objetivo difundir a pesquisa cientifica e o estudo das neurociências para o público geral.

The Brain and Obesity

By Marcelo O. Dietrich, M.D., and Tamas L. Horvath, D.V.M., Ph.D.

For most of human history, food was not available at all times; storing extra energy helped ensure survival. Humans thus evolved to eat whenever food is available—an approach that, in today's world of food ubiquity, contributes to widespread obesity. Now, researchers are uncovering the brain circuitry responsible for this default "eat" message. Marcelo Dietrich and Tamas Horvath tell the story of false starts and measured successes in obesity research. They propose that developing successful obesity therapy may require combining drug therapy with psychological or psychiatric approaches, as well as exercise. In the sidebar, they examine the antithesis of obesity: anorexia nervosa.

In 1994, a scientific finding shot through the research world and then raced far beyond, raising wonder and, particularly among discouraged people struggling with severe weight problems, great hope. The report described a molecule, leptin (from the Greek *leptos*, meaning thin), present in Humans and other animals, that acted to powerfully influence eating in experiments with obese mice in the laboratory (Zhang et al., 1994). With good reason, experts speculated freely about defeating obesity, giving appropriate cautions about the need for more research, and the discussion filled the airwaves and pages of newspapers and magazines for months. Had the Internet been as widespread then as now, it too would have spilled over. But then leptin was gone, dethroned as the "next big thing" by the further research that failed to demonstrate an effect in people. Disappointment and frustration returned for those who had hoped leptin would be salvation.

But the breakthrough and subsequent experiments with leptin did not leave scientists disappointed. Far from it: They had turned an essential corner on the road to understanding the brain and obesity, and much has been discovered in the fifteen years since. In this article, we will explain what we now understand about one of the master controllers of this very intricate brain-body relationship. We also offer a surprise ending—on a pessimistic note for some, but then maybe not.

Understanding “energy balance”

When thinking about obesity, it is important to remember that consuming food to store energy is fundamental for survival—and that nature has done all it can to thwart interference with this mechanism. It is also important to keep in mind that in our first few millions of years, daily life was very different from our modern concept of society, and the biological underpinning and forces that shape our current way of being have diverged very little from other living creatures. Thus, for us and them, much of development has been about preserving and synchronizing opportunities to obtain and consume food to maintain a precise balance between food intake and energy expenditure (energy balance).

In the wild, sources of food were few and widely dispersed. Early humans had to migrate to find food and safe places to rest. Because agriculture developed only later on the evolutionary scale (by most estimates, only 10,000 years ago) this migratory behavior required high levels of daily activity. Additionally, because food was scarce, it was essential for us to develop a biological system to store energy. In humans, the largest depot of stored energy is our fat, specifically, the white adipose tissue. Thus, in the wild, the struggle for life was about seeking, consuming and storing food, and adaptations of brain and body were essential to our thriving in these environmental conditions.

On the other hand, in modern societies humans can obtain food on demand and in many instances have low activity levels (low energy expenditure) resulting in “positive” energy balance—we consume more calories than we burn. This chronic, positive energy balance leads to obesity (accumulation of fat tissue) and its associated problems including diabetes, cardiovascular disorders, cancer and neurodegenerative diseases. Equally striking is that in the last few decades, not only have adults been affected by this, but children have become fat at an alarming rate, making childhood obesity a major health issue for most societies (Cali & Caprio, 2008). Consequently, we are seeing an epidemic of “positive energy balance.”

The role of the brain in maintaining energy balance

The coordination of food intake and energy expenditure (energy balance) is regulated by several brain “nuclei,” identifiable groups of neurons functioning together in

specific brain areas. Some of these nuclei are housed within the hypothalamus, a structure that lies just above the brain-stem and helps to control essential processes such as metabolism and sleep-wake states, body temperature, blood pressure, hunger and thirst and, through connections to other brain circuits, helps regulate brain activities. The hypothalamus is one of the first regions to have developed during evolution.

One of the nuclei helping coordinate food intake and energy expenditure is in the most basal (lowest) part of the hypothalamus and has the form of an arc, giving it its name, the arcuate nucleus (hereafter, Arc). Researchers have focused their attention on the Arc in recent decades due to its singular role in energy balance and because it is located in one of the few areas in the brain that lacks the blood-brain barrier, the tight-meshed cell structure of blood-vessel walls that keeps most blood-borne molecules from entering the brain.

Within the Arc is the heart of what is believed to be the main system for regulating food intake, the melanocortin hormone system. This system senses substances coming from the blood to regulate food intake and energy expenditure. For example, during a meal, different substances are released in the blood and will enter the Arc and signal to the melanocortin system to end the meal. To sense these substances, the melanocortin system in the Arc is composed of two side-by-side groups of specialized neurons with opposing actions. One neuronal group produces melanocortin-stimulating hormones (MSH) that suppress appetite, while the other neuronal group produces molecules that inhibit these hormones' actions and stimulate appetite.

More technically, the first neuronal group (suppressing appetite) produces proopiomelanocortin (POMC), which ultimately produces large peptides that are broken down by enzymes into small peptides including the melanocortin-stimulating hormones (MSH). These hormones bind to and activate melanocortin receptors on neurons that will signal the rest of the brain that food is not needed. Adjacent to the POMC cells is the second neuronal group, appetite-stimulating neurons, which produce a pair of molecules— neuropeptide Y (NPY) and agouti-related protein (AgRP). These oppose the action of MSH by binding to the same melanocortin

receptors and inhibiting their activity. The interaction between NPY/AgRP (appetite stimulating) and POMC (appetite inhibiting) neurons will dictate food intake.

Moreover, the brain has a redundant system for promoting feeding. Appetite-stimulating NPY/AgRP neurons also produce the chemical neurotransmitter GABA, which inhibits other neurons, including the POMC neurons. During periods of negative energy balance the appetite stimulating NPY/AgRP neurons are activated and inhibit MSH, by limiting both its production by POMC neurons and its activity on melanocortin receptor expressing cells.

Through this network, then, the brain has a redundant mechanism to promote feeding: (1) by directly prompting food intake by the appetite stimulating molecules NPY and AgRP; and (2) by NPY/AgRP neurons sending signals to inhibit POMC neurons from suppressing appetite. Strikingly, even though this predominant activity of NPY/AgRP neurons is driven by negative energy balance – that is, the need for food - its activity over POMC neurons seems to be the default of the brain wiring. In other words, our brain has the default setting “I am hungry” and the imprint of this setting is located in the Arc through the communication between these two groups of neurons.

This system had profound evolutionary consequences. The redundant mechanism to promote feeding aided in survival when food was scarce, yet whenever food was obtainable, the default wiring of the brain signaled to induce food intake, even when the energy stores (fat tissue) were sufficient to maintain the energy needed for the body’s metabolism. Thus, in our modern society, where food is available at our discretion, this default wiring will signal us to keep eating. This mechanism may be a key contributor to the current worldwide epidemic of obesity.

Enter Leptin and Visions of Treatment

Because the Arc is located low in the brain and close to an area that lacks the blood-brain barrier, it is an important sensor for blood-borne signals. More than a century ago, the great British neurophysiologist, Sir Charles S. Sherrington, suggested that factors arising from the blood were regulating food intake (Sherrington, 1900). Decades later, scientists discovered that a naturally obese mouse (named ob/ob, for its mutant genes) became leaner if it received some blood from a naturally lean mouse

(Coleman & Hummel, 1969; Coleman, 1973; for review, Coleman, 1982). These experiments provided convincing data that something about the blood was driving the massive obese physical characteristics of the ob/ob mice. Since then, growing evidence has shown that the tissues in the brain and the rest of the body crosstalk, almost certainly by the way of the bloodstream, to signal and sense stimuli that regulate food intake (Lenard & Berthoud, 2008).

In 1994, research led by Jeffrey Friedman of Rockefeller University discovered that these obese mice lacked leptin, a hormone produced by fat tissue. Later studies found that leptin enters the brain and signals the Arc neurons to decrease food intake, inducing satiety (banks et al., 1996; Satoh et al., 1997). Then in 2004, innovative research revealed that leptin was able to induce a re-wiring of NPY/AgRP and POMC cells in the Arc in such a way that the network changes from its default signaling of hunger and adapts to a positive energy balance, decreasing appetite (Pinto et al., 2004).

Yet, administering leptin to obese patients to decrease appetite proved ineffective. Only those few individuals with a rare genetic type of obesity (due to mutations in the gene that produces leptin, resembling the ob/ob mice) were cured by leptin treatment. Further investigation proved that, with the exception of patients with this rare genetic mutation, the brain of obese people somehow develop a resistance to leptin, and the cells in the brain stop sensing the levels of leptin in the blood (Scarpace & Zhang, 2009). Thus, in the great majority of the cases of obesity, the brains of these people cannot sense the levels of leptin, so using it to treat obesity is inefficient from the start. Understanding the causes of leptin resistance in obese people may help researchers identify new targets for treatment.

Finding ways to heighten tissue sensitivity to hormone signals is difficult but not impossible, as diabetes management shows. People with type 2 diabetes are treated with compounds to increase their sensitivity to insulin. We hope for the development of a similar drug treatment capable of increasing the central (brain) sensitivity to leptin in obese people. Investigation into such new compounds is still in its infancy because we lack this knowledge.

Researchers have found, in addition to leptin, several other hormones and molecules that regulate food intake by acting directly in the brain. The gastrointestinal system, for instance, has been a target of intense research, because scientists believe it releases many hormones to signal a negative or positive energy balance. Investigators have taken a particular interest in the finding that the gut, mainly the stomach, produces an important appetite-stimulating molecule, called ghrelin, which also acts in the hypothalamus to prompt eating. Ghrelin was found to activate the NPY/AgRP appetite-stimulating neurons in response to negative energy balance (as for example, during fasting or keeping a low-calorie diet) (Shintani et al., 2001; Lawrance et al., 2002; Wang et al., 2002).

Studies investigating how ghrelin affects the activity of NPY/AgRP neurons in the Arc have excited researchers by showing a cascade of events in these cells that end up stimulating food intake (Andrews et al., 2008). This sequence of events suggests several points of possible intervention for new therapies to treat energy balance disorders, mainly obesity. First in this cascade, ghrelin released by the gut enters the brain and stimulates a receptor (one that prompts growth hormone secretion) on the NPY/AgRP cells, increasing their activity. At the same time and related to this, the mitochondrial machinery in the NPY/AgRP cells also increases its activity to deliver enough of the high-energy molecule, ATP, for cell metabolism. The enhanced mitochondrial activity also increases the production of harmful oxygen molecules derived from mitochondrial respiration. These harmful molecules are free radicals that react with other molecules inside the cell and promote cell damage (for example, damaging the DNA). To protect the cell against such oxidative damage, the NPY/AgRP cells call on another mechanism to buffer these molecules, by activating the mitochondria's uncoupling proteins. With appropriate buffering of free radicals by the uncoupling proteins, the NPY/AgRP cells can maintain high firing rates, thereby stimulating food intake.

Understanding this process may affect more than obesity research; it opens many new lines of investigation to target cellular pathways to regulate energy balance, for example by aiming at uncoupling proteins or the cells' methods for buffering free radicals. Besides suggesting an approach to eating problems, the possibility that free radicals play a role in modulating appetite and regulating energy homeostasis

provides a promising avenue for the development of treatments for many diseases related to metabolism. Researchers have developed several compounds that act as antioxidants in the past few years that now can be used to test this promising theory.

Moreover, molecules involved in regulating food uptake, in addition to leptin and ghrelin, have been identified. We won't describe them, but want to list some here as a reminder of how intricately evolution built this regulatory network. For example, the gut has been shown to also produce eating-related molecules including CCK, PYY, GLP1, NAPEs, and many others with equally daunting acronyms. Adipose tissue produces, in addition to leptin, immune system molecules with a role in diabetes and obesity: IL-6, adiponectin, and resistin, to cite just a few. Lastly, classic regulatory hormones like the glucocorticoids produced by the adrenal glands and thyroid hormones also control food intake.

The feasibility of new pharmacological therapies to treat obesity

In the past two decades, researchers have put forth a tremendous effort to understand the biological abnormalities involved in obesity and to describe cellular pathways as possible targets for pharmaceutical treatments. The brevity of leptin's shining moment dashed the hope that a single molecule could eventually serve to treat obese patients by counteracting their positive energy balance. This may be due to the different types of fuel utilization and overall metabolic consequences of the activity of the NPY/AgRP versus POMC neurons may be to blame. The firing of the NPY/AgRP neurons is driven by fatty acids while that of the POMC cells is driven by glucose, with contrasting consequences. The nature of fuel utilization on these two groups of neurons involved in the regulation of energy balance provides evidence that the NPY/AgRP neurons, which promote feelings of hunger and acting to eat in response to negative energy balance, are a priority for survival—an idea supported by these neurons' aggressiveness in silencing the POMC cells.

Add this dominance—not to mention default status—of the "get something to eat" component of the melanocortin system to the evolutionarily programmed rapid adaptability of brain circuits in response to the changing metabolic environment and you can understand why it is a daunting and futile, if not counterproductive, task to attempt to develop a pill that will keep people from feeling hungry.

Although a one-pill solution to obesity is unlikely, several new avenues raise hope for new treatments of this widespread medical condition. We believe that the first important point in managing obesity is to integrate disciplines. Based on the knowledge of the neurobiological basis of food intake a treatment for obese people could be designed as a mixture of compounds given at appropriate times. However, because of the influence of higher brain functions on the regulation of appetite—for example, the influence of the smell, taste, and appearance of food in the stimulation of food intake—a psychological approach to manage obesity should be added to the treatment.

Indeed, we believe that obesity, like other disorders of energy metabolism (see "Anorexia Nervosa: a Mortal Clash between Reward and Hunger"), should also be treated as a psychological/psychiatric disorder. Additionally, because obesity involves not only elevated energy intake but also decreased energy expenditure, an exercise program is mandatory to help in the treatment of obesity. Finally, because obesity develops over many years, obese patients should expect a similar time scale to return to their ideal body weight after starting treatment.

Key references:

Andrews ZB, Liu ZW, Walllingford N, Erion DM, Borok E, Friedman JM, Tschöp MH,Shanabrough M, Cline G, Shulman GI, Coppola A, Gao XB, Horvath TL, Diano S. UCP2 mediates ghrelin's action on NPY/AgRP neurons by lowering free radicals. Nature. 2008 Aug 14;454(7206):846-51.

Banks WA, Kastin AJ, Huang W, Jaspan JB, Maness LM. Leptin enters the brain by a saturable system independent of insulin. Peptides. 1996;17(2):305-11.

Cali AM, Caprio S. Obesity in children and adolescents. J Clin Endocrinol Metab. 2008 Nov;93(11 Suppl 1):S31-6.

Coleman, D.L. (1973) Effects of parabiosis of obese with diabetes and normal mice. Diabetologia, 9, 294-298.

Coleman, D.L. (1982) Diabetes-obesity syndromes in mice. Diabetes, 31, 1-6.

Coleman, D.L. & Hummel, K.P. (1969) Effects of parabiosis of normal with genetically diabetic mice. Am J Physiol, 217, 1298-1304.

Lawrence CB, Snape AC, Baudoin FM, Luckman SM. Acute central ghrelin and GH secretagogues induce feeding and activate brain appetite centers. Endocrinology. 2002 Jan;143(1):155-62. PubMed PMID: 11751604.

Lenard NR, Berthoud HR. Central and peripheral regulation of food intake and physical activity: pathways and genes. Obesity (Silver Spring). 2008 Dec;16 Suppl 3:S11-22.

Pinto, S., Roseberry, A.G., Liu, H., Diano, S., Shanabrough, M., Cai, X., Friedman, J.M. & Horvath, T.L. (2004) Rapid rewiring of arcuate nucleus feeding circuits by leptin. Science, 304, 110-115.

Satoh N, Ogawa Y, Katsuura G, Hayase M, Tsuji T, Imagawa K, Yoshimasa Y, Nishi S, Hosoda K, Nakao K. The arcuate nucleus as a primary site of satiety effect of leptin in rats. Neurosci Lett. 1997 Mar 21;224(3):149-52.

Scarpace PJ, Zhang Y. Leptin resistance: a prediposing factor for diet-induced obesity. Am J Physiol Regul Integr Comp Physiol. 2009 Mar;296(3):R493-500.

Sherrington, C. Sir. Cutaneous Sensation. In Textbook of Physiology (ed. Sharpey-Schaefer, E.A.) 920-1001 (Pentland, Edinburgh, 1900).

Shintani M, Ogawa Y, Ebihara K, Aizawa-Abe M, Miyanaga F, Takaya K, Hayashi T, Inoue G, Hosoda K, Kojima M, Kangawa K, Nakao K. Ghrelin, an endogenous growth hormone secretagogue, is a novel orexigenic peptide that antagonizes leptin action through the activation of hypothalamic neuropeptide Y/Y1 receptor pathway. Diabetes. 2001 Feb;50(2):227-32.

Wang L, Saint-Pierre DH, Taché Y. Peripheral ghrelin selectively increases Fos expression in neuropeptide Y - synthesizing neurons in mouse hypothalamic arcuate nucleus. Neurosci Lett. 2002 May 31;325(1):47-51.

Zhang Y, Proenca R, Maffei M, Barone M, Leopold L, Friedman JM. Positional cloning of the mouse obese gene and its human homologue. Nature, 1994, 372(6505):425-32.

Anorexia nervosa: a mortal clash between reward and hunger

The integration of metabolic signals in the hypothalamus is core to the control of appetite, but the higher brain centers (both cognitive and emotional) also influence "energy balance." The classic cognitive systems associated with taste, smell, visual cues, palatability and psychological factors can override the homeostatic control of food intake tipping the balance that otherwise would be maintained by the hypothalamus's circuits for regulating hunger and satiety. In Western societies where food is highly palatable, rich in energy (calories) and extensively marketed, the influence of the non-homeostatic regulators becomes even more important in understanding the processes involved in disorders of energy balance.

We believe that few disorders suggest this power of the brain's cognitive circuitry more clearly than anorexia nervosa, a psychiatric disorder often characterized by extreme undereating, body weight loss, hyperactivity, and hypothermia. Compared with other psychiatric conditions, this disorder has the highest mortality rate. It is our hypothesis that, in anorexia nervosa, the brain's ancient evolutionary wiring for adapting happily to low food availability is inappropriately activated and finds itself in a life-threatening battle with other brain signals demanding action to obtain nourishment.

One clue to the intensity of this clash is the elevated level of physical activity in patients with this condition, a symptom that has been reported for more than one hundred years. Several studies have found a relationship between obsessive–compulsive characteristics and exercise frequency in women with strenuous daily exercise routines and hospitalized female anorexia nervosa patients (Davis & Kaptein, 2006). In the patient group, preoccupation with weight was associated with the frequency of exercising and pathological attitudes towards exercise. Addictive and obsessive–compulsive personalities contributed to excessive exercise because of the influence of obligatory/pathological ideas about exercise. Among anorexia nervosa patients, those who exercise excessively have more bulimic symptoms, higher levels of general psychopathology about eating and a greater degree of body dissatisfaction, anxiety, somatization, depression and irritability (Davis & Kaptein, 2006).

Mental alertness and continued normal to high activity levels despite insufficient nutrition and weight loss are commonly viewed as being relatively unique to anorexia nervosa patients as compared with individuals with semi-starvation due to other causes such as illness, chemotherapy or famine. The most plausible explanation for both the alertness and the activity is activation of evolutionarily old circuitry leading to reward upon reduced energy intake.

A final clue is another characteristic of anorexia patients: 90 percent are women, mainly in their late teens. This leads us to propose that a cellular mechanism, in association with the changing hormonal milieu that is characteristic of anorexia nervosa patients, unifies and orchestrates activation of key brain circuits, which in turn leads to the behavioral and endocrine manifestation of anorexia nervosa. Our hypothesis is that in anorexia nervosa, the critical interaction that occurs between shifting levels of circulating hormones— specifically ghrelin, leptin and estradiol— alters key groups of neurons, and these together bring about sex-specific structural and functional changes in particular circuits of the midbrain that transmit the chemical dopamine, as well as in the prefrontal cortex and hypothalamus, to promote reward-like behavioral shifts.

We further hypothesize that anorexia nervosa could be reversed by either eliminating ghrelin signaling or suppressing the number of available long chain free fatty acids in the brain. These acids are used as an energy substrate by neuronal cells that are normally activated by ghrelin, thus their elimination would silence the ghrelin-activated neuronal population. Patients who receive controlled leptin and estrogen replacement therapy also might see their anorexic symptoms diminish. Moreover, we predict that if either or both estradiol and leptin levels are maintained by treatment during the initial phase of disease, at-risk patients will be less likely to progress to anorexia nervosa.

Key references

Davis C, Kaptein S. Anorexia nervosa with excessive exercise: a phenotype with close links to obsessive-compulsive disorder. Psychiatry Res. 2006 Jun 15;142(2-3):209-17.

Anexo A-6. Neural regulation of food intake and energy balance

Publicação especial do periódico *Nature Reviews Neuroscience* na forma de um pôster acessível na internet, objetivando educação e divulgação da neurociência básica para um público não especialista.

Anexo A-6. Neural regulation of food intake and energy balance

Publicação especial do periódico *Nature Reviews Neuroscience* na forma de um pôster acessível na internet, objetivando educação e divulgação da neurociência básica para um público não especialista.

nature REVIEWS
NEUROSCIENCE

Neural regulation of food intake and energy balance

Marcelo O. Dietrich and Tamas L. Horvath

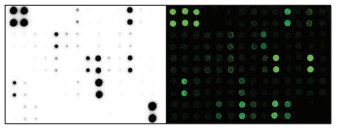

Obesity has reached epidemic proportions worldwide, and the economic cost of treating its health consequences has been estimated at more than US$100 billion in the United States alone. Research efforts are aimed at increasing our understanding of how the brain regulates food intake to identify potential targets for anti-obesity drugs. Information about the body's metabolic state is conveyed to the brain by hormones, peptides and nutrients from the periphery. During a state of hunger, the brain triggers an orexigenic response; conversely, during satiety, the brain prompts an anorexigenic response. In the past few decades, numerous molecules have been identified as playing a part in the regulation of energy balance. Their discovery has helped to unravel a complex network involving peripheral tissues and the brain to coordinate food intake. This poster provides an overview of some of the molecules and circuits involved in the regulation of feeding behaviour.

To adapt to daily variations in energy intake and expenditure, our bodies sense and integrate information about energy availability that is conveyed to the brain by hormones and nutrients from the periphery. These molecules regulate feeding behaviour by acting on neurons in the hypothalamus and the brainstem.

During periods of satiety, the body works towards storage of the acquired nutrients. Satiety is associated with increased sympathetic activity, which promotes both insulin release by the pancreas (and thus stimulates glucose storage in the liver and muscle) and fat deposition (which leads to a rise in leptin levels). Food ingestion results in a release of incretins by the gut. These include GLP1, which stimulates the pancreas to secrete insulin; both GLP1 and insulin are thought to reduce food intake by acting directly in the brain. In pancreatic β-cells, the hormone amylin is co-released with insulin in response to a meal. It is a potent satiety signal, inhibits digestive secretion and slows gastric emptying. The precise brain targets of amylin are not known, but include the area postrema (AP) in the brainstem and the lateral hypothalamus. Two further examples of gut peptides released in response to food intake are PP and OX, which act in the stomach to slow gastric emptying and putatively act in the brain to decrease food intake.

Conversely, during periods of hunger, the hypothalamus regulates the activity of the autonomic nervous system to promote fat release from white adipose tissue and trigger gluconeogenesis in the liver. These changes in peripheral nutrient levels lead to a decrease in the levels of thyroid hormones, insulin and leptin, and to an increase in the level of ghrelin and corticosteroids, which increase food-seeking behaviour through their effect on the brain.

The hormones and peptides mentioned above are only a few among a myriad of molecules thought to be involved in the regulation of energy balance. Research into this complex system continues to identify new candidates that could be pharmacologically targeted to regulate energy balance.

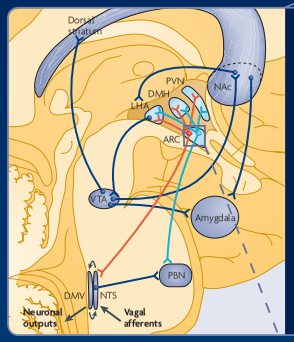

Brain nuclei involved in energy balance regulation

Neurons of the arcuate nucleus (ARC) in the hypothalamus project to the lateral hypothalamus (LHA), which sends projections to the nucleus accumbens (NAc) through the ventral tegmental area (VTA). The NAc is thought to mediate most of the rewarding effects of food intake. The dopaminergic neurons in the VTA also send projections to other brain regions that mediate the hedonic aspects of feeding, such as the amygdala and the dorsal striatum. ARC neurons also project to the parabrachial nucleus (PBN), which mediates food aversion. Furthermore, ARC projections regulate the activity of neurons in the paraventricular nucleus (PVN), the dorsomedial nucleus (DMH) and the ventromedial nucleus (VMN) (not shown) of the hypothalamus, which have a role in maintaining energy balance. In addition, the ARC projects to the nucleus tractus solitarius (NTS) in the brainstem. Local connections in the brainstem, such as that between the NTS and the dorsal motor nucleus of the vagal nerve (DMV), integrate hormonal and neuronal stimuli and so help to regulate feeding behaviour. Red lines indicate basic anorexigenic signals, light blue lines indicate basic orexigenic signals and dark blue lines indicate other, downstream signals.

Signalling in the arcuate nucleus

Two populations of neurons in the ARC have opposite effects on feeding. POMC-expressing neurons are activated by anorexigenic stimuli and release the POMC derivative αMSH, which is an agonist of MC4Rs. These receptors are expressed in neurons in various target nuclei that inhibit feeding behaviour. By contrast, NPY/AGRP-expressing neurons are activated by orexigenic stimuli. They inhibit both POMC-expressing neurons and MC4R-expressing neurons through the release of GABA and AGRP, resulting in the induction of food-seeking behaviour. AGRP acts as a potent endogenous antagonist of MC4Rs, in opposition to αMSH. Projections from NPY/AGRP-expressing neurons are mostly coupled to projections from POMC-expressing neurons, so that MC4R-expressing target neurons receive both negative and positive input.

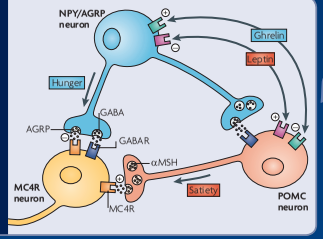

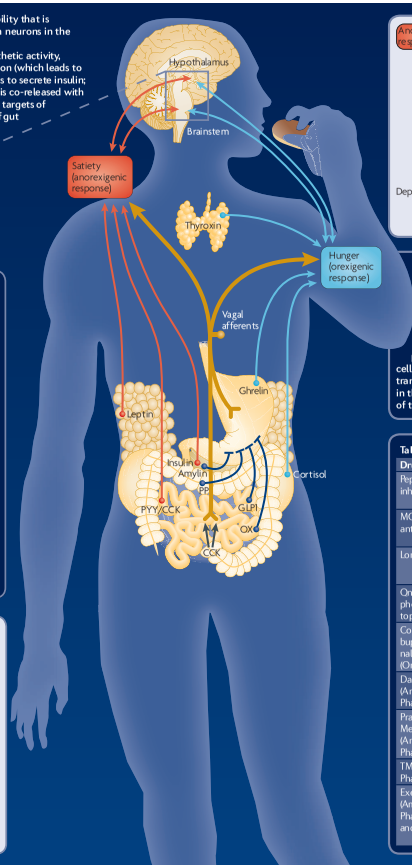

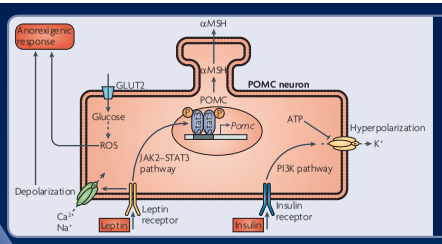

Leptin and insulin signalling

By binding to its receptor in POMC-expressing neurons, leptin activates the JAK2–STAT3 pathway, which ultimately leads to an increase in POMC expression. Subsequently, convertases cleave POMC to generate αMSH. Once released, αMSH binds to and activates MC4R-expressing target neurons, inducing an anorexigenic response. Specific enzymes in the synapse (for example, PRCP) cleave and inactivate αMSH. Leptin can also rapidly depolarize POMC-expressing neurons by opening as yet unidentified, non-specific cation channels.

The binding of insulin to its receptor activates the classical PI3K pathway, which opens K_{ATP} channels and so hyperpolarizes the POMC-expressing neuron. Glucose uptake by neurons occurs through specialized glucose transporters, such as GLUT2. It has been proposed that the increase in glucose levels following feeding leads to an increase in glucose uptake in POMC-expressing cells, which raises levels of ATP and subsequently closes the the K_{ATP} channel. Glucose oxidation also produces ROS, which may be involved in the anorexigenic response.

Model of ghrelin signalling

Ghrelin binds to the GHSR in NPY/AGRP-expressing neurons, leading to an immediate depolarization of the cell membrane and an increase in neuron firing rate. Ghrelin signalling involves phosphorylation of AMPK, with consequent phosphorylation and inhibition of ACC. This decreases the levels of malonyl-CoA, leading to a disinhibition of CPT1, which enables the cell to β-oxidize LCFAs to generate ATP and ROS. ROS activate mitochondrial UCP2, which limits ROS production. This feedback loop between ROS and UCP2 provides a mechanism for cellular homeostasis. The sustained and regulated production of ROS also stimulates the transcription of genes involved in the production of mitochondria (for example, *Nrf1*) and in the orexigenic response (for example, *Npy* and *Agrp*), which helps to sustain the activity of these cells during periods of hunger.

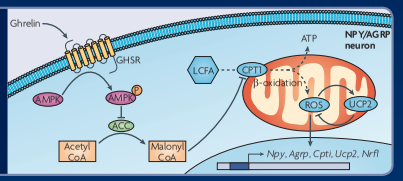

Table | Anti-obesity drugs in development

Drug (company)	Mechanism	Effect in humans	Development stage
Peptidase inhibitors	Inhibit peptidases, such as prolylcarboxypeptidase	• Decreased food intake • Decreased body weight (estimated)	Experimental
MCHR1 antagonists	Inhibits MCHR1	• Decreased food intake • Decreased body weight (estimated)	Experimental Awaiting clinical studies
Lorcaserin (Arena)	Stimulates the 5-hydroxytryptamine (serotonin) receptor 2C	• Decreased body weight (>5%) • No major side effects	Phase III
Onexa: phentermine plus topiramate (Vivus)	Stimulates noradrenaline release Stimulates GABA receptors	• Decreased body weight (>5%) • No major side effects	Phase III
Contrave: bupropion plus naltrexone (Orexigen)	Inhibits dopamine reuptake Inhibits opioid receptors	• Decreased body weight (>5%) • Two cases of seizures reported	Phase III
Davalintide (Amylin Pharmaceuticals)	Mimics the effects of amylin	• Acutely decreased 24-hour food intake in obese subjects	Phase II
Pramlintide/ Metreleptin (Amylin Pharmaceuticals)	Mimics the effects of amylin and leptin	• Decreased body weight	Phase II
TM30339 (7TM Pharma A/S)	A PP analogue that binds to neuropeptide Y4 receptors	• Inhibited food intake • Reduced ghrelin levels	Phase II
Exenatide (Byetta) (Amylin Pharmaceuticals and Eli Lilly)	Mimics incretins such as GLP1	• Decreased body weight in some diabetic subjects	Phase III (obese non-diabetic subjects) Approved for glucose control in some diabetic patients

Obesity

Obesity can dramatically diminish both the quality and length of life. The causes of human obesity may lie in the circuitry of brain areas that regulate food-seeking behaviour in coordination with peripheral hormonal signalling. Pharmacological therapies for treating obesity are limited, mostly because of harmful side effects. Interestingly, an effective option is bariatric surgery, which has been shown to not only decrease body weight but also to improve diabetes, which is commonly associated with obesity. However, the effects of bariatric surgery on metabolism are still not completely understood.

Leptin was discovered in 1994. Individuals with rare mutations in the leptin gene developed profound, early-onset obesity that could be reversed by leptin replacement, which suggested that leptin had potential as an anti-obesity drug. Normally, however, leptin levels increase during the development of obesity. Consequently, the ARC in the hypothalamus becomes less responsive to leptin, thus promoting continuous food intake and fat deposition.

Many pharmacological approaches now attempt to promote or enhance the downstream effects of leptin by stimulating melanocortin signalling, activating POMC-expressing neurons (using serotonin and noradrenaline mimetics) or by activating MC4Rs. In addition, synthetic peptide analogues that mimic the effects of endogenous gut peptides on feeding are being tested alone or in combination with other compounds to promote weight loss [TABLE]. The main objective of these studies is to activate anorexigenic brain areas or to enhance the signalling of other anorexigenic molecules. In addition, molecules that bind to peptide receptors, such as MCHR1 antagonists, are being designed with the aim of inhibiting orexigenic signalling in the brain.

Our increasing understanding of the hormonal, molecular and cellular mechanisms involved in regulating energy balance is opening several new avenues for the pharmaceutical industry to develop and test molecules aimed at treating obesity. These efforts could provide individually tailored treatment options based on the complex genetic and environmental nature of this condition.

Abbreviations

ACC, acetyl-CoA carboxylase; AGRP, agouti-related protein; AMPK, 5′-AMP-activated protein kinase; CCK, cholecystokinin; CPT1, carnitine *O*-palmitoyltransferase 1; GABA, γ-aminobutyric acid; GABAR, γ-aminobutyric acid receptor; GLP1, glucagon-like peptide 1; GLUT2, glucose transporter 2; GHSR, growth hormone secretagogue (ghrelin) receptor; JAK2, Janus kinase 2; K_{ATP} channel, ATP-sensitive K^+ channel; LCFA, long-chain fatty acids; MCH, melanin-concentrating hormone; MCHR1, melanin-concentrating hormone receptor 1; MC4R, melanocortin 4 receptor; αMSH, α-melanocyte-stimulating hormone; NPY, neuropeptide Y; NRF1, nuclear respiratory factor 1; OX, oxyntomodulin; PI3K, phosphoinositide 3-kinase; POMC, pro-opiomelanocortin; PP, pancreatic peptide; PRCP, prolylcarboxypeptidase; PYY, peptide YY; ROS, reactive oxygen species; STAT3, signal transducer and activator of transcription 3; UCP2, uncoupling protein 2.

Contact information

Marcelo O. Dietrich and Tamas L. Horvath are affiliated with the Program on Integrative Cell Signaling and Neurobiology of Metabolism, Section of Comparative Medicine, Yale University, School of Medicine, New Haven, Connecticut 06510, USA.
e-mails: marcelo.dietrich@yale.edu; tamas.horvath@yale.edu

Edited by Monica Hoyos Flight and Leonie Welberg; copyedited by Katie Kingwell and Yukie Ozawa; designed by Kirsten Lee.

http://www.nature.com/nrn/posters/feeding

Anexo A-7. Obesity is Associated with Hypothalamic Injury in Rodents and Humans

Artigo publicado no periódico *Journal of Clinical Investigation.*

Research article

Obesity is associated with hypothalamic injury in rodents and humans

Joshua P. Thaler,[1,2] Chun-Xia Yi,[3] Ellen A. Schur,[2] Stephan J. Guyenet,[1,2] Bang H. Hwang,[1,2,4] Marcelo O. Dietrich,[5] Xiaolin Zhao,[1,2,6] David A. Sarruf,[1,2] Vitaly Izgur,[7] Kenneth R. Maravilla,[7] Hong T. Nguyen,[1,2] Jonathan D. Fischer,[1,2] Miles E. Matsen,[1,2] Brent E. Wisse,[1,2] Gregory J. Morton,[1,2] Tamas L. Horvath,[5,8] Denis G. Baskin,[1,2,4] Matthias H. Tschöp,[3] and Michael W. Schwartz[1,2]

[1]Division of Metabolism, Endocrinology and Nutrition, Diabetes and Obesity Center of Excellence, and [2]Department of Medicine, University of Washington, Seattle, Washington, USA. [3]Metabolic Diseases Institute, Division of Endocrinology, Department of Medicine, University of Cincinnati, Cincinnati, Ohio, USA. [4]Research and Development Service, Department of Veterans Affairs Puget Sound Health Care System, Seattle, Washington, USA. [5]Program in Integrative Cell Signaling and Neurobiology of Metabolism, Section of Comparative Medicine, Yale University School of Medicine, New Haven, Connecticut, USA. [6]Department of Physiology and Pathophysiology, School of Medicine at Xi'an Jiaotong University, Xi'an, China. [7]Department of Radiology, University of Washington, Seattle, Washington, USA. [8]Department of Obstetrics/Gynecology and Reproductive Sciences, Yale University School of Medicine, New Haven, Connecticut, USA.

Rodent models of obesity induced by consuming high-fat diet (HFD) are characterized by inflammation both in peripheral tissues and in hypothalamic areas critical for energy homeostasis. Here we report that unlike inflammation in peripheral tissues, which develops as a consequence of obesity, hypothalamic inflammatory signaling was evident in both rats and mice within 1 to 3 days of HFD onset, prior to substantial weight gain. Furthermore, both reactive gliosis and markers suggestive of neuron injury were evident in the hypothalamic arcuate nucleus of rats and mice within the first week of HFD feeding. Although these responses temporarily subsided, suggesting that neuroprotective mechanisms may initially limit the damage, with continued HFD feeding, inflammation and gliosis returned permanently to the mediobasal hypothalamus. Consistent with these data in rodents, we found evidence of increased gliosis in the mediobasal hypothalamus of obese humans, as assessed by MRI. These findings collectively suggest that, in both humans and rodent models, obesity is associated with neuronal injury in a brain area crucial for body weight control.

Introduction

Obesity has emerged as a major health problem in industrialized nations. Despite substantial progress in understanding the neurobiology of energy homeostasis (the biological process through which energy intake and expenditure are matched to one another so as to promote stability in the amount of fuel stored as fat) (1), little is known regarding how brain systems designed to promote weight stability are altered in common forms of obesity (2, 3).

Growing evidence implicates immune cell–mediated tissue inflammation as an important mechanism linking obesity to insulin resistance in metabolically active organs, such as liver, skeletal muscle, and adipose tissue (4–6). In rodent models of diet-induced obesity (DIO), increased inflammatory signaling in the mediobasal hypothalamus (MBH) similarly contributes to leptin resistance and weight gain (7–12), but the cellular interactions underlying this inflammatory response remain uncharacterized. The goal of the current study was to identify the neuroanatomical correlates of obesity-associated hypothalamic inflammation and to determine whether similar responses occur in humans.

We report that unlike inflammation in peripheral tissues, a process that develops over weeks to months of high-fat diet (HFD) feeding in rodent models (13–15), markers of hypothalamic inflammation are elevated within 24 hours of HFD exposure. Within the first week of HFD, markers of neuron injury also become evident in the hypothalamic arcuate nucleus (ARC) and adjacent median eminence (ARC-ME) in association with reactive gliosis involving recruitment of both microglia and astrocytes. Although initially transient, suggesting an effective neuroprotective response, inflammation and gliosis return and become established with continued HFD exposure. Using an established MRI method (16–19), we also report evidence of increased gliosis in the MBH of obese humans. These findings collectively suggest that, in both humans and rodent models, obesity is associated with injury to a key brain area for energy homeostasis.

Results

Time course of HFD-induced hypothalamic inflammatory gene expression. Consistent with a large volume of literature (7–11, 13, 14, 20), we found that expression of several proinflammatory genes increased by approximately 50% in both hypothalamus (Figure 1A) and liver (Figure 1B) of adult male rats subjected to long-term (20 weeks) consumption of a HFD (60% of calories from fat) relative to that in controls fed standard chow. By comparison, whereas inflammation was not detected in either liver or adipose tissue after only 4 weeks of HFD, hypothalamic inflammation was clearly evident at this earlier time point (Figure 1, C–E). Thus, the effect of HFD feeding to induce hypothalamic inflammatory gene expression seems unlikely to arise from a systemic inflammatory process.

Since rats fed the HFD for 4 weeks gained more than 50 g more body weight and more than 10% more fat mass than chow-fed controls over the same time frame (data not shown), it remains possible that hypothalamic inflammation at this time point is a consequence of obesity. To address this question, we analyzed hypothalamic proinflammatory gene expression in rats during the

Authorship note: Chun-Xia Yi and Ellen A. Schur contributed equally to this work.
Conflict of interest: The authors have declared that no conflict of interest exists.
Citation for this article: *J Clin Invest* doi:10.1172/JCI59660.

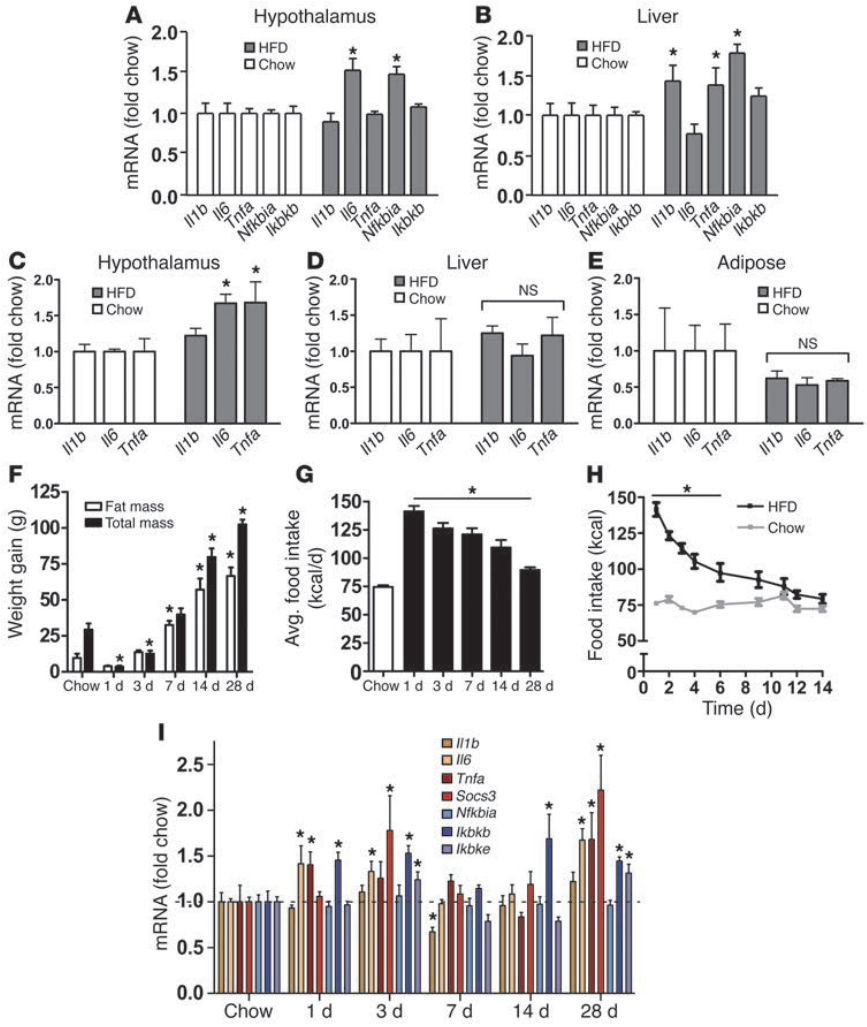

Figure 1

Time course of hypothalamic inflammation after the onset of HFD feeding. (**A** and **B**) Quantification of mRNA encoding proinflammatory cytokines (*Il1b*, *Il6*, *Tnfa*) and NF-κB pathway genes (*Nfkbia*, *Ikbkb*) in (**A**) hypothalamus and (**B**) liver of rats fed either standard chow (white bars) or HFD (gray bars) for 20 weeks (n = 6/group). *P < 0.05 versus chow-fed controls. (**C**–**E**) Effect of 4 weeks of HFD feeding (gray bars) on proinflammatory cytokine gene expression in rat (**C**) hypothalamus, (**D**) liver, and (**E**) white adipose tissue compared with that in chow-fed controls (white bars) (n = 6/group). *P < 0.05 versus chow-fed controls. (**F**) Total weight gain (black bars), fat mass gain (white bars), and (**G**) average (avg) daily food intake (kcal/d) of rats (n = 6/group) fed chow for 2 weeks or HFD for up to 28 days. *P < 0.05 versus chow-fed controls. (**H**) Comparison of daily food intake (kcal) in rats (n = 6/group) fed chow (gray) or HFD (black) for 14 days. *P < 0.05 versus chow-fed controls. (**I**) Time course of induction of mRNA encoding inflammatory mediators, including proinflammatory cytokine (*Il1b*, *Il6*, *Tnfa*), cytokine pathway (*Socs3*), and NF-κB pathway (*Nfkbia*, *Ikbkb*, *Ikbke*) gene expression in the hypothalamus of rats fed chow or HFD for up to 28 days (n = 6/group). All mRNA species were quantified relative to *18S* and *Gapdh* housekeeping gene expression (by ΔΔCT method) and presented as fold change relative to chow-fed controls [fold chow]. The dashed line in **I** represents the level of expression equal to chow-fed controls. *P < 0.05 versus chow.

initial phase of HFD feeding. Relative to that of chow-fed controls, rats placed on the HFD exhibited a transient but robust (50%–100%) increase of food intake (Figure 1, G and H) that gave rise to a small but significant increase of body weight and fat mass by day 7 (Figure 1F). In this cohort, gene expression analysis revealed a complex "on-off-on" pattern, with elevated hypothalamic levels of *Il6*, *Tnfa*, *Socs3*, *Ikbkb*, and *Ikbke* mRNA observed within the first 3 days of HFD exposure, followed by a decline to baseline values from days 7 to 14 and a subsequent return to elevated levels by day 28 (Figure 1I). Thus, increases of hypothalamic proinflammatory gene expression closely mirrored changes of energy intake during the first days of HFD feeding, and both occurred prior to significant expansion of body fat mass (P = NS for fat mass gain of HFD-fed rats at days 1 or 3 compared with chow-fed controls; Figure 1F). C57BL/6 mice displayed a similar, transient increase of proinflammatory gene expression during the first 7 days of HFD feeding

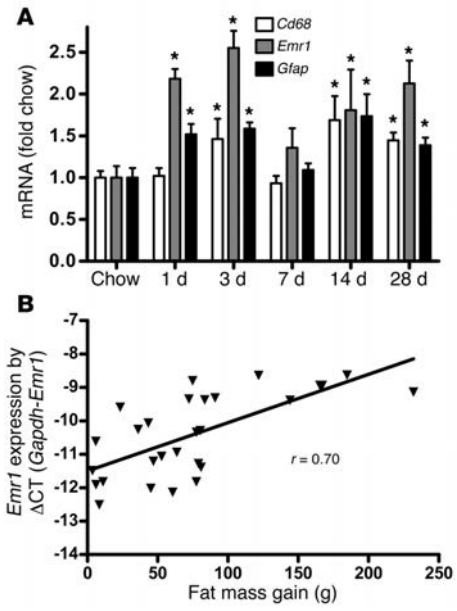

Figure 2
Effect of HFD feeding on hypothalamic microglial markers in rats. (**A**) Time course of hypothalamic microglia-specific (*Cd68* and *Emr1*) and astrocyte-specific (*Gfap*) gene expression in rats fed chow or HFD for up to 28 days (n = 6/group). *P < 0.05 versus chow. (**B**) Correlation of hypothalamic *Emr1* mRNA level (linearized using difference in CT count between the *Gapdh* and the *Emr1* gene [ΔCT]) with change in fat mass (g) over 4 weeks of HFD feeding (r = 0.70; P < 0.001).

(Supplemental Figure 1; supplemental material available online with this article; doi:10.1172/JCI59660DS1), indicating that hypothalamic inflammatory signaling occurs prior to substantial weight gain in mice, as it does in rats.

Markers of gliosis during early HFD feeding. Activation, recruitment, and proliferation of microglia (macrophage-like immune cells of the brain) and astrocytes, collectively termed "reactive gliosis," are hallmarks of the brain response to neuronal injury (21–24). We observed that, in rats fed a HFD for up to 28 days, hypothalamic expression of mRNA encoding myeloid cell–specific markers *Cd68* and *Emr1* (which encodes F4/80) increased by 50%–100% by day 3 (Figure 2A), suggesting an effect of HFD feeding to promote microglial accumulation in this brain area. Interestingly, the level of hypothalamic *Emr1* gene expression was correlated with fat mass gain (r = 0.70; P < 0.001; Figure 2B). Combined with our finding that hypothalamic expression of mRNA encoding the astrocyte marker gene *Gfap* is comparably increased at the same early time point (Figure 2A), these results suggest that the rapid onset of hypothalamic inflammation induced by HFD feeding is associated with robust glial responses.

Using immunohistochemistry to detect the microglia-specific cytoplasmic marker Iba1 (ref. 25 and Figure 3A), we found that microglial number increased in rat ARC by day 3 of HFD exposure compared with that in chow-fed controls (Figure 3, B–D) and remained elevated throughout the initial 2-week period (Figure 3, E and F; quantified in Figure 3G). Concomitantly, microglial cells enlarged (Figure 3H) and adopted a more activated morphology (compare Figure 3I with Figure 3J). In separate cohorts of rats fed a HFD for up to 8 weeks, microglial accumulation in the ARC correlated with the degree of fat mass gain (r = 0.54, P = 0.019; Figure 3K), and animals with greater increases of fat mass also had larger microglia in the ARC (r = 0.52, P = 0.028; Figure 3L). Moreover, changes of both microglial accumulation and cell size appear to be limited to the ARC-ME region, as they were not observed in other hypothalamic (lateral hypothalamic area, ventromedial nucleus) or extrahypothalamic (hippocampus, cerebral cortex) brain areas (Supplemental Figure 2). Since an analogous accumulation of microglia occurred in the ARC-ME of wild-type C57BL/6 mice (Supplemental Figure 3), this effect of HFD feeding is not unique to rats.

The effect of HFD on astroglial responses was assessed in C57BL/6 mice by GFAP immunostaining. As expected, GFAP-positive astrocytes were scattered throughout the ARC-ME of mice fed standard chow, and their processes resembled those in other brain areas (Figure 4A). Within just 1 week of HFD exposure, however, the intensity of GFAP staining in the ARC-ME increased by approximately 50% (Figure 4, B and G). Like hypothalamic inflammatory markers (and unlike the microglial response), this astrocytosis was transient, returning to baseline in mice fed the HFD for 2 to 3 weeks (Figure 4, C and D, respectively; quantified in Figure 4G) but recurring with long-term HFD feeding relative to that in age-matched controls fed chow for the same duration (Figure 4, E and F; quantified in Figure 4H). A similar pattern of hypothalamic gliosis was observed in rats over the first 8 weeks of HFD feeding (data not shown), confirming that comparable microglial, astroglial, and inflammatory responses to HFD occur in both species.

Using immunohistochemistry to detect GFAP, we observed the expected preservation of distinct cell-cell boundaries among astrocytes in the ARC-ME of chow-fed mice (Figure 5A). After just 1 week of HFD exposure, however, astrocytic processes in this brain area coalesced into a dense fibrous network suggestive of a syncytium (Figure 5B), a finding pathognomonic of reactive gliosis (22). This effect was initially transient and resolved between weeks 2 and 3 of HFD (Figure 5, C and D) but reappeared in mice fed a HFD for long intervals (8 months; Figure 5, E and F).

HFD-induced neuronal injury. The rapid onset of inflammation and reactive gliosis observed in the hypothalamus of rats and mice consuming a HFD is a hallmark of the response to neuron injury (e.g., induced by ischemia or excitotoxicity) (21–24). To more directly test the hypothesis that HFD exposure causes ARC neuron injury, we performed immunohistochemical staining to detect induction of the chaperone Hsp72, a component of the neuroprotective response to neuron injury (26), in the ARC-ME of rats fed the HFD for 7 days relative to that of chow-fed controls (Figure 6, A and B). As predicted, Hsp72 immunostaining was increased in HFD-fed rats relative to that in chow-fed controls, and hypothalamic *Hsp72* mRNA expression was also detectably elevated within 3 days of HFD exposure (data not shown). Among ARC neurons in which Hsp72 induction was detected are those containing proopiomelanocortin (POMC) that are components of a critical network for energy balance regulation (ref. 1 and Figure 6, C and D).

We next used electron microscopy to investigate whether autophagy, an independent marker of neuronal stress/injury (27, 28), was induced in POMC neurons from C57BL/6 mice fed the HFD (Figure 6, E–I). After 20 weeks of HFD feeding, the percentage of POMC neurons with detectable autophagosomes increased more than 10 fold (black arrows in Figure 6F; higher-magnification view in Figure 6G), such that the majority of POMC cells examined now exhibited this organelle (6.4% ± 4.1% in chow fed vs. 81.2% ± 8.7% in HFD fed;

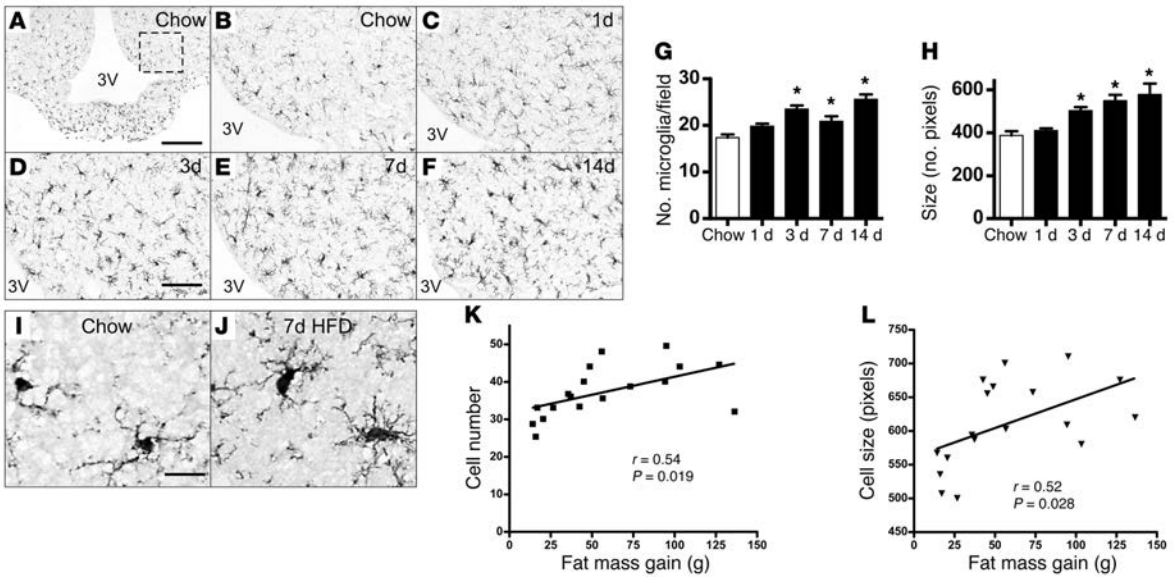

Figure 3

Histochemical analysis of HFD-induced microglial accumulation in rat ARC. Immunohistochemical detection of Iba1 protein, a microglial marker (25), in coronal sections of rat hypothalamus (14 μm) from animals fed either (**A** and **B**) chow or (**C**–**F**) HFD for up to 14 days. (**A**) Low-magnification view (original magnification, ×10) of microglia distributed throughout the MBH. The dashed box indicates the region used for quantification of ARC microglial number and size in **G** and **H**. 3V, third ventricle. Scale bar: 100 μm. (**B**–**F**) Higher-magnification view (original magnification, ×20) of Iba1 immunohistochemistry in the ARC of rats fed (**B**) chow or (**C**) HFD for 1 day, (**D**) 3 days, (**E**) 7 days, or (**F**) 14 days. Scale bar: 50 μm. (**G** and **H**) Quantification of (**G**) mean ARC microglial cell number (per field defined in **A**) and (**H**) microglial cell size (average number of pixels in 10 largest cells) from rats fed either chow or HFD (n = 6/group). *P < 0.05 versus chow. (**I** and **J**) Comparison of microglial fine structure in hypothalamus of rats fed (**I**) chow or (**J**) HFD for 7 days. Microglia from HFD-fed rats manifest a more "ameboid" morphology, characterized by larger cell bodies with thickened and shortened processes. Scale bar: 10 μm. (**K**) Correlation of microglial cell number and fat mass gain (g) over 2–8 weeks of HFD consumption, with indicated linear regression line. (**L**) Correlation of microglial cell size (no. pixels in 10 largest cells/ARC) and fat mass gain (g) over 2 to 8 weeks of HFD consumption, with indicated linear regression line. Each symbol in **K** and **L** represents an animal.

P = 0.00005; Figure 6I). In addition, a disruption of mitochondrial morphology was observed in POMC neurons from mice fed a HFD (white arrows in Figure 6, E and F; higher-magnification view in 6H). Whereas mitochondria in POMC neurons from chow-fed rats uniformly demonstrated homogenous, compact electron-dense lumens with well-organized, parallel-oriented cristae (Figure 6H), mitochondria from HFD-fed animals manifested irregular swellings and less electron-dense lumen with nonparallel cristae that were frequently discontinuous (Figure 6H). Furthermore, the size and shape of the mitochondria varied greatly in the HFD-fed animals but not in the chow-fed animals (Figure 6F, white arrows).

To determine whether cellular injury (Figure 6, A–D) and autophagy (Figure 6, E–I) ultimately give way to permanent alteration of POMC neurons, we quantified POMC-immunopositive cells in long-term HFD-fed mice. This analysis revealed an approximately 25% reduction in the number of POMC cells in the ARC of mice after 8 months of exposure to HFD relative to that of controls fed chow over the same time period (P < 0.05; Figure 6, J–L). Taken together, these results suggest that the hypothalamic response to HFD consumption involves acute injury to — and eventual loss of — ARC POMC neurons.

Evidence of hypothalamic gliosis in obese humans. Based on our findings of reactive gliosis, microglial accumulation, and neuronal injury in rodents with DIO, we investigated whether MBH gliosis is also associated with obesity in humans. We used magnetic resonance images obtained from a retrospective cohort of 34 subjects who had clinical MRI examinations without identified abnormalities. BMI ranged from lean to obese (17.7–44.1 kg/m^2). To determine whether visual evidence of gliosis was present in the brain images, we performed an initial inspection of the MBH for hyperintense signal on T2-weighted coronal sections, a characteristic finding of gliosis in numerous inflammatory, ischemic, and degenerative neural disorders (16–19). By this analysis, no studies were rated as abnormal. To detect gliotic changes below the visual detection threshold, ratios were created to compare mean signal intensity within regions of interest (ROIs) placed in the MBH with ROIs in adjacent amygdalar tissue (ROIs indicated by green circles and arrows in Figure 7, A and B, on representative images from a lean and an obese subject). The putamen was used as a control ROI. Mean signal intensities were highly correlated between ROIs in the right and left hemispheres for all 3 brain regions (MBH: r = 0.99, P < 0.0001; amygdala: r = 0.99, P < 0.0001; putamen: r = 0.97, P < 0.0001), such that MBH/amygdala mean signal ratios were similar on both sides of the brain (left: 1.13 ± 0.12, right: 1.08 ± 0.14; r = 0.54, P = 0.001).

Across all subjects, left MBH/amygdala signal intensity was positively correlated with BMI, both by simple linear regression of mean intensity ratios (r = 0.38, P = 0.027; Figure 7C) and multivariate analysis using MBH signal as the independent variable and amygdala signal as covariate (P < 0.05; data not shown). By comparison, the left MBH/amygdala mean signal ratio was not associated

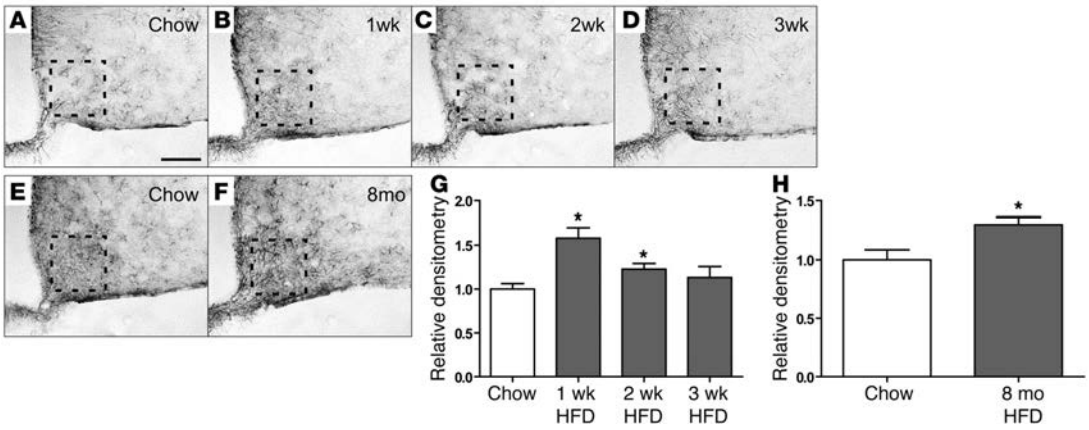

Figure 4
Time course of the effect of HFD feeding on hypothalamic astrocytes. (**A**–**D**) Representative images of astrocytes identified by immunohistochemical detection of GFAP protein in coronal sections of hypothalamus (10 μm) obtained from 10-week-old mice fed either (**A**) chow or HFD for (**B**) 1 week, (**C**) 2 weeks, or (**D**) 3 weeks. (**E** and **F**) GFAP staining of hypothalamic sections from 8-month-old mice fed (**E**) chow or (**F**) HFD. Scale bar: 50 μm. (**G**) Quantification of GFAP staining intensity (mean ± SEM) in the region of the ARC from mice fed either chow or HFD for 1 to 3 weeks (n = 6/group). (**H**) Quantification of GFAP staining intensity (mean ± SEM) in mice fed chow or HFD for 8 months. *P < 0.05 versus chow. The dashed boxes indicate the region used for quantification in **G** and **H**.

with age (r = 0.15; P = NS), and it did not differ by gender (men: 1.14 ± 0.02; women: 1.11 ± 0.03; P = NS). In group comparisons, the left MBH/amygdala mean signal ratio was significantly higher among obese subjects (1.18 ± 0.04; n = 12 with BMI >30 kg/m^2) than that in normal-weight subjects (1.06 ± 0.04; n = 11 with BMI 19–25 kg/m^2; P < 0.05). Interestingly, the association of BMI with increased signal intensity appeared to be limited to the MBH, as BMI was not correlated with putamen/amygdala signal ratios (left: r = 0.10, P = NS; right: r = 0.01, P = NS). Thus, similar to the findings in HFD-fed rodents, our retrospective analysis suggests that obesity in humans is associated with gliosis in the MBH, raising the possibility of a common mechanism of obesity-induced hypothalamic injury across species.

Discussion

Although hypothalamic inflammation is well documented in rodent models of DIO (7–11, 20), neither its underlying mechanisms nor its relevance to human obesity are understood. Here we report that hypothalamic inflammation induced by HFD feeding is a manifestation of neuron injury that in turn triggers a reactive gliosis involving both microglial and astroglial cell populations. Moreover, these responses appear to occur selectively in the ARC and rapidly follow the initiation of a HFD. The transient nature of this hypothalamic response suggests that neuroprotective responses are mounted that limit or reverse the injury during its initial phases, but, with sustained exposure to the HFD, ARC-ME gliosis and injury responses are reestablished. Combined with MRI-based evidence for gliosis in the MBH of obese humans, our findings suggest that, in both humans and rodent DIO models, obesity is associated with neuron injury in a brain area crucial for body weight control.

Several mechanisms have been forwarded to explain obesity-induced inflammation in both peripheral tissues and hypothalamus, including activation of TLR4, induction of endoplasmic reticulum stress, and activation of serine/threonine kinases, such as IKKβ (reviewed in ref. 8). While the contribution made by these mechanisms remains uncertain, the much earlier onset of inflammation in hypothalamus relative to that in peripheral tissues raises the possibility that different processes are involved. Moreover, the nature of the hypothalamic inflammation occurring during the first days of HFD feeding may differ fundamentally from that involved with chronic HFD exposure. The conclusion that the rapid onset of MBH inflammation is a manifestation of neuron injury and associated neuroprotective responses is consistent with previous evidence of apoptosis and glial ensheathment of ARC neurons in animals rendered obese by chronic HFD feeding (29, 30). Moreover, these responses were detected specifically in ARC POMC cells (29, 30), which is consistent with our finding of an approximately 25% reduction in the number of hypothalamic POMC neurons in mice chronically fed a HFD. In this context, it is noteworthy that POMC cells play an essential role to protect against obesity and that loss of these cells is sufficient in and of itself to cause excess weight gain in mice (31).

In experimental models of brain injury, astrocytes play a key neuroprotective role, limiting the extent of both inflammation and neuron loss (21, 22). The reactive gliosis we observed in the MBH of both rats and mice may therefore be neuroprotective in nature, limiting local injury induced by HFD feeding. Consistent with this hypothesis is our finding that the return of proinflammatory markers in the ARC-ME area to basal, preintervention values (on day 7 of HFD feeding) coincides with the appearance of a reactive gliosis in the same brain area. Like markers of inflammation, however, this gliosis is initially transient, but both responses are reestablished as obesity develops (within 4 weeks of HFD feeding). These observations suggest that with sustained exposure the capacity of supportive glial cells to control the damage associated with HFD feeding is exceeded and that neuron injury and loss can no longer be prevented.

This hypothesis is consistent with our finding that during HFD feeding, Hsp72 was rapidly induced in neurons in the ARC-ME. Heat shock proteins are induced in response to many forms of brain injury, including stroke, neurodegenerative disease, epilep-

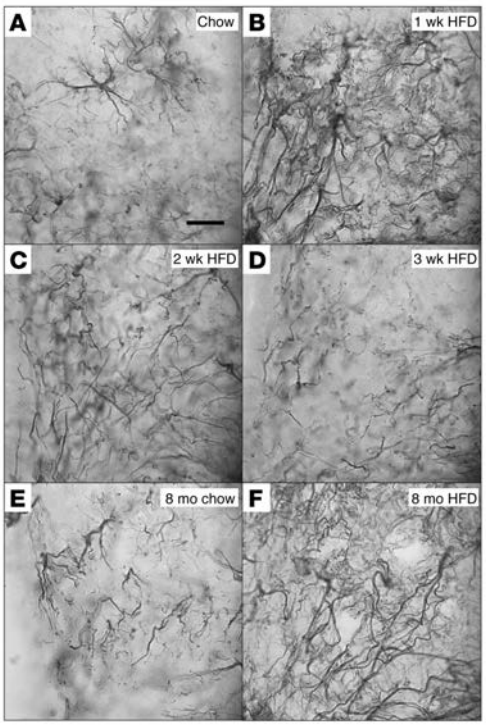

Figure 5
Effect of HFD feeding on ARC astrocyte morphology. High-magnification (original magnification, ×100) examination of astrocyte processes by GFAP immunohistochemistry of sections through mouse ARC. (**A**) Astrocyte processes in the ARC of mice fed chow remain separated into discrete areas. (**B**) One week of HFD feeding is accompanied by the apparent formation of a syncytium of astrocytic processes. (**C**) This astrocyte response is partially resolved by 2 weeks of HFD feeding, with only a few scattered overlapping processes, and, (**D**) by 3 weeks of HFD, glial morphology appears to be fully normalized. (**E**) Mice fed chow for 8 months show increased astrocyte number but no overlap of processes. (**F**) Mice fed HFD for 8 months exhibit severe astrocytosis suggestive of syncytium formation. Scale bar: 10 μm.

sy, and trauma, and overexpression of these proteins can serve a protective role in models of nervous system injury (26, 32). Hsp72 functions as a chaperone and protects neurons from protein aggregation and toxicity (in Parkinson disease, Alzheimer disease, polyglutamine diseases, and amyotrophic lateral sclerosis) as well as apoptosis (in Parkinson disease) (26, 32). It is also a stress marker (temporal lobe epilepsy) and protects cells from inflammation (cerebral ischemic injury) (26, 32). Our findings therefore suggest that rapid induction of Hsp72 in ARC neurons during HFD feeding is part of a neuroprotective response that also involves local microglial and astroglial responses.

Autophagy is a lysosomal degradative pathway that maintains cellular homeostasis by turning over cellular components. Interestingly, this process was recently suggested to participate in the physiological response of MBH neurons to fasting, based on evidence that fasting-induced autophagy liberates nutrient-related signals that regulate neuron firing (33). Beyond the response to starvation, however, autophagy is also a prominent feature of numerous pathological processes (e.g., neurodegeneration) and can lead to apoptosis of neurons and other cell types (27, 28, 34). Although the precise interpretation of increased autophagy in the setting of HFD feeding awaits additional study, recent evidence suggests it may serve to minimize neuronal inflammation and injury (35). Consistent with this interpretation, the apoptosis of ARC POMC cells in rats with DIO (30) and the 25% reduction in POMC cell number we observed in HFD-fed mice support the hypothesis that increased numbers of autophagosomes in this cell population reflect ongoing cell injury and that this protective response along with others, such as upregulated chaperone expression and endoplasmic reticulum stress (11, 36), are ultimately insufficient to prevent cell loss with continued exposure to HFD. This model warrants further study with interventions to determine whether susceptibility to DIO is altered by manipulation of these protective responses.

Although microglia can be activated in a proinflammatory manner and cause tissue damage (37, 38), their diverse roles to regulate and support neuronal function are a topic of intense recent interest (37–39). For example, microglia participate in synaptic pruning both during development (39) and in adult brain (37, 38), and they play an important neuroprotective role under conditions in which the initial insult is directed at neurons (e.g., demyelinating or neurodegenerative disease) (23, 24), rather than at microglia themselves. Available evidence suggests that in the first few days of HFD feeding, the inflammation and neuron injury we have observed in the ARC-ME is not due to actions of microglia. Rather, we hypothesize a neuroprotective effect of these cells based on our findings that (a) accumulation and enlargement of microglia becomes detectable in the ARC only after inflammation is established in this brain area, and (b) this microglial response persists even as local inflammation resolves (albeit transiently). With chronic HFD feeding, however, a pathogenic role for proinflammatory microglia has not been excluded, and future studies are warranted to address this issue. An additional unanswered question is why astrocytosis in the ARC resolves temporarily (along with a decrease of proinflammatory markers) after the first week of HFD feeding, whereas microglial accumulation continues to increase during this time.

It is important to note that the current studies were undertaken in rodent strains known to be genetically predisposed to DIO, and the important question of whether the hypothalamic response to HFD feeding differs in obesity-resistant strains remains unanswered. This point is particularly germane in light of evidence that the balance between excitatory and inhibitory synaptic contacts on ARC neurons is altered by HFD feeding (29, 40) in a manner that differs between animals that are genetically predisposed to DIO and those that are obesity resistant (29). Given the capacity of both microglia and astrocytes to participate in synaptic remodeling and modulate synaptic levels of various neurotransmitters (21–24, 37, 41), it will be of interest in future studies to determine whether hypothalamic responses to HFD feeding are influenced by genetic factors that impact predisposition to DIO.

Based on literature establishing structural MRI as a reliable method for visualizing and quantifying gliosis in human brain (16–19), we undertook a retrospective analysis of T2-weighted magnetic resonance images obtained previously in a cohort of young human subjects undergoing clinical examination. We found hyperintensity of the T2-weighted signal in human MBH that was significantly increased ($P < 0.05$) in obese individuals compared with that in

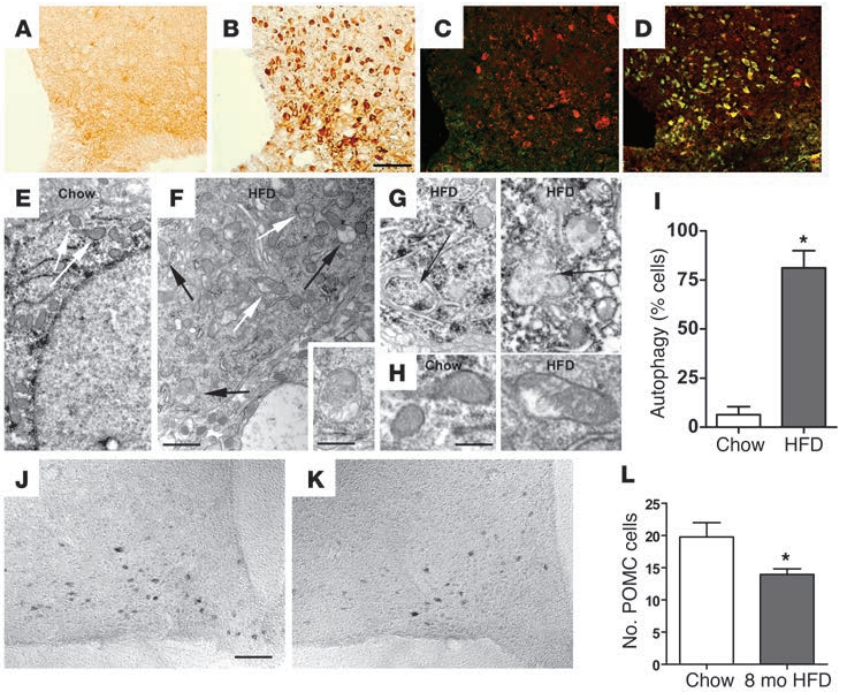

Figure 6
Effect of HFD feeding on hypothalamic markers of neuronal injury and on POMC cell number. (**A**–**D**) Immunohistochemical analysis of the neuronal injury marker Hsp72 in the ARC of rats fed (**A** and **C**) chow or (**B** and **D**) HFD for 7 days. Immunofluorescence in **C** and **D** shows colocalization of Hsp72 (green) with POMC peptide (red). (**E** and **F**) Electron micrograph of a POMC neuron from a mouse fed (**E**) chow or (**F**) HFD for 20 weeks. In **E**, no pathological changes in cytoplasm or mitochondria (white arrows) are observed, whereas, in **F**, mitochondrial integrity is disrupted (white arrows), and mature and developing autophagosomes are present (black arrows). The inset in **F** is a higher-magnification example of an autophagosome. (**G**) Additional high-magnification examples of autophagosomes (black arrows). (**H**) High-magnification images of POMC neuron mitochondria from mice fed chow (parallel-oriented cristae and regular structure) or HFD (nonparallel cristae and irregular shape). (**I**) Quantification of percentage of POMC neurons with autophagosomes (n = 5 cells examined in each of 5 mice). *P < 0.05 versus chow. (**J** and **K**) Representative images of POMC neurons in the ARC of mice fed either (**J**) chow or (**K**) HFD for 8 months. (**L**) Quantification of POMC neuron number in the hypothalamus of mice fed chow or HFD for 8 months (mean ± SEM; n = 8/group). *P < 0.05 versus chow. Scale bar: 50 μm (**A**–**D**, **J**, and **K**); 1 μm (**E** and **F**); 500 nm (**F**, inset); 400 nm (**G** and **H**).

lean individuals, indicative of gliosis. This finding does not constitute definitive proof of increased gliosis, as edema, infection, and tumors can have a similar appearance. However, subjects having preexisting evidence of neurological abnormality were excluded from the study, suggesting that these alternative explanations for increased T2-weighted signal intensity are unlikely. Furthermore, as predicted by our findings in rodents, the gliosis signal was positively correlated to BMI but not to age or gender. Although the magnitude of this increase associated with obesity was modest (which likely reflects, at least in part, limitations inherent in gliosis detection by MRI), these data lend translational relevance to our preclinical studies by suggesting that hypothalamic neuron injury and associated gliosis are a feature of obesity in humans as well as rodents. Although it remains to be determined whether this finding is causally linked to obesity pathogenesis or is simply a marker of the obese state, it seems reasonable to anticipate that damage to a critical brain area for body weight control might play a role in the associated obesity (42), and studies to clarify this issue are a high priority for future research.

In summary, we report that, in rats and mice that are susceptible to DIO, consumption of a HFD rapidly induces neuron injury in a brain area critical for energy homeostasis. Although local responses appear to limit this injury, recovery is transient, eventually giving way to chronic inflammation, neuron loss, and reactive gliosis. Extending these findings is MRI evidence for gliosis in the hypothalamus of obese humans. Collectively, this work identifies a potential link between obesity and hypothalamic injury in humans as well as animal models.

Methods

Animals. Weight-matched male Long-Evans rats (300–350 g; Harlan) or male C57BL/6 mice (20–25 g) were housed individually in a specific pathogen–free environment, maintained in a temperature-controlled room with a 12-hour-light/12-hour-dark cycle, and provided with ad libitum access to water and either standard laboratory chow (3.34 kcal/g; PMI Nutrition International) or a diet containing 60% kcal fat (HFD, 5.24 kcal/g, D12492; Research Diets) for periods ranging from 1 day to 8 months. Body weight and food intake were monitored daily.

Real-time PCR. For expression analyses, RNA from liver, epididymal white adipose tissue, and MBH (rectangular block excised as previously described; ref. 43) was extracted using TRIzol B according to the manufacturers' instructions (MRC). RNA was quantified by spectrophotometry at 260 nm (Nanodrop 1000; Thermo Scientific) and reverse transcribed with avian myeloblastosis virus reverse transcriptase (1 μg; Promega). Levels of mRNA for *Nfkbia*, *Ikbkb*, *Ikbke*, *Il6*, *Il1b*, *Tnfa*, *Gfap*, *Emr1*, *Cd68*, *Gapdh* (internal control), and *18S* RNA (internal control) were measured by semiquantitative real-time PCR on an ABI Prism 7900 HT (Applied Biosystems). The primer sequences were designed using Primer Express (version 2.0.0; Applied Biosystems) as follows: *Nfkbia*, forward, TGCCTGGCCAGTGTAGCAGTCTT, reverse, CAAAGTCACCAAGTGCTCCACGAT; rat *Ikbkb*, forward, AGGGTGACTAAGTCGAGAC, reverse, ACAGCCAGGATATGGTACG; mouse *Ikbkb*, forward, GGCACCTTGGATGACCTAGA, reverse, CCATATCCTGGCTGTCACCT; *Ikbke*, forward, ACCACTAACTACCTGTGGCAT, reverse, ACTGCGAATAGCTTCACGATG; rat *Il6*, forward, CAGAGGATACCACCCACAACAGA, reverse, CAGTGCATCATCGCTGTTCATACA; mouse *Il6*, forward, GTGGCTAAGGACCAAGACCA, reverse, GGTTTGCCGAGTAGACCTCA; *Il1b*, forward, TACAAGGAGAGACAAGCAACGACA, reverse, GATCCACACTCTCCAGCTGCA; rat *Tnfa*, forward, GCTCCCTCTCATCAGTTCCA, reverse, CTCCTCTGCTTGGTGGTTTG; mouse *Tnfa*,

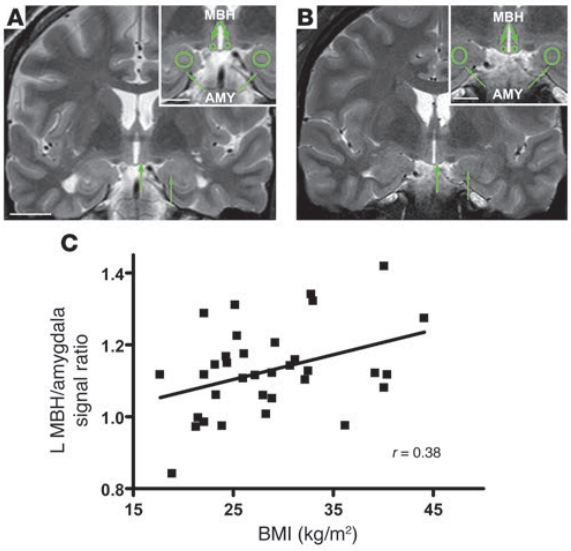

Figure 7
Radiologic evidence of gliosis in the MBH of obese humans. Representative coronal T2-weighted images through the hypothalamus from (**A**) a normal weight and (**B**) an obese subject. Insets show the placement of right and left ROIs (green circles) in the MBH and amygdala (AMY). In the MBH (thick arrows) of the obese subject, signal ratios demonstrated subtle hyperintensity (brightness) relative to the amygdala (thin arrows). Scale bar: 20 mm; 10 mm (insets). (**C**) Correlation of BMI with MBH hyperintensity as measured by left (L) MBH/amygdala signal ratio (n = 34 subjects; r = 0.38; P = 0.027).

forward, CATCTTCTCAAAACTCGAGTGACAA, reverse, TGGGAGTAGATAAGGTACAGCCC; *Gfap*, forward, AACGACTATCGCCGCCAACTG, reverse, CTCTTCCTGTTCGCGCATTTG; rat *Emr1*, forward, AATCGCTGCTGGCTGAATACGG, reverse, CCAGGCAAGGAGGGCAGAGTT; mouse *Emr1*, forward, AATCGCTGCTGGTTGAATACAG, reverse, CCAGGCAAGGAGGACAGAGTT; *Cd68*, forward, CTTCCCACAAGCAGCACAG, reverse, AATGATGAGAGGCAGCAAGAGA; *Gapdh*, forward, AACGACCCCTTCATTGAC, reverse, TCCACGACATACTCAGCAC; and *18S* forward, CGGACAGGATTGACAGATTG, reverse, CAAATCGCTCCACCAACTAA. PCR data were analyzed using the Sequence Detection System software (SDS version 2.2; Applied Biosystems). Expression levels of each gene were normalized to housekeeping genes (*Gapdh* and *18S*) and expressed as a percentage of chow-fed controls. Nontemplate controls were incorporated into each PCR run.

Immunohistochemistry. After fixation-perfusion with 4% paraformaldehyde/PBS, frozen sections in the coronal plane through the rat and mouse hypothalamus were processed for GFAP, Iba1, POMC, and Hsp72 immunoreactivity using standard immunohistochemical procedures. Sections blocked in 5% normal goat, mouse, or donkey serum (Jackson ImmunoResearch Laboratories Inc.) were incubated overnight at 4°C with mouse anti-GFAP (1:10,000; Sigma-Aldrich), mouse anti-Hsp72 (1:1,000; Enzo Life Sciences), rabbit anti-Iba1 (1:1,000; Wako Pure Chemicals), goat anti-Iba1/AIF-1 (1:1,000; Everest Biotech), and anti-POMC (Ab5, 1:10,000; AbCam). Biotinylated anti-rabbit, anti-mouse or anti-goat secondary antibody, ABC reagent, and diaminobenzidine substrate (Vector Laboratories) were used for light microscopic visualization. Immunofluorescence was performed with a combination of Alexa Fluor 488– or Alexa Fluor 594–labeled anti-rabbit, anti-goat, or anti-mouse secondary antibodies (1:500; Invitrogen) and DAPI (Sigma-Aldrich) to identify cell nuclei. GFAP and Iba1 antibodies have been widely validated in the literature as markers for astrocytes and microglia, respectively. In addition, we saw no overlap between these markers and NeuN, a neuronal marker (data not shown). The POMC antibody identified only a small population of neurons in the expected area of the ARC (Figure 6, C, D, J, and K) and hindbrain (data not shown), consistent with the known location of these cells. Hsp72 immunostaining has been used extensively in prior studies (26, 32). In addition, sections incubated with preimmune serum showed no detectable signal (data not shown). While the absence of detectable immunoreactivity in chow-fed controls and presence of positive staining in HFD brains indicates that the Hsp72 antibody staining is not nonspecific, we cannot absolutely rule out the possibility that the antibody may recognize other antigens in hypothalamic neurons of HFD-fed rats.

Images were captured on an Eclipse E600 upright microscope equipped with a color digital camera (Nikon). Quantification was performed in a blinded fashion on anatomically matched brain regions identified in ×20 images. Both sides of bilateral structures (e.g., ARC, VMH, etc.) were counted on 2 to 4 slides per animal, and replicate values from each animal were individually averaged before determining group means (n = 4–8/group). For Iba1 and POMC immunostaining in which discrete cells could be identified, cell number was counted manually within prespecified ROIs using Photoshop (Adobe) or ImageJ (http://rsbweb.nih.gov/ij/). Signal intensity was scored in a semiquantitative fashion and was found to covary with diet group. For microglial cell size (using Iba1) and GFAP immunoreactivity, thresholding was performed in ImageJ, followed by densitometric quantification.

Autophagy analysis. Group-housed C57BL/6 mice fed either standard chow (Purina Lab Chow no. 5001, Ralston Purina Corp.) or 45% kcal HFD (D12451, Research Diets) for 20 weeks were perfused with picric acid, and their brains were processed for electron microscopic examination. Ultrathin sections were cut on a Leica ultramicrotome, collected on Formvar-coated single-slot grids, and analyzed with a Tecnai 12 Biotwin electron microscope (FEI Company). The analysis of autophagosome (intracellular membrane-bound cytosol and organelles) number was performed in an unbiased fashion, as described elsewhere (29, 44). We analyzed 5 POMC neurons identified by POMC immunolabeling in 5 animals per experimental group.

Retrospective study of brain MRIs in humans. We performed a retrospective cohort study to assess for radiologic evidence of MBH gliosis and correlated our findings with BMI levels and obesity. Magnetic resonance brain examinations, using pituitary or epilepsy imaging protocols that used coronal T2-weighted sequences performed between 1/1/2009 and 12/31/2010 at University of Washington Medical Center or Harborview Medical Center, were reviewed for 2 inclusion criteria: (a) availability of good quality coronal views of the hypothalamus and (b) absence of clinical abnormalities that might confound interpretation (e.g., hypothalamic-pituitary axis disease). For 39 studies that met our inclusion criteria, we reviewed electronic medical records to determine body weight at time of exam, height, age, gender, indication for magnetic resonance examination, final diagnosis, comorbidities (e.g., diabetes mellitus), and maximum recorded BMI. Exclusion criteria were as follows: BMI not available; age of less than 18 or more than 70 years; diagnosis of pituitary, hypothalamic, or neurodegenerative disorder (e.g., multiple sclerosis); cerebral atrophy; or history of bariatric surgery. Five subjects were excluded (age >70 [n = 2]; missing height [n = 1]; type 1 diabetes mellitus [n = 1]; CNS disease [n = 1]), yielding a total of 34 study participants (19 men, 15 women; mean age, 38 ± 12 years of age [range 18–63 years of age]; mean BMI, 28.5 ± 6.7 kg/m^2 [range 17.7–44.1 kg/m^2]). The most common indications for examination were hypogonadism (29%), elevated prolac-

tin levels (21%), and seizure (15%). On targeted visual inspection of the MBH, no studies were rated as abnormal, 7 were rated as equivocal (4 left, 1 right, 2 bilaterally), and 27 were rated were normal. There was no difference in the proportion of normal weight versus obese subjects who had an equivocal finding (Fisher's exact = 1.000; P = NS).

Single coronal slices through the hypothalamus, using T2-weighted fast spin echo (with or without fat saturation) or fluid-attenuated inversion recovery sequences, were identified for each subject. The MBH was visually inspected for abnormalities and rated as normal, equivocal, or abnormal. ROIs in the right and left MBH, the right and left amygdala, and the right and left putamen were defined by a neuroradiologist, who was blinded to all clinical information. Mean ROI signal intensity, standard deviation, and area of ROI were measured by using proprietary software on the PACS workstation (Centricity, GE Healthcare). Ratios were calculated by comparing the mean signal intensity in the MBH on each side with that in the ipsilateral amygdala ROI. A control ratio compared mean signal intensity in the putamen with that in the ipsilateral amygdala. Subjects were classified into 2 groups: obese (BMI >30 kg/m^2) and normal weight (BMI 19–24.9 kg/m^2, without any previously recorded BMI >30). Subjects with BMIs outside these ranges were excluded from group analyses, but data from all subjects were used in correlation analyses.

Statistics. All results are expressed as mean ± SEM. Statistical analyses were performed using GraphPad PRISM (version 4.0b; Graph Pad Software). One-way ANOVA with Dunnet's least significant difference post-hoc tests was used to compare mean values against those for chow controls, while 2-tailed Student's t tests were used for 2-group comparisons. For the human MRI study, group differences were assessed by unpaired 2-tailed Student's t test for continuous variables and Fisher's exact test for categorical variables. Normal distributions were confirmed for continuous variables. Pearson's correlation coefficients were calculated, and univariate linear regression was used to test for significance. A secondary analysis was performed as an alternate method to using signal ratios by using mean MBH signal intensity in a multivariate regression, with BMI as the independent variable and mean amygdala signal intensity as a covariate (performed in Stata 9.2, Statacorp). In all instances throughout, P values of less than 0.05 were considered significant.

Study approval. All study protocols involving rats and mice were approved by the Animal Care and Use Committees at the University of Washington, University of Cincinnati, or Yale University and conducted in accordance with the NIH guidelines for care and use of animals. The study involving analysis of human MRI scans was approved by the University of Washington Institutional Review Board (IRB). The IRB granted a waiver of informed consent; because this was a retrospective study that involved minimal risk to the involved subjects, it was not possible to contact all of the subjects, and appropriate safeguards were in place to protect subject confidentiality and privacy.

Acknowledgments

We thank A. Cubelo, L. Nguyen, C. Davis, I. David, and K. Ogimoto for technical assistance with the studies described in this manuscript. This work was supported by a NIH Career Development Award (DK088872) and Diabetes Endocrinology Research Center (DERC) Pilot and Feasibility Award (DK017047) to J. Thaler; NIH grants to M. Schwartz (DK068384, DK083042 and DK052989), M. Tschöp (DK077975), and T. Horvath (DK080000); The Netherlands Organization for Scientific Research – ALW Rubicon to C. Yi; and the Merit Review Research and Research Enhancement Award Programs of the Office of Research and Development, Department of Veterans Affairs to D. Baskin. D. Baskin is the recipient of a Department of Veterans Affairs Senior Research Career Scientist Award. Additional assistance and support was provided by the Nutrition Obesity Research Center (DK035816), Mouse Metabolic Phenotyping Center (U24 DK076126), and Cellular and Molecular Imaging Core of the DERC (DK017047) at the University of Washington.

Received for publication September 30, 2011, and accepted in revised form November 2, 2011.

Address correspondence to: Michael Schwartz, Diabetes and Obesity Center of Excellence, University of Washington School of Medicine, 815 Mercer St., Box 358055, Seattle, Washington 98109, USA. Phone: 206.897.5288; Fax: 206.897.5293; E-mail: mschwart@u.washington.edu.

David A. Sarruf's present address is: Diabetes Pharmacology, Novo Nordisk A/S, Maaloev, Denmark.

1. Morton GJ, Cummings DE, Baskin DG, Barsh GS, Schwartz MW. Central nervous system control of food intake and body weight. *Nature*. 2006; 443(7109):289–295.
2. Myers MG, Cowley MA, Munzberg H. Mechanisms of leptin action and leptin resistance. *Annu Rev Physiol*. 2008;70:537–556.
3. Myers MG Jr, Leibel RL, Seeley RJ, Schwartz MW. Obesity and leptin resistance: distinguishing cause from effect. *Trends Endocrinol Metab*. 2010; 21(11):643–651.
4. Lumeng CN, Saltiel AR. Inflammatory links between obesity and metabolic disease. *J Clin Invest*. 2011;121(6):2111–2117.
5. Schenk S, Saberi M, Olefsky JM. Insulin sensitivity: modulation by nutrients and inflammation. *J Clin Invest*. 2008;118(9):2992–3002.
6. Shoelson SE, Lee J, Goldfine AB. Inflammation and insulin resistance. *J Clin Invest*. 2006; 116(7):1793–1801.
7. De Souza CT, et al. Consumption of a fat-rich diet activates a proinflammatory response and induces insulin resistance in the hypothalamus. *Endocrinology*. 2005;146(10):4192–4199.
8. Thaler JP, Schwartz MW. Minireview: Inflammation and obesity pathogenesis: the hypothalamus heats up. *Endocrinology*. 2010;151(9):4109–4115.
9. Kleinridders A, et al. MyD88 signaling in the CNS is required for development of fatty acid-induced leptin resistance and diet-induced obesity. *Cell Metab*. 2009;10(4):249–259.
10. Milanski M, et al. Saturated fatty acids produce an inflammatory response predominantly through the activation of TLR4 signaling in hypothalamus: implications for the pathogenesis of obesity. *J Neurosci*. 2009;29(2):359–370.
11. Zhang X, Zhang G, Zhang H, Karin M, Bai H, Cai D. Hypothalamic IKKbeta/NF-kappaB and ER stress link overnutrition to energy imbalance and obesity. *Cell*. 2008;135(1):61–73.
12. Posey KA, et al. Hypothalamic proinflammatory lipid accumulation, inflammation, and insulin resistance in rats fed a high-fat diet. *Am J Physiol Endocrinol Metab*. 2009;296(5):E1003–E1012.
13. Kim F, et al. Vascular inflammation, insulin resistance, and reduced nitric oxide production precede the onset of peripheral insulin resistance. *Arterioscler Thromb Vasc Biol*. 2008;28(11):1982–1988.
14. Mori MA, et al. A systems biology approach identifies inflammatory abnormalities between mouse strains prior to development of metabolic disease. *Diabetes*. 2010;59(11):2960–2971.
15. Weisberg SP, McCann D, Desai M, Rosenbaum M, Leibel RL, Ferrante AW Jr. Obesity is associated with macrophage accumulation in adipose tissue. *J Clin Invest*. 2003;112(12):1796–1808.
16. Braffman BH, Zimmerman RA, Trojanowski JQ, Gonatas NK, Hickey WF, Schlaepfer WW. Brain MR: pathologic correlation with gross and histopathology. 2. Hyperintense white-matter foci in the elderly. *AJR Am J Roentgenol*. 1988;151(3):559–566.
17. Briellmann RS, Kalnins RM, Berkovic SF, Jackson GD. Hippocampal pathology in refractory temporal lobe epilepsy: T2-weighted signal change reflects dentate gliosis. *Neurology*. 2002;58(2):265–271.
18. Chung YL, et al. Conflicting MRI signals from gliosis and neuronal vacuolation in prion diseases. *Neuroreport*. 1999;10(17):3471–3477.
19. Marshall VG, Bradley WG Jr, Marshall CE, Bhoopat T, Rhodes RH. Deep white matter infarction: correlation of MR imaging and histopathologic findings. *Radiology*. 1988;167(2):517–522.
20. Posey K, et al. Hypothalamic proinflammatory lipid accumulation, inflammation, and insulin resistance in rats fed a high-fat diet. *Am J Physiol Endocrinol Metab*. 2009;296(5):E1003–E1012.
21. Sofroniew MV. Molecular dissection of reactive astrogliosis and glial scar formation. *Trends Neurosci*. 2009;32(12):638–647.
22. Pekny M, Nilsson M. Astrocyte activation and reactive gliosis. *Glia*. 2005;50(4):427–434.

23. Hanisch UK, Kettenmann H. Microglia: active sensor and versatile effector cells in the normal and pathologic brain. *Nat Neurosci*. 2007; 10(11):1387–1394.
24. Ransohoff RM, Perry VH. Microglial physiology: unique stimuli, specialized responses. *Annu Rev Immunol*. 2009;27:119–145.
25. Ito D, Imai Y, Ohsawa K, Nakajima K, Fukuuchi Y, Kohsaka S. Microglia-specific localisation of a novel calcium binding protein, Iba1. *Brain Res Mol Brain Res*. 1998;57(1):1–9.
26. Sharp FR, Massa SM, Swanson RA. Heat-shock protein protection. *Trends Neurosci*. 1999;22(3):97–99.
27. Chu CT. Autophagic stress in neuronal injury and disease. *J Neuropathol Exp Neurol*. 2006;65(5):423–432.
28. Wong E, Cuervo AM. Autophagy gone awry in neurodegenerative diseases. *Nat Neurosci*. 2010; 13(7):805–811.
29. Horvath TL, et al. Synaptic input organization of the melanocortin system predicts diet-induced hypothalamic reactive gliosis and obesity. *Proc Natl Acad Sci U S A*. 2010;107(33):14875–14880.
30. Moraes JC, et al. High-fat diet induces apoptosis of hypothalamic neurons. *PLoS One*. 2009;4(4):e5045.
31. Gropp E, et al. Agouti-related peptide-expressing neurons are mandatory for feeding. *Nat Neurosci*. 2005;8(10):1289–1291.
32. Turturici G, Sconzo G, Geraci F. Hsp70 and its molecular role in nervous system diseases. *Biochem Res Int*. 2011;2011:618127.
33. Kaushik S, et al. Autophagy in hypothalamic AgRP neurons regulates food intake and energy balance. *Cell Metab*. 2011;14(2):173–183.
34. Alirezaei M, Kemball CC, Whitton JL. Autophagy, inflammation and neurodegenerative disease. *Eur J Neurosci*. 2011;33(2):197–204.
35. Meng Q, Cai D. Defective hypothalamic autophagy directs the central pathogenesis of obesity via the IkappaB kinase beta (IKKbeta)/NF-kappaB pathway. *J Biol Chem*. 2011;286(37):32324–32332.
36. Ozcan L, et al. Endoplasmic reticulum stress plays a central role in development of leptin resistance. *Cell Metab*. 2009;9(1):35–51.
37. Graeber MB. Changing face of microglia. *Science*. 2010;330(6005):783–788.
38. Dheen ST, Kaur C, Ling EA. Microglial activation and its implications in the brain diseases. *Curr Med Chem*. 2007;14(11):1189–1197.
39. Paolicelli RC, et al. Synaptic pruning by microglia is necessary for normal brain development. *Science*. 2011;333(6048):1456–1458.
40. Ravussin Y, et al. Effects of chronic weight perturbation on energy homeostasis and brain structure in mice. *Am J Physiol Regul Integr Comp Physiol*. 2011; 300(6):R1352–R1362.
41. Perea G, Navarrete M, Araque A. Tripartite synapses: astrocytes process and control synaptic information. *Trends Neurosci*. 2009;32(8):421–431.
42. Hochberg I, Hochberg Z. Expanding the definition of hypothalamic obesity. *Obes Rev*. 2010; 11(10):709–721.
43. Thaler JP, et al. Atypical protein kinase C activity in the hypothalamus is required for lipopolysaccharide-mediated sickness responses. *Endocrinology*. 2009; 150(12):5362–5372.
44. Dietrich MO, et al. Agrp neurons mediate Sirt1's action on the melanocortin system and energy balance: roles for Sirt1 in neuronal firing and synaptic plasticity. *J Neurosci*. 2010;30(35):11815–11825.

Supplemental Figure Legends

Figure S1: Hypothalamic inflammation occurs within 3d of HFD consumption in C57Bl6 mice. Quantification of pro-inflammatory cytokine IL-1b and NF-kB pathway (IkBa, IKKb) gene expression in the hypothalamus of C57Bl6 wild-type mice fed Chow or HFD for up to 7d (n=6/group). All mRNA species are quantified relative to GAPDH housekeeping gene expression (by DD CT method) and presented as fold-change relative to Chow-fed controls. *p<0.05 vs Chow; #p = 0.072

Figure S2: HFD does not alter microglial number in brain regions outside the arcuate nucleus in rat. Quantification of microglial cell number in several regions of rat brain derived from the Iba-1 immunostained frozen sections utilized for the analysis in Figure 3. LHA= Lateral hypothalamic area; VMH = ventromedial hypothalamus.

Figure S3: HFD causes microglial accumulation in the mediobasal hypothalamus of C57Bl6 mice. Visualization of microglia by immunodetection of Iba1 protein in 10mm-thick frozen sections of mouse brain (n=8/group) taken from 10wk-old animals fed either A) Chow or B) HFD for 1wk, C) 2wk, or D) 3wk; or E) fed Chow for 8mo or F) HFD for 8mo.

Figure S1: Hypothalamic inflammation occurs within 3d of HFD consumption in C57Bl6 mice.

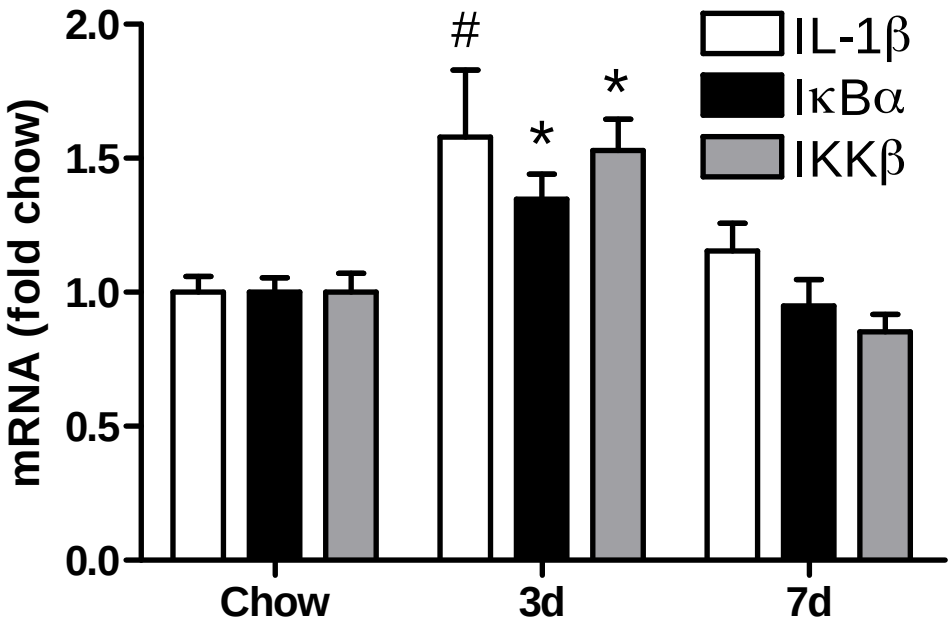

Figure S2: HFD does not alter microglial number in brain regions outside the arcuate nucleus in rat.

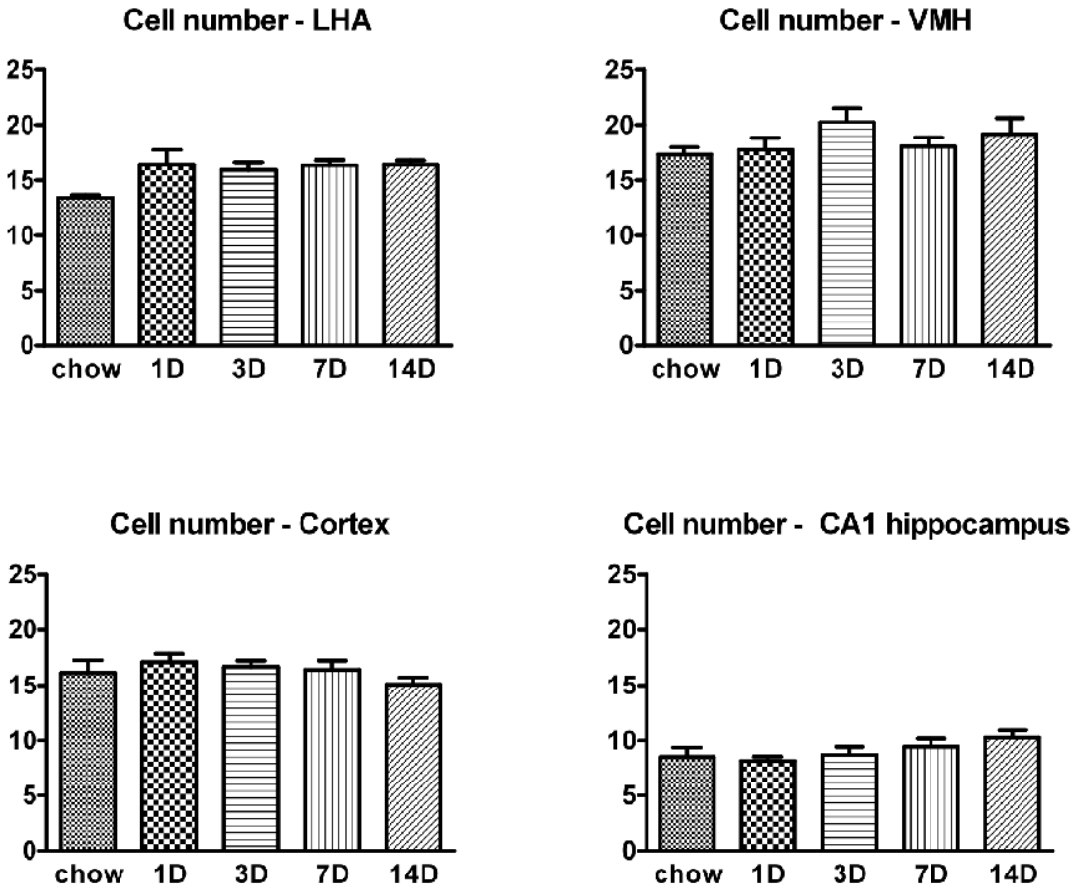

Figure S3: HFD causes microglial accumulation in the mediobasal hypothalamus of C57Bl6 mice.

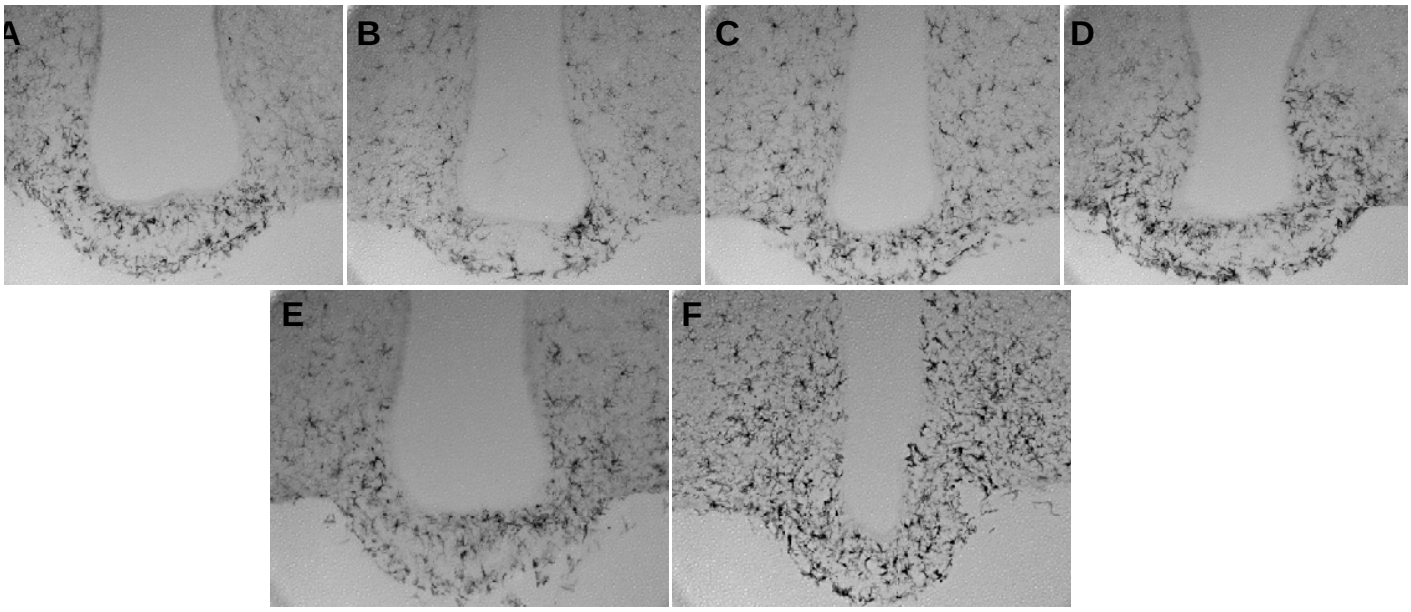

Anexo A-8. Loss of Autophagy in Proopiomelanocortin Neurons Perturbs Axon Growth and Causes Metabolic Dysregulation

Artigo publicado no periódico *Cell Metabolism.*

Please cite this article in press as: Coupé et al., Loss of Autophagy in Pro-opiomelanocortin Neurons Perturbs Axon Growth and Causes Metabolic Dysregulation, Cell Metabolism (2012), doi:10.1016/j.cmet.2011.12.016

Cell Metabolism
Short Article

Loss of Autophagy in Pro-opiomelanocortin Neurons Perturbs Axon Growth and Causes Metabolic Dysregulation

Bérengère Coupé,[1] Yuko Ishii,[1] Marcelo O. Dietrich,[3,4] Masaaki Komatsu,[5,6,7] Tamas L. Horvath,[3] and Sebastien G. Bouret[1,2,*]

[1]The Saban Research Institute, Neuroscience Program, Children's Hospital Los Angeles, University of Southern California, Los Angeles, CA 90027, USA
[2]Inserm, Jean-Pierre Aubert Research Center, U837, University of Lille 2, Lille, 59045, France
[3]Program in Integrative Cell Signaling and Neurobiology of Metabolism, Section of Comparative Medicine, Yale University School of Medicine, New Haven, CT 06520, USA
[4]Department of Biochemistry, Universidade Federal do Rio Grande do Sul, Porto Alegre RS 90035, Brazil
[5]Laboratory of Frontier Science, Tokyo Metropolitan Institute of Medical Science, Bunkyo-ku, Tokyo 113-8613, Japan
[6]Department of Biochemistry, Juntendo University School of Medicine, Bunkyo-ku, Tokyo 113-8421, Japan
[7]PRESTO, Japan Science and Technology Corporation, Kawaguchi 332-0012, Japan
*Correspondence: sbouret@chla.usc.edu
DOI 10.1016/j.cmet.2011.12.016

SUMMARY

The hypothalamic melanocortin system, which includes neurons that produce pro-opiomelanocortin (POMC)-derived peptides, is a major negative regulator of energy balance. POMC neurons begin to acquire their unique properties during neonatal life. The formation of functional neural systems requires massive cytoplasmic remodeling that may involve autophagy, an important intracellular mechanism for the degradation of damaged proteins and organelles. Here we investigated the functional and structural effects of the deletion of an essential autophagy gene, *Atg7*, in POMC neurons. Lack of Atg7 in POMC neurons caused higher postweaning body weight, increased adiposity, and glucose intolerance. These metabolic impairments were associated with an age-dependent accumulation of ubiquitin/p62-positive aggregates in the hypothalamus and a disruption in the maturation of POMC-containing axonal projections. Together, these data provide direct genetic evidence that Atg7 in POMC neurons is required for normal metabolic regulation and neural development, and they implicate hypothalamic autophagy deficiency in the pathogenesis of obesity.

INTRODUCTION

Appetite, energy balance, and metabolism are carefully regulated by the central nervous system (CNS) (see Elmquist et al., 2005; Gao and Horvath, 2007; and Sawchenko, 1998 for reviews). The important components of this neural network include neurons located in the arcuate nucleus of the hypothalamus (ARH), particularly neurons producing pro-opiomelanocortin (POMC). POMC neurons reduce food intake and increase energy expenditure by releasing α-melanocyte-stimulating hormone (αMSH), a product of POMC processing, which activates melanocortin-4 receptors (MC4R) (Cone, 2006). More recent targeted deletion studies have specifically shown the importance of POMC neurons in mediating the physiological actions of metabolic hormones, such as leptin and insulin (Belgardt and Brüning, 2010; Elmquist et al., 2005). POMC neurons provide extensive projections to other parts of the hypothalamus, including the paraventricular (PVH) and dorsomedial (DMH) nuclei of the hypothalamus and the lateral hypothalamic area (LHA), to exert their anorectic effects. Each of these target nuclei also express MC4R (Cone, 2006). Similar to many other functional neural systems, POMC neurons begin to acquire their unique properties during neonatal life. In rodents, arcuate POMC neural circuits develop primarily during the first three weeks of postnatal life, under the influence of both intrinsic and extrinsic cues (Bouret, 2010; Levin, 2006; Sullivan and Grove, 2010). The process of developing highly specialized cellular structures, such as POMC neurons, also requires massive cytoplasmic remodeling. However, the cellular and molecular mechanisms underlying this remodeling process are largely unknown, and its functional relevance remains equally undetermined.

Autophagy is a major cellular degradation process in which parts of the cytoplasm and intracellular organelles are engulfed within double-membraned vesicles, known as autophagosomes, in preparation for the turnover and recycling of these cellular constituents (Klionsky, 2007). Another important function of autophagy is in the supply of nutrients for survival. It also plays an important role in cell growth, development, and homeostasis, where it helps to maintain a balance between the synthesis, degradation, and the subsequent recycling of cellular components (Cecconi and Levine, 2008; Maiuri et al., 2007). In particular, low levels of basal autophagy are important for maintaining the quality of proteins and organelles and are therefore important for the maintenance of cell function and growth. Recent genetic studies have also highlighted the importance of autophagy in physiological regulations. For example, the targeted deletion of

Please cite this article in press as: Coupé et al., Loss of Autophagy in Pro-opiomelanocortin Neurons Perturbs Axon Growth and Causes Metabolic Dysregulation, Cell Metabolism (2012), doi:10.1016/j.cmet.2011.12.016

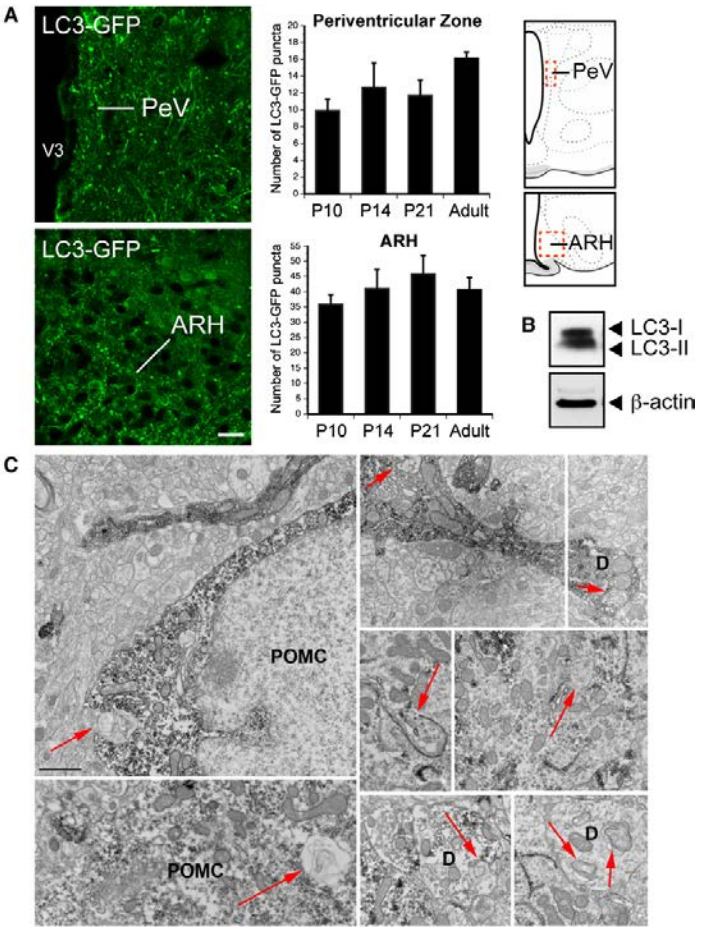

Figure 1. Identification of Autophagy in Hypothalamic POMC Processes

(A) Representative images and quantification of LC3-GFP puncta in the arcuate nucleus (ARH) and the hypothalamic periventricular zone (PeV) of P10, P14, P21, and adult (8- to 9-week-old) mice (n = 4–5 per group). Dashed boxes in the schematics represent the approximate borders of the areas used for quantification.

(B) Immunoblot analysis of LC3 (LC3-I, 18 kDa; LC3-II, 16 kDa) and b-actin (as a loading control) from hypothalami derived from adult mice.

(C) Representative electron micrographs showing autophagosomes (arrows) in POMC-immunolabeled perikarya and processes of P24 wild-type mice. D, dendrites, V3, third ventricle. Values are shown as mean ± SEM. Scale bar, 15 μm (A) and 1 μm (C).

essential autophagy genes have revealed that constitutive autophagy contributes to energy homeostasis (including body weight regulation, adiposity, and glucose homeostasis) by acting on liver physiology (Komatsu et al., 2007a), pancreatic morphology and function (Ebato et al., 2008; Jung et al., 2008), and adipocyte differentiation (Singh et al., 2009; Zhang et al., 2009). In addition, deficiency of autophagy in AgRP neurons causes leanness in adult mice (Kaushik et al., 2011), showing the involvement of hypothalamic autophagy in the control of energy balance.

Although recent advances have indicated that constitutive autophagy contributes to the central control of energy homeostasis, the structural and functional importance of autophagy in hypothalamic anorexigenic neural circuits remains unknown. In the present study, we generated mice deficient in *Atg7*, an essential autophagy gene, specifically in POMC neurons to determine the role of autophagy in this neuronal population. The results indicate that autophagy is important for normal maturation of POMC axonal projections and that the absence of autophagy in POMC neurons results in lifelong metabolic disturbances.

RESULTS

Autophagy Occurs Constitutively in Hypothalamic POMC Processes

To investigate whether autophagy occurs in the postnatal hypothalamus under basal conditions, we used a transgenic mouse in which microtubule-associated protein 1 light chain 3 (LC3) has been fused to green fluorescent protein (GFP). Because LC3 is a reliable marker of autophagosomes, LC3-GFP mice are widely used to monitor autophagy in vivo (Mizushima et al., 2004). LC3-GFP puncta were readily detectable in various regions of the CNS in basal conditions (Figure S1), including in the ARH (Figure 1A). LC3-GFP puncta were found in the ARH as early as postnatal day 10, and the presence of autophagosomes persisted at weaning and into adulthood (Figure 1A). The density of LC3-GFP puncta displayed no significant variations across the ages studied (Figure 1A), and puncta were detected in both perikaryons and processes (Figure 1A). The LC3-GFP signal was not restricted to the ARH; it was also observed in processes located in the periventricular zone of the hypothalamus, which appears to be the major route for ascending ARH efferent connections (Bouret et al., 2004a, 2004b) (Figure 1A). The presence of constitutive autophagy in the hypothalamus was further confirmed by the presence of both LC3 I (soluble form) and LC3 II (membrane-bound form) immunoreactivity in the adult hypothalamus under basal conditions (Figure 1B).

Because POMC is expressed in ARH neurons and in axon terminals traveling throughout the periventricular zone of the hypothalamus (Bouret et al., 2004a), i.e., where basal autophagy was detected, we next investigated whether autophagy occurs specifically in POMC neurons by using electron microscopy. Ultrastructural analysis of material derived from P24 wild-type mice revealed the presence of double-membraned autophagosomes in both neuronal perikarya and neuronal processes of POMC neurons, including dendrites (Figure 1C).

Together, these data indicate that autophagy occurs constitutively in the hypothalamus. The presence of autophagosomes

Please cite this article in press as: Coupé et al., Loss of Autophagy in Pro-opiomelanocortin Neurons Perturbs Axon Growth and Causes Metabolic Dysregulation, Cell Metabolism (2012), doi:10.1016/j.cmet.2011.12.016

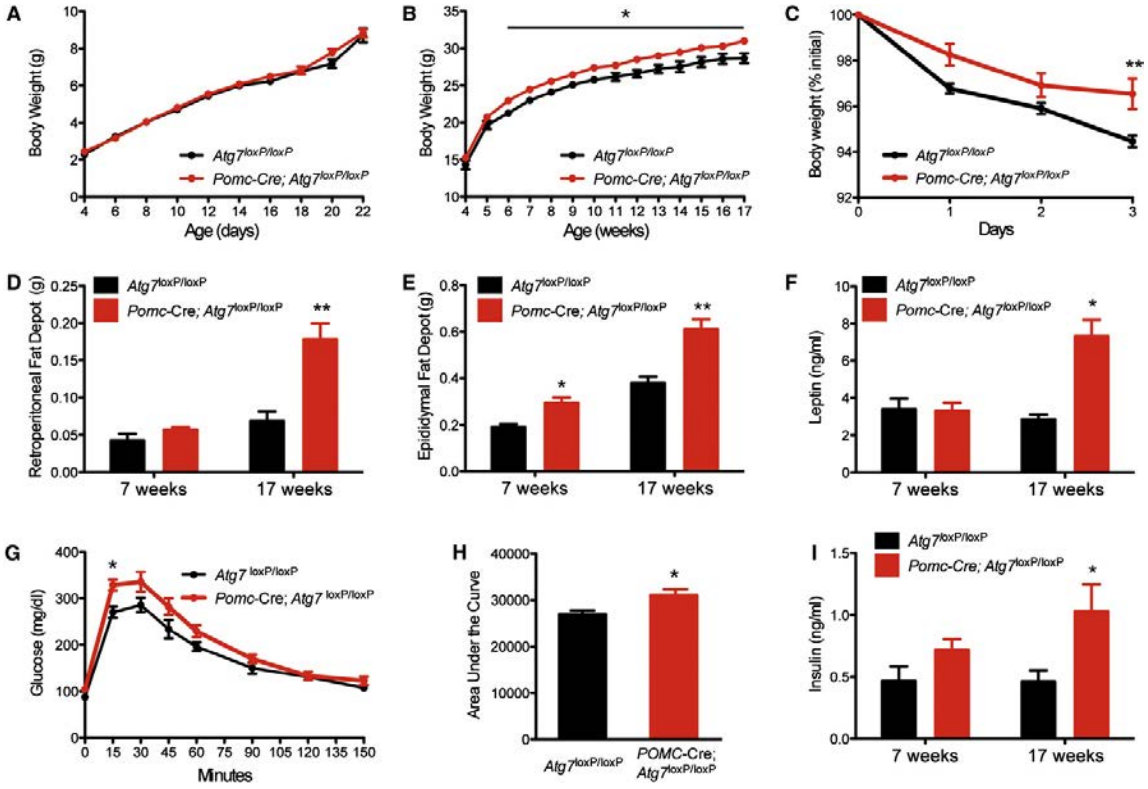

Figure 2. Altered Metabolism in Mice Lacking Autophagy in POMC Neurons

(A and B) Pre- (A) and postweaning (B) growth curves of *Atg7*$^{loxP/loxP}$ (n ≥ 9) and *Pomc*-Cre; *Atg7*$^{loxP/loxP}$ (n = 15) male mice.

(C) Leptin sensitivity of 10-week-old *Atg7*$^{loxP/loxP}$ (n = 6) and *Pomc*-Cre; *Atg7*$^{loxP/loxP}$ (n = 8) male mice.

(D and E) Mass of retroperitoneal (D) and epididymal (E) fat of 7- and 15- to 17-week-old *Atg7*$^{loxP/loxP}$ (n = 4–5) and *Pomc*-Cre; *Atg7*$^{loxP/loxP}$ (n = 5–11) male mice.

(F) Serum leptin and (I) insulin levels in *Atg7*$^{loxP/loxP}$ (n = 8) and *Pomc*-Cre; *Atg7*$^{loxP/loxP}$ (n = 6) male mice from 7 and 15 to 17 weeks of age.

(G and H) Glucose tolerance test (GTT) (G) and area under the GTT curve (H) of 8- to 9-week-old *Atg7*$^{loxP/loxP}$ (n = 7) and *Pomc*-Cre; *Atg7*$^{loxP/loxP}$ (n = 12) male mice.

Values are shown as mean ± SEM. *p < 0.05 versus *Atg7*$^{loxP/loxP}$.

specifically in POMC neuronal processes suggests a role for hypothalamic autophagy in metabolic regulation.

Specific Deletion of Atg7 in POMC Neurons Causes Metabolic Disturbances

To determine the physiological role of autophagy in POMC neurons, we generated mice that lack *Atg7*, an essential autophagy gene, specifically in POMC neurons. We crossed mice carrying an *Atg7*^{loxP} allele (Komatsu et al., 2005) with mice that express *Cre* recombinase in a POMC-specific manner (*Pomc*-Cre) (Balthasar et al., 2004). The resulting *Pomc*-Cre; *Atg7*$^{loxP/loxP}$ mice were born normally and survived to adulthood. *Pomc*-Cre; *Atg7*$^{loxP/loxP}$ mice had body weights undistinguishable from their *Atg7*$^{loxP/loxP}$ control littermates until 6 weeks of age (group, $F_{(1/322)} = 2.08$, $p = 0.1498$; age, $F_{(9/322)} = 159.22$, $p < 0.0001$; interaction, $F_{(9/322)} = 0.39$, $p = 0.9413$) (Figures 2A and 2B). However, starting at 6 weeks of age, mutant mice displayed significantly higher body weights compared with control *Atg7*$^{loxP/loxP}$ mice, and these changes in body weight persisted until 17 weeks of age (group, $F_{(1/311)} = 103.80$, $p < 0.0001$; age, $F_{(13/311)} = 188.66$, $p < 0.0001$; interaction, $F_{(13/311)} = 0.35$, $p = 0.9835$) (Figure 2B). In addition, epididymal and retroperitoneal fat pad weights were also significantly higher in adult *Pomc*-Cre; *Atg7*$^{loxP/loxP}$ mice compared to *Atg7*$^{loxP/loxP}$ mice (Figures 2D and 2E). Moreover, there was a shift in adipocyte size distribution toward larger adipocytes in mutant mice (Figures S2A–S2C). Consistent with these findings, serum leptin levels were also significantly elevated in mutant mice compared to control mice at 17 weeks of age (Figure 2F). Because POMC neurons are major mediators for leptin's regulatory actions, we performed leptin sensitivity tests and found that the weight loss effect of leptin was also attenuated in *Pomc*-Cre; *Atg7*$^{loxP/loxP}$ mice compared to *Atg7*$^{loxP/loxP}$ mice. This attenuation in leptin sensitivity was observed as early as at 7 weeks of age (data not shown) and persisted at 17 weeks of age (group, $F_{(1/39)} = 13.79$, $p = 0.0006$; days of treatment, $F_{(3/39)} = 40.71$, $p < 0.0001$; interaction, $F_{(3/39)} = 2.44$, $p = 0.0786$) (Figure 2C). Whether these metabolic defects are also associated with

Please cite this article in press as: Coupé et al., Loss of Autophagy in Pro-opiomelanocortin Neurons Perturbs Axon Growth and Causes Metabolic Dysregulation, Cell Metabolism (2012), doi:10.1016/j.cmet.2011.12.016

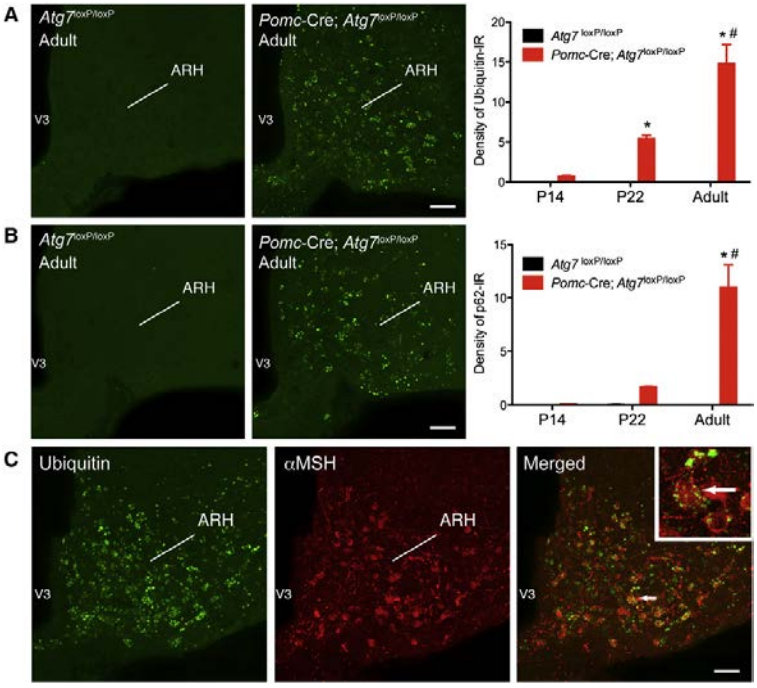

Figure 3. Lack of Autophagy in POMC Neurons Leads to the Gradual Accumulation of Ubiquitin Aggregates in the Arcuate Nucleus

(A and B) Quantification of ubiquitin- (A) and p62-immunoreactivity (B) in the arcuate nucleus (ARH) of P14, P22, and adult (15- to 17-week-old) *Atg7*$^{loxP/loxP}$ (n = 4) and *Pomc*-Cre; *Atg7*$^{loxP/loxP}$ (n = 4) male mice. Confocal images illustrating ubiquitin- (A) and p62-immunoreactivity (B) in the ARH of adult *Atg7*$^{loxP/loxP}$ and *Pomc*-Cre; *Atg7*$^{loxP/loxP}$ mice.

(C) Confocal images showing the presence of ubiquitin-immunoreactivity (green fluorescence) in αMSH-positive cells (red fluorescence) of an adult *Pomc*-Cre; *Atg7*$^{loxP/loxP}$ mouse. The arrow points to a double labeled cell. V3, third ventricle. Values are shown as mean ± SEM. *p < 0.05 versus P14; #p < 0.05 versus P22. Scale bars, 50 μm.

changes in locomotor activity and energy expenditure remains to be investigated.

To examine whether deletion of autophagy in POMC neurons also had consequences for glucose homeostasis, we performed glucose tolerance tests. Fasting glucose levels were significantly elevated in adult *Pomc*-Cre; *Atg7*$^{loxP/loxP}$ mice compared to *Atg7*$^{loxP/loxP}$ mice, and when exposed to a glucose challenge, mutant mice displayed impaired glucose tolerance as compared to control mice (Figures 2G and 2H). Serum insulin levels were also elevated in fed *Pomc*-Cre; *Atg7*$^{loxP/loxP}$ mice compared to *Atg7*$^{loxP/loxP}$ mice at 17 weeks of age (Figure 2I).

Mice deficient in autophagy in POMC neurons also display sexual dimorphism in metabolic regulation. Although female *Pomc*-Cre; *Atg7*$^{loxP/loxP}$ mice displayed higher body weights as early as 9 weeks of age, they did not have changes in glucose tolerance or leptin and insulin levels (Figures S2D–S2G).

Together, these data indicate that the absence of autophagy in POMC neurons has functional consequences on body weight and glucose regulation and these effects are sexually dimorphic.

Lack of Atg7 in POMC Neurons Causes Age-Dependent Accumulation of Ubiquitin and p62 Aggregates in the Arcuate Nucleus

Because defects in autophagy have been shown to cause the accumulation of ubiquitin-containing inclusion cell bodies (Komatsu et al., 2006, 2005), we next evaluated ubiquitin-immunoreactivity (IR) in *Pomc*-Cre; *Atg7*$^{loxP/loxP}$ mice. Hypothalami of control *Atg7*$^{loxP/loxP}$ mice were devoid of ubiquitin-IR. In contrast, numerous inclusions immunopositive for ubiquitin were detected in the hypothalamus of *Pomc*-Cre; *Atg7*$^{loxP/loxP}$ mice (Figure 3A). Notably, the accumulation of ubiquitin was restricted to the ARH (Figure S3A) in an age-dependent manner. A quantitative analysis of the experimental material revealed that although the density of ubiquitin-IR was modest in the ARH of *Pomc*-Cre; *Atg7*$^{loxP/loxP}$ mice at P14, levels of ubiquitin-IR in the ARH were increased 8-fold between P14 and P22 and increased 3-fold between P22 and adult mice, indicating a gradual increase in ubiquitin accumulation in the ARH of mutant mice (Figure 3A).

We also investigated the expression of the polyubiquitin-binding protein p62/SQSTM1, which links ubiquitinated proteins to the autophagy apparatus (Komatsu et al., 2007a). In good agreement with our ubiquitin findings, *Pomc*-Cre; *Atg7*$^{loxP/loxP}$ mice exhibited substantial p62-IR in the ARH as early as P22, and levels of p62-IR continued to increase until adulthood (Figure 3B). Double-labeling experiments further showed that 85% of ubiquitin-immunopositive cells also express POMC (αMSH-IR) and that 95% of αMSH-IR cells are also immunopositive for ubiquitin (Figures 3C and S3B).

Together, these data indicate that deletion of Atg7 in POMC neurons leads to the age-dependent accumulation of ubiquitin and p62 in arcuate neurons. The finding that ubiquitin is largely restricted to αMSH-IR neurons also confirms the selective reduction of autophagy in POMC neurons and suggests that POMC neurons may have biological alterations.

Mice with POMC Neuron-Specific Deletion of Atg7 Display Abnormal Development of POMC Neuronal Projections

To investigate whether autophagy deficiency in POMC neurons causes structural alterations, we analyzed POMC-containing neural projections in *Pomc*-Cre; *Atg7*$^{loxP/loxP}$ and *Atg7*$^{loxP/loxP}$ mice. We paid particular attention to the POMC-derived αMSH projections to the paraventricular nucleus of the hypothalamus (PVH) because of their well-established importance in the neural control of food intake and energy balance (Ellacott and

Please cite this article in press as: Coupé et al., Loss of Autophagy in Pro-opiomelanocortin Neurons Perturbs Axon Growth and Causes Metabolic Dysregulation, Cell Metabolism (2012), doi:10.1016/j.cmet.2011.12.016

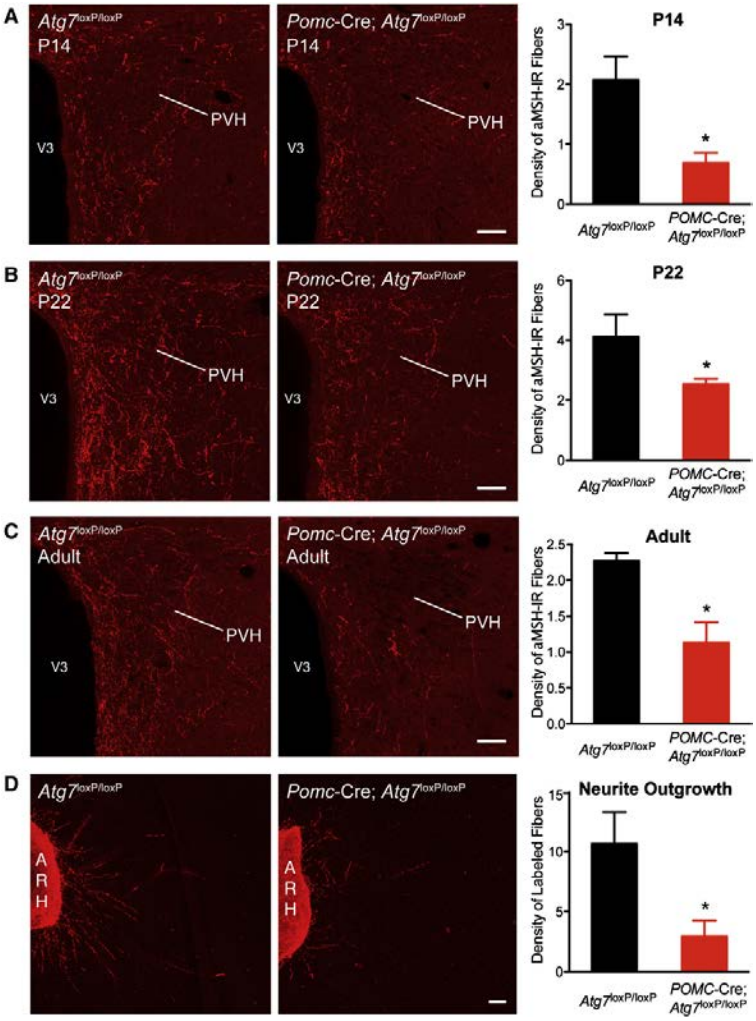

Figure 4. Disruption of POMC Projections in Mice Lacking Autophagy in POMC Neurons

Confocal images and quantification of αMSH-IR fibers in the PVH of P14 (A), P22 (B), and adult (15- to 17-week-old) (C) *Atg7*$^{loxP/loxP}$ (n = 4) and *Pomc*-Cre; *Atg7*$^{loxP/loxP}$ (n = 4) male mice.

(D) Images and quantification of b-endorphin (a POMC-derived peptide)-immunopositive fibers derived from isolated organotypic cultures of the ARH from P4 *Atg7*$^{loxP/loxP}$ and *Pomc*-Cre; *Atg7*$^{loxP/loxP}$ mice. ARH, arcuate nucleus of the hypothalamus; PVH, paraventricular nucleus of the hypothalamus; V3, third ventricle. Values are shown as mean ± SEM. *p < 0.05 versus *Atg7*$^{loxP/loxP}$. Scale bars, 50 μm.

Cone, 2006; Elmquist et al., 2005; Gao and Horvath, 2007; Sawchenko, 1998). Although the overall distribution of αMSH-IR fibers was quite similar between mutant mice and control animals, clear differences were apparent in the density of the labeled fibers. The density of αMSH-IR fibers in the PVH of *Pomc*-Cre; *Atg7*$^{loxP/loxP}$ mice was 1.5-fold to 3-fold lower than that observed in the *Atg7*$^{loxP/loxP}$ mice (Figures 4A–4C). The reduction in αMSH fiber density was observed as early as P14 (Figure 4A) and persisted at P22 (Figure 4B). To determine if the defects in αMSH projections observed in neonatal mutant mice were permanent, we also performed immunohistochemical labeling of αMSH in brain sections from adult *Pomc*-Cre; *Atg7*$^{loxP/loxP}$ and *Atg7*$^{loxP/loxP}$ mice. As observed in neonates, the average density of αMSH-IR fibers in the PVH remained diminished in adult *Pomc*-Cre; *Atg7*$^{loxP/loxP}$ mice relative to that of *Atg7*$^{loxP/loxP}$ mice (Figure 4C). In adults, the density of αMSH-IR fibers in the PVH remained 2-fold lower in mutant mice relative to that of control mice. A substantial disruption in the density of labeled fibers was observed in both the parvicellular and magnocellular parts of the PVH. Similar reductions in αMSH fiber density were also observed in the DMH and LHA (Figures S4D and S4E), indicating that Atg7 deficiency causes extensive disruption of αMSH projections to each of their major terminal fields. To confirm that lack of autophagy in POMC neurons altered the pattern of ARH axonal projections, we implanted a fluorescent axonal tracer DiI into the ARH of *Pomc*-Cre; *Atg7*$^{loxP/loxP}$ and *Atg7*$^{loxP/loxP}$ mice. The density of ARH DiI-labeled fibers was significantly attenuated in the PVH of P14 mutant mice as compared to control mice (Figure S4C).

To confirm that the mutation in *Pomc*-Cre; *Atg7*$^{loxP/loxP}$ mice does not affect the development of other non-POMC circuits, we examined neuronal projections containing AgRP, another neuropeptide system present in the ARH that sends overlapping projections to the PVH. Another reason for studying this neuronal population specifically is because POMC and AgRP/NPY neurons share a common ontological lineage, and it was therefore possible that some of Cre-expressing cells also contain AgRP/NPY (Padilla et al., 2010). However, despite a marked attenuation in the density of αMSH-IR fibers, neural projections containing AgRP appear unaltered in *Pomc*-Cre; *Atg7*$^{loxP/loxP}$ mice (Figure S3C). Consistent with these findings, colocalizations between AgRP- and ubiquitin-IR were rare in mutant mice (Figure S3B). Also, *Agrp* and *Npy* mRNA levels are similar between mutant and control mice (Figures S3D and S3E). In addition, in sharp contrast to *Agrp*-Cre; *Atg7*$^{loxP/loxP}$ mice that are lean (Kaushik et al., 2011), *Pomc*-Cre; *Atg7*$^{loxP/loxP}$ mice have higher body weight and adiposity. Together, these data suggest that the AgRP/NPY system is relatively normal in *Pomc*-Cre; *Atg7*$^{loxP/loxP}$ mice and that the mutation present in *Pomc*-Cre; *Atg7*$^{loxP/loxP}$ mice selectively affects POMC neurons.

Please cite this article in press as: Coupé et al., Loss of Autophagy in Pro-opiomelanocortin Neurons Perturbs Axon Growth and Causes Metabolic Dysregulation, Cell Metabolism (2012), doi:10.1016/j.cmet.2011.12.016

Because autophagy has been suggested to exert neuroprotective actions (Hara et al., 2006; Komatsu et al., 2006, 2007b), we also assessed whether *Atg7* deficiency affects the survival of POMC neurons. The neuroanatomical distribution and number of neurons immunopositive for b-endorphins (a product of POMC neurons) did not differ between *Pomc*-Cre; *Atg7*$^{loxP/loxP}$ and *Atg7*$^{loxP/loxP}$ mice (Figure S4A). Supporting these observations, there were no noticeable differences in the number of TUNEL-positive cells (a marker of apoptosis) or apoptotic blebbed nuclei in the hypothalamus of adult mutant mice as compared to controls (data not shown). In addition, hypothalamic *Pomc* mRNA levels did not differ between *Pomc*-Cre; *Atg7*$^{loxP/loxP}$ and *Atg7*$^{loxP/loxP}$ mice (Figure S4B). These data suggest that the absence of Atg7 does not alter POMC neuron survival. They also indicate that the low density of POMC-derived fibers observed in mutant mice is due to alterations in axon growth as opposed to a reduction in cell number or peptide content in axons.

To determine whether deficiency of *Atg7* might alter the ability of POMC neurons to send axonal projections, we conducted a series of in vitro experiments and evaluated POMC axon growth in both *Pomc*-Cre; *Atg7*$^{loxP/loxP}$ and *Atg7*$^{loxP/loxP}$ mice. After 36 hr in vitro, organotypic ARH explants derived from *Atg7*$^{loxP/loxP}$ control mice exhibit marked POMC axon growth, as revealed by the presence of GAP-43 (a marker of axon growth) and b-endorphin (a marker of POMC neurons) double-labeled fibers extending from the edge of ARH explants (Figure 4D). In contrast, this basal POMC axon growth was severely blunted if the explant was derived from *Pomc*-Cre; *Atg7*$^{loxP/loxP}$ mice (Figure 4D). The overall density of GAP-43-b-endorphin double-labeled neurites extending from explants from *Pomc*-Cre; *Atg7*$^{loxP/loxP}$ mice was 2.5-fold lower than that of *Atg7*$^{loxP/loxP}$ mice (Figure 4D).

Together, these data indicate that *Pomc*-Cre; *Atg7*$^{loxP/loxP}$ mice display an abnormal development of POMC neuronal projections that may be the result of the diminished ability of ARH POMC neurons to extend axons during postnatal development.

DISCUSSION

It is well documented that autophagy, a cellular pathway involved in degrading and recycling various intracellular constituents, plays a major role in the peripheral regulation of metabolism by acting on pancreatic, liver, and adipocyte morphology and function (Ebato et al., 2008; Jung et al., 2008; Komatsu et al., 2007a; Singh et al., 2009; Zhang et al., 2009). More recently, a role for autophagy in the central control of energy metabolism has been identified (Kaushik et al., 2011). However, the precise contribution of autophagy in various subpopulations of hypothalamic neurons involved in metabolic regulation and the structural consequences of autophagy deficiency on the organization of hypothalamic feeding neural circuits remain unknown. In the present study, we reported that autophagy is constitutively active in key parts of the hypothalamus that play a role in feeding and energy balance, including in POMC neurons. By generating mice with a targeted deletion of a key autophagy gene (Atg7) selectively in POMC neurons, we also showed that the loss of autophagy in POMC neurons resulted in increased postweaning body weight, increased adiposity, and perturbations in glucose homeostasis. Autophagy deficiency in POMC neurons also caused an age-dependent accumulation of ubiquitin and p62 and alterations in the maturation of POMC axonal processes.

Neurons were originally thought to be resistant to autophagy induction. This hypothesis was based on the fact that autophagy is induced in almost all tissues, except the brain, following starvation (Mizushima et al., 2004). Nevertheless, there is now a growing appreciation that constitutive autophagy plays an important role in the CNS. Mice that are deficient in either Atg5 or Atg7 in the CNS develop progressive behavioral defects and motor deficits that are usually associated with neurodegenerative diseases (Hara et al., 2006; Komatsu et al., 2006). Consistent with these behavioral observations, the same mutant mice display early signs of neurodegeneration that include massive neuronal loss and abnormal protein aggregation in the cortex and the cerebellum (Hara et al., 2006; Komatsu et al., 2006). A more recent study has implicated autophagy in the central control of energy balance. Mice lacking autophagy specifically in arcuate AgRP neurons have reduced body weight and adiposity and display diminished refeeding response to fasting (Kaushik et al., 2011). Our study extends the role of CNS autophagy in metabolic regulation and brain development. It shows the widespread importance of autophagy in the CNS, particularly in POMC neurons, a major neuronal population promoting negative energy balance. The presence of constitutively active autophagy in ARH neurons and processes is supported by the following observations: LC3, a major constituent of the autophagosome, is expressed in the ARH and the periventricular zone of the hypothalamus (the major route for ascending ARH efferent connections) during postnatal and adult life, and the lack of autophagy (as observed in *Pomc*-Cre; *Atg7*$^{loxP/loxP}$ mice) leads to accumulation of ubiquitin and p62 in the ARH. Moreover, *Pomc*-Cre; *Atg7*$^{loxP/loxP}$ mice, which lack constitutive autophagy, displayed marked structural and physiological alterations. In contrast to mice that lack the autophagy gene in neurons (i.e., *Nestin*-Cre; *Atg5*$^{loxP/loxP}$ or *Nestin*-Cre; *Atg7*$^{loxP/loxP}$ mice), we did not observe significant neuronal loss in *Pomc*-Cre; *Atg7*$^{loxP/loxP}$ mice. Despite a marked reduction in POMC fiber density, POMC cell number was not different between adult control and mutant mice, and there was no evident cell death induction (as evidenced by the absence of TUNEL-positive cells or apoptotic blebbed nuclei) in the hypothalamus of *Pomc*-Cre; *Atg7*$^{loxP/loxP}$ mice. These data suggest that autophagy may exert different functions on different brain regions. They also imply that CNS autophagy is not only important for protection from neurodegenerative diseases, but it is also an important mechanism involved in normal brain development.

The complex patterns of neuronal wiring in the adult hypothalamus depend on a series of events that establish a framework on which functional circuits can be built. The cellular and molecular processes that are involved in the formation of a functioning hypothalamus remain largely unknown. Previous studies have reported autophagy vacuoles in distal axons and have suggested that autophagy plays an important role in axon remodeling and homeostasis during aging (Yue et al., 2009). The present study suggests that autophagy is an important intracellular

process for the normal development of neural projections derived from POMC neurons. The density of αMSH-immunoreactive fibers is markedly attenuated in the hypothalamus of *Pomc*-Cre; *Atg7*$^{loxP/loxP}$ mice, and the disruption in POMC neural projections is found in all major terminal fields of POMC axons, such as the PVH, DMH, and LHA. These observations support the idea that the lack of autophagy alters the ability of POMC neurons to send axonal projections to their target nuclei. Consistent with this hypothesis, the reduction in the density of αMSH-immunoreactive fibers is observed as early as P14, i.e., when POMC neurons extend their axonal projections to their target nuclei (Bouret, 2010; Sullivan and Grove, 2010). Importantly, the density of ARH DiI-labeled fibers is also attenuated in the PVH of mutant mice, suggesting that lack of autophagy causes structural changes in the axonal projection pattern from ARH POMC neurons. Our in vitro studies further support this hypothesis by showing that the ability of ARH POMC neurons to extend their axons is attenuated in explants derived from *Pomc*-Cre; *Atg7*$^{loxP/loxP}$ mice.

Notably, the reduction in axon growth specifically affected POMC axons containing GAP-43 (a marker of axons independent of peptide content), supporting the idea that the reduction in αMSH-immunoreactive fibers found in mutant mice is caused by a reduction in axon density, as opposed to changes in the peptide content in axons. Consistent with this idea, hypothalamic *Pomc* mRNA levels did not differ between *Pomc*-Cre; *Atg7*$^{loxP/loxP}$ and *Atg7*$^{loxP/loxP}$ mice. However, we cannot rule out the possibility that the reduction in immunostaining observed in mutant mice is not due to an increase in peptide release. Nevertheless, a reduction in peptide release is more often associated with a lack of autophagy. For example, glucose-stimulated insulin release in isolated islets is reduced in mice lacking Atg7 specifically in pancreatic beta cells (Ebato et al., 2008). We have also checked the density of fibers containing b-endorphin (another peptide derived from POMC) and found that b-endorphin-containing projections were also reduced in *Pomc*-Cre; *Atg7*$^{loxP/loxP}$ mice (data not shown), supporting the idea that the lack of autophagy does not alter the pattern of POMC peptide processing and specifically affects axon growth.

Optimal brain wiring, including optimal hypothalamic neuronal circuitry, depends on the capacity to change metabolic states in response to external stimuli that vary from early development to adulthood (Elmquist and Flier, 2004; Horvath and Bruning, 2006). Depending on the availability of nutrients (such as proteins) or trophic stimuli (such as hormones), neurons can metabolically switch from an anabolic state to a state of catabolism. Autophagy has long been characterized as a key cellular mechanism for maintaining energy homeostasis during nutrient-poor conditions. Accordingly, short-term food restriction causes induction of autophagy in various tissues, including the hypothalamus (Alirezaei et al., 2010; Kaushik et al., 2011). The present study indicates that under basal conditions, hypothalamic autophagy plays a key role in metabolic regulation. Other cell-intrinsic metabolic-sensing pathways have been implicated in the hypothalamic control of energy balance. These include the kinase mammalian target of rapamycin (mTOR), SIRT1, and AMP-activated protein kinase (Claret et al., 2007; Cota et al., 2006; Minokoshi et al., 2004; Ramadori et al., 2010). The implication of mTOR in the hypothalamic control of appetite regulation is particularly interesting because it also directly regulates autophagy. When nutrients are lacking, mTOR repression shifts cellular metabolism toward autophagy and the recycling of cytosolic constituents. Thus, inadequate mTOR and/or autophagy regulation can lead to overlapping pathological conditions and may predispose an individual to the development of obesity and diabetes. In addition, because leptin directly promotes axon growth from ARH neurons (Bouret et al., 2004b), and because leptin promotes autophagy (Malik et al., 2011), it remains possible that some of the neurotrophic effects of leptin might be mediated through autophagy activation. Similarly, it would be important to determine whether there is an acute role for autophagy regulated by leptin in input organization, membrane properties, and firing frequency of POMC neurons, which in turn, could affect feeding behavior. It is also tempting to speculate that autophagy may support a cellular homeostasis permissive of electrical changes in these neurons during the course of changing metabolic and hormonal milieu.

EXPERIMENTAL PROCEDURES

Animals

Mice were housed in individual cages under specific pathogen-free conditions, maintained in a temperature-controlled room with a 12 hr light/dark cycle, and provided ad libitum access to water and standard laboratory chow (Special Diet Services). Animal usage was in compliance with and approved by the Institutional Animal Care and Use Committee of the Saban Research Institute of the Children's Hospital of Los Angeles. Mice in which LC3 had been fused to GFP were kindly provided by Noboru Mizushima (Mizushima et al., 2004). To generate POMC-specific Atg7 knockout (*Pomc*-Cre; *Atg7*$^{loxP/loxP}$) mice, *Pomc*-Cre mice (C57BL/6 background) (Balthasar et al., 2004) were mated to mice carrying a loxP-flanked Atg7 allele (*Atg7*$^{loxP/loxP}$) (C57BL/6 background) (Komatsu et al., 2005). Breeding colonies were maintained by mating *Pomc*-Cre; *Atg7*$^{loxP/+}$ mice to *Atg7*$^{loxP/loxP}$ mice. Animals were genotyped by PCR as described previously (Balthasar et al., 2004; Komatsu et al., 2005). Cre-negative *Atg7*$^{loxP/loxP}$ mice were used as controls.

Physiological Measures

One day after birth, the litter size was adjusted to seven pups to ensure adequate and standardized nutrition until weaning. Male and female mice ($n \geq 9$ per group) were weighed every 2 days from P4 to P22 (weaning) and weekly from P28 through P119 using an analytical balance. Glucose tolerance was performed at 8–9 weeks of age ($n \geq 7$ per group) by an i.p. administration of glucose (1.5 mg/g body weight) after overnight fasting, and then the blood glucose levels were measured 0, 15, 30, 45, 60, 90, 120, and 150 min following glucose challenge, as previously described (Fan et al., 2000; Howard et al., 2004). Leptin sensitivity test was performed in 7- and 10-week-old male mice ($n \geq 6$ per group). Briefly, mice were injected i.p. with vehicle (5 mM sodium citrate buffer) or leptin (3 mg/kg body weight, Peprotech) according to the following scheme: vehicle injections for 5 days, followed by leptin injections for 3 days. Body weight was measured during the injection period. Retroperitoneal and epididymal fat depots were collected at 7 weeks of age and between 15 and 17 weeks of age ($n \geq 5$ per group) and weighed.

Hormone Assays

Serum leptin and insulin levels were assayed at 7 weeks and between 15 and 17 weeks of age (n = 6–8 per group) using leptin and insulin ELISA kits, respectively (Millipore).

Immunohistochemistry and Image Analysis

Anesthetized male mice were perfused transcardially with 4% paraformaldehyde. The brains were then frozen and sectioned at 30 μm thick and processed for immunofluorescence using standard procedures (Bouret et al., 2004b). The primary antibodies used for IHC were as follows: rabbit anti-GFP (1:10,000,

Invitrogen), sheep anti-αMSH (1:40,000, Millipore), rabbit anti-AgRP (1:1000, Phoenix Pharmaceuticals), rabbit anti-b-endorphin (1:10,000, Millipore), rabbit anti-p62/SQSTM1 (1:1000, Abcam), and rabbit anti-ubiquitin (1:1000, Dako). The primary antibodies were visualized with Alexa Fluor 488 goat anti-rabbit IgGs, or Alexa Fluor 568 goat anti-rabbit IgGs, or Alexa Fluor 568 donkey anti-sheep IgGs (1:200, Invitrogen). Sections were counterstained using bisbenzamide (1:10,000, Invitrogen), to visualize cell nuclei, and coverslipped with buffered glycerol (pH 8.5). Image analysis was performed using ImageJ analysis software (NIH) (Bouret et al., 2008). Additional details appear in Supplemental Experimental Procedures.

Isolated ARH Explant Cultures

Brains were collected from P4 male mice and sectioned 200 μm thick with a vibroslicer as previously described (Bouret et al., 2004b). The ARH was then carefully dissected out of each section under a stereomicroscope. Explants (n = 5–6 cases per group) were cultured onto a rat tail collagen matrix (Upstate). Beginning on the first day in vitro, each explant was transferred to fresh Basal Medium Eagle medium (Invitrogen). After 36 hr, the explants were fixed in paraformaldehyde and neurites extending from the explants were stained with GAP-43 (rabbit, 1:5000, Millipore) and b-endorphin (mouse, 1:5000, Millipore). Image analysis was performed using ImageJ analysis software (NIH) (Bouret et al., 2008). See Supplemental Experimental Procedures for additional information.

Electron Microscopy

P24 wild-type male mice were perfused with 4% paraformaldehyde, and their brains were processed for immunolabeling for POMC using a rabbit anti-POMC precursor antibody (1:4000, Phoenix Pharmaceuticals) for electron microscopy examination. Ultrathin sections were then cut on a Leica ultramicrotome, collected on Formvar-coated single-slot grids, and analyzed with a Tecnai 12 BioTWIN electron microscope (FEI).

Immunoblots

Frozen microdissected hypothalami derived from 15-week-old C57BL/6 wild-type male mice were immunoblotted as described previously (d'Anglemont de Tassigny et al., 2007). Polyclonal antibodies against LC3 (1:300, Cell Signaling) and b-actin (1:1000, Sigma) were used in this experiment.

Statistical Analysis

All values were expressed as means ± SEM. Statistical analyses were conducted using GraphPad PRISM (version 5.0a). Statistical significance was determined using unpaired two-tailed Student's t tests and a two-way ANOVA followed by the Bonferroni post hoc test when appropriate. p values less than 0.05 were considered to be statistically significant.

SUPPLEMENTAL INFORMATION

Supplemental Information includes four figures, Supplemental Experimental Procedures, and Supplemental References and can be found with this article online at doi:10.1016/j.cmet.2011.12.016.

ACKNOWLEDGMENTS

We thank Noboru Mizushima for the generous gift of the LC3-GFP mice. We also would like to thank Li Liu and Julien Maillard for the expert technical assistance. This work was supported by the National Institute of Health (Grant DK84142 to S.G.B. and Grant DK080000 to T.L.H.), the Fondation pour la Recherche Médicale (to S.G.B.), the EU FP7 integrated project (grant agreement #266408, "Full4Health," to S.G.B.), the Agence Nationale de la Recherche (Grant ANR-08-JCJC-0055-01 to S.G.B.), and the American Diabetes Association (Grant ADA 7-08-MN-25 to T.L.H.).

Received: July 14, 2011
Revised: October 24, 2011
Accepted: December 6, 2011
Published online: January 26, 2012

REFERENCES

Alirezaei, M., Kemball, C.C., Flynn, C.T., Wood, M.R., Whitton, J.L., and Kiosses, W.B. (2010). Short-term fasting induces profound neuronal autophagy. Autophagy *6*, 702–710.

Balthasar, N., Coppari, R., McMinn, J., Liu, S.M., Lee, C.E., Tang, V., Kenny, C.D., McGovern, R.A., Chua, S.C., Jr., Elmquist, J.K., and Lowell, B.B. (2004). Leptin receptor signaling in POMC neurons is required for normal body weight homeostasis. Neuron *42*, 983–991.

Belgardt, B.F., and Brüning, J.C. (2010). CNS leptin and insulin action in the control of energy homeostasis. Ann. N Y Acad. Sci. *1212*, 97–113.

Bouret, S.G. (2010). Role of early hormonal and nutritional experiences in shaping feeding behavior and hypothalamic development. J. Nutr. *140*, 653–657.

Bouret, S.G., Draper, S.J., and Simerly, R.B. (2004a). Formation of projection pathways from the arcuate nucleus of the hypothalamus to hypothalamic regions implicated in the neural control of feeding behavior in mice. J. Neurosci. *24*, 2797–2805.

Bouret, S.G., Draper, S.J., and Simerly, R.B. (2004b). Trophic action of leptin on hypothalamic neurons that regulate feeding. Science *304*, 108–110.

Bouret, S.G., Gorski, J.N., Patterson, C.M., Chen, S., Levin, B.E., and Simerly, R.B. (2008). Hypothalamic neural projections are permanently disrupted in diet-induced obese rats. Cell Metab. *7*, 179–185.

Cecconi, F., and Levine, B. (2008). The role of autophagy in mammalian development: cell makeover rather than cell death. Dev. Cell *15*, 344–357.

Claret, M., Smith, M.A., Batterham, R.L., Selman, C., Choudhury, A.I., Fryer, L.G.D., Clements, M., Al-Qassab, H., Heffron, H., Xu, A.W., et al. (2007). AMPK is essential for energy homeostasis regulation and glucose sensing by POMC and AgRP neurons. J. Clin. Invest. *117*, 2325–2336.

Cone, R.D. (2006). Studies on the physiological functions of the melanocortin system. Endocr. Rev. *27*, 736–749.

Cota, D., Proulx, K., Smith, K.A.B., Kozma, S.C., Thomas, G., Woods, S.C., and Seeley, R.J. (2006). Hypothalamic mTOR signaling regulates food intake. Science *312*, 927–930.

d'Anglemont de Tassigny, X., Campagne, C., Dehouck, B., Leroy, D., Holstein, G.R., Beauvillain, J.-C., Buée-Scherrer, V., and Prevot, V. (2007). Coupling of neuronal nitric oxide synthase to NMDA receptors via postsynaptic density-95 depends on estrogen and contributes to the central control of adult female reproduction. J. Neurosci. *27*, 6103–6114.

Ebato, C., Uchida, T., Arakawa, M., Komatsu, M., Ueno, T., Komiya, K., Azuma, K., Hirose, T., Tanaka, K., Kominami, E., et al. (2008). Autophagy is important in islet homeostasis and compensatory increase of beta cell mass in response to high-fat diet. Cell Metab. *8*, 325–332.

Ellacott, K.L., and Cone, R.D. (2006). The role of the central melanocortin system in the regulation of food intake and energy homeostasis: lessons from mouse models. Philos. Trans. R. Soc. Lond. B Biol. Sci. *361*, 1265–1274.

Elmquist, J.K., Coppari, R., Balthasar, N., Ichinose, M., and Lowell, B.B. (2005). Identifying hypothalamic pathways controlling food intake, body weight, and glucose homeostasis. J. Comp. Neurol. *493*, 63–71.

Elmquist, J.K., and Flier, J.S. (2004). Neuroscience. The fat-brain axis enters a new dimension. Science *304*, 63–64.

Fan, W., Dinulescu, D.M., Butler, A.A., Zhou, J., Marks, D.L., and Cone, R.D. (2000). The central melanocortin system can directly regulate serum insulin levels. Endocrinology *141*, 3072–3079.

Gao, Q., and Horvath, T.L. (2007). Neurobiology of feeding and energy expenditure. Annu. Rev. Neurosci. *30*, 367–398.

Hara, T., Nakamura, K., Matsui, M., Yamamoto, A., Nakahara, Y., Suzuki-Migishima, R., Yokoyama, M., Mishima, K., Saito, I., Okano, H., and Mizushima, N. (2006). Suppression of basal autophagy in neural cells causes neurodegenerative disease in mice. Nature *441*, 885–889.

Horvath, T.L., and Bruning, J.C. (2006). Developmental programming of the hypothalamus: a matter of fat. Nat. Med. *12*, 52–53, discussion 53.

Please cite this article in press as: Coupé et al., Loss of Autophagy in Pro-opiomelanocortin Neurons Perturbs Axon Growth and Causes Metabolic Dysregulation, Cell Metabolism (2012), doi:10.1016/j.cmet.2011.12.016

Howard, J.K., Cave, B.J., Oksanen, L.J., Tzameli, I., Bjørbaek, C., and Flier, J.S. (2004). Enhanced leptin sensitivity and attenuation of diet-induced obesity in mice with haploinsufficiency of Socs3. Nat. Med. *10*, 734–738.

Jung, H.S., Chung, K.W., Won Kim, J., Kim, J., Komatsu, M., Tanaka, K., Nguyen, Y.H., Kang, T.M., Yoon, K.-H., Kim, J.-W., et al. (2008). Loss of autophagy diminishes pancreatic beta cell mass and function with resultant hyperglycemia. Cell Metab. *8*, 318–324.

Kaushik, S., Rodriguez-Navarro, J.A., Arias, E., Kiffin, R., Sahu, S., Schwartz, G.J., Cuervo, A.M., and Singh, R. (2011). Autophagy in hypothalamic AgRP neurons regulates food intake and energy balance. Cell Metab. *14*, 173–183.

Klionsky, D.J. (2007). Autophagy: from phenomenology to molecular understanding in less than a decade. Nat. Rev. Mol. Cell Biol. *8*, 931–937.

Komatsu, M., Waguri, S., Chiba, T., Murata, S., Iwata, J., Tanida, I., Ueno, T., Koike, M., Uchiyama, Y., Kominami, E., and Tanaka, K. (2006). Loss of autophagy in the central nervous system causes neurodegeneration in mice. Nature *441*, 880–884.

Komatsu, M., Waguri, S., Koike, M., Sou, Y.S., Ueno, T., Hara, T., Mizushima, N., Iwata, J.-i., Ezaki, J., Murata, S., et al. (2007a). Homeostatic levels of p62 control cytoplasmic inclusion body formation in autophagy-deficient mice. Cell *131*, 1149–1163.

Komatsu, M., Waguri, S., Ueno, T., Iwata, J., Murata, S., Tanida, I., Ezaki, J., Mizushima, N., Ohsumi, Y., Uchiyama, Y., et al. (2005). Impairment of starvation-induced and constitutive autophagy in Atg7-deficient mice. J. Cell Biol. *169*, 425–434.

Komatsu, M., Wang, Q.J., Holstein, G.R., Friedrich, V.L.J., Jr., Iwata, J., Kominami, E., Chait, B.T., Tanaka, K., and Yue, Z. (2007b). Essential role for autophagy protein Atg7 in the maintenance of axonal homeostasis and the prevention of axonal degeneration. Proc. Natl. Acad. Sci. USA *104*, 14489–14494.

Levin, B.E. (2006). Metabolic imprinting: critical impact of the perinatal environment on the regulation of energy homeostasis. Philos. Trans. R. Soc. Lond. B Biol. Sci. *361*, 1107–1121.

Maiuri, M.C., Zalckvar, E., Kimchi, A., and Kroemer, G. (2007). Self-eating and self-killing: crosstalk between autophagy and apoptosis. Nat. Rev. Mol. Cell Biol. *8*, 741–752.

Malik, S.A., Mariño, G., BenYounès, A., Shen, S., Harper, F., Maiuri, M.C., and Kroemer, G. (2011). Neuroendocrine regulation of autophagy by leptin. Cell Cycle *10*, 2917–2923.

Minokoshi, Y., Alquier, T., Furukawa, N., Kim, Y.B., Lee, A., Xue, B., Mu, J., Foufelle, F., Ferré, P., Birnbaum, M.J., et al. (2004). AMP-kinase regulates food intake by responding to hormonal and nutrient signals in the hypothalamus. Nature *428*, 569–574.

Mizushima, N., Yamamoto, A., Matsui, M., Yoshimori, T., and Ohsumi, Y. (2004). In vivo analysis of autophagy in response to nutrient starvation using transgenic mice expressing a fluorescent autophagosome marker. Mol. Biol. Cell *15*, 1101–1111.

Padilla, S.L., Carmody, J.S., and Zeltser, L.M. (2010). Pomc-expressing progenitors give rise to antagonistic neuronal populations in hypothalamic feeding circuits. Nat. Med. *16*, 403–405.

Ramadori, G., Fujikawa, T., Fukuda, M., Anderson, J., Morgan, D.A., Mostoslavsky, R., Stuart, R.C., Perello, M., Vianna, C.R., Nillni, E.A., et al. (2010). SIRT1 deacetylase in POMC neurons is required for homeostatic defenses against diet-induced obesity. Cell Metab. *12*, 78–87.

Sawchenko, P.E. (1998). Toward a new neurobiology of energy balance, appetite, and obesity: the anatomists weigh in. J. Comp. Neurol. *402*, 435–441.

Singh, R., Xiang, Y., Wang, Y., Baikati, K., Cuervo, A.M., Luu, Y.K., Tang, Y., Pessin, J.E., Schwartz, G.J., and Czaja, M.J. (2009). Autophagy regulates adipose mass and differentiation in mice. J. Clin. Invest. *119*, 3329–3339.

Sullivan, E.L., and Grove, K.L. (2010). Metabolic imprinting in obesity. Forum Nutr. *63*, 186–194.

Yue, Z., Friedman, L., Komatsu, M., and Tanaka, K. (2009). The cellular pathways of neuronal autophagy and their implication in neurodegenerative diseases. Biochim. Biophys. Acta *1793*, 1496–1507.

Zhang, Y., Goldman, S., Baerga, R., Zhao, Y., Komatsu, M., and Jin, S. (2009). Adipose-specific deletion of autophagy-related gene 7 (atg7) in mice reveals a role in adipogenesis. Proc. Natl. Acad. Sci. USA *106*, 19860–19865.

Cell Metabolism, Volume *15*

Supplemental Information

Loss of Autophagy in Pro-opiomelanocortin Neurons Perturbs Axon Growth and Causes Metabolic Dysregulation

Bérengère Coupé, Yuko Ishii, Marcelo O. Dietrich, Masaaki Komatsu, Tamas L. Horvath, Sebastien G. Bouret

Supplemental Figure 1

Cell group	Relative Fluorescence Intensity
Nucleus accumbens	+
Caudoputamen	+
Primary somatomotor area	+++
Olfactory tubercle	+
Primary somatosensory area	++(+)
Anteroventral preoptic nucleus	++
Anteroventral periventricular nucleus hypothalamus	++
Lateral septum	(+)
Magnocellular nucleus	+
Median preoptic nucleus	+
Medial preoptic area	+
Medial septal nucleus	(+)
Bed nuclei stria terminalis	+
Globus pallidus	+
Lateral preoptic area	(+)
Medial preoptic nucleus	+
Suprachiasmatic nucleus	++
Septofimbrial nucleus	(+)
Substantia innominata	+
Anterior hypothalamic nucleus	+
Arcuate hypothalamic nucleus	++
Anteromedial nucleus thalamus	-
Field CA3, Ammon's horn	+++
Lateral hypothalamic area	+
Periventricular hypothalamic nucleus	++
Ventromedial hypothalamic nucleus	+
Field CA1, Ammon's horn	+++
Dorsomedial hypothalamic nucleus	+
Mediodorsal nucleus thalamus	-
Posterior amygdalar nucleus	+
Parafascicular nucleus	+
Posterior hypothalamic nucleus	+
Dorsal premammillary nucleus	(+)
Supramammillary nucleus	+
Ventral posteromedial nucleus thalamus	(+)
Anterior pretectal nucleus	(+)
Medial mammillary nucleus, body	++
Midbrain reticular nucleus	+
Primary visual area	++
Ventral tegmental area	+++
Substantia nigra	++
Central linear nucleus raphé	++++
Interpeduncular nucleus	++
Periaqueductal gray	++
Superior colliculus	+
Anterior tegmental nucleus	+
Superior central nucleus raphé	++
Dorsal nucleus raphé	+(+)
Medial longitudinal fascicle	++
Pontine gray	++
Central lobule	++++
Pontine reticular nucleus	++++
Principal sensory nucleus of the trigeminal	++(+)
Pyramid	+++
Nucleus raphé magnus	+++
Gigantocellular reticular nucleus	++
Lateral reticular nucleus	+++
Paragigantocellular reticular nucleus	+++(+)
Spinal nucleus of the trigeminal	+++(+)
XII : hypoglossal nucleus	+++(+)
Cuneate nucleus	+++(+)
Medullary reticular nucleus	+++(+)
Nucleus of the solitary tract	+++(+)
Pyramidal decussation	++++

Supplemental Figure 1, continued

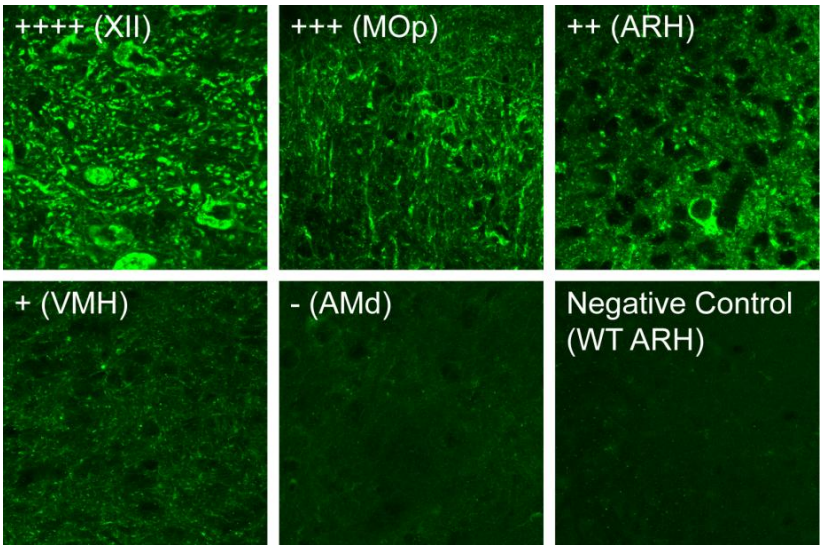

Figure S1. Relative Densities of Autophagosomes in LC3-GFP Adult Mouse Brain

Qualitative estimates of the relative densities of autophagic vacuoles, by considering the signal strength in a given nucleus. A four-point scale was used to rate the density of immunofluorescence observed: ++++, highest density (*e.g.,* hypoglossal nucleus, XII); +++, high density (*e.g.*, primary somatomotor area, MOp); ++, moderate density (*e.g.*, arcuate nucleus, ARH); +, low density but consistently above background (*e.g.*, ventromedial nucleus, VMH); -, background density (*e.g.*, anteromedial nucleus thalamus) and similar to negative control GFP antibody staining in a wild-type (WT) mouse. The nomenclature used herein was previously described by Swanson (Swanson, 1998).

Supplemental Figure 2

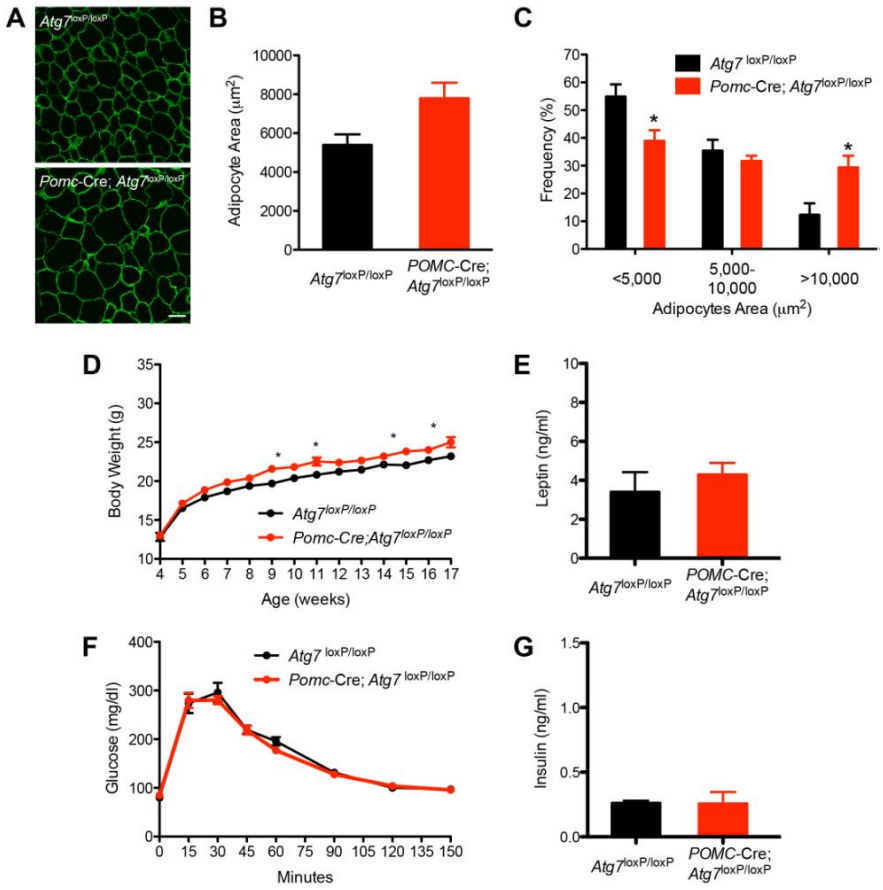

Figure S2. Increased Adipocyte Size in Male Mice Lacking Autophagy in POMC Neurons and Metabolic Regulation in *Pomc*-Cre; *Atg7*$^{loxP/loxP}$ Female Mice

(A) Confocal images illustrating adipocytes (immunostained for perilipin) in the epididymal fat of adult (15- to 17-week-old) *Atg7*$^{loxP/loxP}$ (n = 3) and *Pomc*-Cre; *Atg7*$^{loxP/loxP}$ (n = 3) male mice.

(B and C) Quantification of the (B) adipocyte cell surface area and the (C) frequency distribution of the adipocyte cell surface area of *Atg7*$^{loxP/loxP}$ (n = 3) and *Pomc*-Cre; *Atg7*$^{loxP/loxP}$ (n = 3) male mice at 15-17 weeks of age.

(D) Post-weaning growth curves of *Atg7*$^{loxP/loxP}$ (n = 9) and *Pomc*-Cre; *Atg7*$^{loxP/loxP}$ (n = 12) female mice.

(E–G) Serum leptin (E) and insulin levels (G) in *Atg7*$^{loxP/loxP}$ (n = 4) and *Pomc*-Cre; *Atg7*$^{loxP/loxP}$ (n = 3) female mice from 15-17 weeks of age. (F) Glucose tolerance test (GTT) of 8- to 9-week-old *Atg7*$^{loxP/loxP}$ (n = 6) and *Pomc*-Cre; *Atg7*$^{loxP/loxP}$ (n = 12) female mice. Values are shown as mean ± SEM. **P* < 0.05 versus *Atg7*$^{loxP/loxP}$. Scale bar, 50 um.

Supplemental Figure 3

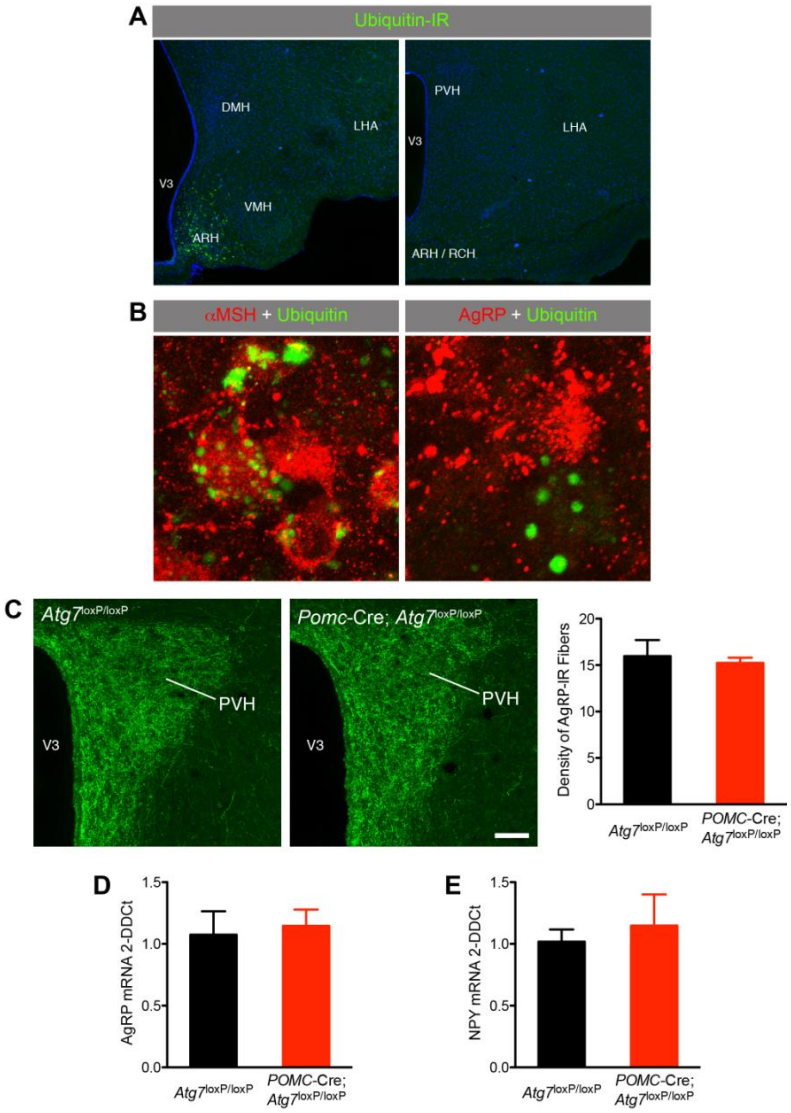

Figure S3. The AgRP Neural System Is Unaffected in *Pomc*-Cre; *Atg7*$^{loxP/loxP}$

(A) Confocal images illustrating ubiquitin-immunoreactivity in the arcuate nucleus (ARH) of *Pomc*-Cre; *Atg7*$^{loxP/loxP}$ mice.

(B) The vast majority of ubiquitin-immunoreactive cells (*green* fluorescence) also contain aMSH-immunoreactivity (*red* fluorescence); colocalizations between ubiquitin- (*green* fluorescence) and AgRP-immunoreactivity (*red* fluorescence) were rare in mutant mice.

(C) Confocal images and quantification of AgRP-immunoreactive fibers in the paraventricular nucleus (PVH) of adult (15- to 17-week-old) *Atg7*$^{loxP/loxP}$ (n = 4) and *Pomc*-Cre; *Atg7*$^{loxP/loxP}$ (n = 4) male mice.

(D and E) Relative expression of (D) *Agrp* and (E) *Npy* mRNA levels in the hypothalamus of adult *Atg7*$^{loxP/loxP}$ (n ≥ 4) and *Pomc*-Cre; *Atg7*$^{loxP/loxP}$ (n ≥ 4) male mice. V3, third ventricle. ARH, arcuate nucleus. DMH, dorsomedial nucleus, LHA, lateral hypothalamic area, RCH, retrochiasmatic area, VMH, ventromedial nucleus. Values are shown as mean ± SEM. Scale bar, 100 um (A), 10 um (C), and 50 um (C).

Supplemental Figure 4

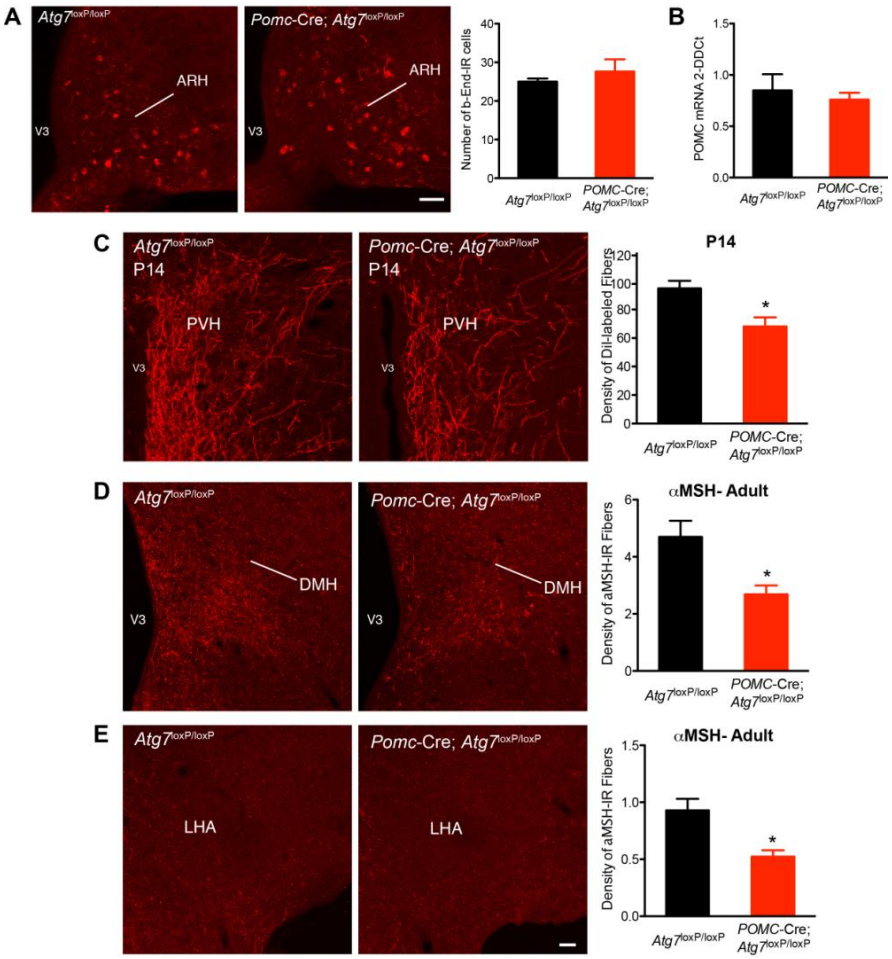

Figure S4. Lack of Autophagy in POMC Neurons Disrupts ARH Neural Projections but Does Not Alter POMC Cell Number nor *Pomc* mRNA Expression

(A) b-endorphin-immunopositive cells in the arcuate nucleus (ARH) of adult (15- to 17-week-old) *Atg7*$^{loxP/loxP}$ (n = 4) and *Pomc*-Cre; *Atg7*$^{loxP/loxP}$ (n = 4) male mice.

(B) Relative expression of *Pomc* mRNA levels in the hypothalamus of adult *Atg7*$^{loxP/loxP}$ (n ≥ 4) and *Pomc*-Cre; *Atg7*$^{loxP/loxP}$ (n ≥ 4) male mice.

(C) Confocal images and quantification of the density of arcuate DiI-labeled fibers innervating the paraventricular nucleus (PVH) in P14 *Pomc*-Cre; *Atg7*$^{loxP/loxP}$ (n = 4) and *Atg7*$^{loxP/loxP}$ (n = 6) mice.

(D and E) Confocal images and quantification of aMSH-IR fibers in (D) the dorsomedial nucleus (DMH) and (E) the lateral hypothalamic area (LHA) of adult (15- to 17-week-old) *Atg7*$^{loxP/loxP}$ (n = 4) and *Pomc*-Cre; *Atg7*$^{loxP/loxP}$ (n = 4) male mice. V3, third ventricle. Values are shown as mean ± SEM. **P* < 0.05 versus *Atg7*$^{loxP/loxP}$. Scale bar, 50 um (A, B), 20 um (C, D).

Supplemental Experimental Procedures

DiI Implants

P14 male mice (n = 4–6 per group) were perfused with 4% paraformaldehyde. The brains were removed and numerically coded to insure unbiased processing and analysis, and 1,10-dioctadecyl-3,3,30,30-tetramethylindocarbocyanine perchlorate (DiI; Santa Cruz) crystals were implanted as described previously (Bouret et al., 2004b; Bouret et al., 2008). Briefly, an insect pin was used to place a crystal of DiI (15um in diameter) into the ARH of each brain under visual guidance. After incubation in the dark for 2 weeks at 37□C, sections were collected through the hypothalamus from each brain and evaluated by confocal microscopy as described below.

Quantitative Analysis of Fiber Density

For the histological experiments, two sections through the ARH (for b-endorphin, ubiquitin, and p62 staining) and the PVH, DMH, and LHA (for aMSH and AgRP staining and DiI labeling) from animals of each experimental group (n = 4 animals per group) were acquired using a Zeiss LSM 710 confocal system equipped with a 20X objective. For the *in vitro* experiments, sections through the ARH explant were acquired using a Zeiss LSM 710 confocal system equipped with a 20X objective. For the quantification of LC3-GFP puncta (n = 4-5 animals per group), two sections through the ARH and the periventricular zone of the hypothalamus were acquired using a Zeiss LSM 710 confocal system equipped with a 63X objective. Image analysis was performed using ImageJ analysis software (NIH).

For the quantitative analysis of fiber density (for aMSH, AgRP, and DiI) and the quantification of ubiquitin- and p62-immunoreactivity, each image plane was binarized to isolate labeled fibers from the background and to compensate for differences in

fluorescence intensity. The integrated intensity was then calculated for each image, which reflects the total number of pixels in the binarized image. This procedure was conducted on each image plane in the stack, and the values for all of the image planes in a stack were summed. The resulting value is an accurate index of the density of the processes in the volume sampled (Bouret et al., 2008).

For the quantitative analysis of cell number, numbers of b-endorphin-immunopositive cells in the ARH were manually counted. The average number of cells counted in two ARH sections from each mouse was used for statistical comparisons.

The NIH ImageJ macro called GFP-LC3 (http://imagejdocu.tudor.lu/author/rkd8/) (Dagda et al., 2008) was used to quantify the number of LC3-GFP puncta.

Histomorphological Assessment of White Adipose Tissue

Male mice were anesthetized at 15-17 weeks of age (n = 3 per group). Epididymal adipose tissue was collected, fixed in a 4% paraformaldehyde solution, sectioned at 5 um, and then stained with a Perilipin A antibody (1:1,000, Sigma) using standard procedures. Images were taken with a Zeiss LSM 710 confocal microscope with a 20X objective. Determination of mean size (μm^2) was measured using Image J software (NIH, Image J 1.39 T). The average adipocyte size measured from three sections in each mouse was used for statistical comparisons.

Measurement of *Pomc* , *Agrp* and *Npy* mRNA

Hypothalami of 15-17 weeks-old male mice fed *ad libitum* were dissected. Total RNA was isolated using the RNeasy Lipid Tissue Mini Kit (Qiagen). cDNA were generated with the high capacity cDNA Reverse Transcription Kit (Applied Biosystem). Quantitative real time PCR analysis was performed using TaqMan Fast universal PCR Mastermix. mRNA expression was calculated using the 2-DDCt method after normalization with

Gapdh as a housekeeping gene. Inventoried TaqMan® Gene expression assays *Pomc (*Mm00435874_m1), *Npy* (Mm03048253_m1), *Agrp* (Mm00475829_g1) and *Gapdh* (Mm99999915_g1) were used. All assays were performed using an Applied Biosystems Prism 7900HT fast sequence detection system.

Supplemental References

Dagda, R.K., Zhu, J., Kulich, S.M., and Chu, C.T. (2008). Mitochondrially localized ERK2 regulates mitophagy and autophagic cell stress: implications for Parkinson's disease. Autophagy *4*, 770–782.

Anexo A-9. Sirtuins and metabolism

Artigo em preparação a ser submetido ao periódico *Physiology Reviews*.

Sirtuins and Metabolism

Ruben Nogueiras, Nilika Chaudhary, Kirk Habegger, Alexander Banks, Marcelo O. Dietrich, Tamas Horvath, David Sinclair, Paul Pfluger, and Matthias Tschoep

ABSTRACT

The sirtuins are a family of highly conserved NAD^+-dependent deacetylases that act as cellular sensors that detect low energy availability and modulate metabolic processes accordingly. Two sirtuins that are central to the control of metabolic processes are mammalian SIRT1 and SIRT3, which are localized to the nucleus and mitochondria, respectively. Both are activated by high NAD^+ levels and inhibited by high NADH levels, conditions caused by low cellular energy status. By deacetylating a variety of proteins that induce catabolic processes while inhibiting anabolic processes, SIRT1 and SIRT3 coordinately increase cellular energy stores to ultimately maintain cellular energy homeostasis. Defects in the pathways controlled by SIRT1 and SIRT3 are known to result in various metabolic disorders. Consequently, activation of Sirtuins by genetic or pharmacological means can elicit multiple metabolic benefits that protect mice from diet-induced obesity, type 2 diabetes, and non-alcoholic fatty liver disease.

I. INTRODUCTION

From budding yeast to humans, fundamental principals of cellular energy metabolism are nearly identical. In all living organisms, cellular energy is produced and expended using highly homologous pathways and energy is stored and transferred using universal "energy currencies" such as ATP and NADH. The tight balance between such anabolic and catabolic pathways ensures that cells do not deplete themselves from essential energy, which would ultimately cause cellular damage or death. Accordingly, evolutionary conserved mechanisms have been established to protect cells from low cellular energy availability and to store excess energy for future use. Such mechanisms include the mTOR signaling pathway to detect branched-chain amino acids like leucine, Carbohydrate Responsive Element Binding Protein (ChREBP) to respond to elevated glucose levels, 5' adenosine monophosphate-activated protein kinase (AMPK) to sense low cellular ATP levels, the Ghrelin O-acetyl transferase (GOAT) to detect medium chain-fatty acids, and sirtuins to detect NAD^+/NADH levels. This review will focus on the two most prominent sirtuins regarding their roles on energy homeostasis in mammals, SIRT1 and SIRT3, and will give an overview on the manifold metabolic benefits elicited by both fuel sensors.

A. Historical Background

Almost a century ago, the Nobel laureate Francis Peyton Rous reported that chronic calorie restriction (CR) elicits beneficial metabolic effects on the spontaneous occurrence of tumors in rats (Rous 1914). At the same time, Osborne et al. showed that calorie restriction of young rats (1.5 to 6 months of age) restores fertility at a later age, and prolongs life-span (Osborne, Mendel et al. 1917). While initially these findings were widely ignored, a growing number of studies in the following decades corroborated these benefits of CR, and accumulated evidence demonstrated that CR also protects from other age-related diseases, such as chronic kidney failure. In 1960, Berg and Simms proposed that the reduction in body fat plays a decisive role in mediating the beneficial effects of calorie restriction on fertility, age-related pathologies, and longevity in the rats (Berg and Simms 1960). Subsequent studies however suggested that the benefits of calorie restriction may be due to the decrease in the absolute amount of calories consumed (Bertrand, Lynd et al. 1980). More recently, this concept has been challenged (Mair, Piper and Partridge 2005) and evidence point to the effect of specific amino acids in determining the effects of long term calorie restriction on life span and fertility (Grandison, Piper and Partridge, 2009; Miller et al, 2005). In the past two decades, new techniques made it possible to focus also on the molecular underpinnings of metabolic benefits through calorie restrictions. Several mechanisms have been identified that were shown to play a role, such as the attenuation of oxidative damage, decreases in insulin and glucose levels, an impairment of the Growth hormone-IGF1 axis, or an activation of the deacetylase family of sirtuins.

In parallel to the work on calorie restriction, a genetic screen for long-lived mutants of *Saccharomyces cerevisiae* led to the discovery that the silent information regulation-2 (Sir2) gene could slow aging in this species (Sinclair, Mills et al. 1997; Kaeberlein, McVey et al. 1999). Later on, Sir2 was identified as NAD^+-dependent deacetylase for histone proteins that is required for calorie restriction to extend yeast lifespan (Imai, Armstrong et al. 2000; Lin, Kaeberlein et al. 2002), and structurally and functionally

highly similar homologues were identified in numerous other organisms. This review will summarize current research on sirtuin physiology and function with particular emphasis on metabolic effects from pharmacologically, genetically, or physiologically inducted sirtuin manipulation.

B. Overview

The mammalian sirtuins are a family of NAD^+-dependent enzymes with homology to the *Saccharomyces cerevisiae* gene silent information regulator 2 (Sir2). Humans have seven sirtuins, SIRT1-SIRT7. SIRT1, the most studied member of this family, plays an important role in several processes ranging from cell cycle regulation to energy homeostasis. SIRT3 has recently emerged as sirtuin member with considerable impact on mitochondrial energy metabolism and function.

The basic sirtuin structure and function have remained highly conserved across species, from bacteria to humans. In humans, sirtuins exist throughout the body; for example, SIRT1 is expressed in many tissues including the brain, liver, pancreas, adipose tissue, muscle and heart. Sirtuins may function as deacetylases and/or ADP-ribosyltransferases. Sirtuins with deacetylase activity remove the acetyl groups from acetylated lysine residues of numerous target proteins, including histones and transcription factors. Section II details the structure, function and localization of sirtuins.

Sirtuins are cellular energy sensors that require NAD^+ for their enzymatic activity. As a result, their activity is directly linked with metabolism. Certain cellular stressors or a low energy state in the cell increases the NAD^+/NADH ratio, decreases nicotinamide levels and activates sirtuins (Lin, Kaeberlein et al. 2002; Anderson, Bitterman et al. 2003). Section III describes the relationship of NAD^+, calorie restriction and the sirtuin family, as well as the mechanisms for sirtuin-catalyzed NAD^+-dependent reactions.

Mammalian SIRT1deacetylates a host of target proteins that are important for apoptosis and the cell cycle, circadian rhythms, mitochondrial function and metabolism. In particular, much current research focuses on the impact of SIRT1 in glucose homeostasis, lipid metabolism and energy balance. While SIRT1 plays an important role in metabolic function, sirtuins 3-5 are localized in mitochondria and may regulate mitochondrial energy metabolism. SIRT3, the most studied of the mitochondrial sirtuins, deacetylates a number of mitochondrial proteins and might also play a role in regulating ATP production. Section IV focuses on the molecular targets of SIRT1 and SIRT3.

Mammalian sirtuins are not only regulated by NAD^+/NADH ratio or cellular stressors, but also by a number of endogenous proteins involved in signal transduction and transcription, as well by a number of microRNAs. Section V will describe the complex regulation of SIRT1 and SIRT3 by endogenous factors.

Sirtuins 1 and 3 are expressed in a wide variety of tissues, and target numerous proteins. Section VI depicts how the activation of SIRT1 influences metabolically active tissues, such as liver, skeletal muscle, pancreas, adipose tissue or brain, by inducing a wide range of physiological processes. Section VII will focus on the specific roles of SIRT3 in diverse metabolically active tissues.

Several mouse models have been used to characterize the metabolic functions of sirtuins. Inbred whole-body SIRT1 knockout mice are born underweight and do not live past the early postnatal stage. SIRT1 knockout mice on an outbred background exhibit developmental and metabolic abnormalities including cardiac defects and decreased locomotor activity, but they also exhibit improved glucose homeostasis. Several studies focus on liver-specific ablation of SIRT1 and the role of hepatic SIRT1 but many findings are contradictory. In addition to SIRT1 deficiency, SIRT1 overexpression is also under investigation. Mice with global SIRT1 overexpression show resistance to metabolic dysfunction as a result of high-fat diet exposure. Gain and loss of function studies on sirtuins other than SIRT1 have been performed. Of particular importance to metabolic regulation are the mitochondrial sirtuins. Section VIII outlines the metabolic phenotypes of global or tissue-specific SIRT1 and SIRT3 loss- and gain-of-function models, and depicts specific roles of SIRT1 for circadian rhythms and diabetes-induced cardiac function.

Section IX describes the current knowledge on genetic polymorphisms in SIRT1 and SIRT3, and their implication in metabolic diseases.

It has been suggested that pharmacological SIRT1 activation may alleviate metabolic dysfunction associated with obesity or other metabolic disorders. Resveratrol is a proposed SIRT1 activator, but its metabolic benefits when administered pharmacologically in humans are still a matter of controversy. Several small-molecule SIRT1 activators with improved biopotency are under investigation for potential therapeutic metabolic benefits in humans. Section X covers the metabolic consequences of SIRT1 activation by resveratrol and other natural or synthetic ligands.

Finally, section XI gives a general view on future directions and perspectives for sirtuin research.

II. THE STRUCTURE, FUNCTION AND DIVERSITY OF SIRTUINS

A. Sirtuins are highly conserved in evolution

The *Saccharomyces cerevisiae* gene silent information regulator 2 (Sir2) was identified as a NAD^+-dependent histone deacetylase (Imai, Armstrong et al. 2000; Smith, Brachmann et al. 2000) that is involved in life span extension associated with calorie restriction (Lin, Defossez et al. 2000; Anderson, Bitterman et al. 2003). Sir2 homologs, known as sirtuins, have been identified in numerous higher organisms including *Drosophila melanogaster* (Barlow, van Drunen et al. 2001; Newman, Lundblad et al. 2002), *Caenorhabditis elegans* (Tissenbaum and Guarente 2001), mice (Yang, Chen et al. 2000) and humans (Brachmann, Sherman et al. 1995; Frye 1999; Sherman, Stone et al. 1999; Frye 2000). Seven sirtuins (SIRT1-SIRT7) comprise the family of Sir2 homologs in humans (Frye 1999; Frye 2000). Mammalian sirtuins share the conserved sirtuin domain in animal evolution, but vary in subcellular localization and function. Of note, sirtuins have been lost in many species including insects, nematodes and plants

(Greiss and Gartner 2009). Thereby, it seems that the loss of individual sirtuins might be compensated for redundant functions conferred by remaining sirtuin family members (Greiss and Gartner 2009).

In yeast, Sir2 deacetylates the acetyl-lysine residues of histones (Imai, Armstrong et al. 2000) by catalyzing a unique chemical reaction that requires NAD^+ and generates the novel product O-acetyl-ADP-ribose (O-AADPR) (Tanner, Landry et al. 2000; Tanny and Moazed 2001; Chang, Kim et al. 2002; Borra, Langer et al. 2004). As discussed below, this deacetylase activity is conserved in mammalian sirtuins, but they can also catalyze reactions for a number of specific protein substrates in addition to histones (Frye 1999). Furthermore, certain mammalian sirtuins also possess ADP-ribosyltransferase activity (Frye 1999).

Consistent with the evolutionarily conserved activity of Sir2 and its homologs, increased protein levels of Sir2 not only confers longevity benefits to *S. cerevisiae* (Kaeberlein, McVey et al. 1999; Kim, Benguria et al. 1999), but also *C. elegans* (Tissenbaum and Guarente 2001) and *D. melanogaster* (Rogina and Helfand 2004). However, other lines of evidence suggest that Sir2 does not affect life span in flies (Newman, Lundblad et al. 2002). Elevated expression of sirtuins in normal human cells does not extend replicative life span (Michishita, Park et al. 2005) and there is no evidence that a sirtuin can extend the lifespan of a mammal, unless it is under metabolic stress (Baur, Pearson et al. 2006; Pearson, Baur et al. 2008).

Today, we know that biochemical features are highly conserved in sirtuins. Their physiological roles, however, differ between species. While Sir2 in yeast is ostensibly confined to deacetylation of histones, but also controls segregation of protein carbonylation, mammalian sirtuins target multiple proteins, regulating many diverse processes ranging from cell cycle progression and mitochondrial function to metabolism and energy homeostasis.

B. Structural properties of SIRT1 and SIRT3

Among the yeast proteins that comprise the Sir silencing complex (Sir1-4), Sir2 is unique (reviewed in (Gottschling 2000), as it is the only homolog that has been evolutionarily conserved in diverse organisms ranging from bacteria to humans (Brachmann, Sherman et al. 1995; Afshar and Murnane 1999; Frye 1999; Sherman, Stone et al. 1999). Accordingly, all Sir2-like proteins possess a sirtuin core domain containing a series of sequence motifs conserved in many organisms (Brachmann, Sherman et al. 1995). Molecular phylogenetic analyses of a diverse array of organisms (including archaea bacteria, yeasts, plants, protozoans, and metazoans) have shown that the conserved sirtuin core domain sequences of eukaryotic organisms can be grouped into four main classes: SIRT1, SIRT2, and SIRT3 are class I, SIRT4 is class II, SIRT5 is class III, and SIRT6 and SIRT7 are class IV (Frye 2000). Sir2 protein is also unique among the silencing factors in *Saccharomyces cerevisiae* because it silences the rDNA as well as the silent mating-type loci and telomeres (Shore and Nasmyth 1987). Silencing is a universal form of transcriptional regulation in which regions of the genome are reversibly inactivated by changes in chromatin structure. Sir2 is also required to segregate damaged proteins into the mother cell, this sparing the daughter cell (Aguilaniu, Gustafsson et al. 2003), but what the target is and how this relates to mammalian aging is not yet known.

In budding yeast, the sirtuins also include a set of genes known as Homologues of Sir2 (HST1-4), which play roles in gene silencing, DNA repair, and lifespan extension by calorie restriction (Chen and Clark-Walker 1994; Brachmann, Sherman et al. 1995; Derbyshire, Weinstock et al. 1996; Yahiaoui, Taibi et al. 1996; Tsang and Escalante-Semerena 1998; Lamming, Latorre-Esteves et al. 2005). The proteins encoded by the HSTs are ~30-65% identical to Sir2 and are characterized by a conserved core domain, which is up to 84% identical to Sir2 and essential for Sir2 silencing (Sherman, Stone et al. 1999). Homologs of the HSTs do not appear in the genomes of vertebrate organisms thus far sequences.

In order to understand the structural basis of the enzymatic mechanism of the sirtuins, a number of crystal structures have been determined. In Archaeoglobusfulgidus, two crystal structures of Sir2-Af1 complexed with NAD were solved at 2.1 Å and 2.4 Å resolution (Finnin, Donigian et al. 2001; Min, Landry et al. 2001). The structure revealed that the protein consists of a large domain having a Rossmann fold and a small domain containing a three-stranded zinc ribbon motif. NAD is bound in a pocket between the two domains (Min, Landry et al. 2001). On the other hand, the 1.7 Å crystal structure of the 323 amino acid catalytic core of human SIRT2 reveals an NAD-binding domain, which is a variant of the Rossmann fold, and a smaller domain composed of a helical module and a zinc-binding module. Mutagenesis studies suggest that a conserved large groove at the interface of the two domains is the likely site of catalysis (Finnin, Donigian et al. 2001). More recently, several crystal structures for human SIRT3 have been also reported (Jin, Wei et al. 2009) for the apo-structure with no substrate, a structure with a peptide containing acetyl lysine of its natural substrate trapped by a thioacetyl peptide, and a structure with the dethioacetylated peptide bound (Jin, Wei et al. 2009).

C. Tissue distribution of SIRT1

SIRT1 is expressed in a wide range of tissues and organs, and has been detected in the liver, pancreas, heart, muscle and adipose tissue of mice (Imai and Guarente ; Lavu, Boss et al. 2008; Yu and Auwerx 2009). Other reports, utilizing a mCherry reporter gene in C. elegans, identified Sir2 mainly in muscle and intestinal cells (Bamps, Wirtz et al. 2009). In humans and mice, SIRT1 is ubiquitously expressed in the brain especially in areas related to neurodegenerative diseases as the prefrontal cortex, hippocampus and basal ganglia (Zakhary et al., 2010). SIRT1 is also expressed in important metabolic centers of the brain (Ramadori, Lee et al. 2008), including the hypothalamic arcuate, ventromedial, dorsomedial, and paraventricular nuclei and the area postrema and the nucleus of the solitary tract in the hindbrain. During aging, SIRT1 was found to decrease its expression in some specific nuclei in the hypothalamus of mice, but not in all brain regions (Lafontaine-LAcasse, Richard, Picard, 2010). Other studies focusing on the function of SIRT1 in development found that SIRT1 is expressed at high levels in most of the tissues of embryos, where expression was mainly found in the heart and the brain, but also in liver, spleen, kidney, lung, thymus, testis and ovary (Sakamoto, Miura et al. 2004). Overall, these studies suggest that SIRT1 is expressed in a wide variety of tissues.

D. Subcellular distribution of SIRT1

The subcellular localization of SIRT1 likely depends upon cell type, stress status, and molecular interactions. SIRT1 has been observed in both the nucleus and the cytoplasm, where it interacts with both nuclear and cytosolic proteins (Cohen, Lavu et al. 2004; Michishita, Park et al. 2005; Tanno, Sakamoto et al. 2007). For example, SIRT1 is ubiquitously present in the prefrontal cortex, hippocampus and basal ganglia. Throughout the rodent brain and spinal cord, both cytosolic and nuclear localization can be detected, though immunocytochemical and western blot analyses indicate that SIRT1 is predominantly nuclear (Zakhary, Ayubcha et al.). The subcellular localization of SIRT1 can be explained by its primary amino acid signal sequence, which contributes to its intracellular localization. The primarily nuclear localization of SIRT1 can be attributed to two nuclear localization signals. In addition, SIRT1 contains two nuclear export signals (Tanno, Sakamoto et al. 2007). Thus, the extent of cytosolic versus nuclear localization of SIRT1 may be dictated by the relative strengths of the nuclear localization and export signals in each cell type or environmental signal (Haigis and Sinclair).

E. Tissue distribution of SIRT3

Like SIRT1, mammalian SIRT3 is expressed in a variety of tissues. Studies carried out with quantitative RT-PCR in different mouse tissues show the highest expression in kidney, brain and heart, followed by liver and testes, and its levels are low in lung, ovary, spleen and thymus (Jin, Galonek et al. 2009). Similar expression patterns are seen in human tissues (Su, Wiltshire et al. 2004; Wu, Orozco et al. 2009).

F. Subcellular distribution of SIRT3

SIRT3 was the first mammalian sirtuin shown to be localized to mitochondria (Onyango, Celic et al. 2002; Schwer, North et al. 2002; Michishita, Park et al. 2005). It is localized to the mitochondrial matrix and cleavage of its signal sequence is necessary for enzymatic activity (Schwer, North et al. 2002). The major isoform of mouse SIRT3 is a 257 amino acid protein that aligns with the C-terminal portion of human SIRT3 (residues 143-399) (Yang, Chen et al. 2000). However, subsequent reports have questioned the exclusivity of the mitochondrial distribution of SIRT3. This ambiguity likely arises from the two different isoforms (short and full length) of SIRT3, which are expressed in both humans and mice and appear to be differentially distributed in a tissue-specific manner (Pillai, Sundaresan et al. ; Hallows, Albaugh et al. 2008; Sundaresan, Samant et al. 2008). Another report identified several splice variants (M1, M2 and M3) (Cooper, Huang et al. 2009). The variants M1 and M2 appear to be localized to the mitochondria, whereas the M3 splice variant is located also in the nucleus (Cooper, Huang et al. 2009). While full-length mouse SIRT3 has been reported to be exclusively located to the mitochondria (Jin, Galonek et al. 2009), other groups report that in the heart the long form of mSIRT3 can be detected in mitochondria, the cytoplasm and the nucleus (Sundaresan, Samant et al. 2008). However, after over-expression of short and long forms of mSIRT3 in mouse embryonic fibroblasts and H9C2 cells, both forms were located in the nucleus as well as the cytoplasm (Bao, Lu et al.).

As with the mouse SIRT3 protein, there are also two forms of the human SIRT3 protein. hSIRT3 is found in both long and short isoforms (Cooper and Spelbrink 2008),

and initially it was thought that the full length form is localized exclusively to the mitochondria, whereas the short form, which loses the N-terminal 142 residues, is present in the cytoplasm and nucleus (Cooper and Spelbrink 2008). However, recent findings have questioned whether the localization of human SIRT3 to mitochondria is exclusive (Onyango, Celic et al. 2002; Scher, Vaquero et al. 2007; Cooper and Spelbrink 2008). Several studies now suggest that SIRT3 is present in the nucleus under basal conditions but translocates to the mitochondria during cellular stress (Scher, Vaquero et al. 2007).

III. CELLULAR FUEL SENSING BY SIRT1 AND SIRT3

Sirtuins function as cellular energy sensors that are either activated or inhibited by the level of metabolic cofactors and intermediates in the cell, including NAD^+, NADH and nicotinamide (Brachmann, Sherman et al. 1995; Imai, Armstrong et al. 2000; Landry, Sutton et al. 2000; Smith, Brachmann et al. 2000; Bitterman, Anderson et al. 2002; Sauve and Schramm 2004). The main organelle to produce energy for usage in cellular metabolism is the mitochondria. Mitochondria are equipped with machinery to facilitate the oxidation of substrate (*e.g.*, carbohydrates and fatty acids) to produce ATP. This oxidative reaction generates energy, which is stored in reduced carrier molecules (as $FADH_2$ and NADH) that are utilized in the mitochondrial membrane to generate ATP through the oxidative phosphorylation cascade. Thus, the generation of energy (i.e., ATP) in the cells is linked to the production of $FADH_2$ and NADH. When these carriers are oxidized, they become FAD and NAD^+, and all four molecules are important regulators of numerous biochemical reactions inside the cell.

A. Cellular energy: NAD^+/NADH ratios and the NAD^+ salvage pathway

An absolute requirement of the sirtuin reaction is the co-substrate NAD^+, which places the sirtuins at the nexus of cellular energy metabolic regulation, providing a possible link between cytosolic energy status and nuclear signaling. Catabolic reactions such as β-oxidation, glycolysis, protein degradation, and citric acid cycling reduce NAD^+ to NADH. When energy is plentiful, intracellular NADH levels rise while NAD^+ levels drop, although the ratio always favors NAD^+ over NADH (Nicholls and S.J. 2002). NADH from cytosolic metabolism feeds into the mitochondria through the malate-aspartate shuttle to join NADH produced via the citric acid cycle (Bakker, Overkamp et al. 2001). Regardless of their origin, both pools of NADH are oxidized in the mitochondria by the electron transport chain (ETC). Specifically, NADH feeds into the ETC through its oxidation to NAD^+ at Complex I (Hirst 2010). Subsequent reactions of the ETC produce energy that is used to pump protons across the mitochondrial matrix. This generates the proton gradient that drives ATP synthesis via oxidative phosphorylation.

Cellular NAD^+ is derived from two main sources: *de novo* synthesis from the amino acid Tryptophan (McCreanor and Bender 1986) and via the salvage of nicotinamide back to NAD^+. The product of the sirtuin reaction, nicotinamide, acts as a feedback inhibitor by binding in a conserved regulatory pocket on the enzymes called the C-

pocket (Avalos, Celic et al. 2002; Bitterman, Anderson et al. 2002). In yeast, the removal of nicotinamide, and the rate-limiting step of the NAD salvage pathway, is catalyzed by Pnc1, a nicotinamide deaminase that is upregluated in response to caloric restriction and cellular stress (Anderson, Bitterman et al. 2003). Overexpression of NAD salvage genes extends lifespan in a SIR2-dependent manner (Anderson, Bitterman et al. 2002), while deletion of the *PNC1* gene blocks lifespan extension by calorie restriction (Anderson, Bitterman et al. 2003).

In humans, the rate-limiting step of the NAD^+ salvage pathway is catalized, not by Pnc1, but by a nicotinamide phosphoribosyltransferase (named as NAMPT in bacteria, but also known as PBEF), which converts nicotinamide to nicotinamide mononucleotide (Magni, Amici et al. 2004; Revollo, Grimm et al. 2004). Like the yeast *PNC1* gene, the expression of this essential enzyme appears to be regulated by stress (Magni, Amici et al. 2004; Iqbal and Zaidi 2006)(Yang et al, 2008) and its activity is specifically elevated in times of prolonged fasting (Yang, Yang et al. 2007). Additional findings suggest that NAMPT could directly influence the NAD^+/NADH ratio in the cell (Revollo, Grimm et al. 2004; van der Veer, Nong et al. 2005). Furthermore, findings by Revollo et al suggest that overexpression of NAMPT directly increases SIRT1 activity (Revollo, Grimm et al. 2004), further implicating NAD^+ concentration in the regulation of SIRT activity.

Studies in yeast bolstered the hypothesis that the NAD^+/NADH and the NAD+/nicotinamide ratios regulate sirtuin activity. Calorie restriction induces a decrease in both NADH and nicotinamide concentrations and is associated with increased life span and Sir2 activity (Lin, Defossez et al. 2000; Lin, Kaeberlein et al. 2002; Anderson, Bitterman et al. 2003; Lin, Ford et al. 2004; Sauve, Moir et al. 2005). Despite strong genetic evidence, a subsequent biochemical study, however, questioned whether NADH is in sufficient concentrations in vivo to inhibit sirtuins, concluding that the ratio of NAD^+ to nicotinamide is the primary mechanism of sirtuin regulation (Schmidt, Smith et al. 2004).

Studies in mice followed, suggesting that prolonged fasting can induce a 50% increase in hepatic NAD^+, leading to increased SIRT1 activity (Rodgers, Lerin et al. 2005). Similarly, Yang *et al.* demonstrated that food deprivation increased the levels of Nampt together with mitochondrial NAD^+ levels, and that the ensuing stress protection required both SIRT3 and SIRT4 (Yang, Yang et al. 2007). Indeed, the dependency of mitochondrial SIRT3 by NAD^+ has been also clearly demonstrated by multiple studies (Onyango, Celic et al. 2002; Schwer, North et al. 2002; Scher, Vaquero et al. 2007).

B. Mechanism of NAD+-dependent deacetylation

The Sir2 family of class III deacetylases utilizes a distinctive chemical reaction to deacetylate lysine residues. This reaction consumes NAD^+, generating nicotinamide, the deacetylated substrate, and a unique product, O-acetyl-ADP-ribose (O-AADPR) (Tanner, Landry et al. 2000; Tanny and Moazed 2001; Chang, Kim et al. 2002; Borra, Langer et al. 2004). The NAD+-dependent deacetylation reaction is a six step reaction eloquently reviewed by Sauve (Sauve 2010). Briefly, the reaction begins with the binding of NAD+ to the sirtuin catalytic site, a process mediated by highly conserved catalytic phenylalanine (Hoff, Avalos et al. 2006; Hawse, Hoff et al. 2008) and histidine residues (Min, Landry et al. 2001; Sauve, Celic et al. 2001; Smith and Denu 2006). The

first step in the sirtuin-catalyzed deacetylation utilizes amide cleavage of NAD^+ to produce nicotinamide and a peptidylimidate intermediate (Sauve, Celic et al. 2001). This is followed by formation of a 1',2'-acyloxonium via nucleophilic attack of the 2'-OH group of the imidate intermediate. This collapse is facilitated by the conserved catalytic histidine (Min, Landry et al. 2001; Smith and Denu 2006), which acts as an activating base to the 2'-OH group. The nucleophilic attack is followed by hydrolysis to 2'-AADPR via attack by water, releasing the free amino group of the previously acetylated lysine residue, AADPR, and nicotinamide. A caveat of this efficient reaction is its inhibition by the reaction product nicotinamide (Bitterman, Anderson et al. 2002). This product can bind to the active site, reacting with peptidyl imidate to form the reverse reaction yielding NAD^+. In addition to the sirtuin-mediated deacetylation, a spontaneous isomeric transition occurs in the solvent to maintain equilibrium of 2'- and 3-AADPR (Sauve, Celic et al. 2001).

C. Mechanism of NAD+-dependent ADP-ribosylation

In addition to the more widely studied deacetylation reaction, sirtuin enzymes were first identified by their ability to catalyze ADP-ribosylation of target proteins (Frye 1999; Tanny, Dowd et al. 1999). While the mechanisms of ADP-riboslytransfer are still in debate, several reports have proposed a possible mechanism for this reaction (Hawse, Hoff et al. 2008; Fahie, Hu et al. 2009; Hawse and Wolberger 2009; Sauve 2010). A leading hypothesis by Hawse and Wolberger suggests that the targets of sirtuin-mediated ADP-riboslytransfer contain a nucleophilic residue +2 positions from the acetylated lysine. In this mechanism, NAD+ reacts with acetyllysine to form an O-alkyamidate and release nicotinamide. The +2 nucleophilic residue next attacks the O-alkylamidate intermediate to produce ADP-ribosylation, and acetyllysine (Hawse and Wolberger 2009).

D. Regulation of sirtuin activity by nutrient intake and metabolic stressors

Although some exceptions exist, studies in the area of aging have repeatedly shown that caloric restriction (CR) improves glucose metabolism, increased mitochondrial activity, and extends life span in a broad range of species from yeast to mammals (Heilbronn and Ravussin 2003; Hursting, Lavigne et al. 2003; Cooper, Mockett et al. 2004; Harper, Leathers et al. 2006). In yeast, a reduction of glucose from 2% to 0.5% in the media (CR) extends life span about 30%. *SIR2* and respiration are required for this effect (Lin, Kaeberlein et al. 2002; Anderson, Bitterman et al. 2003; Lamming, Latorre-Esteves et al. 2005).

The benefits of CR in yeast are not solely dependent on SIR2. Severe CR (0.05% glucose) extends yeast replicative life span but does not require *SIR2* nor mitochondrial respiration (Kaeberlein, Kirkland et al. 2004; Kaeberlein, Hu et al. 2005). Moreover, Sir2 has no effect on yeast survival under starvation (Fabrizio, Gattazzo et al. 2005) or in worms under CR (Bishop, Lu et al.).

It is important to point out that the amount of yeast Sir2 protein does not increase during CR (Anderson, Bitterman et al. 2003), and there are alternative hypotheses concerning

the mechanism for CR-mediated longevity. Surprisingly, Sir2 levels and NAD^+ concentrations are not elevated following CR in yeast (Anderson, Bitterman et al. 2002). Instead, enzymatic activity is believed to increases in response to changes in the concentrations of nicotinamide and NADH. The gene that controls nicotimanide levels in yeast is named pyrazinamidase/nicotinamidase 1 (*PNC*1). This gene encodes an enzyme that deaminatesnicotinamide. Both *SIR2* and *PNC1* seem to work together and are essential for lifespan extension by calorie restriction and low-intensity stress in yeast and in mammals (Anderson, Bitterman et al. 2003). The authors further describe *PNC1* as responsive to all stimuli that extend lifespan, which is consistent with the hypothesis that the ability of dietary manipulations to extend lifespan in mammals is mediated, in part, by the induction of enzymes that increase the rate at which nicotinamide is recycled back to NAD^+ (Yang, Lavu et al. 2006).

While there are seven known mammalian homologs of Sir2, SIRT1 appears to be the one that most closely resembles the yeast Sir2 enzyme (Frye 2000). CR studies in rodent models have shown that CR increases SIRT1 in several metabolically relevant tissues including brain, kidney, liver, white adipose tissue and skeletal muscle (Cohen, Miller et al. 2004). The CR-stimulated increase in SIRT1 protein is accompanied by increased NAD^+, suggesting elevated activity in addition to the elevated enzyme levels (Nakahata, Kaluzova et al. 2008). Supporting the link between CR and SIRT1, analysis of genetically elevated SIRT1 suggest phenotypes that are highly reminiscent of those displayed during treatment with CR and SIRT1 agonists (Baur, Pearson et al. 2006; Lagouge, Argmann et al. 2006; Milne, Lambert et al. 2007). Nevertheless, the hypothesis that SIRT1 activity is increased in all tissues after CR has been recently called into question by a report showing that SIRT1 activity in the liver is decreased by CR, and this reduction by CR is correlated with the reduced role of this organ in fat synthesis (Chen, Bruno et al. 2008), though the time of day organs are harvested, which mammal is examined, and the type of CR, are all variables that may explain differences between studies.

Overexpression of SIRT1 in mice is associated with positive metabolic outcomes. Specifically, these mice display a decrease in adiposity, serum cholesterol, and insulin; as well as increased resistance to obesity-generated glucose intolerance and insulin resistance (Bordone, Cohen et al. 2007; Banks, Kon et al. 2008). On the other hand, studies utilizing mice deficient of the SIRT1 gene have also provided insight into its role in the physiology of CR (Ahn, Kim et al. 2008). Specifically, the global deletion of SIRT1 in mice elicits a shortened life span, which is resistant to CR-mediated increases (Chen, Steele et al. 2005; Li, Xu et al. 2008).

In addition to its activation during CR, SIRT1 is also activated in the presence of oxidative stress (Brunet, Sweeney et al. 2004; Kobayashi, Furukawa-Hibi et al. 2005; St-Pierre, Drori et al. 2006). This activity is important in the context of tissue preservation. For example, the SIRT1-mediated deacetylation of FOXO appears to protect β-cells from oxidative stress (Kitamura, Kitamura et al. 2005; Kitamura and Ido Kitamura 2007). Similarly, while HFD exposure induces oxidative stress via NF-κB (Carlsen, Haugen et al. 2009), SIRT1 over-expression has been shown to increase antioxidant defense enzymes and inhibit NFkappaB activation, thereby providing powerful protection from hepatic inflammation, glucose intolerance, and NAFLD (Pfluger, Herranz et al. 2008). Likewise, the effect of SIRT1 in neuronal tissues appears to be protective in the context of oxidative stress. Recent studies have suggested that

SIRT1 is responsible for protection from neuronal, and specifically axon, degeneration (Araki, Sasaki et al. 2004; Kim, Nguyen et al. 2007; van Ham, Thijssen et al. 2008). Although SIRT1 is known to protect tissues from oxidative damage, work by several groups suggest that SIRT1 may also have a role in providing genetic stability during times of oxidative damage. Specifically, SIRT1 deacetylates several genes important for DNA repair (Yuan and Seto 2007; Yuan, Zhang et al. 2007), and prevents immediate cell death in favor of senescent growth arrest (Sedelnikova, Horikawa et al. 2004). Additionally, SIRT1 is directly recruited to sites of broken DNA and helps recruit key DNA repair proteins such as Rad51 and Nbs1 (Oberdoerffer, Michan et al. 2008). Further supporting a role in genetic stability, $SIRT1^{-/-}$ embryos exhibit impaired DNA repair and increased chromosomal abnormalities (Wang, Sengupta et al. 2008) and overexpression of SIRT1 reduces aneuploidy and delays lymphoma (Oberdoerffer, Michan et al. 2008).

E. Regulation of SIRT3 activity by nutrient intake and metabolic stressors

During caloric restriction, expression of SIRT3 is increased in the mitochondria of murine skeletal and cardiac muscle, as well as in white and brown adipose tissues (Shi, Wang et al. 2005; Sundaresan, Samant et al. 2008; Palacios, Carmona et al. 2009). This is of interest as SIRT3 is known to deacetylate and activate acetyl-CoA-synthase (AceCS), the enzyme responsible for formation of acetyl-CoA from acetate (Schwer, Bunkenborg et al. 2006). AceCS is critical during times of prolonged fasting, where the ketone acetate must first be converted to acetyl-CoA before it can be utilized as a metabolite in the citric acid cycle. Conversely, in genetically obese mice, SIRT3 and genes important for mitochondrial function show decreased expression in brown adipose tissue (Shi, Wang et al. 2005).

IV. MOLECULAR TARGETS OF SIRT1 & SIRT3

SIRT1 interacts with and regulates a number of histone and non-histone proteins substrates. The wide variety of endogenous targets is correlated with the different biological functions modulated by this deacetylase. It has roles in developmental and aging regulation, energy metabolism, inflammation, and the repair of DNA double-strand break, amongst others.

A. Cytosolic and nuclear targets of SIRT1

1. Histones

Histones are proteins that are essential for the tight packaging of DNA into chromatin. The level of histone acetylation has been shown to regulate gene transcription. Specifically, increased acetylation prevents histones from binding and condensing DNA, thus enabling more transcription; whereas deacetylation promotes histone binding and decreases transcription. Each year, different reports identify new histones deacetylated by SIRT1, and among a wide list, it is included histone 1 on lysine 27

(H1K27) (Kuzmichev, Margueron et al. 2005), histone 3 on lysines 9, 14, 18 and 56 (H3K9, H3K14, H3K18, H3K56) (Imai, Armstrong et al. 2000; Vaquero, Scher et al. 2004; Yuan, Pu et al. 2009), and histone 4 on lysines 12 (H4K12) and 6 (H4K16) (Imai, Armstrong et al. 2000; Fu, Liu et al. 2006; Vaquero, Sternglanz et al. 2007). What drives the selection of SIRT1 substrates is not understood; the lack of significant substrate specificity has increased the difficulty of identifying bone fide targets for deacetylation (Blander, Olejnik et al. 2005). Hence credence is given to studies wherein gain and loss of SIRT1 function have reciprocal effects on substrate acetylation.

2. p53

SIRT1 has been shown to target and deacetylate the lysine residues of not only histones but numerous protein substrates as well. This diversity of function has important implications for mammalian cell survival and senescence. The substrates of SIRT1 that regulate apoptosis and cell cycle regulation include transcription factors and DNA repair factors. p53 is an important tumor suppressing protein that regulates many cellular activities, such as cell cycle regulation, DNA repair, and programmed cell death. As SIRT1 binds and deacetylates p53 to decrease its transcriptional activity, p53 is suggested to play a central role in SIRT1-mediated functions in tumorigenesis and senescence.(Luo, Nikolaev et al. 2001; Vaziri, Dessain et al. 2001; Langley, Pearson et al. 2002; Cheng, Mostoslavsky et al. 2003). For this reason, SIRT1 was originally considered to be a potential tumor promoter. However, new evidence suggests that SIRT1 acts as a tumor suppressor based on its role in negatively regulating beta-catenin and surviving (Yi and Luo). Therefore, even though the interaction between SIRT1 and p53 is clear, the current role of the SIRT1/p53 pathway on tumorigenesis is controversial.

3. Ku70

Ku70 is one of the two subunits (Ku70 and Ku80) of the Ku protein. The Ku protein plays a key role in multiple nuclear processes, including DNA repair, chromosome maintenance, transcription regulation, and recombination (Rathaus, Lerrer et al. 2009). It has been reported that SIRT1 prevents apoptosis by interactions with Ku70 (Boulton and Jackson 1998; Cohen, Miller et al. 2004; Jeong, Juhn et al. 2007; Li, Yokota et al. 2007; Anekonda and Adamus 2008). In response to calorie restriction, SIRT1 deacetylates Ku70, which in turn reduces stress-induced apoptosis by sequestering Bax, a pro-apoptotic factor, from mitochondria (Cohen, Miller et al. 2004). SIRT1 can also bind and deacetylate Ku70 to increase DNA repair activity in cells subjected to radiation exposure (Jeong, Juhn et al. 2007).

4. FOXO1, 3 & 4

The Forkhead box, group O (FOXO) subfamily of forkhead transcription factors are able to sense nutrient availability and regulates various cellular processes, including apoptosis and the cell cycle (Accili and Arden 2004; Dansen and Burgering 2008). SIRT1 deacetylates the FOXO proteins increasing their nuclear retention and transcriptional activity (Qiang, Banks et al. ; Daitoku, Hatta et al. 2004; Kitamura, Kitamura et al. 2005). Activation of certain members of the FOXO family can increase resistance to oxidative stress (Kops, Dansen et al. 2002), and SIRT1 is responsible for potentiating this function (van der Horst, Tertoolen et al. 2004). Specifically, SIRT1

regulates FOXO3 by both inhibiting FOXO3-induced apoptosis and potentiating the ability of FOXO3 to induce cell cycle arrest and resist oxidative stress (Brunet, Sweeney et al. 2004; van der Horst, Tertoolen et al. 2004). Other studies suggest that SIRT1 modulation of FOXO1 is important for proper glucose homeostasis, angiogenesis, and feeding behaviors (Sasaki, Kim et al. ; Liu, Dentin et al. 2008; Erion, Yonemitsu et al. 2009).

5. p300

p300 is an acetyltransferase that regulates numerous signaling pathways by facilitating transcriptional activity of a broad array of transcription factors through modular subdomains. It was demonstrated that SIRT1 interacts with and represses p300 transactivation in a NAD-dependent manner (Bouras, Fu et al. 2005). SIRT1 repression involves a transcriptional repression domain of p300 named CRD1, which has two residues (Lys-1020 and Lys-1024) that are essential for SIRT1 repression and serve as substrates for SIRT1deacetylation(Bouras, Fu et al. 2005). These residues also serve as acceptor lysines for modification by the small ubiquitin-like modifier (SUMO) protein. The SUMO-specific protease SSP3 relieved SIRT1 repression of p300, indicating that p300 serves as a deacetylase substrate for SIRT1 through a conserved SUMO consensus motif (Bouras, Fu et al. 2005).

6. HSF1

Heat shock factor 1 (HSF1) increases transcription of heat shock proteins in response to cell stress (Hu and Mivechi 2003). These proteins act to stabilize other proteins thereby reducing protein misfolding. In regards to SIRT1, a recent study shows that SIRT1 deacetylates HSF1, increasing its binding activity with heat shock promoter Hsp70 (Westerheide, Anckar et al. 2009).

7. PPARγ

The peroxisome proliferator-activated receptor gamma (PPAR-gamma) belongs to the nuclear hormone receptor superfamily and regulates gene expression upon heterodimerization with the retinoid X receptor by ligating to peroxisome proliferator response elements (PPREs) in the promoter region of target genes. PPARγ is considered to be one of the master regulators of adipocyte differentiation (Tontonoz, Hu et al. 1994). It has been shown that upon food withdrawal, SIRT1 stimulates fat mobilization in white adipose tissue by repressing PPARγ (Picard, Kurtev et al. 2004). The mechanism by which SIRT1 represses PPARγ involves the cofactors NCoR (nuclear receptor co-repressor) and SMRT (silencing mediator of retinoid and thyroid hormone receptors) (Picard, Kurtev et al. 2004). These effects are also observed in 3T3-L1 adipocytes, where activation of SIRT1 inhibits adipogenesis, whereas the inhibition of SIRT1 increases adipogenesis (Picard, Kurtev et al. 2004).

8. PGC-1α

PGC-1α is the inducible coactivator-1α of PPARγ, which is expressed at low levels in the liver during the fed state, but at high levels after food deprivation (Herzig, Long et al. 2001). PGC-1α plays a critical role in the regulation of hepatic gluconeogenesis and fatty acid oxidation. Consistent with this role, increased expression of PGC-1α in the

liver results in enhanced hepatic glucose production (Herzig, Long et al. 2001). As discussed in more detail below, SIRT1 deacetylates PGC-1α (Rodgers, Lerin et al. 2005) and this appears to be a crucial signal for the actions of SIRT1 at hepatic level.

9. PPARα

Peroxisome proliferator-activated receptor alpha (PPARα) is a ligand-activated transcription factor that belongs to the steroid hormone receptor superfamily. PPARα is expressed predominantly in tissues that have a high level of fatty acid catabolism, such as liver, heart, and muscle, where it regulates the expression of a number of genes critical for lipid and lipoprotein metabolism. Hepatic deletion of SIRT1 leads to impaired PPARα signaling and decreases fatty acid beta-oxidation, whereas overexpression of SIRT1 activates PPARα (Purushotham, Schug et al. 2009). Importantly, the actions of SIRT1 on PPARα require the deacetylation of PGC-1α (Purushotham, Schug et al. 2009).

10. LXRs

The liver X receptors (LXRs) alpha and beta (LXRα and LXRβ) are nuclear receptors that act as cholesterol sensors. SIRT1deacetylates a single conserved lysine (K432 in LXRα and K433 in LXRβ) and induces LXRα and LXRβ activity and thereby, exerts important regulatory action on cholesterol homeostasis (Li, Zhang et al. 2007). Consistent with this SIRT1 mediated regulation, SIRT1ko mice have lower levels of HDL cholesterol, while LDL cholesterol is unaffected (Li, Zhang et al. 2007). Moreover, SIRT1ko mice show a reduced cholesterol transport in macrophages and the liver, and this leads to an accumulation of hepatic cholesterol (Li, Zhang et al. 2007).

11. SREBP-1c

Sterol regulatory element-binding protein (SREBP) 1c is a master regulator which controls and upregulates the enzymes involved in fatty acid synthesis. It has been demonstrated that SIRT1deacetylates and inhibits SREBP1c activity in the liver (Ponugoti, Kim et al.), and it appears that the lipolytic action of SIRT1 in the liver is dependent on SREBP1c (Ponugoti, Kim et al.).

12. UCP-2

Uncoupling protein 2 (UCP2) belongs to the family of mitochondrial carriers. Moreover, UCP2 promotes longevity by shifting a given cell towards fatty acid fuel utilization (Andrews). SIRT1 represses mitochondrial uncoupling protein 2 (UCP2) transcription by binding directly to its promoter (Bordone, Motta et al. 2006). Consistently, it was observed that transgenic mice overexpressing SIRT1 in pancreatic beta cells have lower levels of UCP2 in islets, resulting in enhanced insulin secretion in isolated islets (Moynihan, Grimm et al. 2005). Additionally, the effects of SIRT1 inhibition in the brain decreasing food intake and promoting synaptic changes are abrogated in mice knockout for UCP2 (Dietrich el al., J Neuroscience 2010).

13. PTP1B

PTP1B is a member of the protein tyrosine phosphatase family. PTP1B plays a crucial role as an insulin receptor phosphatase, and PTP1B-deficient mice are more sensitive to insulin, have improved glucose metabolism and are resistant to diet-induced obesity (Elchebly, Payette et al. 1999). It has been shown that the beneficial effects of SIRT1 activation on insulin sensitivity are, at least partially, mediated by the repression of PTP1B transcription at the chromatin level (Sun, Zhang et al. 2007). Resveratrol, which may be an activator of SIRT1, also suppresses PTP1B, which might be a key step for enhancing insulin sensitivity (Sun, Zhang et al. 2007).

14. MyoD

The transcription factors of the MyoD family have essential functions in myogenic lineage determination and skeletal muscle development. These myogenic regulatory factors activate muscle-specific transcription of numerous genes. SIRT1 has been shown to retard muscle differentiation through its interaction with MyoD (Fulco, Schiltz et al. 2003). However, SIRT1 does not interact directly with MyoD, but forms a complex with the acetyltransferase p300/CBP-associated factor (PCAF), and then deacetylates both PCAF and MyoD (Fulco, Schiltz et al. 2003).

15. TIP60

The histone acetyltransferase TIP60 can acetylate many substrates, including histones and p53, promoting apoptosis. SIRT1deacetylates and inactivates TIP60 activity in vivo, suggesting that SIRT1 plays an important role in the control of histone acetyltransferase activity and function in response to DNA damage (Wang and Chen).

16. NF-kappaB

The nuclear factor kappa enhancer binding protein (NF-kappaB) regulates diverse biological processes including immunity, inflammation, and apoptosis. The interaction between SIRT1 and the NF-κB signaling pathway was first reported to be involved in the cigarette smoke-mediated proinflammatory cytokine release (Yang, Wright et al. 2007). This interaction was observed in a monocyte-macrophage cell line and in inflammatory cells of rat lungs. However, one important role of NF-κB is to mediate pancreatic β-cell damage. Studies in isolated rat islets or RINm5F cells have demonstrated that overexpression of SIRT1 completely blocked cytokines induced cell damage (Lee, Song et al. 2009), indicating that the SIRT1/NF-κB pathway plays an important role mediating beta-cell damage. Overexpression of SIRT1 was further shown to attenuate hepatic NFkB activation *in vitro* and *in vivo* (Pfluger, Herranz et al. 2008).

17. IRS

Studies performed in vitro have shown that resveratrol inhibited the phosphorylation of insulin receptor substrate 1 (IRS1) Ser307 and IRS2 Thr348, which are markers of insulin resistance (Draznin 2006), thereby, indicating that resveratrol improves insulin resistance (Frojdo, Durand et al.). In agreement with this, SIRT1 overexpression increased the phosphorylation of PKB, a moleculae that is downstream the IRS, in

muscle cells and HEK293 cells, whereas the inhibition of SIRT1 has opposite actions (Frojdo, Durand et al.). Another *in vitro* report demonstrated that the suppression of SIRT1 activity inhibited the tyrosine phosphorylation of insulin receptor substrate 2 (IRS2) in HEK293 cells (Zhang 2007). In neurons, the inhibition of SIRT1 increases the acetylation and reduced the phosphorylation of IRS2 (Li, Xu et al. 2008). The reduced activity of SIRT1 also reduced Ras activation and ERK1/2 phosphorylation (both markers of oxidized proteins and lipids) (Li, Xu et al. 2008). Thus, this article suggests that SIRT1 can protect neurons from oxidative damage.

18. E2F1/p73

E2F1 is known to induce the transcription of several apoptotic genes and can induce apoptosis after DNA damage events through both p53-dependent and p53-independent mechanisms. SIRT1 inhibits E2F1 (Wang, Chen et al. 2006), and this inhibition suppresses p73 transcriptional activity (Dai, Wang et al. 2007; Pediconi, Guerrieri et al. 2009). It seems that SIRT1 interacts with PCAF and E2F1 on the P1p73 promotor (Pediconi, Guerrieri et al. 2009), and thereby can modulate tumor proliferation.

19. MEF2

MEF2 is a family of transcription factors with important functions in muscle cell differentiation and apoptosis (McKinsey, Zhang et al. 2002). SIRT1 can potently induce MEF2 deacetylation during muscle cell differentiation (Zhao, Sternsdorf et al. 2005), indicating that this mechanism might be responsible of the negative regulation of myogenesis by SIRT1.

20. TORC2

The CREB regulated transcription coactivator 2 (CRTC2 or TORC2) plays an essential role in gluconeogenesis. For instance, the stimulation of the gluconeogenic program induced by glucagon requires the dephosphorylation and nuclear translocation of TORC2. SIRT1 reduces TORC2 activity in the liver, while the inhibition of SIRT1 signalling induces TORC2 activity (Liu, Dentin et al. 2008), suggesting that this pathway is an important modulator of the gluconeogenesis (discussed below).

21. PARP1.

Sirtuins and poly(ADP-ribose) polymerases (PARPs) act as survival and death inducing factors. These two protein families are both dependent on NAD+ for their activities. In response to DNA damage, SIRT1-dependent deacetylation blocks PARP1 activity, and it protects cells from PARP1-mediated cell death (Kolthur-Seetharam, Dantzer et al. 2006; Rajamohan, Pillai et al. 2009)**.**

B. Mitochondrial targets of SIRT3

The NAD^+-dependent deacetylase SIRT3 is localized in mitochondria (Onyango, Celic et al. 2002; Schwer, North et al. 2002; Michishita, Park et al. 2005; Shi, Wang et al. 2005; Lombard, Alt et al. 2007; Schlicker, Gertz et al. 2008) and plays an important role in mitochondrial metabolism (Shi, Wang et al. 2005). To exert these metabolic actions, SIRT3 regulates the expression of many mitochondrial proteins through a reversible deacetylation process (Hallows, Lee et al. 2006; Schwer, Bunkenborg et al. 2006).

1. AceCS2

Acetyl-CoA synthase 2 (AceCS2) was the first SIRT3 mitochondrial protein substrate to be identified (Hallows, Lee et al. 2006; Schwer, Bunkenborg et al. 2006) and is an enzyme that catalyzes the production of Acetyl-CoA from acetate (Fujino, Kondo et al. 2001). AceCS2 undergoes regulation by reversible acetylation; SIRT3deacetylates and activates AceCS2, whereas acetylation of AceCS2 inhibits its activity (Hallows, Lee et al. 2006; Schwer, Bunkenborg et al. 2006). Since Acetyl-CoA is an important regulator of several metabolic pathways including cholesterol and fatty acid biosynthesis, it is possible that SIRT3 modulates those biological actions.

2. HMGCS2

Hydroxyl methylglutaryl CoA synthase 2 (HMGCS2), the rate-limiting step in β-hydroxybutyrate synthesis, was shown to deacetylated and activated by SIRT3 (Shimazu, Hirschey et al.). Upon fasting, SIRT3-mediatedHMGCS2 activation was required to induce the production of ketone bodies (Shimazu, Hirschey et al.).

3. GDH

Glutamate dehydrogenase (GDH) is a key metabolic enzyme in the mitochondrial matrix that is colocalized with SIRT3 in the mitochondrial matrix (Schlicker, Gertz et al. 2008). SIRT3deacetylates and activates GDH in vitro (Schlicker, Gertz et al. 2008) and in vivo (Lombard, Alt et al. 2007).

4. p53

SIRT3 suppresses p53 activity leading to growth arrest and senescence (Li, Banck et al.). This was demonstrated in the EJ-p53 cell line, where SIRT3 co-localizes with p53 in the mitochondria before inducing cell arrest (Li, Banck et al.). A close interaction between SIRT3 and p53 also plays an important function in mouse preimplantation in vitro (Kawamura, Uchijima et al.), even though mice lacking SIRT3 are fertile.

5. Ku70

SIRT3 protects cardiomyocytes from stress-induced cell death by deacetylating Ku70, leading to the interaction between Ku70 and the proapoptotic protein Bax. This pathway is associated with a protective function of SIRT3 on cardyomiocytes under stress conditions (Sundaresan, Samant et al. 2008; Sundaresan, Gupta et al. 2009).

6. Foxo3a

SIRT3 activates Foxo3a in cardiomyocytes leading to the activation of a molecular pathway involving ROS/Ras/MAPK/ERK and PI3K/Akt, which finally inhibits cardiac hypertrophy (Sundaresan, Gupta et al. 2009). The actions of SIRT3 on cardiomyocytes have been also demonstrated in vivo, as mice lacking SIRT3 shows signs of cardiac hypertrophy at 8 weeks of age (Sundaresan, Gupta et al. 2009). Similar results were obtained in *C. elegans*, where daf-16, the homolog of the human FOXO family was also deacetylated by SIRT3(Jacobs, Pennington et al. 2008).

7. p300/H3-K56

Acetylation of histone H3 core domain lysine 56 (H3-K56) is essential for the compaction of DNA into chromatin, and the histone acetyltransferase p300 acetylates H3-K56 in vivo. Human SIRT3 deacetylates H3K-56 (Vempati, Jayani et al.), indicating that SIRT3 regulates the DNA damage response pathway.

8. Cyclophilin D

Increasing evidence implicates a multi-protein complex called the mitochondrial permeability transition pore (mPTP) in the decline in mitochondrial function with age. Acute triggering of the mPTP can lead to apoptosis whereas low-level, chronic triggering results in mitochondrial swelling, membrane de-polarization, and the destruction of defective mitochondria by autophagy. SIRT3 deacetylates the regulatory component of the mPTP, cyclophilin D (CypD) on lysine 166, adjacent to the binding site of cyclosporine A, a CypD inhibitor (Hafner, Dai et al. ; Shulga, Wilson-Smith et al.). Consistent with this, cardiac myocytes from mice lacking SIRT3 exhibit an age-dependent increase in mitochondrial swelling due to increased mPTP opening (Hafner, Dai et al.). $SIRT3^{-/-}$ mice show accelerated signs of aging in the heart including cardiac hypertrophy and fibrosis at 13 months of age and are hypersensitive to heart stress. Deacetylation of cyclophilin D also induces dissociation of hexokinase II from the mitochondria prevents cell death (Shulga, Wilson-Smith et al.), which produces a transition from a reliance on glycolysis to oxidative phosphorylation (Shulga, Wilson-Smith et al.).

9. MRPL10

The mitochondrial ribosomal protein L10 (MRPL10) plays an important function in the acetylation in the mitochondrial chromosome. SIRT3 overexpression in C2C12 cells induces the deacetylation of MRPL10 and thereby diminishes the synthesis of proteins in the mitochondria (Yang, Cimen et al.). Consistent with these findings, the inhibition of SIRT3 in those cells leads to an increased synthesis of mitochondrial proteins (Yang, Cimen et al.).

10. SDH

Succinate dehydrogenase (SDH) is a unique enzyme, as it participates in both Krebs cycle and oxidative phosphorylation in mitochondria. Therefore, it is essential for mitochondrial metabolism and its deletion is lethal. One of its subunits, named SDhA is

a substrate for SIRT3, allowing this sirtuin to regulate oxidative phosphorylation (Cimen, Han et al.).

11. OTC

SIRT3 was shown to deacetylate and thereby activate ornithine transcarbamoylase (OTC), a rate-limiting enzyme in the urea cycle (Hallows, Yu et al.). Calorie restriction increased both SIRT3 and OTC activity; in SIRT3 null mice, low OTC activity during fasting was connected with increased orotic acid levels, indicating a disturbed nitrogen balance. Hallow et al further conducted LC/MS analyses of mitochondrial proteins in SIRT3 null and WT mice, and revealed a number of novel SIRT3 targets involved in beta-oxidation and amino acid catabolism (Hallows, Yu et al.).

12. ICDH2

The isocitrate dehydrogenase 2 (ICDH2) is another key metabolic regulator in the mitochondrial matrix that is also colocalized with SIRT3 in the mitochondrial matrix.ICDH2 is also deacetylated and activated by SIRT3 (Schlicker, Gertz et al. 2008), and this effect was shown to be abolished by a sirtuin inhibitor. The precise acetylation sites for ICDH2 (K75 and K241) were found to be deacetylated by SIRT3 (Schlicker, Gertz et al. 2008). The increased activity of ICDH2 promotes regeneration of antioxidants and catalyzes the citric acid cycle (Schlicker, Gertz et al. 2008). Very recently, the deacetylationof ICDH2 by SIRT3 was shown to augment the mitochondrial glutathione antioxidant defense system in mice via increasing NADPH levels and the ratio of reduced-to-oxidized glutathione in mitochondria (Someya, Yu et al.). Importantly, calorie restriction-induced SIRT3 activation was thereby linked to the prevention from extensive age-related oxidative damage (Someya, Yu et al.).

13. MnSOD

Recently, SIRT3 was shown to deacetylatemanganese superoxide dismutase (MnSOD), thereby increasing MnSOD activity (Tao, Coleman et al.). Such SIRT3-mediated MnSOD activation consequently decreased mitochondrial superoxide. Conversely, SIRT3 ablation in mice decreased hepatic MnSOD activity, which might contribute to the tumor-permissive environment seen in $SIRT3^{-/-}$ animals. Accordingly, SIRT3-/- mice displayed higher susceptibility to radiation-induced liver damage (Tao, Coleman et al.).

14. ATP and the electron transport chain

A recent study shows that SIRT3 deacetylates one or more proteins of the electron transport chain Complex I, including NDUFA9 (Ahn, Kim et al. 2008). Complex I activity is inhibited in SIRT3(-/-) mice and potentiated in mitochondria that have been exposed to increased levels of SIRT3 (Ahn, Kim et al. 2008). These results suggest that SIRT3 plays an important role in regulating ATP synthesis in mitochondria and thus is a potential regulator of mitochondrial energy metabolism (Ahn, Kim et al. 2008).

V. ENDOGENOUS REGULATORS OF SIRT1 & SIRT3

Besides the classical activation of sirtuins by increased NAD^+/NADH ratios, a number of other endogenous processes regulate SIRT1 and SIRT3 activity. Transcription of sirtuins can be controlled by a number of transcription factors and transcriptional co-activators or repressors. Further, mRNA stability of sirtuins depends on the presence of specific microRNAs. Last, sirtuin activity can be regulated by post-translational modifications through protein-protein interaction, stimulating or repressing sirtuin activity.

A. Endogenous regulators of SIRT1

1. E2F1

E2F1 induces SIRT1 expression at the transcriptional level (Wang, Chen et al. 2006; Brooks and Gu 2009). E2F1 is also a substrate of SIRT1 and deacetylation of E2F1 inhibits its activity as a transcriptional activator. This action is modulated by the interaction of SIRT1 with PCAF, which controls the E2F1/p73 apoptotic pathway (Pediconi, Guerrieri et al. 2009). Accordingly, the down-regulation of SIRT1 increases E2F1 transcriptional and apoptotic functions (Wang, Chen et al. 2006; Brooks and Gu 2009). Therefore, this SIRT1–E2F1 negative feedback loop might act as a regulatory switch that can determine the apoptotic fate of a cell.

2. p53

In addition to being a target for SIRT1deacetylation, p53 can also repress SIRT1 transcription through binding to two response elements within the SIRT1 promoter. p53-null mice have increased levels of SIRT1 in different tissues and several p53-null tumour cell lines display SIRT1 overexpression (Nemoto, Fergusson et al. 2004; Ford, Jiang et al. 2005). Therefore, SIRT1 and p53 also form a regulatory feedback loop since SIRT1 is known to deacetylate p53.

3. HIC1

The growth regulator and tumour repressor gene Hypermethylated In Cancer 1 (HIC1) also suppresses SIRT1 transcription. HIC1, C terminal binding protein 1 (CTBP1) and SIRT1 form a co-repressor complex (Chen, Wang et al. 2005) that binds enhancer elements upstream of the SIRT1 promoter and inhibits SIRT1 expression. In both mouse and human prostate cancer cells, as well as Hic−/− mouse embryonic fibroblasts, reduction or ablation of HIC1 is associated with an increase in SIRT1 expression levels (Huffman, Grizzle et al. 2007), indicating one possible explanation of the increased levels of SIRT1 during tumorigenesis.

4. HuR

HuR is a ubiquitously expressed RNA-binding protein that stabilizes mRNAs and regulates translation to protein. The tumour suppressor HuR (also known as ELAVL1) is an mRNA binding protein that binds the 3′ UTR of SIRT1 mRNA, stabilizes the SIRT1 mRNA, and increases SIRT1 expression levels (Abdelmohsen, Pullmann et al.

2007). Moreover, HUR gene expression correlates with the reduced levels of SIRT1 expression in aged senescent cells (Abdelmohsen, Pullmann et al. 2007).

5. miR-34a

MicroRNAs are posttranscriptional gene regulators that are differentially expressed under several physiological conditions. The microRNA miR-34a, also binds the 3′ UTR of SIRT1 mRNA (Yamakuchi, Ferlito et al. 2008; Yamakuchi and Lowenstein 2009). In contrast to HUR, miR-34a prevents translation of SIRT1 and so inhibits SIRT1deacetylase activity, subsequently inducing the accumulation of acetylated p53.

6. miR-199a

In addition to miR-34a, miR-199a has also been associated with SIRT1 regulation. Knockdown of miR-199a results in the upregulation of SIRT1 and the hypoxia-inducible factor 1 alpha (Hif-1alpha) (Rane, He et al. 2009). As this report found that miR-199a levels were decreased in cardiac myocytes upon hypoxia, the data indicate that SIRT1 is important for hypoxic damage (Rane, He et al. 2009).

7. DBC1

Deleted in breast cancer 1 (DBC1, also known as KIAA1967) is an inhibitor of SIRT1 activity (Kim, Kho et al. 2007; Kim, Chen et al. 2008; Zhao, Kruse et al. 2008). Moreover, reduction of DBC1 inhibits p53-mediated apoptosis after induction of double-stranded DNA breaks owing to SIRT1-mediated p53 deacetylation. Although little is known about the normal function of DBC1, its loss in several cancer cell lines and its inhibition of SIRT1 suggest it may have an important role in tumorigenesis.

8. AROS

Active regulator of SIRT1 (AROS, also known as RPS19BP1) is a 142 amino acid nuclear protein, which directly activates SIRT1 activity and attenuates p53-dependent transcriptional activation (Kim, Kho et al. 2007). Consistent with this role, reduction of AROS increased cell susceptibility to apoptosis after DNA damage (Kim, Kho et al. 2007).

9. Necdin

Necdin is a member of the melanoma-associated antigen (MAGE) family of proteins. These proteins play multiple functions in cellular regulation, including tumorigenesis or neuronal differentiation and survival. Necdin has been shown to negatively regulating p53 by potentiating SIRT1-mediated deacetylation of p53 (Hasegawa and Yoshikawa 2008). Inhibition of p53 acetylation through a necdin–SIRT1–p53 complex prevents p53-mediated apoptosis in response to DNA damage.

10. AMPK

AMPK controls the expression of genes involved in energy metabolism in mouse skeletal muscle by acting in coordination with SIRT1. AMPK increases SIRT1 activity

by increasing cellular NAD+ levels (Canto, Gerhart-Hines et al. 2009). Interestingly, this interaction between SIRT1 and AMPK seems to be reciprocal, as SIRT1 activation stimulates fatty acid oxidation and indirectly activates AMPK (Feige, Lagouge et al. 2008).

11. Foxo3a

Forkhead box O-class (FOXO) transcription factors function as tumor-suppressor proteins by inhibiting cell proliferation, promoting apoptotic cell death and protecting cells from DNA damage and oxidative stress. Foxo3a stimulates SIRT1 transcription through two p53 binding sites present in the SIRT1 promoter (Nemoto, Fergusson et al. 2004). Consistently, knockdown of Foxo3a expression inhibits the starvation-induced increase in SIRT1 expression (Nemoto, Fergusson et al. 2004).

12. c-Myc

c-Myc regulates processes involved in many if not all aspects of cell fate. c-Myc and SIRT1 form a negative feedback loop that inhibits c-Myc–induced cellular transformation. On one hand, c-Myc binds to the SIRT1 promoter and induces SIRT1 expression (Yuan, Minter-Dykhouse et al. 2009). However, SIRT1 interacts with and deacetylates c-Myc, resulting in decreased c-Myc stability and subsequent suppression of SIRT1 expression (Yuan, Minter-Dykhouse et al. 2009).

13. SHP

Orphan nuclear receptor Small Heterodimer Partner (SHP) is a transcriptional corepressor of a wide variety of nuclear receptors. It has been reported that SHP interacts and co-localizes with SIRT1, inhibiting the transcriptional activity of SIRT1 (Chanda, Xie et al.).

B. Endogenous regulators of SIRT3

Little is known about endogenous regulators of SIRT3. One report suggested that PGC-1α stimulates mouse SIRT3 activity in both muscle cells and hepatocytes (Kong, Wang et al.). In agreement with this, SIRT3 knockdown suppressed the actions of PGC-1α on mitochondrial biogenesis in myotubes (Kong, Wang et al.).

VI. METABOLIC TISSUES TARGETED BY SIRT1

A. The roles of SIRT1 in liver metabolism

1. SIRT1 and hepatic glucose metabolism

In liver, SIRT1 is upregulated during negative energy balance as occurs during fasting and calorie restriction (Cohen, Miller et al. 2004; Nemoto, Fergusson et al. 2004; Al-Regaiey, Masternak et al. 2005; Rodgers, Lerin et al. 2005; Nie, Erion et al. 2009). In 2005, research led by Puigserver and collaborators (Rodgers, Lerin et al. 2005) revealed

that during fasting SIRT1 stimulates gluconeogenesis, while inhibiting glycolysis, by deacetylating the transcriptional coactivator PGC-1α. The authors showed that SIRT1 interacts with, and deacetylates, PGC-1α in a NAD^+-dependent manner (Nemoto, Fergusson et al. 2005; Rodgers, Lerin et al. 2005). Importantly, the regulation of PGC-1α by SIRT1 was found to be essential for fasting or pyruvate mediated increases of gluconeogenic genes (*PEPCK* and *G6Pase*) and glucose output in cultured hepatocytes. Furthermore, this deacetylation also acts to decrease the expression of glycolytic genes (*glucokinase* and *LPK*) (Rodgers, Lerin et al. 2005). This effect of SIRT1 stimulating hepatic glucose output during fasting was later confirmed in mice (Rodgers and Puigserver 2007; Erion, Yonemitsu et al. 2009).

SIRT1 has been shown to regulate hepatic glucose metabolism by interacting with the FOXO family of transcriptional factors (Kaestner, Knochel et al. 2000; Kobayashi, Furukawa-Hibi et al. 2005). FOXO are transcription factors that are inactivated by the PI3k-Akt/PKB pathway in response to hormonal signaling (Barthel, Schmoll et al. 2005; Greer and Brunet 2005). When phosphorylated, these transcription factors are inactive and are localized in the cytosol; upon de-phosphorylation, they have nuclear localization and are active (Zhao, Gan et al. 2004). Several groups have shown the close and intricate interaction between SIRT1 and FOXO. Motta et al. (2004) found that SIRT1 binds to FOXO3a, and promotes its deacetylation with consequent inhibition of FOXO3a transcriptional activity (Motta, Divecha et al. 2004). On the other hand, FOXO3a induced by starvation promotesSIRT1 expression in a p53 dependent manner (Nemoto, Fergusson et al. 2004). Additionally, SIRT1 was also shown to interact and deacetylate FOXO1 (Yang, Hou et al. 2005) and FOXO4 (Kobayashi, Furukawa-Hibi et al. 2005). The FOXO family of transcription factors has shown to stimulate the expression of genes involved in gluconeogenesis (*pepck* and *g6pase*) (Yeagley, Guo et al. 2001; Wolfrum, Asilmaz et al. 2004), while decreasing expression of glucose kinase (gk) (Ayala, Streeper et al. 1999; Schmoll, Walker et al. 2000; Zhang, Patil et al. 2006). During prolonged fasting, FOXO1 activity supported by SIRT1 seems to be a key element in the maintenance of glucose production (Liu, Dentin et al. 2008). SIRT1 activation has been shown to stimulate Foxo1 translocation to hepatocyte nuclei (Frescas, Valenti et al. 2005). Under conditions of SIRT1 activation or oxidative stress, Foxo1 is confined to a nuclear subdomain where it boosts transcription of genes that promote gluconeogenesis and hepatic glucose production (Frescas, Valenti et al. 2005). Importantly, mutations of the FoxO1 coactivator-interacting LXXLL motif, eliminated FoxO1 interaction with SIRT1, indicating that this motif is essential for SIRT1 actions mediated by FXO1 (Nakae, Cao et al. 2006).

SIRT1 is also known to regulate gluconeogenesis via its interaction with STAT3 (Nie, Erion et al. 2009). STAT3 suppresses gluconeogenesis by inhibiting the transcription of *PEPCK1* and *g6pase* (Inoue, Ogawa et al. 2004; Inoue, Ogawa et al. 2006), and its activity is dependent on the phosphorylation of amino acid residues. STAT3 contains several lysine sites that are acetylated. This acetylation has been shown to regulate the activity and phosphorylation of this protein. SIRT1 deacetylases STAT3, thus decreasing STAT3 activity and it is inhibitory effect on gluconeogenesis. Therefore, activation of SIRT1 during fasting stimulates gluconeogenesis by inhibiting STAT3 while activating PGC-1α and FOXO1.

In contrast, a number of studies suggest that the activation of SIRT1 inhibits insulin-induced hepatic glucose production in obese rats (Milne, Lambert et al. 2007).

Moreover, a recently identified fasting-inducible switch, consisting of SIRT1 and p300, causes a transfer between two key regulators of glucose production (Liu, Dentin et al. 2008). The switch occurs during nutrient deprivation, when regulation of the gluconeogenic program is shifted from CREB-regulated transcription coactivator 2 (CRTC2, also TORC2) to Foxo1 (Liu, Dentin et al. 2008). During early fasting, glucagon induces p300/CBP-mediated acetylation of CRTC2, which briefly increases gluconeogenic activity. During prolonged fasting, SIRT1deacetylates and downregulates CRTC2 and promotes a Foxo1-mediated gluconeogenic program (Liu, Dentin et al. 2008), therefore SIRT1 may also act to suppress hepatic glucose production during the late phases of fasting (Liu, Dentin et al. 2008).

2. SIRT1 and hepatic fatty acid metabolism

SIRT1 plays a prominent role in the regulation of hepatic fatty acid metabolism. Specifically, SIRT1 regulated hepatic lipid metabolism by activating the AMPK (AMP-activated protein kinase)/LKB1 signaling pathway (Hou, Xu et al. 2008). Notably, LKB1 was essential to produce downstream effects of SIRT1 on fatty acid oxidation and lipogenesis (Hou, Xu et al. 2008). In a hyperglycemic environment, SIRT1-mediated activation of AMPK prevents lipid accumulation and FAS upregulation(Hou, Xu et al. 2008). Consistent with this regulation, mice fed on high fat diet treated with resveratrol or the SIRT1 agonist SRT1720 exhibited improved liver physiology and metabolic function (Baur, Pearson et al. 2006; Milne, Lambert et al. 2007; Pfluger, Herranz et al. 2008).

3. SIRT1 and hepatic cholesterol metabolism

SIRT1also plays an important role in cholesterol homeostasis. The cholesterol-sensing liver X receptor (LXR) proteins are nuclear receptors involved in maintaining cholesterol homeostasis. LXRs act to enhance the reverse transport of cholesterol from peripheral tissues by stimulating the expression of the ATP-binding cassette transporter A1 (ABCA1). These transport proteins direct cholesterol to apolipoprotein AI to form high density lipoproteins (Li, Zhang et al. 2007). SIRT1 interacts with and deacetylates the LXRs, influencing several targets including the ABCA1 (Li, Zhang et al. 2007), and therefore, regulating HDL production (Attie 2007).

B. The roles of SIRT1 in pancreatic β-cells

1. SIRT1 and in insulin secretion

In addition to the regulation of hepatic glucose metabolism, SIRT1 has also been linked to glucose-stimulated insulin secretion in pancreatic beta cells (Moynihan, Grimm et al. 2005; Bordone, Motta et al. 2006). A selective increase in the dosage of SIRT1 in pancreatic beta cells improves glucose tolerance and insulin release in response to glucose and KCl (Moynihan, Grimm et al. 2005). Conversely, SIRT1 knock down in beta cells had opposite effect on insulin secretion (Bordone, Motta et al. 2006). This effect appears to be partially induced via SIRT1-mediated repression of *ucp2* (Bordone, Motta et al. 2006). Intriguingly, this improved insulin sensitivity is not exclusive to the beta cell. SIRT1 was shown to improve insulin sensitivity by decreasing the transcription of *ptp1b in vitro* in myotubes (Sun, Zhang et al. 2007). PTP1B acts as a negative regulator of insulin receptor signaling, and its downregulation improves insulin

sensitivity (Elchebly, Payette et al. 1999). Transgenic mice with mild overexpression of SIRT1 also showed improved glucose tolerance in several models of insulin resistance, an effect that was mediated by decrease hepatic production of glucose and increase adiponectin levels, and not by differences in beta cell sensing of glucose (Banks, Kon et al. 2008).

2. SIRT1 and β-cell protection

SIRT1 also plays a role in pancreatic beta-cell protection. In the hyperglycemic state, oxidative stress can induce pancreatic beta cell failure (Kitamura, Kitamura et al. 2005). SIRT1, Foxo1 and Pml (promyelocytic leukemia protein) form a complex that upregulatestranscription factors (NeuroD and MafA) to protect beta cells from hyperglycemia-induced damage (Kitamura, Kitamura et al. 2005). Also, the SIRT1-mediated regulation of NF-κB may prevent pancreatic beta-cell toxicity (Lee, Song et al. 2009). SIRT1 has been shown to regulate NF-κB (nuclear factor kappa-light-chain-enhancer of activated B cells) by deacetylating lysine 310 on its relA/p65 subunit (Yeung, Hoberg et al. 2004).

C. The roles of SIRT1 in skeletal muscle metabolism

1. SIRT1 and skeletal muscle fatty acid metabolism

When skeletal muscle is nutrient-deprived, glucose oxidation shifts to fatty acid oxidation. SIRT1 is activated during low energy states and therefore it makes sense that SIRT1 would induce fatty acid oxidation as the cell shifts from glucose consumption to fatty acid oxidation (Gerhart-Hines, Rodgers et al. 2007). In skeletal muscle, SIRT1 deacetylates PGC-1alpha to induce mitochondrial fatty acid oxidation in a glucose-scarce environment (Gerhart-Hines, Rodgers et al. 2007). SIRT1deacetylates and activates acetyl-CoA synthetase (AceCS) 1, which can induce substantial fatty acid synthesis (Hallows, Lee et al. 2006). AceCS1 is regulated by reversible acetylation, a process in which acetylation inactivates AceCS1 and SIRT1-induced deacetylation reactivates it. In vivo studies have shown that mice treated with the potential SIRT1 activator resveratrol (the specificity of resveratrol for SIRT1 activation is critically discussed in chapter X), significantly increased their aerobic capacity (Lagouge, Argmann et al. 2006). The effects of resveratrol were also associated with an induction of genes for oxidative phosphorylation and mitochondrial biogenesis. Furthermore, these effects were largely explained by the deacetylation of PGC-1alpha and subsequent increases in PGC-1alpha activity (Lagouge, Argmann et al. 2006). Importantly, resveratrol protected these mice against diet-induced-obesity and insulin resistance (Lagouge, Argmann et al. 2006). SIRT1 may also act on uncoupling protein 3 (UCP3), a mitochondrial protein expressed in skeletal muscle that lowers membrane potential and prevents fatty acid accumulation (Amat, Solanes et al. 2007). This regulation occurs via SIRT1-mediated deacetylation of histones near the UCP3 promoter, thereby preventing UCP3 transcription and subsequently the accumulation of fatty acids (Amat, Solanes et al. 2007).

2. SIRT1 and skeletal muscle glucose metabolism

As discussed in Section IV (A.13.), in vitro studies demonstrated that SIRT1 improves insulin sensitivity by repressing the protein tyrosine phosphatase 1B (PTP1B) gene in skeletal myotube cells (Sun, Zhang et al. 2007). PTP1B is a key insulin receptor phosphatase, and PTP1B-deficient mice have been shown to be more insulin-sensitive and more resistant to diet-induced obesity compared with controls (Elchebly, Payette et al. 1999). In vivo studies have also shown that resveratrol was able to increase glucose uptake, an effect independent of insulin and dependent on AMPK, through the increase of the intrinsic activity of the glucose transporter GLUT4 (Breen, Sanli et al. 2008).

3. SIRT1 and skeletal muscle muscle differentiation

Sir2 was shown to negatively regulate muscle gene expression and differentiation. To exert these actions, Sir2 does not directly interact with muscle transcriptional regulators, but ratherassociates with the complex PCAF/GCN5. In the presence of PCAF/GCN5, Sir2 associates with and deacetylates both transcriptional factors PCAF and myogenic determining factor (MyoD) (Fulco, Schiltz et al. 2003). Moreover, in C2C12 myotubes, when MyoD is present with SIRT1 on the PGC-1-alpha promoter, PGC-1alpha overexpression increases due to positive feedback of PGC-1alpha on its own promoter (Amat, Planavila et al. 2009). Therefore, MyoD enhances the overexpression of PGC-1alpha in a SIRT1-dependent manner (Amat, Planavila et al. 2009).

D. The roles of SIRT1 in white adipose tissue metabolism

1. SIRT1 and adipose tissue fatty acid metabolism

SIRT1 favors lipolysis and fatty acid mobilization in response to fasting by repressing PPAR-γ (Picard, Kurtev et al. 2004), which is essential for adipogenesis. SIRT1 interacts with PPARγ DNA binding sites, but it is unclear whether SIRT1deacetylates PPARγ directly (Picard, Kurtev et al. 2004). Activation of SIRT1 inhibits differentiation and proliferation in pig preadipocytes, whereas inhibition of SIRT1 activates adipocyte differentiation substantially (Bai, Pang et al. 2008). In pig preadipocytes, SIRT1 may inhibit Foxo1 or other genes associated with pig adipocyte development (Bai, Pang et al. 2008).

2. SIRT1 and adipose tissue glucose metabolism

SIRT1 also regulates the production and/or the secretion of insulin-sensitizing factors such as adiponectin and FGF21 through the regulation of FOXO1 and PPARγ (Qiao and Shao 2006; Banks, Kon et al. 2008; Wang, Qiang et al. 2008). These studies suggest that in adipocytes, PPARγ selectively represses the expression of a group of genes containing FGF21. However, in vivo studies have yet to corroborate these findings. Moreover, the adipocytes of mice lacking the leptin receptor (*db/db* mice), which develop obesity and type 2 diabetes, show lower levels of FOXO1 and SIRT1 than their littermates (Subauste and Burant 2007), whereas the activation of SIRT1 by resveratrol rescued FOXO1 levels in the adipocytes of *db/db* mice (Subauste and Burant 2007). The beneficial role of SIRT1 on glucose metabolism might be at least partially explained by the activation of adiponectin. Adiponectin is an important regulator of

energy homeostasis, and its expression is reduced in obesity and type II diabetes. SIRT1 activates Foxo1, which forms a transcription complex with CCAAT/enhancer-binding protein alpha (C/EBPalpha), thus promoting adiponectin gene transcription (Qiao and Shao 2006). SIRT1 may also play a role in the attenuation of ROS. In adipocytes exposed to high levels of free fatty acids, activation of SIRT1 leads to nuclear translocation of Foxo1 and is accompanied with a parallel decrease in ROS production (Subauste and Burant 2007). SIRT1-mediated activation of Foxo1 may therefore protect from obesity-induced inflammation and subsequently insulin resistance.

E. CNS SIRT1 regulates metabolic control

SIRT1 is present in metabolically important areas of the brain, including hypothalamic nuclei such as the arcuate, ventromedial, dorsomedial and paraventricular nuclei, as well as the area postrema and the nucleus of the solitary tract in the hindbrain (Ramadori, Lee et al. 2008). SIRT1 protein levels are modulated by nutrient status, since fasting increased the hypothalamic levels of SIRT1, and this change was blunted in the hypothalamus of leptin deficient mice (Ramadori, Lee et al. 2008). Specifically, SIRT1 mRNA is expressed in pro-opiomelanocortin neurons, which are essential integrators of proper glucose homeostasis and body weight regulation (Ramadori, Lee et al. 2008). Consistent with this finding, several studies suggest that SIRT1 regulates food intake and body weight through the central melanocortin system of the brain (Dietrich et al., 2010) (Sasaki, Kim et al. ; Cakir, Perello et al. 2009). For instance, a decrease in hypothalamic SIRT1 signaling by pharmacological inhibition or by siRNA prevents FoxO1 deacetylation and downregulates food intake and body weight gain (Dietrich et al., 2010) (Cakir, Perello et al. 2009). Central administration of an orexigenic melanocortin receptor antagonist reversed the effects of SIRT1 inhibition (Cakir, Perello et al. 2009) (Dietrich et al., 2010), supporting the hypothesis that hypothalamic SIRT1 interacts with the central melanocortin system in a FoxO1 dependent-manner. During fasting, increased SIRT1 expression represses Foxo1 activity through increased deacetylation (Cakir, Perello et al. 2009). Increased SIRT1 expression also appears to activate S6K signaling (Cakir, Perello et al. 2009). Consistently, the overexpression of SIRT1 in the mediobasal hypothalamus rescues hyperphagia and body weight gain induced by constitutive nuclear Foxo1 expression and thereby, suppresses the expression of the orexigenic neuropeptide AgRP (Sasaki, Kim et al.).

In contrast to these findings, studies by Dietrich et al. suggest that pharmacological inhibition of brain SIRT1 decreased the activity of AgRP neurons and the inhibitory tone of POMC neurons (Dietrich, Antunes et al.). This inhibition of SIRT1 decreased food intake through the central melanocortin receptors in a UCP2 dependent manner (Dietrich, Antunes et al.). Moreover, pharmacological blockade of SIRT1 in the central nervous system prevents the orexigenic action of ghrelin (Dietrich el al., 2010) (Velasquez, Martinez et al.). Consistent with these pharmacological results, the selective disruption of SIRT1 in AgRP neurons in mice using the cre-lox approach blunted electric responses of Agrp neurons to ghrelin and decreased food intake (Dietrich, Antunes et al.). Also, the Agrp-Sirt1 KO mice displayed decrease fat mass and impaired metabolic response to fast (Dietrich et al., 2010).

There is also controversial data surrounding intracerebroventricular (ICV) infusion of the proposed SIRT1 activator resveratrol. Chronic ICV infusion of resveratrol

significantly decreased insulin resistance and normalized blood glucose levels in diet-induced obese and diabetic mice (Ramadori, Gautron et al. 2009). Interestingly, despite diminshed Iκ-Bα mRNA levels after icv resveratrol infusion, hypothalamic NF-κB signaling was augmented via deacetylation of RelA/p65 and total RelA/p65 protein (Ramadori, Gautron et al. 2009).

The mechanism/s behind these controversial effects has yet to be determined, but it is important to note that several studies suggest that resveratrol is not an activator of SIRT1, and therefore, the effects observed after central administration of resveratrol are not exerted through hypothalamic SIRT1. Also, the opposite results obtained after pharmacological inhibition of SIRT1 might be explained by the different animal backgrounds used or different methodology, however, these relevant aspects remain to be elucidated.

Additional studies have reported the effect of the lack of SIRT1 in the entire brain as well as in POMC neurons. Mice lacking SIRT1 in the brain showed defects in somatotropic signaling and in responding to caloric restriction (Cohen, Supinski et al. 2009). More specifically, brain SIRT1 specific ko mice are dwarfed and old mice are glucose intolerant and display altered caloric restriction responses (Cohen, Supinski et al. 2009). Another report investigating the lack of SIRT1 in POMC neurons found that these mice were heavier than their littermates and had more perigonadal fat due to lower energy expenditure (Ramadori, Fujikawa et al.). The deletion of SIRT1 in POMC neurons also abolished the capacity of leptin to activate phosphoinositol 3-kinase (PI3K) signaling in POMC neurons and altered BAT and perigonadal WAT metabolism (Ramadori, Fujikawa et al.).

In addition to genetic disruption of SIRT1 signaling in the central nervous system, the effect of overexpression of SIRT1 in the brain has been also studied. Elevated levels of SIRT1 in hypothalamic dorsomedial and lateral nucleus increased body temperature and physical activity in response to caloric restriction (Satoh, Brace et al.). In summary, central SIRT1 signaling seems to be a key mediator of energy metabolism and the physiological response to calorie restriction, however, the exact mechanisms of central SIRT1 action remain to be elucidated.

F. Roles of SIRT1 in other tissues involved in metabolic control

SIRT1 is expressed in a number of additional tissues that are important for metabolic control. For instance, SIRT1 is expressed in kidneys were it was shown to protect from oxidative injury (He, Wang et al.) and hypoxia (Kume, Uzu et al.), potentially via deacetylation and activaton of HIF-2 alpha (Dioum, Chen et al. 2009). SIRT1 is further expressed in a number of myeloid cells, where it can exert metabolic control. For instance, macrophage SIRT1 was shown to improve insulin sensitivity by attenuating inflammatory pathways (Yoshizaki, Schenk et al.). To date, nothing is known on the role of SIRT1 in metabolically relevant tissues such as the thyroid glands or the adrenals. In the intestine, SIRT1 is known to suppress intestinal tumorigenesis and colon cancer growth (Firestein, Blander et al. 2008), however, nothing is known yet on potential roles of intestinal SIRT1 in metabolic control.

VII. METABOLIC TISSUES TARGETED BY SIRT3

A. Roles of SIRT3 in liver metabolism

Gene and protein expression of SIRT3 in the liver were activated by fasting (Hirschey, Shimazu et al.) and decreased when the animals were fed high fat diet (HFD) (Bao, Scott et al. ; Kendrick, Choudhury et al.). HFD feeding in SIRT3 ko mice induced an increase in the acetylation of several hepatic proteins, suggesting that SIRT3 is a crucial regulator of hepatic mitochondrial function(Kendrick, Choudhury et al.). Mechanistic findings have shown that palmitate modulates oxygen consumption and ROS levels in hepatocytes in a SIRT3-dependent manner (Bao, Scott et al.). Palmitate increases oxygen consumption in hepatocytes, and the inhibition of SIRT3 abolished those actions (Bao, Scott et al.). Similar results were obtained in mice lacking SIRT3, as a palmitate test in these mice induced lipotoxicity in hepatocytes, whereas this effect was abrogated when SIRT3 levels were restored (Bao, Scott et al.). The relevance of SIRT3 in hepatic metabolism was also confirmed in another study showing that SIRT3 overexpression in hepatocytes decreases the accumulation of lipids (Shi, Fan et al.). This effect appeared to be mediated by the activation of AMPK and ACC (Shi, Fan et al.): when AMPK was inhibited by compound C, SIRT3 failed to decrease lipid accumulation (Shi, Fan et al.). In this line, another study demonstrated that SIRT3 induced fatty acid oxidation through the deacetylation of long chain acyl coenzyme A dehydrogenase (LCAD) and mice lacking SIRT3 showed lower fatty acid oxidation (Hirschey, Shimazu et al.). Very recently, it was further suggested that hepatic ketone body production is regulated by SIRT3; HMGCS2, the rate limiting enzyme in the synthesis of b-hydroxybutyrate, needs deacetylation to induce the physiological response to prolonged fasting (Shimazu, Hirschey et al.).

B. The roles of SIRT3 in skeletal muscle metabolism

Skeletal muscle plays an important role in the regulation of lipid metabolism, as lipid catabolism provides a high percentage of the energy usage for resting muscle. Similar to its regulation in the liver, SIRT3 levels are decreased in the muscle of mice fed HFD, whereas it is increased after fasting and caloric restriction (Palacios, Carmona et al. 2009). In addition to its regulation by nutritional status, muscle SIRT3 is also modulated by exercise, astrained mice showed higher SIRT3 levels when compared to non-exercised mice (Hokari, Kawasaki et al. ; Palacios, Carmona et al. 2009). Furthermore, the lack of SIRT3 inactivates AMPK and pCREB, leading to the inhibition of PGC-1α activity in muscle (Palacios, Carmona et al. 2009).

C. The roles of SIRT3 in adipose tissue function

SIRT3 has been detected at high levels in brown adipose tissue (BAT), while lower levels were found in white adipose tissue (Shi, Wang et al. 2005). In BAT, SIRT3 is activated by caloric restriction and cold exposure, and increased temperatures reverse the higher levels of SIRT3(Hirschey, Shimazu et al. ; Shi, Wang et al. 2005). Furthermore, constitutive expression of SIRT3 in brown adipocytes increases the expression of PGC-1α and UCP1, leading to higher thermogenesis and oxygen consumption (Shi, Wang et al. 2005).

VIII. GENETIC MODELS OF SIRT1 & SIRT3 UNRAVEL NEW ROLES IN METABOLIC CONTROL AND CIRCADIAN RHYTHMS

A. SIRT1 gain- and loss-of-function models and metabolic dysfunction.

1. Global SIRT1 deficiency affects metabolic control

Early studies of lower organisms lacking Sir2 demonstrated that Sir2 deficiency eliminates the life-extending effects of calorie restriction in yeast (Lin, Defossez et al. 2000) and decreases life span of flies (Astrom, Cline et al. 2003). In SIRT1 deficient mice, the results are somewhat controversial and different phenotypes have been found. Inbred SIRT1-null mice were born underweight and showed early postnatal lethality (McBurney, Yang et al. 2003). Specifically, SIRT1 knockouts died between E9.5 and E14.5 and exhibit problems with proper DNA repair and histone modulation (Wang, Sengupta et al. 2008). Accordingly, the lack of SIRT1 also produced important developmental defects of the retina and heart (Cheng, Mostoslavsky et al. 2003).Male (inbred) SIRT1-null mice were shown to be sterile, potentially due to reduced expression (and thus signaling) of hypothalamic gonadotropin-releasing hormone and luteinizing hormone (Kolthur-Seetharam, Teerds et al. 2009) and thus attenuated spermatogenesis (Coussens, Maresh et al. 2008). Nevertheless, approximately half the SIRT1-null mice on an outbred background survived past adulthood (McBurney, Yang et al. 2003). Outbred SIRT1-null mice were visibly smaller (25%) than their littermates at 2-4 months, and this difference peaked (40%) when the mice were 13-20 months-old (Boily, Seifert et al. 2008). The surviving mice have a characteristic defect in eyelid development rendering them sightless (McBurney, Yang et al. 2003). This body weight difference was not due to food intake, which was similar to that of wild-type mice; in fact, SIRT1-null mice were hyperphagic when food intake was normalized to body weight. However, these mice were hypermetabolic, contained inefficient liver mitochondria, and had elevated rates of lipid oxidation (Boily, Seifert et al. 2008).

When the caloric intake was restricted 40%, SIRT1 knockout mice did not show the increased physical activity as in wild type mice, and their metabolic rate was lower (Boily, Seifert et al. 2008). These findings are similar to those observed after 9 months of CR, showing that SIRT1 null mice failed to increase their physical activity, even though they performed better than wild type mice on an accelerationg treadmill or rotaroad (Chen, Steele et al. 2005). Importantly, calorie restriction did not extend the life span of SIRT1-null mice (Boily, Seifert et al. 2008). Notably, although mice lacking SIRT1 had reduced levels of markers of oxidative damage in the brain, the life span of these mice was shorter under both normal and caloric restricted conditions (Li, Xu et al. 2008). In mice, life span is often determined by the individuals and strain-specific susceptibility to develop tumors, and SIRT1 might increase life span by decreasing tumor rates. However, controversy also surrounds the functions of SIRT1 on tumorigenesis. While one study suggested that SIRT1-null mice developed tumors at an increased rate relative to wild-type mice (Wang, Sengupta et al. 2008), subsequent studies refuted that claim; SIRT1-null mice developed tumors at normal rates and

resveratrol treatment did not have a protective effect against tumorigenesis (Boily, He et al. 2009).

The complete lack of SIRT1 has differential metabolic effects on glucose homeostasis and lipid metabolism. Studies by Bordone et al. showed that SIRT1 deficiency seems to improve glucose homeostasis (Bordone, Motta et al. 2006). Global SIRT1-knockout mice demonstrated improved glucose tolerance with decreased levels of insulin and blood glucose (Bordone, Motta et al. 2006). SIRT1 suppressed the uncoupling protein 2 (UCP2), which inhibited insulin secretion. Accordingly,SIRT1 knockout mice showed high UCP2 expression (Bordone, Motta et al. 2006). It is possible, though, that an improvement in glucose homeostasis could be due simply to the reduced body weight, fat mass and size of the SIRT1-knockout mice. On the other hand, partial lack of SIRT1 (SIRT1 +/- mice) led to liver steatosis when mice were fed mediate-fat diet (Xu, Gao et al.). The steatosis was accompanied by an elevated liver/body ratio, liver size and hepatic lipid deposition (Xu, Gao et al.). Therefore, it seems that the disruption of SIRT1 activity may cause beneficial effects on glucose but it favors lipid deposition in the liver.

Li and colleagues determined that global SIRT1 deficiency also affects cholesterol regulation (Li, Zhang et al. 2007). The liver X receptors (LXRs) are important for cholesterol and triglyceride homeostasis (Li, Zhang et al. 2007). SIRT1-null mice demonstrated abnormal cholesterol homeostasis due to the decreased expression of LXR targets and, as a consequence, a reduction of reverse cholesterol transport as well as high-density lipoproteins (HDL) (Li, Zhang et al. 2007), but low-density lipoprotein (LDL) cholesterol was unchanged compared to wild-type mice (Li, Zhang et al. 2007).

2. Liver-specific SIRT1 knockdown affects metabolic control

The metabolic consequences of SIRT1 deficiency in liver-specific SIRT1-knockout mice are even more variable and disputed than those of global SIRT1-knockout mice. In 2007, Rodgers and Puigserver observed that hepatic SIRT1 knockdown in mice led to mild hypoglycemia, decreased glucose production, increased insulin sensitivity, decreased blood cholesterol levels, and increased levels of cholesterol and free fatty acids in the liver during fasting (Rodgers and Puigserver 2007). These results were consistent with SIRT1 regulation of gluconeogenesis, cholesterol homeostasis and free fatty acid oxidation in the liver (Rodgers and Puigserver 2007). Most of these results were observed only under fasting conditions (Rodgers and Puigserver 2007), and the over-expression of SIRT1 reversed many of these changes. However, another study suggests that SIRT1 knockdown in the liver may be beneficial in a rat model of type II diabetes (Erion, Yonemitsu et al. 2009). The knockdown of SIRT1in those rats improved insulin sensitivity, lowered fasting glucose levels, decreased hepatic glucose production and decreased plasma total cholesterol levels (Erion, Yonemitsu et al. 2009).

Studies in liver-specific SIRT1-knockout mice on a high-calorie ‘western’ diet suggested that these mice had at least some protectionfrom accumulating fat, as compared with wild-type mice. In contrast, while under calorie restriction, the liver-specific knockout mice displayed the same phenotype as wild-type mice. These observations suggested that hepatic SIRT1 may be inactivated during calorie restriction

in normal mice and activated while on a high-calorie diet (Chen, Bruno et al. 2008). As discussed before, these results are in direct contrast to the dogma that calorie restriction universally increases SIRT1 activity, and new questions are brought to light concerning the unique role of hepatic SIRT1(Chen, Bruno et al. 2008). Contradicting the above findings, a 2009 study by Purushotham et al. suggested that hepatic SIRT1 knockout was harmful for mice that were challenged with a high-fat diet (Purushotham, Schug et al. 2009). These mice developed many metabolic problems including liver steatosis, hepatic inflammation and endoplasmic reticulum stress (Purushotham, Schug et al. 2009).

Overall, based on the existing evidence collected in SIRT1-null mice, it is difficult to conclude on the precise role of hepatic SIRT1 in regulating glucose, cholesterol and lipid metablism. Factors like species differences, methodological differences (viral knockdown vs. germline mutation), the overall problem of genetic background (inbred vs. outbred), and the compromised health of SIRT1-null mice make it hard to evaluate the role of hepatic SIRT1.

3. Beneficial effects of global SIRT1 overexpression on systemic metabolism

As happened with global SIRT1 deletion, the overexpression of SIRT1 in mice also showed different results regarding their body weight or their feeding behavior. However, most studies show compelling evidence that SIRT1 overexpression offers substantial benefits on serum cholesterol and insulin levels, and increased resistance to high-fat diet induced glucose intolerance and insulin resistance (Bordone, Cohen et al. 2007; Banks, Kon et al. 2008; Pfluger, Herranz et al. 2008). Mice over-expressing SIRT1 under the control of a beta-actin promoter were leaner and more metabolically active than their standard-diet fed littermates. In addition, they had lower cholesterol, insulin and fasting glucose levels and improved glucose tolerance (Bordone, Cohen et al. 2007). Furthermore, these transgenic mice performed better on a rotarod assay (Bordone, Cohen et al. 2007). All these characteristics resembled the phenotype showed by mice under CR. However, subsequent studies in mice that over-expressed SIRT1 under its own promotor showed slightly different results (Banks, Kon et al. 2008; Pfluger, Herranz et al. 2008). Banks et al. showed that on a standard diet SIRT1 transgenic mice had normal insulin sensitivity but decreased food intake and locomotor activity, resulting in decreased energy expenditure but normal body weight (Banks, Kon et al. 2008). Concommitant overexpression of SIRT1 in environmental and genetic models of insulin resistance and diabetes improved glucose tolerance due to decreased hepatic glucose production and increased adiponectin levels, however, body weight and body composition remained unchanged (Banks, Kon et al. 2008). Accordingly, SIRT1 overexpression did not protect mice from high-fat diet induced obesity (Banks, Kon et al. 2008). Pfluger et al. also failed to find a protection from diet-induced obesity in diet-induced obese mice (Pfluger, Herranz et al. 2008). However, contrary to previous studies, SIRT1 transgenic mice displayed higher energy expenditure, which was compensated by a parallel increase in food intake (Pfluger, Herranz et al. 2008). Nevertheless, in agreement with previous studies, high-fat diet fed SIRT1overexpressor mice displayed lower lipid-induced inflammation along with better glucose tolerance, and were protected from hepatic steatosis (Pfluger, Herranz et al. 2008). The mechanisms modulating these actions involved the induction of antioxidant proteins

MnSOD and Nrf1, possibly via stimulation of PGC-1α, and a lower activation of proinflammatory cytokines, such as TNFalpha and IL-6, via down-modulation of NFκB activity (Pfluger, Herranz et al. 2008).

4. Pancreatic beta cell-specific SIRT1 overexpression improves glucose homeostasis

In RINm5F cells or isolated rat islets, the pharmacological stimulation and ectopic expression of SIRT1completely prevented cytokine-mediated cytotoxicity, indicating that SIRT1 participates in the maintenance of normal insulin-secreting responses to glucose in isolated rat islets (Lee, Song et al. 2009). In addition, SIRT1 positively regulated insulin secretion in pancreatic beta cells by repressing UCP2 (Bordone, Motta et al. 2006). These results were later corroborated in mice with genetic manipulation of SIRT1 in the pancreas. For instance, the Imai laboratory has studied beta cell-specific SIRT1-overexpressing (BESTO) transgenic mice over the past few years (Moynihan, Grimm et al. 2005; Ramsey, Mills et al. 2008). In these mice, the higher dosage of SIRT1 potentiated glucose-stimulated insulin secretion and improved glucose tolerance (Moynihan, Grimm et al. 2005), potentially via SIRT1-mediated inhibition of uncoupling protein 2 (UCP2) (Moynihan, Grimm et al. 2005). However, when BESTO mice were ageing to 18-24 months, this beneficial glucose-stimulated insulin secretion was lost (Ramsey, Mills et al. 2008).

B. SIRT3 gain- and loss-of-function models and mitochondrial function.

Mice deficient in SIRT3 were viable and did not show any metabolic disorder. They had normal body weight, body composition, oxygen consumption, respiratory quotient and physical activity (Lombard, Alt et al. 2007). They also responded normally to food deprivation, and adaptive thermogenesis was not altered (Lombard, Alt et al. 2007). However, the lack of SIRT3 induced global mitochondrial lysine acetylation through the maintenance of basal ATP levels (Kim, Patel et al. ; Lombard, Alt et al. 2007; Ahn, Kim et al. 2008). Another important effect of the global deficiency of SIRT3 was that these mice had increased stress-induced superoxide levels and genomic instability, leading to a tumour-permissive phenotype (Kim, Patel et al.). Prolonged SIRT3 expression in the mitochondria of murine adipocytes potentiates cellular respiration, lowered membrane potential, and attenuated reactive oxygen species production (Shi, Wang et al. 2005).

In addition to modulating metabolism, SIRT3 controls mitochondrial membrane potential by deacetylating and inhibiting the regulatory component of the mPTP, cyclophilin D (CypD) (Hafner, Dai et al.). Cardiac myocytes from mice lacking SIRT3 experience an age-dependent increase in mPTP opening and accelerated signs of aging in the heart, known phenotypes of excessive mPTP opening. Knockout mice experience cardiac hypertrophy and fibrosis at 13 months of age and are also sensitive to transverse aortic constriction (TAC), as evidenced by cardiac hypertrophy, fibrosis, and increased mortality. Together, these findings in the mouse knockout show that SIRT3 is critical for delaying mitochondrial dysfunction during aging.

.

C. SIRT1 AND THE MOLECULAR CLOCK

Animals are capable of maintaining an autonomous rhythm that closely resembles the 24-hour daily cycle, even in constant light conditions (Szymanski 1918). This autonomous circadian oscillation is connected to body's metabolism, and alterations in the circadian cycle can have enormous impact on metabolism. The master clock of mammals is located in the suprachiasmatic nucleus (SCN) of the basal hypothalamus (Weaver 1998). Lesion of the SCN abolished the cyclic nature of locomotor activity in rodents (Moore and Eichler 1972; Stephan and Zucker 1972; Ibuka and Kawamura 1975; Stetson and Watson-Whitmyre 1976; Ibuka, Inouye et al. 1977; Ibuka, Nihonmatsu et al. 1980). However, transplantation of SCN grafts to the lesioned SCN could restore the oscillatory behavior in lesioned animals (Ralph, Foster et al. 1990; Ralph and Hurd 1996; Silver, LeSauter et al. 1996). The nature of the oscillatory behavior of the transplanted graft was located intracellularly, as evidenced by the fact that when neurons from the SCN are dissociated in cell culture their oscillatory (circadian) activity is maintained for many days. Even though the SCN maintains the body's circadian rhythm, several other tissues maintain an independent oscillatory rhythm, which in most cases resembles the 24-hour light-dark cycle. In contrast to the SCN, where the light is the main circadian regulatory input, cellular energy metabolism (feeding) serves as a potent synchronizer of oscillations in peripheral tissues (and other brain nuclei).

Recently, NAD^+ has been shown to have a circadian rhythm in mammalian cells that is due to the salvage pathway (a two-step reaction that converts nicotinamidetonicotinamide mononucleotide (NMN) to NAD^+) (Magni, Amici et al. 1999; Nakahata, Sahar et al. 2009; Ramsey, Yoshino et al. 2009). The two enzymes responsible for catalyzing these reactions arenicotinamidephophoribosyltransferase (NAMPT) and NMN adenylytransferases (NMNAT).(Emanuelli, Carnevali et al. 2001; Revollo, Grimm et al. 2004). What makes this scenario interesting for the understanding of sirtuins' physiology is that SIRT1 utilizes NAD^+ in its biochemical reaction to generate nicotinamide. Thus, NAMPT, NMNAT and SIRT1 close a loop in a biochemical cascade from nicotinamide down to NMN,NAD^+ and finally nicotinamide (Nakahata, Sahar et al. 2009; Ramsey, Yoshino et al. 2009).

It is intuitive to hypothesize that if NAD^+ fluctuates according to the circadian cycle, then SIRT1 activity should vary as well, because it is linked to NAD^+ levels. Several reports shed light on these mechanisms, showing that SIRT1 interacts with CLOCK to generate a protein complex (SIRT1-CLOCK). CLOCK is a protein that was discovered by Takahashi's group in 1994 and is the main regulator of the autonomous circadian rhythm in cells (62). CLOCK is a transcription factor from the group of bHLH (basic helix-loop-helix) that dimerizes with BMAL1 to regulate the transcription of several circadian genes (e.g., Cryptochrome and Period genes) (17, 26, 51). Accumulation of the transcripts (Cry and Per) lead them to complex with CLOCK-BMAL1, silencing the transcription of circadian genes (31, 61, 69). Interestingly, CLOCK is a histone acetyltransferase (HAT) (13) that directly acetylates histone H3 and its partner BMAL1. These acetylation reactions are essential for the binding and regulation of the transcription of the circadian genes (39). Moreover, when Per2 binds to the CLOCK-BMAL1 complex, it is also acetylated (2). SIRT1 was shown to bind to the CLOCK complex and exert its deacetylase activity leading to degradation of the complex and inactivation of circadian gene transcription (2, 39). Thus, SIRT1 deacetylase activity affects the CLOCK complex by regulating acetyl residues and consequently driving

degradation of the complex. Additionally, the CLOCK-BMAL1 complex was shown to bind to the Nampt promoter and up-regulates NAMPT expression (40, 47). Increases in NAMPT levels contribute to enhance the levels of NAD^+, which in turn activates SIRT1. SIRT1 in turn deacetylates the CLOCK complex and releases it from the DNA, decreasing the transcription of NAMPT. With less NAMPT, levels of NAD+ decrease, and consequently, SIRT1 activity. This NAMPT-SIRT1 loop acts to fine-tune the circadian oscillation of the CLOCK-BMAL1 complex, linking metabolism variances to the circadian rhythm (40, 47). The data described here was found in mammalian cells and in peripheral tissues (liver). A brain correlate in the SCN has not been described, but the widespread expression of SIRT1 in most (if not all) cells suggest that this pathway may occur in several other systems. However, NAMPT is thought to be not expressed in the brain tissue (48), or at least, in very small quantities. Specific groups of neurons could express NAMPT and be able to utilize this cycle to regulate their clock rhythmicity. Thus, the heterogeneity of the brain tissue, and the very low (if any) levels of NAMPT in the brain necessitate further research to understand how metabolic oscillations signal to neurons, mainly in SCN.

Absence of SIRT1 lead to dysregulation of circadian rhythms (Wijnen 2009). Dysregulation of circadian rhythms lead to metabolic dysfunction and correlates with obesity as well as other metabolic problems (Turek, Joshu et al. 2005). Thus, a relationship may exist among SIRT1, circadian rhythms, NAD^+ and metabolic dysfunction.

D. SIRT1 AND DIABETES-INDUCED CARDIAC DYSFUNCTION

SIRT1 conferred cardioprotection in the heart (Alcendor, Kirshenbaum et al. 2004; Pillai, Isbatan et al. 2005; Alcendor, Gao et al. 2007) during oxidative stress (Pillai, Gupta et al. 2006). Resveratrol, a proposed SIRT1 activator (reviewed in XIII), prevented hypoxia-induced apoptosis in cardiomyocytes through SIRT1-mediated Foxo1 regulation (Chen, Yu et al. 2009). SIRT1-mediated cardiac benefits occured when SIRT1 expression levels were low to moderate; in contrast, high doses of SIRT1exacerbated oxidative stress and induced cardiomyopathy (Alcendor, Gao et al. 2007).

Hyperglycemia during diabetes can cause significant cardiac deterioration and dysfunction. Recent studies have demonstrated that diabetes-induced cardiac dysfunction may be alleviated through activation of the SIRT1 pathway (Dong and Ren 2007; Vahtola, Louhelainen et al. 2008; Sulaiman, Matta et al. 2009). SIRT1 regulated angiogenic activity in endothelial cells by deacetylating and inhibiting the forkhead transcription factor Foxo1 (Potente, Ghaeni et al. 2007), which is a negative regulator of angiogenesis (ref). In the diabetic state, repression of Foxo1 activity causes endothelial dysfunction and diminished angiogenesis. A study by Balestrieri et al. proposed that SIRT1 is an important regulator of EPC dysfunction in a high-glucose environment (Balestrieri, Rienzo et al. 2008). When EPCs were exposed to a high glucose environment, downregulation of EPC activity correlated with reduced SIRT1 expression and elevated acetyl-Foxo1 expression (Balestrieri, Rienzo et al. 2008). In addition to these effects on EPCs, SIRT1 has been implicated in cardiac dysfunction. Cardiac dysfunction in diabetic cardiomyopathy reduced sarcoplasmic calcium ATPase

(SERCA2a) expression levels. Sulaiman et al. showed that activation of SIRT1 by resveratrol increased levels of SERCA2a mRNA and improved cardiac function in mice injected with streptozotocin, a chemical used to model Type I diabetes in animals (Sulaiman, Matta et al. 2009).

According to Orimo et al., the mechanism of SIRT1's beneficial action was through p53 regulation (Orimo, Minamino et al. 2009). The authors describe that hyperglycemia induced vascular senescence unless SIRT1 was introduced or p53 was removed; activation of SIRT1 by resveratrol lessened the extent of vascular dysfunction in diabetic mice, specifically through the SIRT1-p53 pathway (Orimo, Minamino et al. 2009).

IX. GENETIC POLYMORPHISMS OF SIRT1 AND SIRT3 IN HUMANS

A. Genetic polymorphisms of SIRT1

Very little is known about the genetic variation of SIRT1 and its effects on energy homeostasis in humans and the data are somewhat confusing. Arecent report has examined the relation between variants in SIRT1 and obesity in 1,068 obese patients and 313 normal-weight control subjects (Peeters, Beckers et al. 2008). The authors found that males but not females with a SIRT1 single nucleotide polymorphism (SNP) were associated with increased visceral adiposity (Peeters, Beckers et al. 2008). A similar study using a large sample-size population of 6251 elderly subjects (population-based Rotterdam Study) found that there were two variants in SIRT1 that were associated with lower body mass index,decreased risk of obesity, and lower weight gain (Zillikens, van Meurs et al. 2009). In a smaller study using 389 patients with metabolic syndrome and 547 controls, a significant association between one SIRT1 SNP and metabolic syndrome was found (Cruz, Valladares-Salgado et al.). However, another study performed in 917 overweight individuals investigating the associations of SIRT1 SNPs with metabolic responsedid not find an association of SIRT1 SNPs with baseline BMI or with BMI change after 9 months follow-up (Weyrich, Machicao et al. 2008).

The genetic variation of SIRT1 and its effects on human longevity is also poorly studied. One report using DNA from 1573 long-lived individuals (centenarians and nonagenarians) found no evidence between the 5 SNPs analyzed and longevity (Flachsbart, Croucher et al. 2006). Similar findings were observed in another population-based Leiden85-plus Study of 1245 subjects (Kuningas, Putters et al. 2007). Therefore, it seems that SNPs for SIRT1 are not related with human longevity, but further studies using larger-size populations are needed to elucidate this issue.

B. Genetic polymorphisms of SIRT3

The knowledge about the potential role and genetic alterations of SIRT3 in humans is even lower than for SIRT1. SIRT3 is located at the telomeric terminal on 11p15.5 chromosome, and studies performed in people over 100 years have demonstrated that there is a correlation between longevity and polymorphism of four genes located in this region (De Luca, Rose et al. 2001). The researchers found a SNP marker in exon 3 of the SIRT3 gene, and there was a male-specific relationship between this marker and longevity (Rose, Dato et al. 2003). Another study using 640 individuals found two human SIRT3 SNPs and suggested that SIRT3 increased cellular respiration (Dransfeld, Alborzinia et al.). Another work assessed the association between SIRT3 not only with age, but also with endurance exercise (Lanza, Short et al. 2008). The results showed that the protein levels of SIRT3 in muscle were lower in old sedentary subjects when compared to young sedentary subjects (Lanza, Short et al. 2008). However, they failed to show any statistical difference between ages in endurance-trained individuals (Lanza, Short et al. 2008).

X. METABOLIC CONSEQUENCES OF PHARMACOLOGICAL SIRT1 ACTIVATION

A. Resveratrol – a specific SIRT1 activator?

Early studies showing the role of Sir2/SIRT1 in the mechanisms responsible for the effects of calorie restriction in prolonging lifespan (Kaeberlein, McVey et al. 1999; Lin, Defossez et al. 2000; Tissenbaum and Guarente 2001) raised the possibility that SIRT1 could be implicated in glucose metabolism and insulin sensitivity, key factors impaired during aging. Initial screening studies identified the polyphenol resveratrol as a potent activator of SIRT1(Howitz, Bitterman et al. 2003). Utilizing this chemical tool to stimulate SIRT1 activity in vivo, several groups reported benefits of resveratrol in models of metabolic disorders (Baur, Pearson et al. 2006; Lagouge, Argmann et al. 2006). Resveratrol administration was shown to protect against detrimental effects of high-fat diet exposure, such as glucose intolerance, insulin resistance or lifespan reduction, however, no beneficial effects on body weight could be observed (Baur, Pearson et al. 2006; Lagouge, Argmann et al. 2006; Ajmo, Liang et al. 2008), potentially through activation of SIRT1. However, other studies failed to show activation of SIRT1 by resveratrol (Kaeberlein, McDonagh et al. 2005; Pacholec, Chrunyk et al. 2010), and suggested that previous reports on a specific activation of SIRT1 by resveratrol could be due to an interaction between resveratrol and the fluorophore used in the assay (Kaeberlein, McDonagh et al. 2005; Pacholec, Chrunyk et al. 2010). This report was challenged by a subsequent report showing that the fluorphore is dispensible for SIRT1 activation to occur (Dai, Kustigian et al.). Instead, the authors suggest that the fluorphore mimics a bulky-hydrophobic amino acid in natural substrates Resveratrol has been shown to be a broad-spectrum indirect activator of several proteins, such as AMPK, an important enzyme for energy and glucose homeostasis (Baur, Pearson et al. 2006; Dasgupta and Milbrandt 2007; Park, Kim et al. 2007; Chan, Dolinsky et al. 2008; Hwang, Kwon et al. 2008; Shang, Chen et al. 2008; Um, Park et al. 2010). AMPK senses the levels of ATP in the cell milieu. Metformin, a well-known activator of AMPK, is widely used to treat type-2 diabetes. Several reports

showed that AMPK and SIRT1 share similar molecular pathways, and activation of SIRT1 by resveratrol could be a consequence of AMPK activation (Um, Park et al. 2010). Indeed, it was recently reported that the effects of resveratrol improving metabolic parameters in models of metabolic disorders are dependent on the expression of the AMPK subunit alpha (Um, Park et al. 2010). In this report, the authors tested the effects of resveratrol in AMPKα1 and AMPKα2 knockouts mice; resveratrol failed to improve insulin sensitive, glucose tolerance and mitochondria biogenesis in an AMPK-dependent manner, and failed to decrease fat mass. The authors also showed that resveratrol increased the NAD^+/NADH ratio, which is known to activate SIRT1 activity (Um, Park et al. 2010). This effect was also dependent on the expression of AMPK, thus shedding light on a possible indirect mechanism by which SIRT1 is activated by resveratrol through modulation of NAD^+/NADH levels via AMPK (Canto, Gerhart-Hines et al. 2009).

On the other hand, SIRT1 regulates LKB1, an upstream regulator of AMPK, (Zu, Liu et al. ; Hou, Xu et al. 2008). Thus the effects of resveratrol may be mediated by inhibtion of LKB1. Indeed, knockdown of LKB1 reduces the ability of resveratrol to protect cells from mitochondrial dysfunction (Shin, Cho et al. 2009). Clearly, the interplay between SIRT1 and AMPK is complex, is not possible to conclude whether resveratrol acts on AMPK independently of SIRT1. The testing of resveratrol in a SIRT1 knockout mouse would likely clarify this debate (for further review see (Haigis and Sinclair ; Canto and Auwerx 2009).

B. Natural SIRT1 activators

It is well known that nicotinamide adenine dinucleotides (NAD+ and NADH) are essential mediators of energy homeostasis (Berger, Ramirez-Hernandez et al. 2004). Consequently, increased intracellular levels of NAD+ activate sirtuin-dependent metabolic control. Thus, compounds that modulate NAD/NADH ratio are likely to also exert effects on SIRT1-medulated metabolic control. Indeed, β-lapachone, an o-naphthoquinoneextracted from bark of the lapacho tree (Tabebuiaavellanedae), has been shown to stimulate NADH oxidation through interaction with NADH: quinoneoxidoreductase 1 (NQO1); treatment of diet-induced obese and leptin-deficient ob/ob mice with β-lapachone markedly increased fatty acid oxidation and ameliorated the symptoms broadly summarized as metabolic syndrome, such as increased adiposity, glucose intolerance, dyslipidemnia and fatty liver (Hwang, Kim et al. 2009). Therefore, the pharmacological administration of β-lapachone mimics effects of SIRT1 activation/overexpression, and as a matter of fact, the treatment with β-lapachone increased SIRT1 mRNA expression in muscle and WAT (Hwang, Kim et al. 2009).

Kaempferol, a flavonoid with anti- and pro-oxidant activity present in various natural sources, was shown to activate SIRT3 in myelogenous leukemia cell line K562 and promyelocitic human leukemia U937 (Marfe, Tafani et al. 2009). Consistently, down-regulation of SIRT3 in these cell lines abolished the actions of Kaempferol (Marfe, Tafani et al. 2009). Since Kaempferol induced apoptosis, it seems possible that SIRT3 might play an important function in the mitochondrially-mediated apoptosis.

C. Novel synthetic SIRT1 activators improve metabolic control

After the discovery of resveratrol as a SIRT1 activator, several synthetic small molecule activators of SIRT1 were reported (Milne, Lambert et al. 2007). These molecules, 1000 times more potent than resveratrol but structurally distinct (Milne, Lambert et al. 2007), were shown to act through the same enzymatic mechanism, i.e. binding to an allosteric site exposed in the enzyme-substrate complex and thereby lowering the K_M of SIRT1 for its acetylated peptide substrates. Importantly, these molecules, unlike resveratrol, exhibited good oral bioavailability in rodents, and their administration substantially improved both glucose and insulin homeostasis in ob/ob mice, diet induced obese mice, and Zuckerfa/fa rats (Milne, Lambert et al. 2007). Consistent with these findings, the same researchers have shown that these activators recapitulate many of the molecular events downstream of CR in vivo, such as enhancing mitochondrial biogenesis, improving metabolic signaling pathways, and blunting pro-inflammatory pathways in mice fed a high fat, high calorie diet (Smith, Kenney et al. 2009). Similarly, an independent group treated mice with nonalcoholic fatty liver disease (NAFLD) with one of these activators named SRT1720, and found that the compound reduced the expression of lipogenic enzymes, the serum lipid profiles, the expressions of marker genes for oxidative stress and inflammatory cytokines in the liver of mice with NAFLD (Yamazaki, Usui et al. 2009). SRT1720 administration was further shown to enhance endurance and protect from diet-induced obesity and insulin resistance, potentially by enhancing oxidative metabolism in skeletal muscle, liver, and brown adipose tissue (Feige, Lagouge et al. 2008). *In vitro* studies using SRT1720 have shown that this drug increases insulin-stimulated glucose uptake in adipocytes (Yoshizaki, Milne et al. 2009).

However, a recent study attributed activation of SIRT1 to drug binding to the fluorphore, casting doubts on the specificity of these molecules (Pacholec, Bleasdale et al.). In contrast to the two independent studies, in vivo administration of SRT1720 was lethal to mice and failed to decrease plasma glucose or improve mitochondrial capacity in mice fed a high fat diet, though insulin levels were decreased (Pacholec, Bleasdale et al.). This report concludes that these synthetic activators, as well as resveratrol, exhibit multiple off-target activities against receptors, enzymes, transporters, and ion channels and therefore, are not direct activators of SIRT1 (Pacholec, Bleasdale et al.). Since this report, activation of SIRT1 has been shown to occur on natural peptides and that the enzyme kinetics for activation by SRT1720 and other small molecules are consistent with an allosteric activation mechanism (Dai, Kustigian et al.).

XI. FUTURE PERSPECTIVES

Decades of biomedical progress and the vast improvements in our living conditions allow us to lead productive lives into old age. At the same time, however, we have to face unprecedented negative impacts of our Western lifestyle, resulting in the rapid rise in obesity and its co-morbidities diabetes and fatty liver disease. Although major efforts are being made to attenuate such negative impacts of our Western lifestyle on obesity and its sequelae, to date there are no efficient pharmacological treatment options for weight control available, and surgical options such as bariatric surgeries, albeit being

highly efficient, may not (yet) be feasible for large proportions of the affected population. In addition, although changes in life style may hold the greatest promise to avoid obesity and metabolic disorders for a majority of us, dietary regiments such as calorie restriction and exercise have repeatedly been shown to not lead to adequate weight loss if not continued with highest perseverance and diligence. Furthermore, drugs that can mimic caloric restriction hold the promise of being able to prevent and treat numerous other diseases such as cancer and heart disease.

Although pharmacological or genetic activation of sirtuins, and particularly SIRT1, resembles the beneficial effects of caloric restriction, making them attractive drug, we should not forget that sirtuins act on many different transcription factors which are involved in numerous biological activities. Clinical trials will be necessary to address if SIRT1 analogs have beneficial effects in obese and/or diabetic patients.
SIRT3 is still a largely unexplored drug target. Although there are promising *in vitro* studies over-expressing SIRT3, to our knowledge, there are no specific SIRT3 activators available, and its potential pharmacological actions *in vivo* remain completely unknown. Again, SIRT3 targets a range of molecules with many different actions, so the issue regarding the specificity of SIRT3 activators is very similar to SIRT1.

One can bet without any risk that new targets modulated by SIRT1 and SIRT3 will appear in the near future, and some of those targets will be important for several metabolic actions. To precisely dissect the molecular pathways modulating sirtuins is a crucial step in elucidating the real potential of these deacetylases, and will require years of investigation. With the information obtained on sirtuins to date, it seems that this big challenge deserves to be weighed out, and we will certainly enjoy more exciting studies on this topic during the next years.

XII. REFERENCES

Abdelmohsen, K., R. Pullmann, Jr., et al. (2007). "Phosphorylation of HuR by Chk2 regulates SIRT1 expression." Mol Cell **25**(4): 543-57.

Accili, D. and K. C. Arden (2004). "FoxOs at the crossroads of cellular metabolism, differentiation, and transformation." Cell **117**(4): 421-6.

Afshar, G. and J. P. Murnane (1999). "Characterization of a human gene with sequence homology to Saccharomyces cerevisiae SIR2." Gene **234**(1): 161-8.

Aguilaniu, H., L. Gustafsson, et al. (2003). "Asymmetric inheritance of oxidatively damaged proteins during cytokinesis." Science **299**(5613): 1751-3.

Ahn, B. H., H. S. Kim, et al. (2008). "A role for the mitochondrial deacetylase Sirt3 in regulating energy homeostasis." Proc Natl Acad Sci U S A **105**(38): 14447-52.

Ajmo, J. M., X. Liang, et al. (2008). "Resveratrol alleviates alcoholic fatty liver in mice." Am J Physiol Gastrointest Liver Physiol **295**(4): G833-42.

Al-Regaiey, K. A., M. M. Masternak, et al. (2005). "Long-lived growth hormone receptor knockout mice: interaction of reduced insulin-like growth factor i/insulin signaling and caloric restriction." Endocrinology **146**(2): 851-60.

Alcendor, R. R., S. Gao, et al. (2007). "Sirt1 regulates aging and resistance to oxidative stress in the heart." Circ Res **100**(10): 1512-21.

Alcendor, R. R., L. A. Kirshenbaum, et al. (2004). "Silent information regulator 2alpha, a longevity factor and class III histone deacetylase, is an essential endogenous apoptosis inhibitor in cardiac myocytes." Circ Res **95**(10): 971-80.

Amat, R., A. Planavila, et al. (2009). "SIRT1 controls the transcription of the peroxisome proliferator-activated receptor-gamma Co-activator-1alpha (PGC-1alpha) gene in skeletal muscle through the PGC-1alpha autoregulatory loop and interaction with MyoD." J Biol Chem **284**(33): 21872-80.

Amat, R., G. Solanes, et al. (2007). "SIRT1 is involved in glucocorticoid-mediated control of uncoupling protein-3 gene transcription." J Biol Chem **282**(47): 34066-76.

Anderson, R. M., K. J. Bitterman, et al. (2002). "Manipulation of a nuclear NAD+ salvage pathway delays aging without altering steady-state NAD+ levels." J Biol Chem **277**(21): 18881-90.

Anderson, R. M., K. J. Bitterman, et al. (2003). "Nicotinamide and PNC1 govern lifespan extension by calorie restriction in Saccharomyces cerevisiae." Nature **423**(6936): 181-5.

Andrews, Z. B. "Uncoupling protein-2 and the potential link between metabolism and longevity." Curr Aging Sci **3**(2): 102-12.

Anekonda, T. S. and G. Adamus (2008). "Resveratrol prevents antibody-induced apoptotic death of retinal cells through upregulation of Sirt1 and Ku70." BMC Res Notes **1**: 122.

Araki, T., Y. Sasaki, et al. (2004). "Increased nuclear NAD biosynthesis and SIRT1 activation prevent axonal degeneration." Science **305**(5686): 1010-3.

Astrom, S. U., T. W. Cline, et al. (2003). "The Drosophila melanogaster sir2+ gene is nonessential and has only minor effects on position-effect variegation." Genetics **163**(3): 931-7.

Attie, A. D. (2007). "ABCA1: at the nexus of cholesterol, HDL and atherosclerosis." Trends Biochem Sci **32**(4): 172-9.

Avalos, J. L., I. Celic, et al. (2002). "Structure of a Sir2 enzyme bound to an acetylated p53 peptide." Mol Cell **10**(3): 523-35.

Ayala, J. E., R. S. Streeper, et al. (1999). "Conservation of an insulin response unit between mouse and human glucose-6-phosphatase catalytic subunit gene promoters: transcription factor FKHR binds the insulin response sequence." Diabetes **48**(9): 1885-9.

Bai, L., W. J. Pang, et al. (2008). "Modulation of Sirt1 by resveratrol and nicotinamide alters proliferation and differentiation of pig preadipocytes." Mol Cell Biochem **307**(1-2): 129-40.

Bakker, B. M., K. M. Overkamp, et al. (2001). "Stoichiometry and compartmentation of NADH metabolism in Saccharomyces cerevisiae." FEMS Microbiol Rev **25**(1): 15-37.

Balestrieri, M. L., M. Rienzo, et al. (2008). "High glucose downregulates endothelial progenitor cell number via SIRT1." Biochim Biophys Acta **1784**(6): 936-45.

Bamps, S., J. Wirtz, et al. (2009). "The Caenorhabditis elegans sirtuin gene, sir-2.1, is widely expressed and induced upon caloric restriction." Mech Ageing Dev **130**(11-12): 762-70.

Banks, A. S., N. Kon, et al. (2008). "SirT1 gain of function increases energy efficiency and prevents diabetes in mice." Cell Metab **8**(4): 333-41.

Bao, J., Z. Lu, et al. "Characterization of the murine SIRT3 mitochondrial localization sequence and comparison of mitochondrial enrichment and deacetylase activity of long and short SIRT3 isoforms." J Cell Biochem **110**(1): 238-47.

Bao, J., I. Scott, et al. "SIRT3 is regulated by nutrient excess and modulates hepatic susceptibility to lipotoxicity." Free Radic Biol Med **49**(7): 1230-7.

Barlow, A. L., C. M. van Drunen, et al. (2001). "dSIR2 and dHDAC6: two novel, inhibitor-resistant deacetylases in Drosophila melanogaster." Exp Cell Res **265**(1): 90-103.

Barthel, A., D. Schmoll, et al. (2005). "FoxO proteins in insulin action and metabolism." Trends Endocrinol Metab **16**(4): 183-9.

Baur, J. A., K. J. Pearson, et al. (2006). "Resveratrol improves health and survival of mice on a high-calorie diet." Nature **444**(7117): 337-42.

Berg, B. N. and H. S. Simms (1960). "Nutrition and longevity in the rat. II. Longevity and onset of disease with different levels of food intake." J Nutr **71**: 255-63.

Berger, F., M. H. Ramirez-Hernandez, et al. (2004). "The new life of a centenarian: signalling functions of NAD(P)." Trends Biochem Sci **29**(3): 111-8.

Bertrand, H. A., F. T. Lynd, et al. (1980). "Changes in adipose mass and cellularity through the adult life of rats fed ad libitum or a life-prolonging restricted diet." J Gerontol **35**(6): 827-35.

Bishop, N. A., T. Lu, et al. "Neural mechanisms of ageing and cognitive decline." Nature **464**(7288): 529-35.

Bitterman, K. J., R. M. Anderson, et al. (2002). "Inhibition of silencing and accelerated aging by nicotinamide, a putative negative regulator of yeast sir2 and human SIRT1." J Biol Chem **277**(47): 45099-107.

Blander, G., J. Olejnik, et al. (2005). "SIRT1 shows no substrate specificity in vitro." J Biol Chem **280**(11): 9780-5.

Boily, G., X. H. He, et al. (2009). "SirT1-null mice develop tumors at normal rates but are poorly protected by resveratrol." Oncogene **28**(32): 2882-93.

Boily, G., E. L. Seifert, et al. (2008). "SirT1 regulates energy metabolism and response to caloric restriction in mice." PLoS One **3**(3): e1759.

Bordone, L., D. Cohen, et al. (2007). "SIRT1 transgenic mice show phenotypes resembling calorie restriction." Aging Cell **6**(6): 759-67.

Bordone, L., M. C. Motta, et al. (2006). "Sirt1 regulates insulin secretion by repressing UCP2 in pancreatic beta cells." PLoS Biol **4**(2): e31.
Borra, M. T., M. R. Langer, et al. (2004). "Substrate specificity and kinetic mechanism of the Sir2 family of NAD+-dependent histone/protein deacetylases." Biochemistry **43**(30): 9877-87.
Boulton, S. J. and S. P. Jackson (1998). "Components of the Ku-dependent non-homologous end-joining pathway are involved in telomeric length maintenance and telomeric silencing." Embo J **17**(6): 1819-28.
Bouras, T., M. Fu, et al. (2005). "SIRT1 deacetylation and repression of p300 involves lysine residues 1020/1024 within the cell cycle regulatory domain 1." J Biol Chem **280**(11): 10264-76.
Brachmann, C. B., J. M. Sherman, et al. (1995). "The SIR2 gene family, conserved from bacteria to humans, functions in silencing, cell cycle progression, and chromosome stability." Genes Dev **9**(23): 2888-902.
Breen, D. M., T. Sanli, et al. (2008). "Stimulation of muscle cell glucose uptake by resveratrol through sirtuins and AMPK." Biochem Biophys Res Commun **374**(1): 117-22.
Brooks, C. L. and W. Gu (2009). "How does SIRT1 affect metabolism, senescence and cancer?" Nat Rev Cancer **9**(2): 123-8.
Brunet, A., L. B. Sweeney, et al. (2004). "Stress-dependent regulation of FOXO transcription factors by the SIRT1 deacetylase." Science **303**(5666): 2011-5.
Cakir, I., M. Perello, et al. (2009). "Hypothalamic Sirt1 regulates food intake in a rodent model system." PLoS One **4**(12): e8322.
Canto, C. and J. Auwerx (2009). "PGC-1alpha, SIRT1 and AMPK, an energy sensing network that controls energy expenditure." Curr Opin Lipidol **20**(2): 98-105.
Canto, C., Z. Gerhart-Hines, et al. (2009). "AMPK regulates energy expenditure by modulating NAD+ metabolism and SIRT1 activity." Nature **458**(7241): 1056-60.
Carlsen, H., F. Haugen, et al. (2009). "Diet-induced obesity increases NF-kappaB signaling in reporter mice." Genes Nutr **4**(3): 215-22.
Cimen, H., M. J. Han, et al. "Regulation of succinate dehydrogenase activity by SIRT3 in mammalian mitochondria." Biochemistry **49**(2): 304-11.
Cohen, D. E., A. M. Supinski, et al. (2009). "Neuronal SIRT1 regulates endocrine and behavioral responses to calorie restriction." Genes Dev **23**(24): 2812-7.
Cohen, H., C. Miller, et al. (2004). "Calorie restriction promotes mammalian cell survival by inducing the SIRT1 deacetylase." Science **305**(5682): 390-2.
Cohen, H. Y., S. Lavu, et al. (2004). "Acetylation of the C terminus of Ku70 by CBP and PCAF controls Bax-mediated apoptosis." Mol Cell **13**(5): 627-38.
Cohen, H. Y., C. Miller, et al. (2004). "Calorie restriction promotes mammalian cell survival by inducing the SIRT1 deacetylase." Science **305**(5682): 390-2.
Cooper, H. M., J. Y. Huang, et al. (2009). "A new splice variant of the mouse SIRT3 gene encodes the mitochondrial precursor protein." PLoS One **4**(3): e4986.
Cooper, H. M. and J. N. Spelbrink (2008). "The human SIRT3 protein deacetylase is exclusively mitochondrial." Biochem J **411**(2): 279-85.
Cooper, T. M., R. J. Mockett, et al. (2004). "Effect of caloric restriction on life span of the housefly, Musca domestica." FASEB J **18**(13): 1591-3.
Coussens, M., J. G. Maresh, et al. (2008). "Sirt1 deficiency attenuates spermatogenesis and germ cell function." PLoS One **3**(2): e1571.

Cruz, M., A. Valladares-Salgado, et al. "Candidate gene association study conditioning on individual ancestry in patients with type 2 diabetes and metabolic syndrome from Mexico City." Diabetes Metab Res Rev **26**(4): 261-70.

Chan, A. Y., V. W. Dolinsky, et al. (2008). "Resveratrol inhibits cardiac hypertrophy via AMP-activated protein kinase and Akt." J Biol Chem **283**(35): 24194-201.

Chanda, D., Y. B. Xie, et al. "Transcriptional corepressor SHP recruits SIRT1 histone deacetylase to inhibit LRH-1 transactivation." Nucleic Acids Res **38**(14): 4607-19.

Chang, J. H., H. C. Kim, et al. (2002). "Structural basis for the NAD-dependent deacetylase mechanism of Sir2." J Biol Chem **277**(37): 34489-98.

Chen, C. J., W. Yu, et al. (2009). "Resveratrol protects cardiomyocytes from hypoxia-induced apoptosis through the SIRT1-FoxO1 pathway." Biochem Biophys Res Commun **378**(3): 389-93.

Chen, D., J. Bruno, et al. (2008). "Tissue-specific regulation of SIRT1 by calorie restriction." Genes Dev **22**(13): 1753-7.

Chen, D., A. D. Steele, et al. (2005). "Increase in activity during calorie restriction requires Sirt1." Science **310**(5754): 1641.

Chen, W. Y., D. H. Wang, et al. (2005). "Tumor suppressor HIC1 directly regulates SIRT1 to modulate p53-dependent DNA-damage responses." Cell **123**(3): 437-48.

Chen, X. J. and G. D. Clark-Walker (1994). "sir2 mutants of Kluyveromyces lactis are hypersensitive to DNA-targeting drugs." Mol Cell Biol **14**(7): 4501-8.

Cheng, H. L., R. Mostoslavsky, et al. (2003). "Developmental defects and p53 hyperacetylation in Sir2 homolog (SIRT1)-deficient mice." Proc Natl Acad Sci U S A **100**(19): 10794-9.

Dai, H., L. Kustigian, et al. "SIRT1 activation by small molecules - kinetic and biophysical evidence for direct interaction of enzyme and activator." J Biol Chem.

Dai, J. M., Z. Y. Wang, et al. (2007). "SIRT1 interacts with p73 and suppresses p73-dependent transcriptional activity." J Cell Physiol **210**(1): 161-6.

Daitoku, H., M. Hatta, et al. (2004). "Silent information regulator 2 potentiates Foxo1-mediated transcription through its deacetylase activity." Proc Natl Acad Sci U S A **101**(27): 10042-7.

Dansen, T. B. and B. M. Burgering (2008). "Unravelling the tumor-suppressive functions of FOXO proteins." Trends Cell Biol **18**(9): 421-9.

Dasgupta, B. and J. Milbrandt (2007). "Resveratrol stimulates AMP kinase activity in neurons." Proc Natl Acad Sci U S A **104**(17): 7217-22.

De Luca, M., G. Rose, et al. (2001). "Sex-specific longevity associations defined by Tyrosine Hydroxylase-Insulin-Insulin Growth Factor 2 haplotypes on the 11p15.5 chromosomal region." Exp Gerontol **36**(10): 1663-71.

Derbyshire, M. K., K. G. Weinstock, et al. (1996). "HST1, a new member of the SIR2 family of genes." Yeast **12**(7): 631-40.

Dietrich, M. O., C. Antunes, et al. "Agrp neurons mediate Sirt1's action on the melanocortin system and energy balance: roles for Sirt1 in neuronal firing and synaptic plasticity." J Neurosci **30**(35): 11815-25.

Dioum, E. M., R. Chen, et al. (2009). "Regulation of hypoxia-inducible factor 2alpha signaling by the stress-responsive deacetylase sirtuin 1." Science **324**(5932): 1289-93.

Dong, F. and J. Ren (2007). "Fidarestat improves cardiomyocyte contractile function in db/db diabetic obese mice through a histone deacetylase Sir2-dependent mechanism." J Hypertens **25**(10): 2138-47.

Dransfeld, C. L., H. Alborzinia, et al. "SIRT3 SNPs validation in 640 individuals, functional analyses and new insights into SIRT3 stability." Int J Oncol **36**(4): 955-60.

Draznin, B. (2006). "Molecular mechanisms of insulin resistance: serine phosphorylation of insulin receptor substrate-1 and increased expression of p85alpha: the two sides of a coin." Diabetes **55**(8): 2392-7.

Elchebly, M., P. Payette, et al. (1999). "Increased insulin sensitivity and obesity resistance in mice lacking the protein tyrosine phosphatase-1B gene." Science **283**(5407): 1544-8.

Emanuelli, M., F. Carnevali, et al. (2001). "Molecular cloning, chromosomal localization, tissue mRNA levels, bacterial expression, and enzymatic properties of human NMN adenylyltransferase." J Biol Chem **276**(1): 406-12.

Erion, D. M., S. Yonemitsu, et al. (2009). "SirT1 knockdown in liver decreases basal hepatic glucose production and increases hepatic insulin responsiveness in diabetic rats." Proc Natl Acad Sci U S A **106**(27): 11288-93.

Fabrizio, P., C. Gattazzo, et al. (2005). "Sir2 blocks extreme life-span extension." Cell **123**(4): 655-67.

Fahie, K., P. Hu, et al. (2009). "Side chain specificity of ADP-ribosylation by a sirtuin." FEBS J **276**(23): 7159-76.

Feige, J. N., M. Lagouge, et al. (2008). "Specific SIRT1 activation mimics low energy levels and protects against diet-induced metabolic disorders by enhancing fat oxidation." Cell Metab **8**(5): 347-58.

Finnin, M. S., J. R. Donigian, et al. (2001). "Structure of the histone deacetylase SIRT2." Nat Struct Biol **8**(7): 621-5.

Firestein, R., G. Blander, et al. (2008). "The SIRT1 deacetylase suppresses intestinal tumorigenesis and colon cancer growth." PLoS One **3**(4): e2020.

Flachsbart, F., P. J. Croucher, et al. (2006). "Sirtuin 1 (SIRT1) sequence variation is not associated with exceptional human longevity." Exp Gerontol **41**(1): 98-102.

Ford, J., M. Jiang, et al. (2005). "Cancer-specific functions of SIRT1 enable human epithelial cancer cell growth and survival." Cancer Res **65**(22): 10457-63.

Frescas, D., L. Valenti, et al. (2005). "Nuclear trapping of the forkhead transcription factor FoxO1 via Sirt-dependent deacetylation promotes expression of glucogenetic genes." J Biol Chem **280**(21): 20589-95.

Frojdo, S., C. Durand, et al. "Phosphoinositide 3-kinase as a novel functional target for the regulation of the insulin signaling pathway by SIRT1." Mol Cell Endocrinol **335**(2): 166-76.

Frye, R. A. (1999). "Characterization of five human cDNAs with homology to the yeast SIR2 gene: Sir2-like proteins (sirtuins) metabolize NAD and may have protein ADP-ribosyltransferase activity." Biochem Biophys Res Commun **260**(1): 273-9.

Frye, R. A. (2000). "Phylogenetic classification of prokaryotic and eukaryotic Sir2-like proteins." Biochem Biophys Res Commun **273**(2): 793-8.

Fu, M., M. Liu, et al. (2006). "Hormonal control of androgen receptor function through SIRT1." Mol Cell Biol **26**(21): 8122-35.

Fujino, T., J. Kondo, et al. (2001). "Acetyl-CoA synthetase 2, a mitochondrial matrix enzyme involved in the oxidation of acetate." J Biol Chem **276**(14): 11420-6.

Fulco, M., R. L. Schiltz, et al. (2003). "Sir2 regulates skeletal muscle differentiation as a potential sensor of the redox state." Mol Cell **12**(1): 51-62.
Gerhart-Hines, Z., J. T. Rodgers, et al. (2007). "Metabolic control of muscle mitochondrial function and fatty acid oxidation through SIRT1/PGC-1alpha." Embo J **26**(7): 1913-23.
Gottschling, D. E. (2000). "Gene silencing: two faces of SIR2." Curr Biol **10**(19): R708-11.
Greer, E. L. and A. Brunet (2005). "FOXO transcription factors at the interface between longevity and tumor suppression." Oncogene **24**(50): 7410-25.
Greiss, S. and A. Gartner (2009). "Sirtuin/Sir2 phylogeny, evolutionary considerations and structural conservation." Mol Cells **28**(5): 407-15.
Hafner, A. V., J. Dai, et al. "Regulation of the mPTP by SIRT3-mediated deacetylation of CypD at lysine 166 suppresses age-related cardiac hypertrophy." Aging (Albany NY) **2**(12): 914-23.
Haigis, M. C. and D. A. Sinclair "Mammalian sirtuins: biological insights and disease relevance." Annu Rev Pathol **5**: 253-95.
Hallows, W. C., B. N. Albaugh, et al. (2008). "Where in the cell is SIRT3?--functional localization of an NAD+-dependent protein deacetylase." Biochem J **411**(2): e11-3.
Hallows, W. C., S. Lee, et al. (2006). "Sirtuins deacetylate and activate mammalian acetyl-CoA synthetases." Proc Natl Acad Sci U S A **103**(27): 10230-5.
Hallows, W. C., W. Yu, et al. "Sirt3 promotes the urea cycle and fatty acid oxidation during dietary restriction." Mol Cell **41**(2): 139-49.
Harper, J. M., C. W. Leathers, et al. (2006). "Does caloric restriction extend life in wild mice?" Aging Cell **5**(6): 441-9.
Hasegawa, K. and K. Yoshikawa (2008). "Necdin regulates p53 acetylation via Sirtuin1 to modulate DNA damage response in cortical neurons." J Neurosci **28**(35): 8772-84.
Hawse, W. F., K. G. Hoff, et al. (2008). "Structural insights into intermediate steps in the Sir2 deacetylation reaction." Structure **16**(9): 1368-77.
Hawse, W. F. and C. Wolberger (2009). "Structure-based mechanism of ADP-ribosylation by sirtuins." J Biol Chem **284**(48): 33654-61.
He, W., Y. Wang, et al. "Sirt1 activation protects the mouse renal medulla from oxidative injury." J Clin Invest **120**(4): 1056-68.
Heilbronn, L. K. and E. Ravussin (2003). "Calorie restriction and aging: review of the literature and implications for studies in humans." Am J Clin Nutr **78**(3): 361-9.
Herzig, S., F. Long, et al. (2001). "CREB regulates hepatic gluconeogenesis through the coactivator PGC-1." Nature **413**(6852): 179-83.
Hirschey, M. D., T. Shimazu, et al. "SIRT3 regulates mitochondrial fatty-acid oxidation by reversible enzyme deacetylation." Nature **464**(7285): 121-5.
Hirst, J. (2010). "Towards the molecular mechanism of respiratory complex I." Biochem J **425**(2): 327-39.
Hoff, K. G., J. L. Avalos, et al. (2006). "Insights into the sirtuin mechanism from ternary complexes containing NAD+ and acetylated peptide." Structure **14**(8): 1231-40.
Hokari, F., E. Kawasaki, et al. "Muscle contractile activity regulates Sirt3 protein expression in rat skeletal muscles." J Appl Physiol **109**(2): 332-40.
Hou, X., S. Xu, et al. (2008). "SIRT1 regulates hepatocyte lipid metabolism through activating AMP-activated protein kinase." J Biol Chem **283**(29): 20015-26.

Howitz, K. T., K. J. Bitterman, et al. (2003). "Small molecule activators of sirtuins extend Saccharomyces cerevisiae lifespan." Nature **425**(6954): 191-6.
Hu, Y. and N. F. Mivechi (2003). "HSF-1 interacts with Ral-binding protein 1 in a stress-responsive, multiprotein complex with HSP90 in vivo." J Biol Chem **278**(19): 17299-306.
Huffman, D. M., W. E. Grizzle, et al. (2007). "SIRT1 is significantly elevated in mouse and human prostate cancer." Cancer Res **67**(14): 6612-8.
Hursting, S. D., J. A. Lavigne, et al. (2003). "Calorie restriction, aging, and cancer prevention: mechanisms of action and applicability to humans." Annu Rev Med **54**: 131-52.
Hwang, J. H., D. W. Kim, et al. (2009). "Pharmacological stimulation of NADH oxidation ameliorates obesity and related phenotypes in mice." Diabetes **58**(4): 965-74.
Hwang, J. T., D. Y. Kwon, et al. (2008). "Resveratrol protects ROS-induced cell death by activating AMPK in H9c2 cardiac muscle cells." Genes Nutr **2**(4): 323-6.
Ibuka, N., S. I. Inouye, et al. (1977). "Analysis of sleep-wakefulness rhythms in male rats after suprachiasmatic nucleus lesions and ocular enucleation." Brain Res **122**(1): 33-47.
Ibuka, N. and H. Kawamura (1975). "Loss of circadian rhythm in sleep-wakefulness cycle in the rat by suprachiasmatic nucleus lesions." Brain Res **96**(1): 76-81.
Ibuka, N., I. Nihonmatsu, et al. (1980). "Sleep-wakefulness rhythms in mice after suprachiasmatic nucleus lesions." Waking Sleeping **4**(2): 167-73.
Imai, S., C. M. Armstrong, et al. (2000). "Transcriptional silencing and longevity protein Sir2 is an NAD-dependent histone deacetylase." Nature **403**(6771): 795-800.
Imai, S. and L. Guarente "Ten years of NAD-dependent SIR2 family deacetylases: implications for metabolic diseases." Trends Pharmacol Sci **31**(5): 212-20.
Inoue, H., W. Ogawa, et al. (2006). "Role of hepatic STAT3 in brain-insulin action on hepatic glucose production." Cell Metab **3**(4): 267-75.
Inoue, H., W. Ogawa, et al. (2004). "Role of STAT-3 in regulation of hepatic gluconeogenic genes and carbohydrate metabolism in vivo." Nat Med **10**(2): 168-74.
Iqbal, J. and M. Zaidi (2006). "TNF regulates cellular NAD+ metabolism in primary macrophages." Biochem Biophys Res Commun **342**(4): 1312-8.
Jacobs, K. M., J. D. Pennington, et al. (2008). "SIRT3 interacts with the daf-16 homolog FOXO3a in the mitochondria, as well as increases FOXO3a dependent gene expression." Int J Biol Sci **4**(5): 291-9.
Jeong, J., K. Juhn, et al. (2007). "SIRT1 promotes DNA repair activity and deacetylation of Ku70." Exp Mol Med **39**(1): 8-13.
Jin, L., H. Galonek, et al. (2009). "Biochemical characterization, localization, and tissue distribution of the longer form of mouse SIRT3." Protein Sci **18**(3): 514-25.
Jin, L., W. Wei, et al. (2009). "Crystal structures of human SIRT3 displaying substrate-induced conformational changes." J Biol Chem **284**(36): 24394-405.
Kaeberlein, M., D. Hu, et al. (2005). "Increased life span due to calorie restriction in respiratory-deficient yeast." PLoS Genet **1**(5): e69.
Kaeberlein, M., K. T. Kirkland, et al. (2004). "Sir2-independent life span extension by calorie restriction in yeast." PLoS Biol **2**(9): E296.
Kaeberlein, M., T. McDonagh, et al. (2005). "Substrate-specific activation of sirtuins by resveratrol." J Biol Chem **280**(17): 17038-45.

Kaeberlein, M., M. McVey, et al. (1999). "The SIR2/3/4 complex and SIR2 alone promote longevity in Saccharomyces cerevisiae by two different mechanisms." Genes Dev **13**(19): 2570-80.
Kaeberlein, M., M. McVey, et al. (1999). "The SIR2/3/4 complex and SIR2 alone promote longevity in Saccharomyces cerevisiae by two different mechanisms." Genes Dev **13**(19): 2570-80.
Kaestner, K. H., W. Knochel, et al. (2000). "Unified nomenclature for the winged helix/forkhead transcription factors." Genes Dev **14**(2): 142-6.
Kawamura, Y., Y. Uchijima, et al. "Sirt3 protects in vitro-fertilized mouse preimplantation embryos against oxidative stress-induced p53-mediated developmental arrest." J Clin Invest **120**(8): 2817-28.
Kendrick, A. A., M. Choudhury, et al. "Fatty liver is associated with reduced SIRT3 activity and mitochondrial protein hyperacetylation." Biochem J.
Kim, D., M. D. Nguyen, et al. (2007). "SIRT1 deacetylase protects against neurodegeneration in models for Alzheimer's disease and amyotrophic lateral sclerosis." EMBO J **26**(13): 3169-79.
Kim, E. J., J. H. Kho, et al. (2007). "Active regulator of SIRT1 cooperates with SIRT1 and facilitates suppression of p53 activity." Mol Cell **28**(2): 277-90.
Kim, H. S., K. Patel, et al. "SIRT3 is a mitochondria-localized tumor suppressor required for maintenance of mitochondrial integrity and metabolism during stress." Cancer Cell **17**(1): 41-52.
Kim, J. E., J. Chen, et al. (2008). "DBC1 is a negative regulator of SIRT1." Nature **451**(7178): 583-6.
Kim, S., A. Benguria, et al. (1999). "Modulation of life-span by histone deacetylase genes in Saccharomyces cerevisiae." Mol Biol Cell **10**(10): 3125-36.
Kitamura, T. and Y. Ido Kitamura (2007). "Role of FoxO Proteins in Pancreatic beta Cells." Endocr J **54**(4): 507-15.
Kitamura, Y. I., T. Kitamura, et al. (2005). "FoxO1 protects against pancreatic beta cell failure through NeuroD and MafA induction." Cell Metab **2**(3): 153-63.
Kobayashi, Y., Y. Furukawa-Hibi, et al. (2005). "SIRT1 is critical regulator of FOXO-mediated transcription in response to oxidative stress." Int J Mol Med **16**(2): 237-43.
Kolthur-Seetharam, U., F. Dantzer, et al. (2006). "Control of AIF-mediated cell death by the functional interplay of SIRT1 and PARP-1 in response to DNA damage." Cell Cycle **5**(8): 873-7.
Kolthur-Seetharam, U., K. Teerds, et al. (2009). "The histone deacetylase SIRT1 controls male fertility in mice through regulation of hypothalamic-pituitary gonadotropin signaling." Biol Reprod **80**(2): 384-91.
Kong, X., R. Wang, et al. "Sirtuin 3, a new target of PGC-1alpha, plays an important role in the suppression of ROS and mitochondrial biogenesis." PLoS One **5**(7): e11707.
Kops, G. J., T. B. Dansen, et al. (2002). "Forkhead transcription factor FOXO3a protects quiescent cells from oxidative stress." Nature **419**(6904): 316-21.
Kume, S., T. Uzu, et al. "Calorie restriction enhances cell adaptation to hypoxia through Sirt1-dependent mitochondrial autophagy in mouse aged kidney." J Clin Invest **120**(4): 1043-55.
Kuningas, M., M. Putters, et al. (2007). "SIRT1 gene, age-related diseases, and mortality: the Leiden 85-plus study." J Gerontol A Biol Sci Med Sci **62**(9): 960-5.

Kuzmichev, A., R. Margueron, et al. (2005). "Composition and histone substrates of polycomb repressive group complexes change during cellular differentiation." Proc Natl Acad Sci U S A **102**(6): 1859-64.
Lagouge, M., C. Argmann, et al. (2006). "Resveratrol improves mitochondrial function and protects against metabolic disease by activating SIRT1 and PGC-1alpha." Cell **127**(6): 1109-22.
Lamming, D. W., M. Latorre-Esteves, et al. (2005). "HST2 mediates SIR2-independent life-span extension by calorie restriction." Science **309**(5742): 1861-4.
Landry, J., A. Sutton, et al. (2000). "The silencing protein SIR2 and its homologs are NAD-dependent protein deacetylases." Proc Natl Acad Sci U S A **97**(11): 5807-11.
Langley, E., M. Pearson, et al. (2002). "Human SIR2 deacetylates p53 and antagonizes PML/p53-induced cellular senescence." Embo J **21**(10): 2383-96.
Lanza, I. R., D. K. Short, et al. (2008). "Endurance exercise as a countermeasure for aging." Diabetes **57**(11): 2933-42.
Lavu, S., O. Boss, et al. (2008). "Sirtuins--novel therapeutic targets to treat age-associated diseases." Nat Rev Drug Discov **7**(10): 841-53.
Lee, J. H., M. Y. Song, et al. (2009). "Overexpression of SIRT1 protects pancreatic beta-cells against cytokine toxicity by suppressing the nuclear factor-kappaB signaling pathway." Diabetes **58**(2): 344-51.
Li, S., M. Banck, et al. "p53-induced growth arrest is regulated by the mitochondrial SirT3 deacetylase." PLoS One **5**(5): e10486.
Li, X., S. Zhang, et al. (2007). "SIRT1 deacetylates and positively regulates the nuclear receptor LXR." Mol Cell **28**(1): 91-106.
Li, Y., W. Xu, et al. (2008). "SirT1 inhibition reduces IGF-I/IRS-2/Ras/ERK1/2 signaling and protects neurons." Cell Metab **8**(1): 38-48.
Li, Y., T. Yokota, et al. (2007). "Bax-inhibiting peptide protects cells from polyglutamine toxicity caused by Ku70 acetylation." Cell Death Differ **14**(12): 2058-67.
Lin, S., P. Defossez, et al. (2000). "Requirement of NAD and SIR2 for life-span extension by calorie restriction in Saccharomyces cerevisiae." Science **289**(5487): 2126-8.
Lin, S. J., P. A. Defossez, et al. (2000). "Requirement of NAD and SIR2 for life-span extension by calorie restriction in Saccharomyces cerevisiae." Science **289**(5487): 2126-8.
Lin, S. J., E. Ford, et al. (2004). "Calorie restriction extends yeast life span by lowering the level of NADH." Genes Dev **18**(1): 12-6.
Lin, S. J., M. Kaeberlein, et al. (2002). "Calorie restriction extends Saccharomyces cerevisiae lifespan by increasing respiration." Nature **418**(6895): 344-8.
Liu, Y., R. Dentin, et al. (2008). "A fasting inducible switch modulates gluconeogenesis via activator/coactivator exchange." Nature **456**(7219): 269-73.
Liu, Y., R. Dentin, et al. (2008). "A fasting inducible switch modulates gluconeogenesis via activator/coactivator exchange." Nature **456**(7219): 269-73.
Lombard, D. B., F. W. Alt, et al. (2007). "Mammalian Sir2 homolog SIRT3 regulates global mitochondrial lysine acetylation." Mol Cell Biol **27**(24): 8807-14.
Luo, J., A. Y. Nikolaev, et al. (2001). "Negative control of p53 by Sir2alpha promotes cell survival under stress." Cell **107**(2): 137-48.
Magni, G., A. Amici, et al. (2004). "Enzymology of NAD+ homeostasis in man." Cell Mol Life Sci **61**(1): 19-34.

Magni, G., A. Amici, et al. (1999). "Enzymology of NAD+ synthesis." Adv Enzymol Relat Areas Mol Biol **73**: 135-82, xi.
Marfe, G., M. Tafani, et al. (2009). "Kaempferol induces apoptosis in two different cell lines via Akt inactivation, Bax and SIRT3 activation, and mitochondrial dysfunction." J Cell Biochem **106**(4): 643-50.
McBurney, M. W., X. Yang, et al. (2003). "The mammalian SIR2alpha protein has a role in embryogenesis and gametogenesis." Mol Cell Biol **23**(1): 38-54.
McCreanor, G. M. and D. A. Bender (1986). "The metabolism of high intakes of tryptophan, nicotinamide and nicotinic acid in the rat." Br J Nutr **56**(3): 577-86.
McKinsey, T. A., C. L. Zhang, et al. (2002). "MEF2: a calcium-dependent regulator of cell division, differentiation and death." Trends Biochem Sci **27**(1): 40-7.
Michishita, E., J. Y. Park, et al. (2005). "Evolutionarily conserved and nonconserved cellular localizations and functions of human SIRT proteins." Mol Biol Cell **16**(10): 4623-35.
Milne, J. C., P. D. Lambert, et al. (2007). "Small molecule activators of SIRT1 as therapeutics for the treatment of type 2 diabetes." Nature **450**(7170): 712-6.
Min, J., J. Landry, et al. (2001). "Crystal structure of a SIR2 homolog-NAD complex." Cell **105**(2): 269-79.
Moore, R. Y. and V. B. Eichler (1972). "Loss of a circadian adrenal corticosterone rhythm following suprachiasmatic lesions in the rat." Brain Res **42**(1): 201-6.
Motta, M. C., N. Divecha, et al. (2004). "Mammalian SIRT1 represses forkhead transcription factors." Cell **116**(4): 551-63.
Moynihan, K. A., A. A. Grimm, et al. (2005). "Increased dosage of mammalian Sir2 in pancreatic beta cells enhances glucose-stimulated insulin secretion in mice." Cell Metab **2**(2): 105-17.
Nakae, J., Y. Cao, et al. (2006). "The LXXLL motif of murine forkhead transcription factor FoxO1 mediates Sirt1-dependent transcriptional activity." J Clin Invest **116**(9): 2473-83.
Nakahata, Y., M. Kaluzova, et al. (2008). "The NAD+-dependent deacetylase SIRT1 modulates CLOCK-mediated chromatin remodeling and circadian control." Cell **134**(2): 329-40.
Nakahata, Y., S. Sahar, et al. (2009). "Circadian control of the NAD+ salvage pathway by CLOCK-SIRT1." Science **324**(5927): 654-7.
Nemoto, S., M. M. Fergusson, et al. (2004). "Nutrient availability regulates SIRT1 through a forkhead-dependent pathway." Science **306**(5704): 2105-8.
Nemoto, S., M. M. Fergusson, et al. (2005). "SIRT1 functionally interacts with the metabolic regulator and transcriptional coactivator PGC-1{alpha}." J Biol Chem **280**(16): 16456-60.
Newman, B. L., J. R. Lundblad, et al. (2002). "A Drosophila homologue of Sir2 modifies position-effect variegation but does not affect life span." Genetics **162**(4): 1675-85.
Nicholls, D. G. and F. S.J. (2002). Bioenergetics 3, Academic Press.
Nie, Y., D. Erion, et al. (2009). "STAT3 inhibition of gluconeogenesis is downregulated by SirT1." Nat Cell Biol **11**(4): 492-500.
Oberdoerffer, P., S. Michan, et al. (2008). "SIRT1 redistribution on chromatin promotes genomic stability but alters gene expression during aging." Cell **135**(5): 907-18.
Onyango, P., I. Celic, et al. (2002). "SIRT3, a human SIR2 homologue, is an NAD-dependent deacetylase localized to mitochondria." Proc Natl Acad Sci U S A **99**(21): 13653-8.

Orimo, M., T. Minamino, et al. (2009). "Protective role of SIRT1 in diabetic vascular dysfunction." Arterioscler Thromb Vasc Biol **29**(6): 889-94.
Osborne, T. B., L. B. Mendel, et al. (1917). "The Effect of Retardation of Growth Upon the Breeding Period and Duration of Life of Rats." Science **45**(1160): 294-5.
Pacholec, M., J. E. Bleasdale, et al. "SRT1720, SRT2183, SRT1460, and resveratrol are not direct activators of SIRT1." J Biol Chem **285**(11): 8340-51.
Pacholec, M., B. Chrunyk, et al. (2010). "SRT1720, SRT2183, SRT1460, and resveratrol are not direct activators of SIRT1." J Biol Chem.
Palacios, O. M., J. J. Carmona, et al. (2009). "Diet and exercise signals regulate SIRT3 and activate AMPK and PGC-1alpha in skeletal muscle." Aging (Albany NY) **1**(9): 771-83.
Palacios, O. M., J. J. Carmona, et al. (2009). "Diet and exercise signals regulate SIRT3 and activate AMPK and PGC-1alpha in skeletal muscle." Aging (Albany NY) **1**(9): 771-83.
Park, C. E., M. J. Kim, et al. (2007). "Resveratrol stimulates glucose transport in C2C12 myotubes by activating AMP-activated protein kinase." Exp Mol Med **39**(2): 222-9.
Pearson, K. J., J. A. Baur, et al. (2008). "Resveratrol delays age-related deterioration and mimics transcriptional aspects of dietary restriction without extending life span." Cell Metab **8**(2): 157-68.
Pediconi, N., F. Guerrieri, et al. (2009). "hSirT1-dependent regulation of the PCAF-E2F1-p73 apoptotic pathway in response to DNA damage." Mol Cell Biol **29**(8): 1989-98.
Peeters, A. V., S. Beckers, et al. (2008). "Association of SIRT1 gene variation with visceral obesity." Hum Genet **124**(4): 431-6.
Pfluger, P. T., D. Herranz, et al. (2008). "Sirt1 protects against high-fat diet-induced metabolic damage." Proc Natl Acad Sci U S A **105**(28): 9793-8.
Picard, F., M. Kurtev, et al. (2004). "Sirt1 promotes fat mobilization in white adipocytes by repressing PPAR-gamma." Nature **429**(6993): 771-6.
Pillai, J. B., M. Gupta, et al. (2006). "Poly(ADP-ribose) polymerase-1-deficient mice are protected from angiotensin II-induced cardiac hypertrophy." Am J Physiol Heart Circ Physiol **291**(4): H1545-53.
Pillai, J. B., A. Isbatan, et al. (2005). "Poly(ADP-ribose) polymerase-1-dependent cardiac myocyte cell death during heart failure is mediated by NAD+ depletion and reduced Sir2alpha deacetylase activity." J Biol Chem **280**(52): 43121-30.
Pillai, V. B., N. R. Sundaresan, et al. "Mitochondrial SIRT3 and heart disease." Cardiovasc Res **88**(2): 250-6.
Ponugoti, B., D. H. Kim, et al. "SIRT1 deacetylates and inhibits SREBP-1C activity in regulation of hepatic lipid metabolism." J Biol Chem.
Ponugoti, B., D. H. Kim, et al. "SIRT1 deacetylates and inhibits SREBP-1C activity in regulation of hepatic lipid metabolism." J Biol Chem **285**(44): 33959-70.
Potente, M., L. Ghaeni, et al. (2007). "SIRT1 controls endothelial angiogenic functions during vascular growth." Genes Dev **21**(20): 2644-58.
Purushotham, A., T. T. Schug, et al. (2009). "Hepatocyte-specific deletion of SIRT1 alters fatty acid metabolism and results in hepatic steatosis and inflammation." Cell Metab **9**(4): 327-38.
Qiang, L., A. S. Banks, et al. "Uncoupling of acetylation from phosphorylation regulates FoxO1 function independent of its subcellular localization." J Biol Chem **285**(35): 27396-401.

Qiao, L. and J. Shao (2006). "SIRT1 regulates adiponectin gene expression through Foxo1-C/enhancer-binding protein alpha transcriptional complex." J Biol Chem **281**(52): 39915-24.
Rajamohan, S. B., V. B. Pillai, et al. (2009). "SIRT1 promotes cell survival under stress by deacetylation-dependent deactivation of poly(ADP-ribose) polymerase 1." Mol Cell Biol **29**(15): 4116-29.
Ralph, M. R., R. G. Foster, et al. (1990). "Transplanted suprachiasmatic nucleus determines circadian period." Science **247**(4945): 975-8.
Ralph, M. R. and M. W. Hurd (1996). "Pacemaker interactions in the mammalian circadian system." Braz J Med Biol Res **29**(1): 77-85.
Ramadori, G., T. Fujikawa, et al. "SIRT1 deacetylase in POMC neurons is required for homeostatic defenses against diet-induced obesity." Cell Metab **12**(1): 78-87.
Ramadori, G., L. Gautron, et al. (2009). "Central administration of resveratrol improves diet-induced diabetes." Endocrinology **150**(12): 5326-33.
Ramadori, G., C. E. Lee, et al. (2008). "Brain SIRT1: anatomical distribution and regulation by energy availability." J Neurosci **28**(40): 9989-96.
Ramsey, K. M., K. F. Mills, et al. (2008). "Age-associated loss of Sirt1-mediated enhancement of glucose-stimulated insulin secretion in beta cell-specific Sirt1-overexpressing (BESTO) mice." Aging Cell **7**(1): 78-88.
Ramsey, K. M., J. Yoshino, et al. (2009). "Circadian clock feedback cycle through NAMPT-mediated NAD+ biosynthesis." Science **324**(5927): 651-4.
Rane, S., M. He, et al. (2009). "Downregulation of miR-199a derepresses hypoxia-inducible factor-1alpha and Sirtuin 1 and recapitulates hypoxia preconditioning in cardiac myocytes." Circ Res **104**(7): 879-86.
Rathaus, M., B. Lerrer, et al. (2009). "DeubiKuitylation: a novel DUB enzymatic activity for the DNA repair protein, Ku70." Cell Cycle **8**(12): 1843-52.
Revollo, J. R., A. A. Grimm, et al. (2004). "The NAD biosynthesis pathway mediated by nicotinamide phosphoribosyltransferase regulates Sir2 activity in mammalian cells." J Biol Chem **279**(49): 50754-63.
Rodgers, J. and P. Puigserver (2007). "Fasting-dependent glucose and lipid metabolic response through hepatic sirtuin 1." Proc Natl Acad Sci U S A **104**(31): 12861-6.
Rodgers, J. T., C. Lerin, et al. (2005). "Nutrient control of glucose homeostasis through a complex of PGC-1alpha and SIRT1." Nature **434**(7029): 113-8.
Rodgers, J. T. and P. Puigserver (2007). "Fasting-dependent glucose and lipid metabolic response through hepatic sirtuin 1." Proc Natl Acad Sci U S A **104**(31): 12861-6.
Rogina, B. and S. L. Helfand (2004). "Sir2 mediates longevity in the fly through a pathway related to calorie restriction." Proc Natl Acad Sci U S A **101**(45): 15998-6003.
Rose, G., S. Dato, et al. (2003). "Variability of the SIRT3 gene, human silent information regulator Sir2 homologue, and survivorship in the elderly." Exp Gerontol **38**(10): 1065-70.
Rous, P. (1914). "The Influence of Diet on Transplanted and Spontaneous Mouse Tumors." J Exp Med **20**(5): 433-51.
Sakamoto, J., T. Miura, et al. (2004). "Predominant expression of Sir2alpha, an NAD-dependent histone deacetylase, in the embryonic mouse heart and brain." FEBS Lett **556**(1-3): 281-6.
Sasaki, T., H. J. Kim, et al. "Induction of hypothalamic Sirt1 leads to cessation of feeding via agouti-related peptide." Endocrinology **151**(6): 2556-66.

Satoh, A., C. S. Brace, et al. "SIRT1 promotes the central adaptive response to diet restriction through activation of the dorsomedial and lateral nuclei of the hypothalamus." J Neurosci **30**(30): 10220-32.
Sauve, A. A. (2010). "Sirtuin chemical mechanisms." Biochim Biophys Acta.
Sauve, A. A., I. Celic, et al. (2001). "Chemistry of gene silencing: the mechanism of NAD+-dependent deacetylation reactions." Biochemistry **40**(51): 15456-63.
Sauve, A. A., R. D. Moir, et al. (2005). "Chemical activation of Sir2-dependent silencing by relief of nicotinamide inhibition." Mol Cell **17**(4): 595-601.
Sauve, A. A. and V. L. Schramm (2004). "SIR2: the biochemical mechanism of NAD(+)-dependent protein deacetylation and ADP-ribosyl enzyme intermediates." Curr Med Chem **11**(7): 807-26.
Scher, M. B., A. Vaquero, et al. (2007). "SirT3 is a nuclear NAD+-dependent histone deacetylase that translocates to the mitochondria upon cellular stress." Genes Dev **21**(8): 920-8.
Schlicker, C., M. Gertz, et al. (2008). "Substrates and regulation mechanisms for the human mitochondrial sirtuins Sirt3 and Sirt5." J Mol Biol **382**(3): 790-801.
Schmidt, M. T., B. C. Smith, et al. (2004). "Coenzyme specificity of Sir2 protein deacetylases: implications for physiological regulation." J Biol Chem **279**(38): 40122-9.
Schmoll, D., K. S. Walker, et al. (2000). "Regulation of glucose-6-phosphatase gene expression by protein kinase Balpha and the forkhead transcription factor FKHR. Evidence for insulin response unit-dependent and -independent effects of insulin on promoter activity." J Biol Chem **275**(46): 36324-33.
Schwer, B., J. Bunkenborg, et al. (2006). "Reversible lysine acetylation controls the activity of the mitochondrial enzyme acetyl-CoA synthetase 2." Proc Natl Acad Sci U S A **103**(27): 10224-9.
Schwer, B., B. J. North, et al. (2002). "The human silent information regulator (Sir)2 homologue hSIRT3 is a mitochondrial nicotinamide adenine dinucleotide-dependent deacetylase." J Cell Biol **158**(4): 647-57.
Sedelnikova, O. A., I. Horikawa, et al. (2004). "Senescing human cells and ageing mice accumulate DNA lesions with unrepairable double-strand breaks." Nat Cell Biol **6**(2): 168-70.
Shang, J., L. L. Chen, et al. (2008). "Resveratrol improves non-alcoholic fatty liver disease by activating AMP-activated protein kinase." Acta Pharmacol Sin **29**(6): 698-706.
Sherman, J. M., E. M. Stone, et al. (1999). "The conserved core of a human SIR2 homologue functions in yeast silencing." Mol Biol Cell **10**(9): 3045-59.
Shi, T., G. Q. Fan, et al. "SIRT3 reduces lipid accumulation via AMPK activation in human hepatic cells." J Dig Dis **11**(1): 55-62.
Shi, T., F. Wang, et al. (2005). "SIRT3, a mitochondrial sirtuin deacetylase, regulates mitochondrial function and thermogenesis in brown adipocytes." J Biol Chem **280**(14): 13560-7.
Shimazu, T., M. D. Hirschey, et al. "SIRT3 deacetylates mitochondrial 3-hydroxy-3-methylglutaryl CoA synthase 2 and regulates ketone body production." Cell Metab **12**(6): 654-61.
Shin, S. M., I. J. Cho, et al. (2009). "Resveratrol protects mitochondria against oxidative stress through AMP-activated protein kinase-mediated glycogen synthase kinase-3beta inhibition downstream of poly(ADP-ribose)polymerase-LKB1 pathway." Mol Pharmacol **76**(4): 884-95.

Shore, D. and K. Nasmyth (1987). "Purification and cloning of a DNA binding protein from yeast that binds to both silencer and activator elements." Cell **51**(5): 721-32.

Shulga, N., R. Wilson-Smith, et al. "Sirtuin-3 deacetylation of cyclophilin D induces dissociation of hexokinase II from the mitochondria." J Cell Sci **123**(Pt 6): 894-902.

Silver, R., J. LeSauter, et al. (1996). "A diffusible coupling signal from the transplanted suprachiasmatic nucleus controlling circadian locomotor rhythms." Nature **382**(6594): 810-3.

Sinclair, D. A., K. Mills, et al. (1997). "Accelerated aging and nucleolar fragmentation in yeast sgs1 mutants." Science **277**(5330): 1313-6.

Smith, B. C. and J. M. Denu (2006). "Sir2 protein deacetylases: evidence for chemical intermediates and functions of a conserved histidine." Biochemistry **45**(1): 272-82.

Smith, J. J., R. D. Kenney, et al. (2009). "Small molecule activators of SIRT1 replicate signaling pathways triggered by calorie restriction in vivo." BMC Syst Biol **3**: 31.

Smith, J. S., C. B. Brachmann, et al. (2000). "A phylogenetically conserved NAD+-dependent protein deacetylase activity in the Sir2 protein family." Proc Natl Acad Sci U S A **97**(12): 6658-63.

Someya, S., W. Yu, et al. "Sirt3 mediates reduction of oxidative damage and prevention of age-related hearing loss under caloric restriction." Cell **143**(5): 802-12.

St-Pierre, J., S. Drori, et al. (2006). "Suppression of reactive oxygen species and neurodegeneration by the PGC-1 transcriptional coactivators." Cell **127**(2): 397-408.

Stephan, F. K. and I. Zucker (1972). "Circadian rhythms in drinking behavior and locomotor activity of rats are eliminated by hypothalamic lesions." Proc Natl Acad Sci U S A **69**(6): 1583-6.

Stetson, M. H. and M. Watson-Whitmyre (1976). "Nucleus suprachiasmaticus: the biological clock in the hamster?" Science **191**(4223): 197-9.

Su, A. I., T. Wiltshire, et al. (2004). "A gene atlas of the mouse and human protein-encoding transcriptomes." Proc Natl Acad Sci U S A **101**(16): 6062-7.

Subauste, A. R. and C. F. Burant (2007). "Role of FoxO1 in FFA-induced oxidative stress in adipocytes." Am J Physiol Endocrinol Metab **293**(1): E159-64.

Sulaiman, M., M. J. Matta, et al. (2009). "Resveratrol, an activator of SIRT1 up-regulates sarcoplasmic calcium ATPase and improves cardiac function in diabetic cardiomyopathy." Am J Physiol Heart Circ Physiol.

Sun, C., F. Zhang, et al. (2007). "SIRT1 improves insulin sensitivity under insulin-resistant conditions by repressing PTP1B." Cell Metab **6**(4): 307-19.

Sundaresan, N. R., M. Gupta, et al. (2009). "Sirt3 blocks the cardiac hypertrophic response by augmenting Foxo3a-dependent antioxidant defense mechanisms in mice." J Clin Invest **119**(9): 2758-71.

Sundaresan, N. R., S. A. Samant, et al. (2008). "SIRT3 is a stress-responsive deacetylase in cardiomyocytes that protects cells from stress-mediated cell death by deacetylation of Ku70." Mol Cell Biol **28**(20): 6384-401.

Szymanski, J. (1918). "Versuche uber die Fahigkeit der Hunde zur Bildung von optischen Association." Pfluger's Arch. f. d. ges. Physiol **171**.

Tanner, K. G., J. Landry, et al. (2000). "Silent information regulator 2 family of NAD-dependent histone/protein deacetylases generates a unique product, 1-O-acetyl-ADP-ribose." Proc Natl Acad Sci U S A **97**(26): 14178-82.

Tanno, M., J. Sakamoto, et al. (2007). "Nucleocytoplasmic shuttling of the NAD+-dependent histone deacetylase SIRT1." J Biol Chem **282**(9): 6823-32.
Tanny, J. C., G. J. Dowd, et al. (1999). "An enzymatic activity in the yeast Sir2 protein that is essential for gene silencing." Cell **99**(7): 735-45.
Tanny, J. C. and D. Moazed (2001). "Coupling of histone deacetylation to NAD breakdown by the yeast silencing protein Sir2: Evidence for acetyl transfer from substrate to an NAD breakdown product." Proc Natl Acad Sci U S A **98**(2): 415-20.
Tao, R., M. C. Coleman, et al. "Sirt3-mediated deacetylation of evolutionarily conserved lysine 122 regulates MnSOD activity in response to stress." Mol Cell **40**(6): 893-904.
Tissenbaum, H. and L. Guarente (2001). "Increased dosage of a sir-2 gene extends lifespan in Caenorhabditis elegans." Nature **410**(6825): 227-30.
Tissenbaum, H. A. and L. Guarente (2001). "Increased dosage of a sir-2 gene extends lifespan in Caenorhabditis elegans." Nature **410**(6825): 227-30.
Tontonoz, P., E. Hu, et al. (1994). "Stimulation of adipogenesis in fibroblasts by PPAR gamma 2, a lipid-activated transcription factor." Cell **79**(7): 1147-56.
Tsang, A. W. and J. C. Escalante-Semerena (1998). "CobB, a new member of the SIR2 family of eucaryotic regulatory proteins, is required to compensate for the lack of nicotinate mononucleotide:5,6-dimethylbenzimidazole phosphoribosyltransferase activity in cobT mutants during cobalamin biosynthesis in Salmonella typhimurium LT2." J Biol Chem **273**(48): 31788-94.
Turek, F. W., C. Joshu, et al. (2005). "Obesity and metabolic syndrome in circadian Clock mutant mice." Science **308**(5724): 1043-5.
Um, J. H., S. J. Park, et al. (2010). "AMP-activated protein kinase-deficient mice are resistant to the metabolic effects of resveratrol." Diabetes **59**(3): 554-63.
Vahtola, E., M. Louhelainen, et al. (2008). "Forkhead class O transcription factor 3a activation and Sirtuin1 overexpression in the hypertrophied myocardium of the diabetic Goto-Kakizaki rat." J Hypertens **26**(2): 334-44.
van der Horst, A., L. G. Tertoolen, et al. (2004). "FOXO4 is acetylated upon peroxide stress and deacetylated by the longevity protein hSir2(SIRT1)." J Biol Chem **279**(28): 28873-9.
van der Veer, E., Z. Nong, et al. (2005). "Pre-B-cell colony-enhancing factor regulates NAD+-dependent protein deacetylase activity and promotes vascular smooth muscle cell maturation." Circ Res **97**(1): 25-34.
van Ham, T. J., K. L. Thijssen, et al. (2008). "C. elegans model identifies genetic modifiers of alpha-synuclein inclusion formation during aging." PLoS Genet **4**(3): e1000027.
Vaquero, A., M. Scher, et al. (2004). "Human SirT1 interacts with histone H1 and promotes formation of facultative heterochromatin." Mol Cell **16**(1): 93-105.
Vaquero, A., R. Sternglanz, et al. (2007). "NAD+-dependent deacetylation of H4 lysine 16 by class III HDACs." Oncogene **26**(37): 5505-20.
Vaziri, H., S. K. Dessain, et al. (2001). "hSIR2(SIRT1) functions as an NAD-dependent p53 deacetylase." Cell **107**(2): 149-59.
Velasquez, D. A., G. Martinez, et al. "The central Sirtuin 1/p53 pathway is essential for the orexigenic action of ghrelin." Diabetes **60**(4): 1177-85.
Vempati, R. K., R. S. Jayani, et al. "p300-mediated acetylation of histone H3 lysine 56 functions in DNA damage response in mammals." J Biol Chem **285**(37): 28553-64.

Wang, C., L. Chen, et al. (2006). "Interactions between E2F1 and SirT1 regulate apoptotic response to DNA damage." Nat Cell Biol **8**(9): 1025-31.
Wang, H., L. Qiang, et al. (2008). "Identification of a domain within peroxisome proliferator-activated receptor gamma regulating expression of a group of genes containing fibroblast growth factor 21 that are selectively repressed by SIRT1 in adipocytes." Mol Cell Biol **28**(1): 188-200.
Wang, J. and J. Chen "SIRT1 regulates autoacetylation and histone acetyltransferase activity of TIP60." J Biol Chem **285**(15): 11458-64.
Wang, R. H., K. Sengupta, et al. (2008). "Impaired DNA damage response, genome instability, and tumorigenesis in SIRT1 mutant mice." Cancer Cell **14**(4): 312-23.
Weaver, D. R. (1998). "The suprachiasmatic nucleus: a 25-year retrospective." J Biol Rhythms **13**(2): 100-12.
Westerheide, S. D., J. Anckar, et al. (2009). "Stress-inducible regulation of heat shock factor 1 by the deacetylase SIRT1." Science **323**(5917): 1063-6.
Weyrich, P., F. Machicao, et al. (2008). "SIRT1 genetic variants associate with the metabolic response of Caucasians to a controlled lifestyle intervention--the TULIP Study." BMC Med Genet **9**: 100.
Wijnen, H. (2009). "Circadian rhythms. A circadian loop asSIRTs itself." Science **324**(5927): 598-9.
Wolfrum, C., E. Asilmaz, et al. (2004). "Foxa2 regulates lipid metabolism and ketogenesis in the liver during fasting and in diabetes." Nature **432**(7020): 1027-32.
Wu, C., C. Orozco, et al. (2009). "BioGPS: an extensible and customizable portal for querying and organizing gene annotation resources." Genome Biol **10**(11): R130.
Xu, F., Z. Gao, et al. "Lack of SIRT1 (Mammalian Sirtuin 1) activity leads to liver steatosis in the SIRT1+/- mice: a role of lipid mobilization and inflammation." Endocrinology **151**(6): 2504-14.
Yahiaoui, B., A. Taibi, et al. (1996). "A Leishmania major protein with extensive homology to silent information regulator 2 of Saccharomyces cerevisiae." Gene **169**(1): 115-8.
Yamakuchi, M., M. Ferlito, et al. (2008). "miR-34a repression of SIRT1 regulates apoptosis." Proc Natl Acad Sci U S A **105**(36): 13421-6.
Yamakuchi, M. and C. J. Lowenstein (2009). "MiR-34, SIRT1 and p53: the feedback loop." Cell Cycle **8**(5): 712-5.
Yamazaki, Y., I. Usui, et al. (2009). "Treatment with SRT1720, a SIRT1 Activator, Ameliorates Fatty Liver with Reduced Expression of Lipogenic Enzymes in MSG Mice." Am J Physiol Endocrinol Metab.
Yang, H., S. Lavu, et al. (2006). "Nampt/PBEF/Visfatin: a regulator of mammalian health and longevity?" Exp Gerontol **41**(8): 718-26.
Yang, H., T. Yang, et al. (2007). "Nutrient-sensitive mitochondrial NAD+ levels dictate cell survival." Cell **130**(6): 1095-107.
Yang, S. R., J. Wright, et al. (2007). "Sirtuin regulates cigarette smoke-induced proinflammatory mediator release via RelA/p65 NF-kappaB in macrophages in vitro and in rat lungs in vivo: implications for chronic inflammation and aging." Am J Physiol Lung Cell Mol Physiol **292**(2): L567-76.
Yang, Y., H. Cimen, et al. "NAD+-dependent deacetylase SIRT3 regulates mitochondrial protein synthesis by deacetylation of the ribosomal protein MRPL10." J Biol Chem **285**(10): 7417-29.

Yang, Y., H. Hou, et al. (2005). "Suppression of FOXO1 activity by FHL2 through SIRT1-mediated deacetylation." EMBO J **24**(5): 1021-32.
Yang, Y. H., Y. H. Chen, et al. (2000). "Cloning and characterization of two mouse genes with homology to the yeast Sir2 gene." Genomics **69**(3): 355-69.
Yeagley, D., S. Guo, et al. (2001). "Gene- and activation-specific mechanisms for insulin inhibition of basal and glucocorticoid-induced insulin-like growth factor binding protein-1 and phosphoenolpyruvate carboxykinase transcription. Roles of forkhead and insulin response sequences." J Biol Chem **276**(36): 33705-10.
Yeung, F., J. E. Hoberg, et al. (2004). "Modulation of NF-kappaB-dependent transcription and cell survival by the SIRT1 deacetylase." Embo J **23**(12): 2369-80.
Yi, J. and J. Luo "SIRT1 and p53, effect on cancer, senescence and beyond." Biochim Biophys Acta **1804**(8): 1684-9.
Yoshizaki, T., J. C. Milne, et al. (2009). "SIRT1 exerts anti-inflammatory effects and improves insulin sensitivity in adipocytes." Mol Cell Biol **29**(5): 1363-74.
Yoshizaki, T., S. Schenk, et al. "SIRT1 inhibits inflammatory pathways in macrophages and modulates insulin sensitivity." Am J Physiol Endocrinol Metab **298**(3): E419-28.
Yu, J. and J. Auwerx (2009). "The role of sirtuins in the control of metabolic homeostasis." Ann N Y Acad Sci **1173 Suppl 1**: E10-9.
Yuan, J., K. Minter-Dykhouse, et al. (2009). "A c-Myc-SIRT1 feedback loop regulates cell growth and transformation." J Cell Biol **185**(2): 203-11.
Yuan, J., M. Pu, et al. (2009). "Histone H3-K56 acetylation is important for genomic stability in mammals." Cell Cycle **8**(11): 1747-53.
Yuan, Z. and E. Seto (2007). "A functional link between SIRT1 deacetylase and NBS1 in DNA damage response." Cell Cycle **6**(23): 2869-71.
Yuan, Z., X. Zhang, et al. (2007). "SIRT1 regulates the function of the Nijmegen breakage syndrome protein." Mol Cell **27**(1): 149-62.
Zakhary, S. M., D. Ayubcha, et al. "Distribution analysis of deacetylase SIRT1 in rodent and human nervous systems." Anat Rec (Hoboken) **293**(6): 1024-32.
Zhang, J. (2007). "The direct involvement of SirT1 in insulin-induced insulin receptor substrate-2 tyrosine phosphorylation." J Biol Chem **282**(47): 34356-64.
Zhang, W., S. Patil, et al. (2006). "FoxO1 regulates multiple metabolic pathways in the liver: effects on gluconeogenic, glycolytic, and lipogenic gene expression." J Biol Chem **281**(15): 10105-17.
Zhao, W., J. P. Kruse, et al. (2008). "Negative regulation of the deacetylase SIRT1 by DBC1." Nature **451**(7178): 587-90.
Zhao, X., L. Gan, et al. (2004). "Multiple elements regulate nuclear/cytoplasmic shuttling of FOXO1: characterization of phosphorylation- and 14-3-3-dependent and -independent mechanisms." Biochem J **378**(Pt 3): 839-49.
Zhao, X., T. Sternsdorf, et al. (2005). "Regulation of MEF2 by histone deacetylase 4- and SIRT1 deacetylase-mediated lysine modifications." Mol Cell Biol **25**(19): 8456-64.
Zillikens, M. C., J. B. van Meurs, et al. (2009). "SIRT1 genetic variation is related to BMI and risk of obesity." Diabetes **58**(12): 2828-34.
Zu, Y., L. Liu, et al. "SIRT1 promotes proliferation and prevents senescence through targeting LKB1 in primary porcine aortic endothelial cells." Circ Res **106**(8): 1384-93.

Anexo A-10. Physiological modulation of the purinergic system induced by exercise influences nociception in mice: investigation of the mechanism of action

Artigo em preparação; periódico ainda não definido.

Physiological modulation of the purinergic system induced by exercise influences nociception in mice: investigation of the mechanism of action.

Marcelo O. Dietrich[1], André P. Schmidt[1,2], Catiele Antunes[1], Cristhine Schallenberger[1], Ana Elisa Böhmer[1], Luis Valmor C. Portela[1], Diogo O. Souza[1] (✉)

[1]Graduate Program in Biochemistry, Department of Biochemistry, ICBS, Federal University of Rio Grande do Sul, Porto Alegre, RS, Brazil. [2]Anesthesia and Perioperative Medicine Service at Hospital de Clínicas de Porto Alegre (HCPA), Federal University of Rio Grande do Sul, Porto Alegre, RS, Brazil.

(✉) Diogo O. Souza

Avenida Ramiro Barcelos, 2600-Anexo

Zip code: 90035-003

Porto Alegre - RS – Brazil

Phone: (55-51) 33085557 / 33085558

Fax: (55-51) 33085540 / 33085535

E-mail: diogo@ufrgs.br

Abstract

Adenosine and adenosine 5´-trifosphate (ATP) exert a modulatory role in pain conduction already well described. In this direction, several clinical and preclinical studies point the use of adenosine and its analogs in pain treatment. In the same way, exercise appears under great clinical interest. Regular physical activity, an essential component of a healthy lifestyle, recently has been shown to mediate central nervous system adaptations, to protect neurons from various brain insults, to promote neurogenesis and improve the performance in learning tasks. Although exercise effects involve alterations in plasticity, it is not known whether exercise has antinociceptive actions neither if it has a role in the regulation of purinergic system. We hypothesized that exercise, as a physiological intervention, may modulate the purinergic system in the blood-cerebrospinal (CSF) barrier and reduce pain. To address these issues, we evaluated the effects of voluntary exercise in animal models of nociception. Additionally, we sought to determine the mechanisms implicated in the analgesic effects of this training, focusing on the adenosinergic system, largely involved in nociception. We demonstrated that exercise is antinociceptive in the tail-flick, hot-plate and capsaicin tests in mice. Additionally, we demonstrated that exercise produced an increase in the CSF levels of adenosine and in the immunocontent of adenosine A_1 receptors in spinal cord. The administration of A_1 but not A_{2a} adenosine-receptor antagonist prevented the antinociceptive effects of exercise. Altogether, our findings suggest that the analgesic effects of exercise are partially mediated by its modulatory effects on the purinergic system in the central nervous system.

Keywords: Adenosine, Exercise, Purines, Pain, Antinociception.

Introduction

Adenosine and ATP, as part of purinergic system, exert multiple influences on pain transmission at peripheral and spinal sites. Although the ability of adenine-based purines to alter nociceptive transmission peripherally and centrally has been recognized for some time (Collier et al., 1966; Yarbrough and McGuffin-Clineschmidt, 1981) the last decade has seen the development of a particular interest in the role of purines in nociception. At peripheral nerve terminals in rodents, adenosine A_1 receptor activation produces antinociception by decreasing, while adenosine A_2 receptor activation produces pronociceptive or pain enhancing properties by increasing, cyclic AMP levels in the sensory nerve terminal. Adenosine receptor knockout mice, especially A_1R and A_{2A}R mice, have proven very useful to delineate mechanisms underlying adenosinergic effects on pain transmission. The use of such mice has revealed a role for A_1 receptors in mediating antinociception (Johansson et al., 2001; Wu et al., 2005) and of A_{2A} receptors in mediating hyperalgesia (Ledent et al., 1997; Hussey et al., 2007). Endogenous adenosine systems contribute to antinociceptive properties of caffeine, opioids, noradrenaline, 5-hydroxytryptamine, tricyclic antidepressants and transcutaneous electrical nerve stimulation (Keil and DeLander, 1996; Sawynok, 1998). At both peripheral and spinal sites, the manipulation of endogenous adenosine levels by inhibition of adenosine kinase can produce antinociception by activating adenosine A_1 receptor mechanisms (Sawynok, 1998).

Regular physical activity, an essential component of a healthy lifestyle, recently has been shown to mediate central nervous system (CNS) adaptations (Cotman and Berchtold, 2002). Animal studies have demonstrated that exercise protects neurons from

various brain insults (Carro et al., 2000; Larsen et al., 2000; Tillerson et al., 2003), promotes neurogenesis (van Praag et al., 1999a) and improves the performance in learning tasks (Fordyce and Farrar, 1991; van Praag et al., 1999b). Many studies have linked functional improvements, such as those reported for memory and cognition (Fordyce and Farrar, 1991; van Praag et al., 1999b) to changes in the number, structure and function of neuron (van Praag et al., 1999a). Recent studies indicate that physical activity produces these changes by altering genes involved in synaptic plasticity (Farmer et al., 2004; Dishman et al., 2006) and affects the modulation of glutamatergic synapses by increasing glutamate receptors in postsynaptic densities from cortical mice brain (Dietrich et al., 2005).

In parallel with the development of adenosine-based pharmaceuticals, there is an increasing recognition about the role of endogenous adenosine in other therapeutic modalities, such as the regular exercise activity. Studies provide strong support that physical activity beneficially alters several functions in the CNS. Although exercise effects involve alterations in plasticity, it is not known whether exercise has a role in pain transmission neither in the regulation of purinergic system. Therefore, we hypothesized that exercise, as a physiological intervention, may modulate the purinergic system in the CNS, in particular in the blood-(cerebrospinal fluid) CSF barrier, and reduce pain. To address these issues, we evaluated the effects of voluntary exercise in animal models of nociception. Additionally, we sought to determine the mechanisms involved in the analgesic effects of exercise, focusing on the adenosinergic system, largely involved in nociception.

Material and Methods

Animals: Male adult Swiss albino mice (30-40 g) were kept on a 12 hour

light/dark cycle (light on at 7:00 am) at temperature of 22 ± 1ºC, housed in plastic cages (five per cage) with tap water and commercial food *ad libitum.* Mice were divided in two groups: sedentary (Sed) and voluntarily physical active (exercise - Ex) groups. Animals from Ex group had free access, during 45 days, to a running wheel which was located within the living cage; Sed group stayed for the same time in similar conditions without running wheels. In all nociceptive behavioral experiments, the animals were acclimatized to the laboratory for at least 1 h before testing, and used only once throughout the experiments. The ethical guidelines for investigations of experimental pain in conscious animals (Zimmermann, 1983) and our institutional protocols for experiments with animals, designed to avoid suffering and limit the number of animals sacrificed, were followed throughout. The number of animals and intensities of noxious stimuli used were the minimum necessary to demonstrate the consistent effects of the drug treatments.

Drugs: Capsaicin, caffeine, naloxone, morphine and purine nucleoside phosphorylase (PNP) were purchased from Sigma Chemicals (St Louis, MO, USA). DPCPX (8-cyclopentyl-1,3-dipropylxanthine) was purchased from Tocris (Northpoint, UK). Immucillin-H and SCH58261 (5-amino-2-(2-furyl)-7-phenylethyl-pyrazolo-[4,3-e]-1,2,4-triazolo[1,5c]pyrimidine) were provided by S. Weiss (Vernalis, UK). The anesthetic sodium thiopental was obtained from Cristália (SP, Brazil). Capsaicin and Immucillin-H were diluted in DMSO (dimethyl sulfoxide, 5% and 1% respectively). All other solutions were dissolved in saline (NaCl 0.9%) and buffered with 0.1 N NaOH or 0.1 N HCl to pH 7.4 when necessary. All other chemicals were of high grade quality.

Surgical procedure: Surgery and i.c.v. infusion techniques were according to (Schmidt et al., 2000). Mice were anaesthetized with sodium thiopental (60 mg/kg, 10 ml/kg, i.p.). In an stereotaxic apparatus, the skin of the skull was removed and a 27

gauge 7 mm guide cannula was placed at 1 mm posterior to bregma, 1 mm right from de midline and 1 mm above the lateral brain ventricle. Through a 2 mm at the cranial bone, the cannula was implanted 1.5 mm ventral to the superior surface of the skull, and fixed with jeweler acrylic cement. Experiments were performed 48 hours after surgery.

Tail-flick: Nociception was assessed with a tail-flick apparatus (Albrasch Electronic Equipments, Brazil), as described in detail elsewhere (D´Amour and Smith, 1941). A source of light was positioned below the tail, focused on a point 2.3 cm rostral to the tip of the tail and the time that the mouse took to withdraw its tail from the noxious stimulus was recorded. Deflection of the tail activates a photocell and automatically terminated the trial. The light intensity was adjusted in order to obtain baseline tail flick latency (TFL) of 3-4 s. A cut-off time of 10 s was employed in order to prevent tissue damage (a mouse that did not flick by 10 s was considered as fully analgesic). On day one, the animals were habituated with the tail flick apparatus through three separate measures (data not shown). On day two, baseline tail flick latency was measured for each mouse prior to the treatments. Animals displaying at least two TFL of 10 s on the baseline were excluded from the study. Each animal was tested before treatments in order to obtain the baseline. Data are expressed as the changes in the tail-flick latencies according to the following formula: $\Delta T(s)$ = post-drug latency – pre-drug latency.

Hot-plate: The hot-plate test was used to measure the response latencies according to the method described by (Eddy and Leimbach, 1953), with minor modification. Animals were placed into a glass cylinder of 24 cm diameter on the heated (55 ± 0.5 °C) Hot Plate apparatus (Ugo Basile, model-DS 37, Italy) surface. The time between placement of the animal on the hot-plate and the occurrence of licking of the hindpaws or jumping off the surface was recorded as response latency. On day one, the

animals were habituated with the turned off apparatus. On day two, mice were tested and animals displaying baseline latencies higher than 15 s were excluded; an automatic 20 s cut-off was used to prevent tissue damage. Each animal was tested before treatments in order to obtain the baseline. Data are expressed as the changes in the tail-flick latencies according to the following formula: $\Delta T(s)$ = post-drug latency – pre-drug latency.

Hole-board: The hole-board apparatus (Ugo Basile, Italy) consisted of gray Perspex panels (40 x 40 cm, 2.2 cm thick) with 16 equidistant holes 3 cm in diameter in the floor. Photocells below the surface of the holes automatically recorded the number of head-dips. The board was positioned 15 cm above the table and divided into nine squares of 10 x 10 cm with a water-resistant marker. Each animal was placed singly in the center of the board facing away from the observer and its behavior recorded for 5 min. The number of head-dips, crossings (number of squares crossed with all four paws), rearings, groomings, and defecations was recorded, as well as the latency to start the locomotion (Vinade et al., 2003).

Measurement of motor performance: In order to evaluate non-specific muscle relaxant or neurotoxic effects, we tested the effects of exercise in the rotarod test and in the spontaneous locomotor activity test. The rotarod apparatus (Ugo Basile, Italy) consists of a rotating (18 rpm) bar (2.5 cm diameter), subdivided by disks into six compartments. As previously described (Leal et al., 2000), mice were initially trained to remain on the rotarod apparatus for 120 sec. Those not remaining on the bar for at least two out of three consecutive trials were discarded. On the day after training, the latency to fall from the rotarod (one trial with a maximum of 60 sec) was determined. The method for the spontaneous locomotor activity was adapted from (Creese et al., 1976). Activity cages (45 x 25 x 20 cm, Albarsch Electronic Equipment, Brazil), equipped with three parallel photocells, automatically record the number of crossings during 15 min.

Spontaneous alternation performance: Spontaneous alternation performance was assessed in a Y-maze. Each of the three arms was 30 cm long, 20 cm high and 6 cm wide, and converged to an equal angle. Each mouse was placed at the end of one arm and allowed to freely move through the maze for 8 min. The series of arm entries was recorded visually. An alternation was defined as entries in all three arms on consecutive occasions. The percentage of alternation was calculated as (total of alternation/total arm entries - 2) X 100, according to (Maurice et al., 1996).

Inhibitory avoidance: Mice are shocked when leaving a platform in a training session making them more prone to remain in the platform during a subsequent test session. The training apparatus was a 50x25x25-cm plastic box with a 2-cm high, 46-cm wide platform at the center of the training apparatus. The floor of the apparatus was made of parallel 0.1-cm caliber stainless-steel bars spaced 1.0-cm apart. In the training session, the animal was placed on a platform and the latency to step down the four paws on the grid was measured with a device; upon stepping down, mice received a 2 s intermittent foot shock (three 0.5s shocks, 0.2mA, with a 0.25s interval between them). Test session step-down latency 10 min and 24 h later was taken as a short- and long-time memory, to a ceiling time of 180 s. No foot shock was given in the test session.

Cerebrospinal fluid (CSF) sampling: Mice were anesthetized with sodium thiopental (60 mg/kg, 10 ml/kg, i.p.) and placed in a stereotaxic apparatus, where the CSF was drawn (10 - 20 µl per mouse) by direct puncture of the *cisterna magna* with an insulin syringe (27 gauge x 1/2 in length), with the help of a magnifying glass. All samples were centrifuged at 10,000g in an Eppendorf centrifuge during 5 min to obtain cell-free supernatants and stored in separate tubes at -70^{o}C until analysis were conducted.

HPLC procedure: High-performance liquid chromatography (HPLC) was

performed with CSF cell-free supernatants aliquots for determination of purines concentration, according to (Domanski et al., 2006). CSF concentrations of the following purines were determined: adenosine triphosphate (ATP), adenosine diphosphate (ADP), adenosine monophosphate (AMP), adenosine, guanosine triphosphate (GTP), guanosine diphosphate (GDP), guanosine monophosphate (GMP), guanosine, inosine monophosphate (IMP), inosine, hypoxanthine, xanthine, and uric acid. Analyses were performed with Shimadzu Class-VP chromatography system consisting of a quaternary gradient pump with vacuum degassing and piston desalting modules, Shimadzu SIL-10AF auto injector valve with 50 μL loop, and an UV detector. Separations were achieved on a Supelco C18 250 mm x 4.6 mm, 5 μm particle size column. The mobile phase flowed at a rate of 1.2 mL/min and the column temperature was 24 ^{o}C. Buffer composition remained unchanged (A: 150 mmol/L phosphate buffer, pH 6.0, containing 150 mmol/L potassium chloride; B: 15% acetonitrile in buffer A). The gradient profile was modified to the following content of buffer B in the mobile phase: 0% at 0.00 min, 2% at 0.05 min, 7% at 2.45 min, 50% at 10.00 min, 100% at 11.00 min, and 0% at 12.40 min. Samples of 10 μL were injected into the injection valve loop. Absorbance was read at 254 nm. CSF concentrations of purines are expressed as mean ± SEM in μM.

Electrophoresis and Western blot analysis: mice were sacrificed by decapitation and the spinal cord from both groups was collect out. Spinal cords were homogenized in 5% SDS solution containing protease inhibitor cocktail (Sigma, São Paulo/Brazil) and kept at -70°C. Protein content was further determined by using Bicinchoninic acid assay using bovine serum albumin (BSA) as standard (Pierce, São Paulo/Brazil). Proteins from spinal cord preparations were separated by 12% SDS-PAGE mini-gels and transferred to nitrocellulose membrane using a Trans-Blot system (Bio-Rad, Porto Alegre, Brazil). After blocking for 2 h at room temperature with 5% milk in Tris-buffered saline, pH 7.6

containing 0.1% Tween 20 (TBS–T), the membranes were incubated overnight at 4 °C with either a rabbit anti-adenosine A_1 receptor antibody (1:1000 dilution from Affinity Bioreagents) or anti-adenosine A_{2A} receptor antibody (1:5000 dilution from Sigma). After primary antibodies incubation, membranes were washed and incubated with alkaline phosphatase-conjugated secondary antibodies for 2 h at room temperature and developed with ECL (Amersham, São Paulo/Brazil). The autoradiographic films were scanned and densitometric analyses were performed using public domain NIH Image Program (developed at the U.S. National Institutes of Health and available on the internet at http://rsb.info.nih.gov/nih-image/). We used Coomassie blue stain in gels, analyzed by NIH Image, and Ponceau S red stain in membranes to be sure the same quantity of protein was loaded in each lane (5 Ag/lane). The results were presented by A_1 or A_{2A} receptor arbitrary units.

Statistical analysis: Data are expressed as mean ± SEM. Differences among groups were determined by one-way analysis of variance (ANOVA), followed by Student-Newman-Keuls test when applicable. $P < 0.05$ was considered of statistical significance.

Results

Involvement of adenosine in the antinociceptive effects of exercise

We first explored if exercise could promote analgesia in animal models of nociception. The results presented in Fig. 1A shows that exercise was able to decrease pain sensation against i.pl. capsaicin. Fig. 1B shows that the non-selective opioid-receptor antagonist naloxone completely prevented morphine- and exercise-induced antinociception. Fig. 1C shows that i.p. administration of adenosine produced antinociception in the i.pl. capsaicin tests in sedentary mice and its effect was prevented

by pretreatment with caffeine (10 $mg.kg^{-1}$, i.p.), a non-selective adenosine receptor antagonist, and the same effect was observed in exercise mice. Next, we investigated if the pretreatment with A_1 or A_{2A} adenosine-receptor antagonists would be able to prevent the effect of exercise against capsaicin test. The results depicted in Fig. 1D shows that the selective A_1 adenosine-receptor antagonist DPCPX (0.1 $mg.kg^{-1}$), but not the selective A_{2A} adenosine-receptor antagonist SCH58261 (0.5 $mg.kg^{-1}$) prevented antinociception induced by adenosine and exercise in the capsaicin pain tests.

Effects of exercise in promote analgesia against i.pl. capsaicin was reproduced in tail-flick model. Fig. 2A shows that exercise promoted analgesia either on tail flick test. As expected, morphine 3.0 $mg.kg^{-1}$, which was taken as a positive control, strongly impaired the nociceptive response in tail flick test ($P < 0.001$) when administered to sedentary mice. Naloxone prevented morphine- and exercise-induced antinociception. However, in this pain model, neither caffeine nor DPCPX prevented the antinociceptive effects of exercise (Figs 2C and 2D). Actually, SCH58261 presented a slight increase in antinociceptive effects of exercise.

Exercise was able to reduce pain in a third model of nociception, hot plate-induced pain (Fig. 3A). In addition (Fig. 3B), the non-selective opioid-receptor antagonist naloxone, which had no intrinsic effect over nociception, completely prevented morphine- and exercise-induced antinociception. Fig. 1C shows that i.p. administration of adenosine produced antinociception on hot plate test in sedentary mice and its effect was prevented by pretreatment with caffeine, the same occurring with antinociceptive effects of exercise. In relation to adenosine-receptor antagonist effects (Fig. 3D), we observed that DPCPX and SCH58261 had a similar effect to that observed in capsaicin test: reversion and maintenance of adenosine and exercise antinociception, respectively.

Spinal cord immunocontent of adenosine receptors and CSF purine levels are modulated by exercise

We investigated the mechanisms implicated in the analgesic effects of exercise, focusing in the adenosinergic system, largely involved in nociception. Since adenosine is widely distributed through the organs, not exclusively in the CNS, we decided to verify adenosine-receptors immunocontent in spinal cord, a critical site for conduction of pain signals to the brain. Western blotting approach was performed and we immunodetected adenosine receptors in the spinal cord. We found out an increased immunocontent of A_1 receptors (fig.4A), but not of A_{2A} receptors (fig.4B**).**

Once the cerebrospinal fluid is rapidly distributed in the up-to-down direction with rapid penetration of the spinal cord tissue, we looked in the CSF levels of adenosine and its metabolites. CSF concentrations of adenosine as well GTP, GDP and guanosine were significantly increased in exercised mice in comparison with sedentary control, in spite of a significant decrease hypoxanthine, xanthine and uric acid (Fig. 5). Exercise did not affect ATP, ADP, AMP, GMP, IMP and inosine CSF levels.

Two interconnected compartments are responsible for the control of extracellular purines and need to be distinguished: the vascular endothelium forming the blood–brain barrier within the brain interstitial compartment, and the choroid epithelium forming the blood–CSF barrier. Thus, we decided to study the purine hydrolysis by choroid plexus which is implicated in the active clearance of purines from CSF to blood. Fig. 6 (A-D) shows the nucleotides hydrolysis by choroid plexus. When we analyzed all the purines and its metabolites at the baseline (Fig. 6A), no difference is evident, but when we look to a curve of time, we found that ADP levels are increased in the 5^{th} minute (Fig 6A). No effect was found in a time curve for GTP, GDP, GMP and guanosine (Fig. 6C). When

we looked for metabolites, we found an increase in inosine levels as well as a decrease in xanthine and uric acid (Fig. 6D).

Inhibition of purine metabolism causes antinociception

Because the enzyme that converts adenosine in hypoxanthine is PNP, a ubiquitous enzyme essential for purine metabolism which is active in rodent's CSF, we postulated exercise has a PNP-inhibitor-like effect, accumulating adenosine, and decreasing levels of its downstream metabolites. To confirm our hypothesis, we injected mice i.c.v. with the PNP inhibitor immucillin-H and checked if it mimics the effects of exercise in nociception. Indeed, we used immucillin-H 12.5 μM injected into the CSF to achieve a final CSF concentration of 1 μM. Immucillin-H promoted notable analgesia in a similar fashion as did exercise (Fig. 7). In other group, we injected mice i.c.v. with PNP (2 units/mouse) and no effect was observed.

Exercise and antinociception memory (neuroplasticity)

Considering that we demonstrated that exercise is able to reduce pain in three different models of pain, we decided to investigate if these effects would be maintained with the interruption of training. Thus, we let mice in running wheels for 45 days and after 30 days of detraining, animals returned to exercise for 15 days. Pain tests were performed in these three moments: training, detraining and retraining. Analgesic effects were observed in capsaicin and tail-flick tests during training from the 7^{th} day through the 45^{th} day (Fig. 8). However, on hot-plate model, analgesic effects were observed only in the 7^{th} day of training. On detraining period, any effect was observed on capsaicin, tail-flick and hot-plate models. When animals returned to exercise, significant analgesia was observed in capsaicin model (during 3^{rd}, 7^{th} and 15^{th}) session tests and tail-flick

model (during 7th and 15th session tests), but no difference was observed in hot plate-induce pain.

Exercise and behavioral tests

In the hole-board model, exercise did not affect latency to first head-dip, and the number of head-dips, rearings, groomings and defecations, but decreased the number of crossings (Fig. 9). No effect on motor performance in the rotarod test was observed. Additionally, exercise reduced spontaneous locomotor activity on the 3rd and 30th day locomotion as measured by activity cages as shown in Fig. 10A, but did not affect the time exploring the center (Fig. 10B) neither the spontaneous alternation performance in the Y-maze (Fig. 10C). As we observed an effect memory-like in analgesic properties of exercise, it was necessary to analyze memory *per se*. Then, to evaluate memory, animals were submitted to inhibitory avoidance task. We evaluated short- and long-term memory and no difference was observed between sedentary and exercise groups (Fig. 10D).

Discussion

It has been shown that regular physical activity mediates central nervous system (CNS) adaptations (Cotman and Berchtold, 2002) and is involve in the modulation of various brain processes (Fordyce and Farrar, 1991; Carro et al., 2000; Larsen et al., 2000; Tillerson et al., 2003). The present results indicate that 45 days of voluntary exercise presents antinociceptive effects against three models of pain, capsaicin, tail-flick and hot-plate. Additionally, we showed that non-selective opioid-receptor antagonist naloxone completely prevented exercise-induced antinociception. These results indicate that exercise effects on antinociception are related to opioid and adenosine (A_1) receptors.

In this work we showed that exercise effects are due, at less in part, to modulation of the purinergic system. Treatment with adenosine showed analgesic effects as already described elsewhere (Gyllenhammar and Nordfors, 2001). The peripheral actions of adenosine in rodents depend very much upon the adenosine receptor subtype activated. Adenosine can alter pain transmission by actions on both nociceptive afferent and transmission neurons, and these actions are mediated primarily by adenosine A_1 receptors (Sawynok, 1998; Sawynok et al., 1999). Thus, the exogenous administration of adenosine A_1 agonists locally to the hindpaw of the rat produces antinociception in a pressure hyperalgesia model (Taiwo and Levine, 1990) and in the formalin model (Karlsten et al., 1992). In contrast, local administration of adenosine A_2 receptor agonists enhances pain responses in both models (Taiwo and Levine, 1990; Karlsten et al., 1992), an action most likely due to adenosine A_{2A} receptor activation (Doak and Sawynok, 1995). In this work, when mice were pretreated with caffeine, a non-selective adenosine receptor antagonist, the antinociceptive effect was abolished either in sedentary control mice that received adenosine after pretreatment and in exercise group. It is important to consider that the local administration of caffeine has not demonstrated any antinociceptive properties, perhaps because of its mixed profile of activity against both adenosine A_1 and A_2 receptors (Doak and Sawynok, 1995). The present results provide the first direct evidence that adenosine A_1 receptors are involved in analgesic effects of exercise in mice. Administration of DPCPX, a selective A_1 adenosine-receptor antagonist entirely prevented the analgesic effect of exercise. This action is not share with A_{2A} receptors once its inhibition had no effect over exercise antinociception. By western blotting approach, we immunodetected adenosine receptor levels in the spinal cord and we found out an increased immunocontent of A_1 receptor but not of A_{2a} receptor. It is additional evidence that A_1 receptors mediate the antinociceptive effects of

exercise.

Endogenous adenosine can be released from brain, spinal cord and peripheral tissues, and the regulation of such release by various pharmacological agents can alter pain processing through activation of adenosine A_1 receptors on neurons, and perhaps other receptors on adjacent structures. In the CSF, adenosine, GTP, GDP and guanosine were significantly increased in exercise mice in comparison with sedentary control, in spite of a significant decrease hypoxanthine, xanthine and uric acid. It is an evidence that exercise may modulate the endogenous levels of adenosine probably by decrease its degradation and thus assign antinociceptive benefits.

Following these results, we found that hydrolysis of purines by choroid plexus is affected by exercise. We observed an increase in CSF levels of ADP at 5 min with a concomitant decrease in xanthine at 5 min. It is an indicative of central accumulation of ADP, a precursor of adenosine. It was already described that the concentration of adenosine in the brain interstitial fluid under resting conditions remains low, probably between 120 and 220 nM, despite constant production from both extracellular and intracellular sources (Latini and Pedata, 2001). Here, we observed that adenosine levels did not change with exercise, but ADP levels are significantly increased, an effect that could be an indicative of central accumulation of ADP, a precursor of adenosine.

In physiological conditions, adenosine may enter brain interstitial fluid from the blood through the blood–brain barrier and may be removed by brain endothelial cells, followed by either an efflux to blood or metabolic degradation. *In vivo* this system probably serves to excrete the purine metabolites from cerebrospinal fluid into the blood (Berlin, 1969). Thus, the choroid plexus may serve as an excretory mechanism for endogenous purine metabolites from brain, thereby regulating their levels in the CSF.

Besides the modulation of purinergic system in the blood-CSF barrier by exercise

and its antinociceptive effects, evidence to the participation of this system in the exercise effects appears from experiments with Immucillin-H, a PNP-inhibitor. While PNP is an enzyme that converts adenosine in hypoxanthine, its inhibition is responsible for accumulate adenosine and decrease levels of its metabolites. Administration of immucillin-H promoted notable analgesia in a similar fashion as did exercise and PNP administration had no effect. It is in accordance with the modulation of CSF levels of purines by exercise. Mice trained in running wheels for 45 days showed antinociception against pain models in parallel with an increased in CSF adenosine levels and a concomitant decrease in its metabolites. In the same way, when we block the degradation of adenosine with Immucillin, increasing its levels, we observed the same effects showed by exercise.

Recently, evidence has accumulated suggesting that physical activity enhances cognition in rodents (Suominen-Troyer et al., 1986; Rogers et al., 1990; van Praag et al., 1999b; Winter et al., 2007) and researchers have shown that in hippocampus, a brain area important for learning and memory, presents a robust increase in new neurons associated with exercise (van Praag et al., 1999b; van Praag et al., 1999a). Here we showed that animals trained during 45 days have an important reduction in pain sensibility, notable already in the 7^{th} day of training. However, after activity has been interrupted, the antinociception is lost. Interestingly, with a retraining, the antinociception against capsaicin-induced pain returns since the 3^{rd} day and in tail flick model returns in the 7^{th} day, but no effect was detectable on hot plate model. In inhibitory avoidance task no difference was observed between groups. Then, these effects along the time seem to be related to a spinal cord neuroplasticity induced by exercise (memory-like effect at a spinal cord level).

In summary, to the best of our knowledge, this is the first study investigating the

antinociceptive effects of voluntary exercise in traditional animal pain models. Exercise-induced antinociception may be related to modulatory effects in the purinergic system, probably due to a decrease in degradation of adenosine with its subsequent accumulation in the CSF and an increase in the immunocontent of adenosine A_1 receptors at the spinal cord. Considering that the clinical use of adenosine and its analogs is not a reality, the non-pharmacological approaches appear as a good option to control pain sensation. Exercise, as a physiological intervention, arises as possible mechanism to control pain and modulate purinergic system besides being able to improve systemic functions and brain health.

Acknoledgements:

Supported by the FINEP research grant “Rede Instituto Brasileiro de Neurociência (IBN-Net)” # 01.06.0842-00, CNPq, CAPES, FAPERGS, UFRGS.

References

Berlin RD (1969) Purines: active transport by isolated choroid plexus. Science 163:1194-1195.

Calcagnetti DJ, Fleetwood SW, Holtzman SG (1990) Pharmacological profile of the potentiation of opioid analgesia by restraint stress. Pharmacol Biochem Behav 37:193-199.

Carro E, Nunez A, Busiguina S, Torres-Aleman I (2000) Circulating insulin-like growth factor I mediates effects of exercise on the brain. J Neurosci 20:2926-2933.

Collier HO, James GW, Schneider C (1966) Antagonism by aspirin and fenamates of bronchoconstriction and nociception induced by adenosine-5'-triphosphate. Nature 212:411-412.

Cotman CW, Berchtold NC (2002) Exercise: a behavioral intervention to enhance brain health and plasticity. Trends Neurosci 25:295-301.

Creese I, Burt DR, Snyder SH (1976) Dopamine receptor binding predicts clinical and pharmacological potencies of antischizophrenic drugs. Science 192:481-483.

D´Amour FE, Smith DL (1941) A method for determining loss of pain sensation. J Pharmacol Exp Ther 72:74-79.

Dietrich MO, Mantese CE, Porciuncula LO, Ghisleni G, Vinade L, Souza DO, Portela LV (2005) Exercise affects glutamate receptors in postsynaptic densities from cortical mice brain. Brain Res 1065:20-25.

Dishman RK, Berthoud HR, Booth FW, Cotman CW, Edgerton VR, Fleshner MR, Gandevia SC, Gomez-Pinilla F, Greenwood BN, Hillman CH, Kramer AF, Levin BE, Moran TH, Russo-Neustadt AA, Salamone JD, Van Hoomissen JD, Wade CE, York DA, Zigmond MJ (2006) Neurobiology of exercise. Obesity (Silver Spring) 14:345-356.

Doak GJ, Sawynok J (1995) Complex role of peripheral adenosine in the genesis of the response to subcutaneous formalin in the rat. Eur J Pharmacol 281:311-318.

Domanski L, Sulikowski T, Safranow K, Pawlik A, Olszewska M, Chlubek D, Urasinska E, Ciechanowski K (2006) Effect of trimetazidine on the nucleotide profile in rat kidney with ischemia-reperfusion injury. Eur J Pharm Sci 27:320-327.

Eddy NB, Leimbach D (1953) Synthetic analgesics. II. Dithienylbutenyl- and dithienylbutylamines. J Pharmacol Exp Ther 107:385-393.

Farmer J, Zhao X, van Praag H, Wodtke K, Gage FH, Christie BR (2004) Effects of voluntary exercise on synaptic plasticity and gene expression in the dentate gyrus of adult male Sprague-Dawley rats in vivo. Neuroscience 124:71-79.

Fordyce DE, Farrar RP (1991) Enhancement of spatial learning in F344 rats by physical activity and related learning-associated alterations in hippocampal and cortical cholinergic functioning. Behav Brain Res 46:123-133.

Gyllenhammar E, Nordfors LO (2001) Systemic adenosine infusions alleviated neuropathic pain. Pain 94:121-122.

Hussey MJ, Clarke GD, Ledent C, Hourani SM, Kitchen I (2007) Reduced response to the formalin test and lowered spinal NMDA glutamate receptor binding in adenosine A2A receptor knockout mice. Pain 129:287-294.

Johansson B, Halldner L, Dunwiddie TV, Masino SA, Poelchen W, Gimenez-Llort L, Escorihuela RM, Fernandez-Teruel A, Wiesenfeld-Hallin Z, Xu XJ, Hardemark A, Betsholtz C, Herlenius E, Fredholm BB (2001) Hyperalgesia, anxiety, and decreased hypoxic neuroprotection in mice lacking the adenosine A1 receptor. Proc Natl Acad Sci U S A 98:9407-9412.

Karlsten R, Gordh T, Post C (1992) Local antinociceptive and hyperalgesic effects in the formalin test after peripheral administration of adenosine analogues in mice.

Pharmacol Toxicol 70:434-438.

Keil GJ, 2nd, DeLander GE (1996) Altered sensory behaviors in mice following manipulation of endogenous spinal adenosine neurotransmission. Eur J Pharmacol 312:7-14.

Larsen JO, Skalicky M, Viidik A (2000) Does long-term physical exercise counteract age-related Purkinje cell loss? A stereological study of rat cerebellum. J Comp Neurol 428:213-222.

Latini S, Pedata F (2001) Adenosine in the central nervous system: release mechanisms and extracellular concentrations. J Neurochem 79:463-484.

Leal MB, de Souza DO, Elisabetsky E (2000) Long-lasting ibogaine protection against NMDA-induced convulsions in mice. Neurochem Res 25:1083-1087.

Ledent C, Vaugeois JM, Schiffmann SN, Pedrazzini T, El Yacoubi M, Vanderhaeghen JJ, Costentin J, Heath JK, Vassart G, Parmentier M (1997) Aggressiveness, hypoalgesia and high blood pressure in mice lacking the adenosine A2a receptor. Nature 388:674-678.

Maurice T, Lockhart BP, Privat A (1996) Amnesia induced in mice by centrally administered beta-amyloid peptides involves cholinergic dysfunction. Brain Res 706:181-193.

Rogers RL, Meyer JS, Mortel KF (1990) After reaching retirement age physical activity sustains cerebral perfusion and cognition. J Am Geriatr Soc 38:123-128.

Sawynok J (1998) Adenosine receptor activation and nociception. Eur J Pharmacol 347:1-11.

Sawynok J, Reid A, Liu XJ (1999) Acute paw oedema induced by local injection of adenosine A(1), A(2) and A(3) receptor agonists. Eur J Pharmacol 386:253-261.

Schmidt AP, Lara DR, Maraschin JF, Perla AS, Souza DO (2000) Guanosine and

GMP prevent seizures induced by quinolinic acid in mice. Brain Res 864:40-43.

Suominen-Troyer S, Davis KJ, Ismail AH, Salvendy G (1986) Impact of physical fitness on strategy development in decision-making tasks. Percept Mot Skills 62:71-77.

Taiwo YO, Levine JD (1990) Direct cutaneous hyperalgesia induced by adenosine. Neuroscience 38:757-762.

Tillerson JL, Caudle WM, Reveron ME, Miller GW (2003) Exercise induces behavioral recovery and attenuates neurochemical deficits in rodent models of Parkinson's disease. Neuroscience 119:899-911.

van Praag H, Kempermann G, Gage FH (1999a) Running increases cell proliferation and neurogenesis in the adult mouse dentate gyrus. Nat Neurosci 2:266-270.

van Praag H, Christie BR, Sejnowski TJ, Gage FH (1999b) Running enhances neurogenesis, learning, and long-term potentiation in mice. Proc Natl Acad Sci U S A 96:13427-13431.

Vinade ER, Schmidt AP, Frizzo ME, Izquierdo I, Elisabetsky E, Souza DO (2003) Chronically administered guanosine is anticonvulsant, amnesic and anxiolytic in mice. Brain Res 977:97-102.

Winter B, Breitenstein C, Mooren FC, Voelker K, Fobker M, Lechtermann A, Krueger K, Fromme A, Korsukewitz C, Floel A, Knecht S (2007) High impact running improves learning. Neurobiol Learn Mem 87:597-609.

Wu WP, Hao JX, Halldner L, Lovdahl C, DeLander GE, Wiesenfeld-Hallin Z, Fredholm BB, Xu XJ (2005) Increased nociceptive response in mice lacking the adenosine A1 receptor. Pain 113:395-404.

Yarbrough GG, McGuffin-Clineschmidt JC (1981) In vivo behavioral assessment of central nervous system purinergic receptors. Eur J Pharmacol 76:137-144.

Zimmermann M (1983) Ethical guidelines for investigations of experimental pain in conscious animals. Pain 16:109-110.

Legends:

Figure 1: Effects of exercise against i.pl. capsaicin test in mice. Columns represent mean time spent licking the injected hindpaw and vertical bars represent SEM. (A) Effects of exercise against capsaicin-induced pain. (B) Effects of pretreatment with naloxone (1 $mg.kg^{-1}$) on morphine-(3 $mg.kg^{-1}$) or exercise-induced antinociception. (C) Effects of pretreatment with caffeine (10 $mg.kg^{-1}$) on adenosine-(100 $mg.kg^{-1}$) or exercise-induced antinociception. (D) Effects of pretreatment with DPCPX (0.1 $mg.kg^{-1}$) or SCH58261 (0.5 $mg.kg^{-1}$) on adenosine-(100 $mg.kg^{-1}$) or exercise-induced antinociception. N = 8 – 10 animals per group. * = $P < 0.05$ and ** = $P < 0.01$ as compared to control, one-way ANOVA followed by Student-Newman-Keuls test.

Figure 2: Effects of exercise against the tail-flick test in mice. Columns represent the changes in the tail-flick latencies according to the following formula: $\Delta T(s)$ = post-drug latency – pre-drug latency and vertical bars represent SEM. (A) Effects of exercise in the tail-flick test. (B) Effects of pretreatment with naloxone (1 $mg.kg^{-1}$) on morphine-(3 $mg.kg^{-1}$) or exercise-induced antinociception. (C) Effects of pretreatment with caffeine (10 $mg.kg^{-1}$) on adenosine-(100 $mg.kg^{-1}$) or exercise-induced antinociception. (D) Effects of pretreatment with DPCPX (0.1 $mg.kg^{-1}$) or SCH58261 (0.5 $mg.kg^{-1}$) on adenosine-(100 $mg.kg^{-1}$) or exercise-induced antinociception. N = 8 – 10 animals per group. * = $P < 0.05$, ** = $P < 0.01$ and *** = $P < 0.01$ as compared to control, one-way ANOVA followed by Student-Newman-Keuls test.

Figure 3: Effects of exercise against the hot-plate test in mice. Columns represent the changes in the tail-flick latencies according to the following formula: $\Delta T(s)$ = post-drug latency – pre-drug latency and vertical bars represent SEM. (A) Effects of exercise in the

hot-plate test. (B) Effects of pretreatment with naloxone (1 $mg.kg^{-1}$) on morphine-(3 $mg.kg^{-1}$) or exercise-induced antinociception. (C) Effects of pretreatment with caffeine (10 $mg.kg^{-1}$) on adenosine-(100 $mg.kg^{-1}$) or exercise-induced antinociception. (D) Effects of pretreatment with DPCPX (0.1 $mg.kg^{-1}$) or SCH58261 (0.5 $mg.kg^{-1}$) on adenosine-(100 $mg.kg^{-1}$) or exercise-induced antinociception. N = 8 – 10 animals per group. * = $P < 0.05$, ** = $P < 0.01$ and *** = $P < 0.01$ as compared to control, one-way ANOVA followed by Student-Newman-Keuls test.

Figure 4: Effect of 45 days of voluntary exercise on the immunocontent of A_1 e A_{2A} adenosine-receptors (panels A e B, respectively) in spinal cord from mice. Representative Western blot lanes are shown. Histograms represent arbitrary units in sedentary controls and exercise mice through densitometric quantification of immunoblots. Columns represent mean and vertical bars represent SEM. N = 4 – 5. Sed = sedentary group; Ex = voluntary exercise group. * = $P < 0.05$ as compared to control (sedentary), unpaired Student-*t*-test.

Figure 5: Effects of 45 days of voluntary exercise on CSF levels of adenosine triphosphate (ATP), adenosine diphosphate (ADP), adenosine monophosphate (AMP), adenosine, guanosine triphosphate (GTP), guanosine diphosphate (GDP), guanosine monophosphate (GMP), guanosine (GUO), inosine monophosphate (IMP), inosine (INO), hypoxanthine (HX), xanthine (XA), and uric acid (UA). The columns represent means (μM) and vertical bars represent SEM. N = 10 animals per group. * = $P < 0.05$ as compared to control (sedentary), one-way ANOVA followed by Student-Newman-Keuls test.

Figure 6: Effects of 45 days of voluntary exercise on the concentration of purines exposed to the choroid plexus *ex vivo*. (A) Basal secretion of purines from choroid plexus. Adenosine triphosphate (ATP), adenosine diphosphate (ADP), adenosine monophosphate (AMP), adenosine, guanosine triphosphate (GTP), guanosine diphosphate (GDP), guanosine monophosphate (GMP), guanosine (GUO), inosine monophosphate (IMP), inosine (INO), hypoxanthine (HX), xanthine (XA), and uric acid (UA); (B), (C) and (D) represent medium concentration of purines after exposition to ATP (1 mM). (B) Time curve of ATP, ADP, AMP and adenosine; (C) Time curve of GTP, GDP, GMP and guanosine; (D) Time curve of INO, HX, XA and UA. The columns represent means (μM) and vertical bars represent SEM. N = 10 animals per group. * = $P < 0.05$ compared to control (sedentary), unpaired Student-*t*-test.

Figure 7: Effects of Immucillin-H (ImmH – 12.5 μM) and PNP (2 units per mouse) against i.pl. capsaicin-induced pain. Mice were treated with an i.c.v. injection of Immucillin-H, PNP or vehicle (DMSO 1%). After 5 min, animals received an i.pl. injection of capsaicin. N = 10 animals per group. * = $P < 0.01$ compared to vehicle (control), one-way ANOVA followed by Student-Newman-Keuls test.

Figure 8: Time curve of exercise against i.pl. capsaicin, tail-flick and hot-plate pain tests in mice. Animals were trained for 45 days, detrained for 30 days e retrained for 15 days. Tests were performed in different times during training, detraining and retraining. (A) Capsaicin-induced pain, (B) tail-flick (C) hot-plate. (A) - columns represent mean time spent licking the injected hindpaw and vertical bars represent SEM. (B) and (C) - Columns represent the changes in the tail-flick latencies according to the following formula: ΔT(s) = post-drug latency – pre-drug latency and vertical bars represent SEM.

N = 10 – 15 animals per group. * = $P < 0.05$ as compared to control (sedentary), unpaired Student-*t*-test.

Figure 9: Effects of exercise in the mice hole-board, spontaneous locomotor activity and rotarod tests. (A) head-dips; (B) latency to the first head-dip; (C) squares crossed; (D) rearings; (E) groomings; (F) defecation; (G) Number of crossings (activity test), (H) latency to fall (rotarod test). The columns represent mean and vertical bars represent SEM. N = 8 animals per group. * = $P < 0.05$ as compared to control (sedentary), unpaired Student-*t*-test.

Figure 10: Effects of exercise in memory, anxiety and locomotor parameters in mice. (A) Effects of exercise on locomotor activity; (B) Time exploring the center of a new environment; (C) spontaneous alternation performance in the Y-maze test; (D) Effects of exercise on the inhibitory avoidance task. N = 8 animals per group. * = $P < 0.05$ as compared to control (sedentary), unpaired Student-*t*-test.

Figure 1:

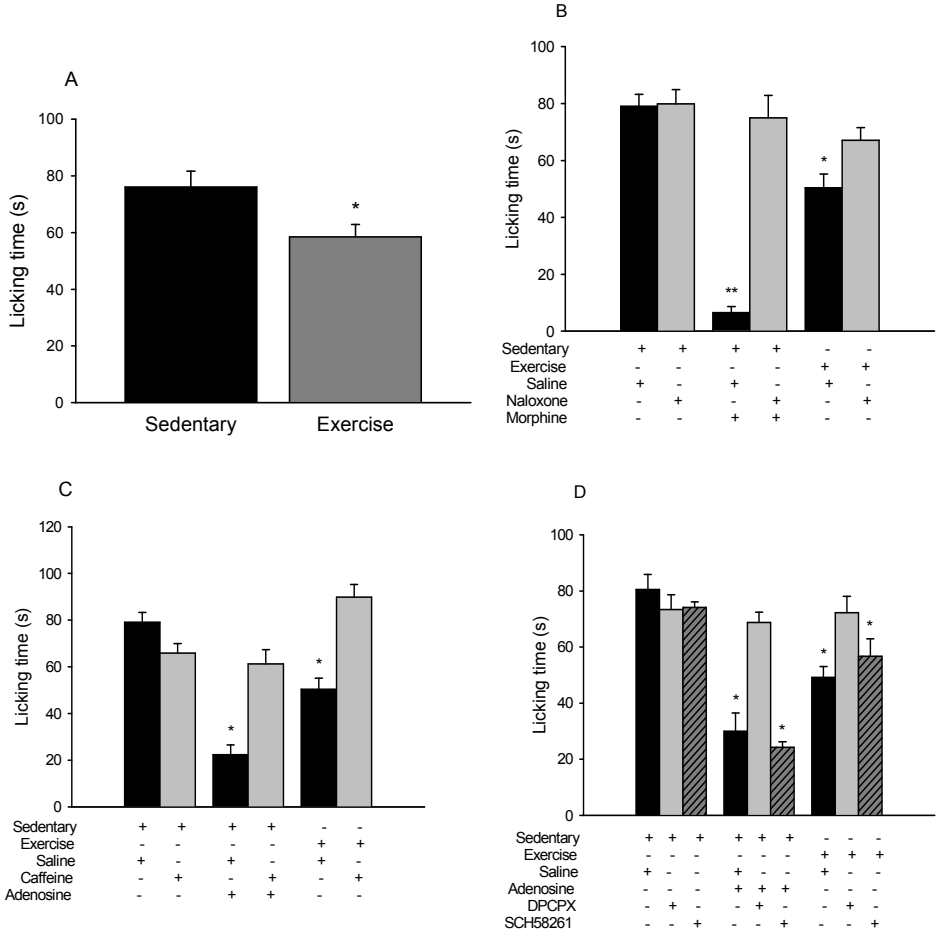
A
Licking time (s)
100
80
60
40
20
0
*
Sedentary
Exercise
B
Licking time (s)
100
80
60
40
20
0
**
*
Sedentary + + + + - -
Exercise - - - - + +
Saline + - + - + -
Naloxone - + - + - +
Morphine - - + + - -
C
Licking time (s)
120
100
80
60
40
20
0
*
*
Sedentary + + + + - -
Exercise - - - - + +
Saline + - + - + -
Caffeine - + - + - +
Adenosine - - + + - -
D
Licking time (s)
100
80
60
40
20
0
*
*
*
*
Sedentary + + + + + + - - -
Exercise - - - - - - + + +
Saline + - - + - - + - -
Adenosine - - - + + + - - -
DPCPX - + - - + - - + -
SCH58261 - - + - - + - - +

Figure 2:

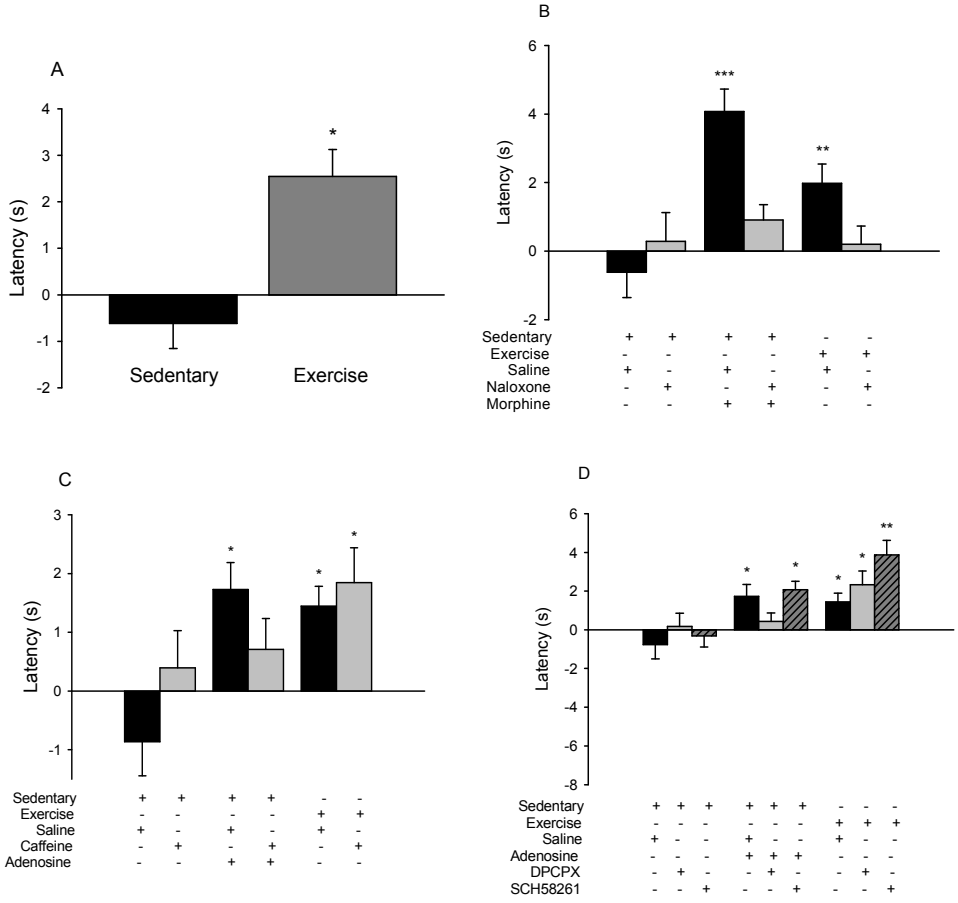
A
Latency (s)
Sedentary
Exercise
B
Latency (s)
Sedentary
Exercise
Saline
Naloxone
Morphine
C
Latency (s)
Sedentary
Exercise
Saline
Caffeine
Adenosine
D
Latency (s)
Sedentary
Exercise
Saline
Adenosine
DPCPX
SCH58261

Figure 3:

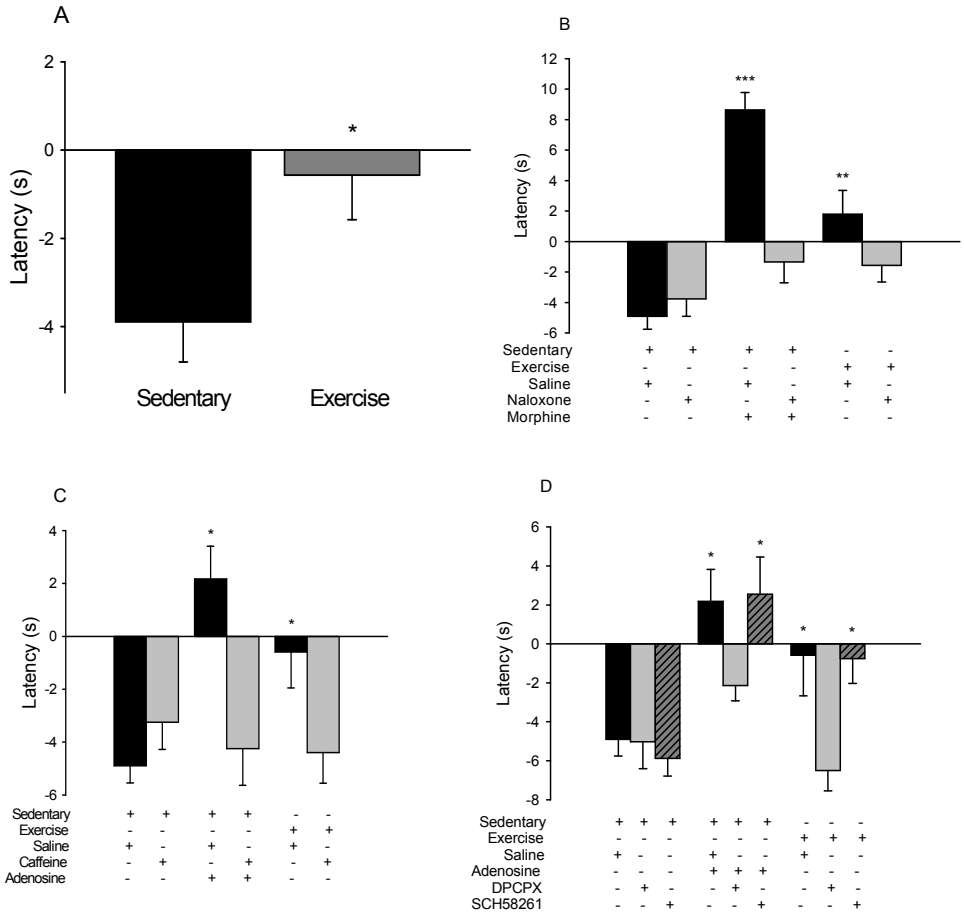
A
Latency (s)
Sedentary
Exercise
B
Latency (s)
Sedentary
Exercise
Saline
Naloxone
Morphine
C
Latency (s)
Sedentary
Exercise
Saline
Caffeine
Adenosine
D
Latency (s)
Sedentary
Exercise
Saline
Adenosine
DPCPX
SCH58261

Figure 4:

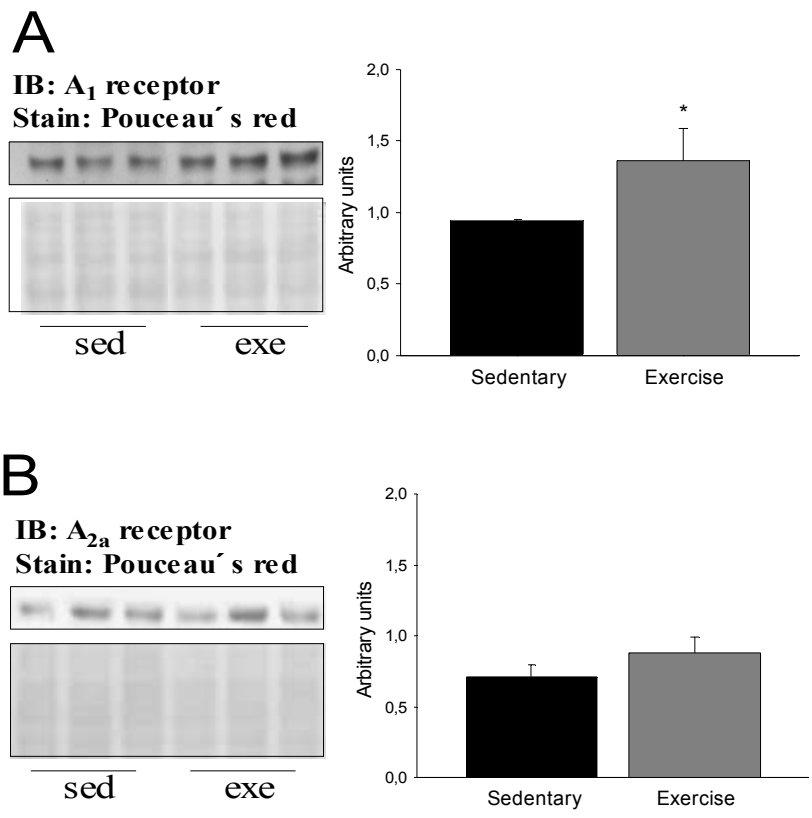
A
IB: A1 receptor
Stain: Pouceau´s red
sed
exe
Arbitrary units
2,0
1,5
1,0
0,5
0,0
*
Sedentary
Exercise
B
IB: A2a receptor
Stain: Pouceau´s red
sed
exe
Arbitrary units
2,0
1,5
1,0
0,5
0,0
Sedentary
Exercise

Figure 5:

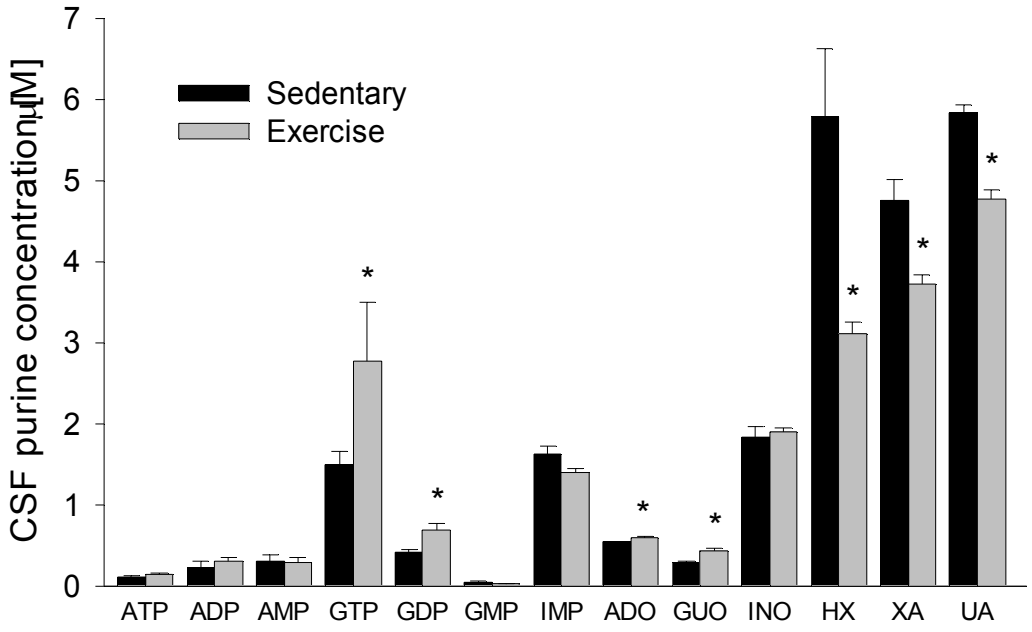
CSF purine concentration [μM]
Sedentary
Exercise
0
1
2
3
4
5
6
7
ATP
ADP
AMP
GTP
GDP
GMP
IMP
ADO
GUO
INO
HX
XA
UA
*

Figure 6:

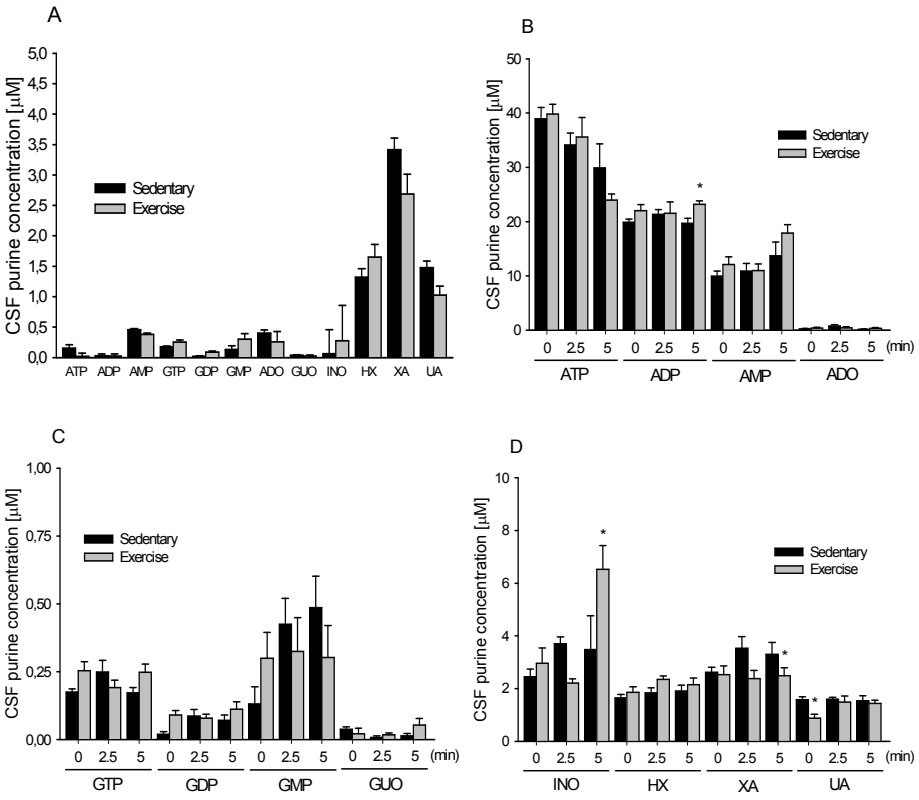
A
CSF purine concentration [µM]
Sedentary
Exercise
ATP ADP AMP GTP GDP GMP ADO GUO INO HX XA UA
B
CSF purine concentration [µM]
Sedentary
Exercise
0 2.5 5 (min)
ATP ADP AMP ADO
C
CSF purine concentration [µM]
Sedentary
Exercise
0 2.5 5 (min)
GTP GDP GMP GUO
D
CSF purine concentration [µM]
Sedentary
Exercise
0 2.5 5 (min)
INO HX XA UA

Figure 7:

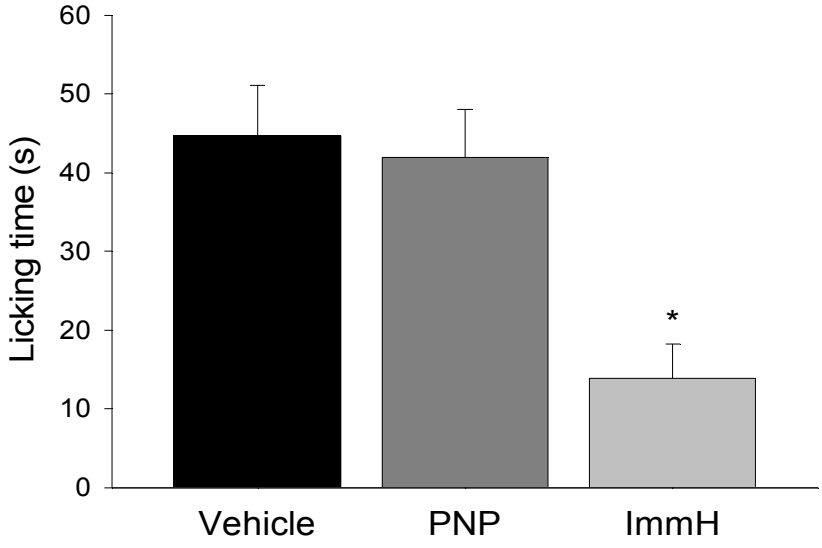

Figure 8:

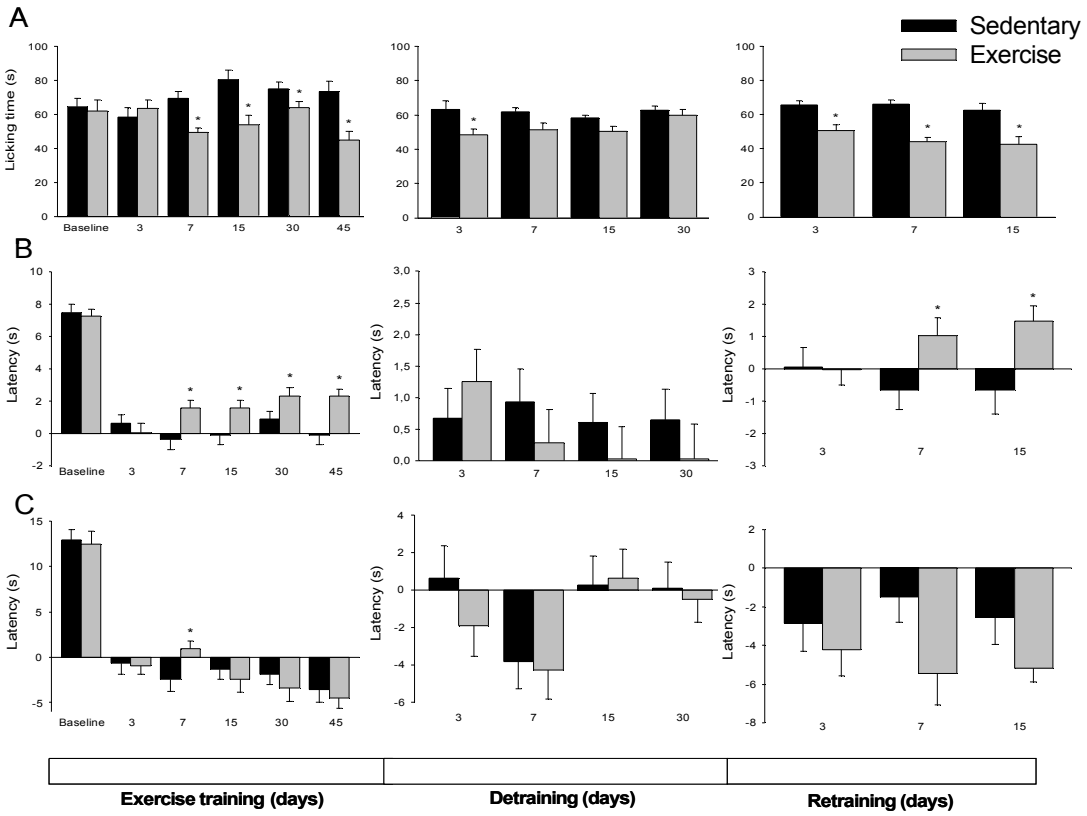
A
Sedentary
Exercise
Licking time (s)
Baseline
3
7
15
30
45
B
Latency (s)
C
Exercise training (days)
Detraining (days)
Retraining (days)

Figure 9:

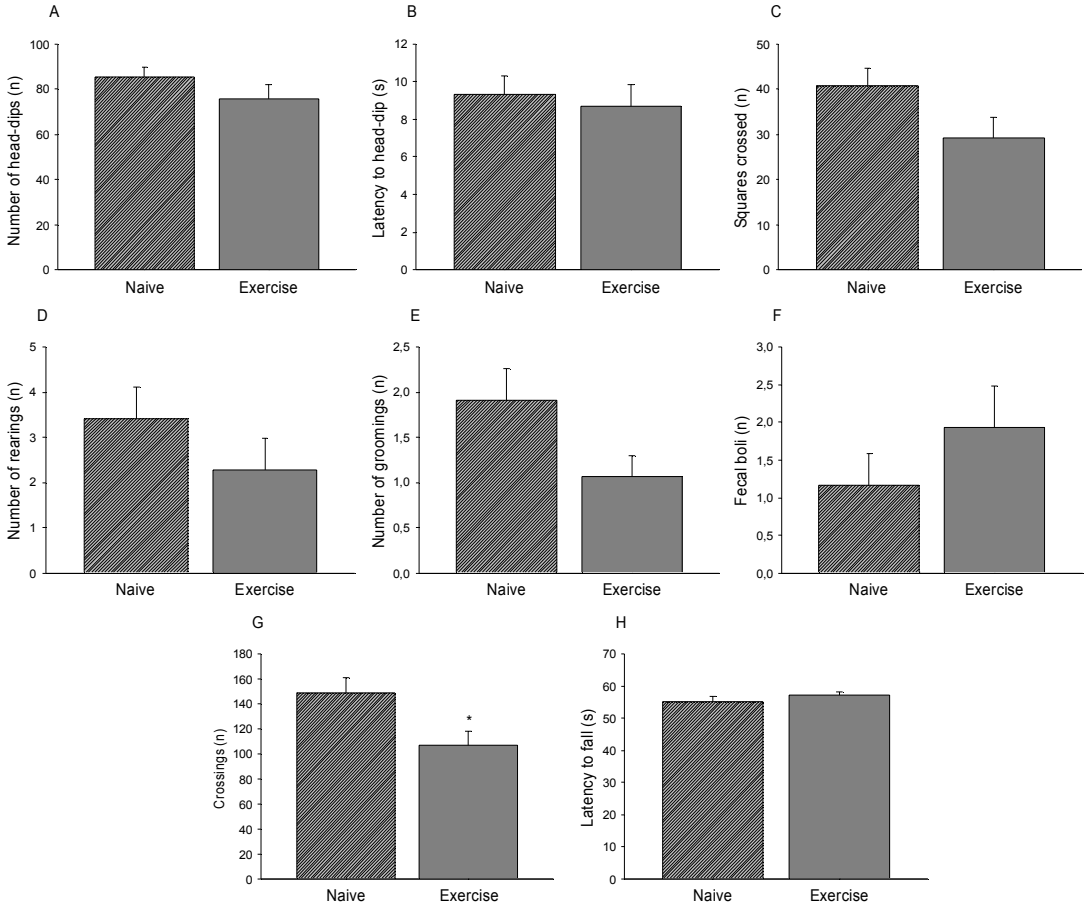
A
Number of head-dips (n)
100
80
60
40
20
0
Naive
Exercise
B
Latency to head-dip (s)
12
10
8
6
4
2
0
Naive
Exercise
C
Squares crossed (n)
50
40
30
20
10
0
Naive
Exercise
D
Number of rearings (n)
5
4
3
2
1
0
Naive
Exercise
E
Number of groomings (n)
2,5
2,0
1,5
1,0
0,5
0,0
Naive
Exercise
F
Fecal boli (n)
3,0
2,5
2,0
1,5
1,0
0,5
0,0
Naive
Exercise
G
Crossings (n)
180
160
140
120
100
80
60
40
20
0
*
Naive
Exercise
H
Latency to fall (s)
70
60
50
40
30
20
10
0
Naive
Exercise

Figure 10:

A

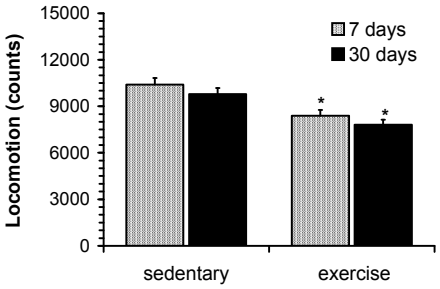

B

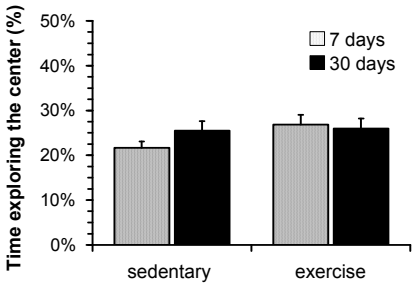

C

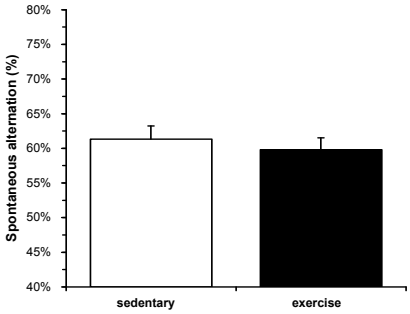

D

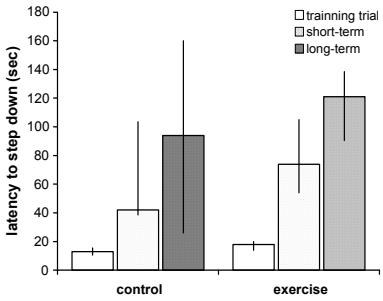

Anexo A-11. Different Effect of High Fat Diet and Physical Exercise in the Hippocampal Signaling

Artigo publicado no periódico *Neurochemistry Research*

Neurochem Res (2008) 33:880–885
DOI 10.1007/s11064-007-9530-7

ORIGINAL PAPER

Different Effect of High Fat Diet and Physical Exercise in the Hippocampal Signaling

Alexandre Pastoris Muller · Martín Cammarota · Marcelo de Oliveira Dietrich · Liane N. Rotta · Luis Valmor Portela · Diogo Onofre Souza · Iván Izquierdo · Lia R. M. Bevilaqua · Marcos Luiz Santos Perry

Accepted: 16 October 2007 / Published online: 22 November 2007

Abstract Obesity is an epidemic disease that may affect brain function. The present study examined the effect of high fat diet (HF) and physical exercise on peripheral tissue and hippocampal signaling. CF-1 mice ($n = 4$, per cage) were divided into groups receiving high fat (HF) or control (CD) diets for 5 months, with or without voluntary exercise. Serum triacylglycerol, total cholesterol, HDLc, liver triacylglycerol and glycogen concentrations were evaluated ($n = 6$). Also, the phosphorylation state of the AKT → ERK 1/2 → CREB pathway (AKT, pAKTser473, ERK 1/2, pERK 1/2, CREB and pCREB, $n = 4$–6) was analyzed in the hippocampus. HF diet caused an increase in AKT phosphorylation at ser473 ($P < 0.05$), while exercise increased the phosphorylation of ERK 1/2 ($P < 0.05$) and CREB ($P < 0.05$). As expected, exercise reversed some of the harmful effects of HF, i.e., increased liver deposition of fat ($P < 0.05$) and fat gain in the abdominal region ($P < 0.05$). In conclusion, the effects of exercise and HF diet on brain signaling appear to affect the hippocampal AKT → ERK 1/2 → CREB pathway in independent ways: HF intake caused increased phosphorylation of AKTser473, while exercise increased ERK 1/2 → CREB signaling. The physiological relevance of these findings in brain function remains to be elucidated.

Keywords High fat diet · Physical exercise · Hippocampal signaling · Obesity

A. P. Muller · M. de Oliveira Dietrich · L. V. Portela · D. O. Souza · M. L. S. Perry (✉)
Departamento de Bioquímica, Programa de Pós-Graduação em Ciências Biológicas-Bioquímica, Instituto de Ciências Básicas da Saúde, Universidade Federal do Rio Grande do Sul, Rua Ramiro Barcelos, 2600 – ANEXO, CEP 90035-003 Porto Alegre, RS, Brazil
e-mails: xandipm@portoweb.com.br; mlsperry@excite.com

M. Cammarota · I. Izquierdo · L. R. M. Bevilaqua
Centro de Memória, Instituto de Pesquisas Biomédicas, Pontifícia Universidade Católica do Rio Grande do Sul, Porto Alegre, RS, Brazil

L. N. Rotta
Universidade Luterana do Brasil, Canoas, RS, Brazil

L. N. Rotta
Fundação Faculdade Federal de Ciências Médicas de Porto Alegre, Porto Alegre, RS, Brazil

Introduction

Obesity is a problem in all westernized countries and more recently in several less industrialized countries such as India and Brazil. Both environmental and genetic factors may contribute to excessive body weight gain and its comorbidities [1]. Obesity associated with abdominal fat deposits is a major risk factor for insulin resistance, type II diabetes, and the 'metabolic syndrome'. Thus, lifestyle interventions aiming to control body weight gain have been proposed to prevent obesity [2]. Physical exercise, a low-cost lifestyle intervention, is known to increase insulin sensitivity, decrease body weight, and improve serum lipid profile [3]. Moreover, there is accumulating evidence that physical exercise has beneficial effects on brain function through incompletely understood mechanisms [4]. Hormones and neurotrophins, as well as proteins involved in intracellular signaling pathways, are putative brain targets modulated by the effects of exercise and diet [5–7].

A classical signaling pathway that is proposed to be regulated by hormones and neurotrophins is the serine/threonine protein kinase B (also knows as AKT) pathway. AKT-mediated intracellular signaling is a key regulator of

cell cycle, apoptosis and cellular responses to insulin in the brain [8]. Through its phosphorylation, AKT can be activated and translocated to the nucleus to regulate gene transcription. Moreover, AKT interacts with other kinases, including mitogen-activated protein kinase (MAPK) family members such as the extracellular signal-regulated kinases (ERK1/ERK2) and cyclic-AMP response element binding protein (CREB) [9]. Recent observations indicate that ERK-associated signaling plays an essential role in cell differentiation and proliferation, and also in long-term synaptic plasticity [10]. Activated ERK translocates to the nucleus and regulates gene transcription via phosphorylation of different transcription factors, including CREB, which are involved in long-term plasticity events within the brain [11]. Both experimental and clinical studies have reported that a high-fat diet may impair overall brain function, whereas exercise has opposite effect [4]. In rat models, a high-fat diet has been found to impair performance on a variety of tasks requiring both the hippocampus and frontal cortex, an effect which has been shown to be associated with the level of saturated fatty acids on diet [11]. Moreover, epidemiological studies have shown that a high intake of saturated fat and cholesterol can contribute to cognitive decline [12]. Albeit the mechanisms by which high-fat diets alter cognitive function are not completely understood, hyperglycemia and glucose intolerance caused by such diet may be a contributing factor. Albeit the increasing rates of obesity and insulin resistance have stimulated interest in the effects of diet composition on peripheral systems, comparatively little work has been done to examine its effects on the brain. Thus, it seems relevant to determine whether a combination of high fat diet and physical exercise would influence and/or interact with specific aspects of brain signaling.

In this sense, this study evaluated hippocampal AKT → ERK 1/2 → CREB signaling, a pathway recognized to be regulated by diet and exercise, which is also putatively involved in several cellular functions including regulation of cell growth, apoptosis, survival and nutrient metabolism [8].

Experimental procedure

Animals and diet

CF-1 male mice, 2 months old, were maintained in a 12-h light/dark cycle at 22–24°C. Mice were maintained during 5 months after being assigned to one of four groups ($n = 4$ per cage): control diet/sedentary (CDS); control diet/exercise (CDE); high fat diet/sedentary (HFS); high fat diet/exercise (HFE). Animals engaged in voluntary physical activity had free access to running wheel throughout the treatment as previously reported [13]. The animals progressively increased the distance ran per day during the first month, reaching a plateau of about 3000 m/day after 30 days and maintaining it until the end of the study. To avoid social isolation we did not maintain animals in individual housing.

Diets containing a standard vitamin and mineral mix with all essential nutrients were provided *ad libitum.* The HF diet contained 60% energy from saturated and unsaturated fat (45% lard and 15% soybean oil), 15% energy from starch and 25% from protein (soybean protein), while the CD contained 15% of energy from saturated fat and unsaturated fat (soybean oil), 60% energy from starch and 25% from protein (soybean protein).

Glucose tolerance test (GTT)

An intraperitoneal injection of glucose (2 mg/g body weight) was performed in 6 h fasted mice after 5 months of treatment (at 2:00 P.M). Blood glucose was monitored with glucose oxidase method (Labtest, MG, Brazil) at 0, 30, 60 and 120 min after glucose injection. Blood was collected from tail.

Blood biochemical evaluation

Two weeks after, to prevent the effect of stress caused by GTT, animals were sacrificed by decapitation. Blood was collected and centrifuged at 2500*g*/10 min. Serum was stored at −20°C until assays were performed. The serum triacylglycerol (TAG), total cholesterol, HDL cholesterol was measured using commercial kits (Labtest, MG, Brazil). The reactions were performed using Labmax equipment (Labtest, MG, Brazil).

Liver measurements and fat pad weights

Liver was dissected and between 90–110 mg of liver were homogenized 1:10 with saline 0.9%; 20 μl of the homogenate were used to determine liver TAG. Liver glycogen was determined by the colorimetric method described by Krisman [14]. Fat tissues from retroperitoneal and epididymal regions were dissected and weighted as previously described [15].

Hippocampal preparation and Western blot analysis

Hippocampus was rapidly dissected and stored at −70°C. Hippocampal homogenates were prepared in buffer (NaF

50 mM, Tris 20 mM, sucrose 0.32 mM, ortovanadate 1 mM, EDTA mM, EGTA 1 mM, phenylmethylsulfonyl fluoride 1 mM) and centrifuged. Supernatants were collected and total protein was measured by a Bradford protein assay. For Western blot analysis, samples containing 30 μg of protein were separated by electrophoresis on a 10% polyacrilamide gel and electrotransfered to PVDF membranes. Non-specific binding sites were blocked with in Tween–Tris buffered saline (TTBS, 100 mM Tris–HCl, pH 7.5, containing 0.9% NaCl and 0.1% Tween-20) containing 5% albumin for 2 h. Membranes were then incubated overnight at 4°C with polyclonal antibodies against AKT, pAKT ser473 (Cell Signalling, 1:1000), CREB, pCREb (Upstate, 1:2000) or ERK 1/2, pERK 1/2 (Upstate, 1:500). After rinsing three times for 10 min each with TTBS, membranes were incubated with secondary antibodies (1:15000 dilution, anti-rabbit, Santa Cruz) during 2 h at room temperature. After rinsing four times for 10 min each with TTBS, membranes were incubated with peroxidase-conjugated for 5 min at room temperature, then displayed on autoradiographic film by chemiluminescence. Signals were digitally scanned and quantified using Opitquant version 02.00 (Packard Instrument Company). This procedure was repeated by at least three times.

Statistical analysis

Results are presented as means ± SEM. Differences between all groups was analyzed by using analysis of variance (ANOVA) with a post-hoc Duncan test. For analyzing differences between treatments we used a two-way ANOVA. To analyze GTT results we used repeated-measures ANOVA. Values were considered statistically different when P values were below 0.05.

Results

Body weight, fat pads weight, serum lipids and liver measurements

Body weight, fat pad weight, serum and liver biochemical analysis are demonstrated in Table 1. The HFS group presented increased fat pad weight in epididymal and retroperitoneal regions as compared to other groups ($P < 0.05$) but no increment in total body weight was observed. The HFS group also showed a high liver TAG concentration compared to other groups ($P < 0.05$). CDE animals showed an increase in serum TAG compared to the HFE group ($P < 0.05$). Body weight, fat pads and liver glycogen were not statistically different when the HFE and CD groups were compared. The HFS group had a lower hepatic glycogen concentration than other groups ($P < 0.05$). Total cholesterol and HDLc were not altered by diet or exercise.

Glucose tolerance test

The results of GTT are presented in Fig. 1a. At 30 min there was an apparent increase in serum glucose levels in both HFS and HFE groups (19% and 50% respectively); however, this effect did not reach statistical significance. At 60 min, glucose levels in the HFS group remained high compared to all other groups ($P < 0.05$, 37%). At 60 min, glucose levels in the HFE group were equal to the CD group.

Immunocontent of AKT and pAKT in hippocampus

Total AKT immunocontent was not different among groups, but HF groups enhanced the phosphorylation of AKTser473 when compared to CD groups (Fig. 1b, F (13.3) = 25.184 $P < 0.05$).

Immunocontent of ERK 1/2 and pERK 1/2, CREB and pCREB in hippocampus

Considering that pAKTser473 was modified by diet, we also evaluated other proteins involved in this signaling pathway. Total immunocontent of ERK1/2 (Fig. 2a) and CREB (Fig. 2b) did not change with diet, but exercise increased phosphorylation status of pERK1/2 (F (5.1) = 10.981 $P < 0.03$, Fig. 2a) and pCREB (F (4.8) = 5.593 $P < 0.05$, Fig. 2b).

Discussion

In this study, we evaluated the effects of both high-fat diet and exercise on metabolic parameters and on the hippocampal AKT → ERK 1/2 → CREB signaling pathway in mice. Research has recently been spurred by the finding that an association exists between the accumulation of TAG in tissues other than adipocytes and the development of insulin resistance [16]. In our work, exercise prevented fat deposition and TAG accumulation in the liver of HF treated mice. Similarly, Gauthier et al. [17] also showed that HF triggered the accumulation of lipid as macrovesicles in liver; but in this study when an exercise training program was pursued at the same time as the HF diet, the

Table 1 Body weight, adiposity, liver and blood measurements in mice after 5 months of treatments

	Body weight (g)	Fat pad retroperitoneal	Fat pad epididymal	Triacylglycerol serum mg%	Liver triacylglycerol mg%	Liver glycogen mg%	Cholesterol mg/dl	HDL cholesterol mg%
CDS	49.7 ± 2.6	0.9 ± 0.2	2.5 ± 0.4	170.0 ± 19[a,b]	3.0 ± 0.4	2.3 ± 0.3	129.2 ± 11.3	41.7 ± 4.1
CDE	45.8 ± 1.6	0.8 ± 0.1	1.7 ± 0.3	188.0 ± 20[a]	2.6 ± 0.2	2.6 ± 0.2	133.8 ± 8.9	45.6 ± 2.8
HFS	50.3 ± 1.7	2.3 ± 0.1[a]	3.6 ± 0.3[a]	137.8 ± 12[a,b]	4.9 ± 0.4[a]	1.3 ± 0.3[a]	138.5 ± 8.0	43.0 ± 3.8
HFE	47.0 ± 2.1	1.1 ± 0.2	2.4 ± 0.5	114.4 ± 22[b]	3.8 ± 0.7	2.2 ± 0.5	144.2 ± 14.9	49.2 ± 2.4

Values are mean ± SEM. Means in a column with distinct letter or different letter differ than other groups with distinct letter or without letter ($P \leq 0.05$). CDS (control diet sedentary, $n = 6$); CDE (control diet exercise $n = 6$); HFS (high fat diet sedentary $n = 6$); HFE (high fat diet exercise $n = 6$)

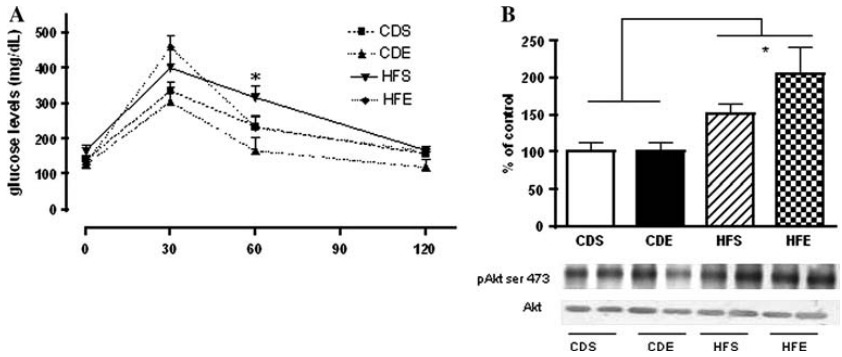

Fig. 1 Glucose tolerance test, AKT and pAKTser473 immunocontent. (**a**) 6 h-fasted mice received an intraperitoneal injection of glucose (2 mg/g of body wt). Blood samples were taken at the times 0, 30, 60 and 120 min from the tail vein of the same animal. Repeated-measures analysis of variance (ANOVA) was used to evaluate statistical significance. Results are expressed as means ± SEM. Serum glucose levels were higher in the HFS group at 60 min ($P = 0.05$) compared to all other groups. (**b**) Representative immunoblots of hippocampal pAKTser473 and AKT with their respective histograms and densitometric analyses. Results are expressed as mean ± SEM. Two-way ANOVA was used to analyze statistical significance. HF diet (sedentary and exercise) increased pAKTser473 immunocontent ($P < 0.05$). CDS (control diet sedentary, $n = 4$); CDE (control diet exercise $n = 4$); HFS (high fat diet sedentary $n = 4$); HFE (high fat diet exercise $n = 4$)

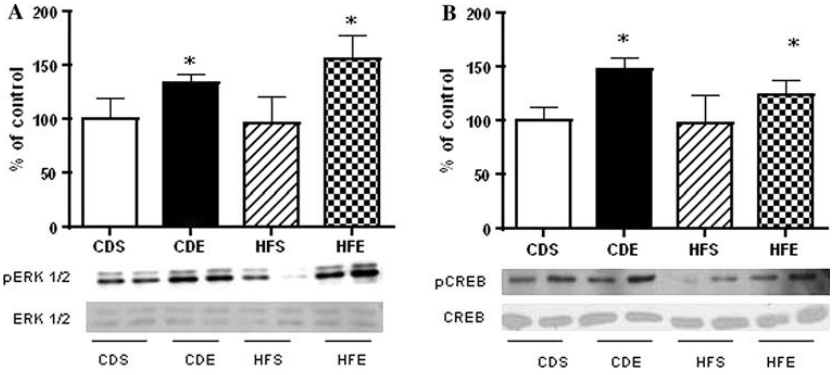

Fig. 2 Determination of ERK 1/2, pERK 1/2, CREB and pCREB immunocontent. Representative immunoblots of hippocampal ERK 1/2, pERK 1/2, CREB and pCREB with their respective histograms and densitometric analyses. Results are expressed as mean ± SEM. Two-way ANOVA was used to analyze statistical significance. (**a**) Exercise increased pERK 1/2 ($P = 0.03$). (**b**) Exercise increased pCREB ($P = 0.05$). * indicates difference in exercise groups in relation to sedentary groups. CDS (control diet sedentary, $n = 6$); CDE (control diet exercise $n = 6$); HFS (high fat diet sedentary $n = 6$); HFE (high fat diet exercise $n = 6$)

induction of hepatic steatosis was completely suppressed. Our results are somewhat convergent with the effect of exercise in reducing liver lipid accumulation induced by HF diet.

The HFS group had altered glucose levels in GTT at 60 min ($P < 0.05$). Moreover, increased AKTser473 phosphorylation was observed in hippocampal tissue from the HFS and HFE groups. It has been extensively reported that cerebral signaling may be influenced by insulin and glucose levels [8, 18–21]. Accordingly, Clodfelder-Miller et al. [22] demonstrated that physiological variations in serum glucose and insulin levels affected brain AKT phosphorylation/dephosphorylation status in the hippocampus. Moreover, streptozotocin-induced hyperglycemia caused persistent AKT hyperphosphorylation, which was postulated to be detrimental for brain function [22]. Here, we speculate that although not statistically significant, the increased glucose levels observed at 30 min in HFS (19%) and HFE (50%) groups could account in some degree for the increased phosphorylation of AKTser473. However, considering that the GTT did not present a clear pattern of glucose intolerance, it is difficult to attribute a causal effect of glucose and/or insulin levels on AKT phosphorylation.

Conversely, Mielke et al. [23] demonstrated that in C57BL/6 mice, consuming a large proportion of calories from saturated fat had limited effect on learning and memory, and also on pAKT. These results suggest that changes in brain function do not appear to be strictly related to changes in peripheral glucose tolerance and neural insulin sensitivity**.** Exercise training did not affect GTT response in CDE group when compared to CDS group, probably because this parameter is already well regulated in sedentary animals (i.e. they may not yet present pathophysiological alterations that can be further optimized by exercise).

The preliminary postulation that the effect of exercise and HF diet might affect the AKT → ERK 1/2 → CREB by similar means was not confirmed by this study. ERK 1/2 is activated in response to many different stimuli including growth factors and hormones and transduces extracellular stimuli into diverse intracellular responses. Moreover, the activation of ERK 1/2 may cause phosphorylation of CREB [9], which is consistently associated with the positive effect of exercise on brain function, at least in part, by promoting increased neurotrophic factor expression and synthesis [4].

In conclusion, the effects of exercise and HF diet on brain signaling affected the AKT–> ERK 1/2 –> CREB in different ways. HF intake caused increase phosphorylation of hippocampal AKTser473 and exercise increased hippocampal ERK 1/2 → CREB signaling. The physiological relevance of these findings for the brain function remains to be elucidated.

References

1. Hendrickx H, McEwen B, der Ouderaa F (2005) Metabolism, mood and cognition in aging: the importance of lifestyle and dietary intervention. Neurobiol Aging 26S:S1–S5
2. Chakravarthy M, Booth F (2004) Eating, exercise, and "thrifty" genotypes: connecting the dots toward an evolutionary understanding of modern chronic diseases. J Appl Physiol 96:3–10
3. Bhattacharya A, Rahman M, Sun D et al (2005) The combination of dietary conjugated linoleic acid and treadmill exercise lowers gain in body fat mass and enhances lean body mass in high fat–fed male Balb/C mice. J Nutr 135:1124–1130
4. Molteni R, Wu A, Vaynman S et al (2004). Exercise reverses the harmful effect of consumption of high fat diet and behavioral plasticity associated on the of brain-derived neurotrophic factor. Neuroscience 123:429–440
5. Adlard P, Victoria P, Viorela P et al (2005) Voluntary exercise decreases amyloid load in a transgenic model of Alzheimer's disease. J Neurosci 25:4217–4221
6. Cotman C, Berchtold N (2002) Exercise: a behavioural intervention to enhance brain health and plasticity. Trends Neurosci 25:295–301
7. Van Praag H, Shubert T, Zhao C et al (2005). Exercise enhances learning and hippocampal neurogenesis in aged mice. J Neurosci 25:8680–8685
8. Lawlor A, Alessi D (2001). PKB/AKT: a key mediator of cell proliferation, survival and insulin responses? J Cell Sci 114: 2903–2910
9. Morikawa E, Ueyama E, Serba E (2004) Fasting-induced activation of mitogen-actived protein kinases (ERK/p38) in the mouse hypothalamus. J Neuroendocrinol 16:105–112
10. Cowan KJ, Storey KB (2003) Mitogen-activated protein kinases: new signaling pathways functioning in cellular responses to environmental stress. J Exp Biol 206:1107–1115
11. Kalmijn S, van Boxtel MP, Ocke M, Verschuren WM, Kromhout D, Launer LJ (2004) Dietary intake of fatty acids and fish in relation to cognitive performance at middle age. Neurology 62:275–280
12. Kalmijn S, Launer LJ, Ott A, Witteman JC, Hofman A, Breteler MM (1997) Dietary fat intake and the risk of incident dementia in the Rotterdam study. Ann Neurol 42:776–782
13. Dietrich M, Mantese C, Porciuncula L, Ghisleni G, Souza D, Portela L (2005). Exercise affects glutamate receptors in postsynaptic densities from cortical mice brain. Brain Res 1065:20–25
14. Krisman R (1962). A method for the colorimetric estimation of glycogen with iodine. Anal Biochem 4:17–23
15. Parekh PI, Petro AN, Miller JM et al (1998) Reversal of diet-induced obesity and diabetes in C57BL/6J mice. Metabolism 77:1089–1096
16. Saltiel AR, Kahn CR (2001) Insulin signaling and the regulation of glucose and lipid metabolism. Nature 414:799–806
17. Gauthier M, Couturier K, Latour J et al (2003). Concurrent exercise prevents high fat- diet induced macrovesicular hepatic steatosis. J Appl Physiol 94:2127–2134
18. Gispen WH, Biessels GJ (2000) Cognition and synaptic plasticity in diabetes mellitus. Trends Neurosci 23:542–549
19. Perros P, Frier BM (1997) The long-term sequelae of severe hypoglycemia on the brain in insulin-dependent diabetes mellitus. Horm Metab Res 29:197–202

20. Parkes M, White KG (2000) Glucose attenuation of memory impairments. Behav Neurosci 114:307–319
21. Messier C (2004) Glucose improvement of memory: a review. Eur J Pharmacol 490:33–57
22. Clodfelder-Miller B, De Sarno P, Zmijewska A et al (2005) Physiological and pathological changes in glucose regulate brain AKT and glycogen synthase kinase-3. J Biol Chem 280:39723–39731
23. Mielke G, Nicolitch K, Avellaneda V, Earlana K, Ahuja T, Mealing G, Messier C (2006) Longitudinal study of the effects of a high-fat diet on glucose regulation, hippocampal function, and cerebral insulin sensitivity in C57BL/6 mice. Behav Brain Res 175: 374–382

ANEXOS B: publicações relacionadas a outros capítulos desta tese

Aqui podem ser encontrados os resumos de dois artigos publicados no periódico *Cell*. Esses artigos foram comentados e revisados criticamente em duas 'previews' que fazem parte do corpo principal desta tese. Ver capítulos III e IV da Parte II.

Anexo B-1. Artigo relacionado ao capítulo IV (Parte II). Loss of GABAergic signaling by AgRP neurons to the parabrachial nucleus leads to starvation.

Reference
Cell. 2009 Jun 26;137(7):1225-34.

Authors
Wu Q, Boyle MP, Palmiter RD.

Abstract
Neurons in the arcuate nucleus that produce AgRP, NPY, and GABA (AgRP neurons) promote feeding. Ablation of AgRP neurons in adult mice results in Fos activation in postsynaptic neurons and starvation. Loss of GABA is implicated in starvation because chronic subcutaneous delivery of bretazenil (a GABA(A) receptor partial agonist) suppresses Fos activation and maintains feeding during ablation of AgRP neurons. Moreover, under these conditions, direct delivery of bretazenil into the parabrachial nucleus (PBN), a direct target of AgRP neurons that also relays gustatory and visceral sensory information, is sufficient to maintain feeding. Conversely, inactivation of GABA biosynthesis in the ARC or blockade of GABA(A) receptors in the PBN of mice promote anorexia. We suggest that activation of the PBN by AgRP neuron ablation or gastrointestinal malaise inhibits feeding. Chronic delivery of bretazenil during loss of AgRP neurons provides time to establish compensatory mechanisms that eventually allow mice to eat.

Anexo B-2. Artigo relacionado ao capítulo V (Parte II). Hunger states switch a flip-flop memory circuit via a synaptic AMPK-dependent positive feedback loop.

Reference
Cell. 2011 Sep 16;146(6):992-1003.

Authors
Yang Y, Atasoy D, Su HH, Sternson SM.

Abstract
Synaptic plasticity in response to changes in physiologic state is coordinated by hormonal signals across multiple neuronal cell types. Here, we combine cell-type-specific electrophysiological, pharmacological, and optogenetic techniques to dissect neural circuits and molecular pathways controlling synaptic plasticity onto AGRP neurons, a population that regulates feeding. We find that food deprivation elevates excitatory synaptic input, which is mediated by a presynaptic positive feedback loop involving AMP-activated protein kinase. Potentiation of glutamate release was triggered by the orexigenic hormone ghrelin and exhibited hysteresis, persisting for hours after ghrelin removal. Persistent activity was reversed by the anorexigenic hormone leptin, and optogenetic photostimulation demonstrated involvement of opioid release from POMC neurons. Based on these experiments, we propose a memory storage device for physiological state constructed from bistable synapses that are flipped between two sustained activity states by transient exposure to hormones signaling energy levels.

ANEXO C: Formação e produção científica durante o doutoramento (2008-2012)

Prêmios

2008 PENS Summer School Award, Frankfurt, Germany.
2009 13th Latin American Young Talent Award in Life Sciences, Brazilian Society for Biochemistry and Molecular Biology and GE Health Care Life Sciences.
2009 Keystone Symposia Scholarship 2010, Keystone Symposia.
2009 OROBOROS Scholarship for attending the 54th Course in High-resolution Respirometry 2009, Oroboros Instruments.

Palestras

1. Diversas aulas ministradas na disciplina "Bioquímica Médica I" do curso de Medicina da Universidade Federal do Rio Grande do Sul (Brasil). Anfitrião: Professor Diogo O. Souza. De 2008-atual.

2. *Effects of voluntary exercise in the central nervous system plasticity in mice*. Section of Comparative Medicine, Yale School of Medicine. 04/2008. Anfitrião: Tamas L. Horvath.

3. *Papel da proteína Sirt1 na regulação do apetite*. Programa de Pós-graduação em Ciências Biológicas: Bioquímica, Universidade Federal do Rio Grande do Sul (Brazil). 01/2010. Anfitrião: Diogo O. Souza.

4. *A view on integrative physiology: the role of the AgRP neurons*. Nanjing University (China). 05/2011. Anfitrião: Qian Gao.

5. *A view on integrative physiology: the role of the AgRP neurons*. Xijing Hospital, Fourth Military Medical University (China). 05/2011. Anfitrião: Professor Hai-long Dong.

6. *A view on integrative physiology: the role of the AgRP neurons*. Dipartimento di Farmacologia Sperimentale, Universitá degli Studi di Napoli Federico II (Nápoles, Itália). 07/2011.

Lista de artigos científicos publicados

1. Muller AP, Cammarota M, **Dietrich MO**, Rotta LN, Portela LV, Souza DO, Izquierdo I, Bevilaqua LR, Perry ML. Different effect of high fat diet and physical exercise in the hippocampal signaling. Neurochem Res. 2008 May;33(5):880-5.

2. **Dietrich MO**, Spuch C, Antequera D, Rodal I, de Yébenes JG, Molina JA, Bermejo F, Carro E. Megalin mediates the transport of leptin across the blood-CSF barrier. Neurobiol Aging. 2008 Jun;29(6):902-12.

3. **Dietrich MO**, Andrews ZB, Horvath TL. Exercise-induced synaptogenesis in the hippocampus is dependent on UCP2-regulated mitochondrial adaptation. J Neurosci. 2008 Oct 15;28(42):10766-71.

4. Nie Y, Erion DM, Yuan Z, **Dietrich MO**, Shulman GI, Horvath TL, Gao Q. STAT3 inhibition of gluconeogenesis is downregulated by SirT1. Nature Cell Biology, p. 1-0, 2009.

5. **Dietrich MO**, Horvath TL. GABA keeps up an appetite for life. Cell. 2009 Jun 26;137(7):1177-9.

6. Maejima Y, Sedbazar U, Suyama S, Kohno D, Onaka T, Takano E, Yoshida N, Koike M, Uchiyama Y, Fujiwara K, Yashiro T, Horvath TL, **Dietrich MO**, Tanaka S, Dezaki K, Oh-I S, Hashimoto K, Shimizu H, Nakata M, Mori M, Yada T. Nesfatin-1-regulated oxytocinergic signaling in the paraventricular nucleus causes anorexia through a leptin-independent melanocortin pathway. Cell Metab. 2009 Nov;10(5):355-65.

7. **Dietrich MO**, Horvath TL. The role of mitochondrial uncoupling proteins in lifespan. Pflugers Arch. 2009.

8. **Dietrich MO**, Horvath TL. Feeding signals and brain circuitry. European Journal of Neuroscience. 2009.

9. **Dietrich MO**, Antunes C, Geliang G, Liu ZW, Borok E, Nie Y, Xu AW, Souza DO, Gao Q, Diano S, Gao XB, Horvath TL. Agrp neurons mediate Sirt1's action on the melanocortin system and energy balance: roles for Sirt1 in neuronal firing and synaptic plasticity. J Neurosci. 2010. Sep 1;30(35):11815-25.

10. Diano S, Liu ZW, Jeong JK, **Dietrich MO**, Ruan H, Kim E, Suyama S, Kelly K, Gyengesi E, Arbiser JL, Belsham DD, Sarruf DA, Schwartz MW, Bennet A, Shanabrough M, Mobbs CV, Yang X, Gao XB, Horvath TL. Peroxisome proliferation-related hypothalamic control of ROS sets melanocortin tone and feeding in diet-induced obesity. Nat Med. 2011 Aug 28;17(9):1121-7.

11. **Dietrich MO**, Horvath TL. Synaptic plasticity of feeding circuits: hormones and hysteresis. Cell. 2011 Sep 16;146(6):863-5.

12. Coupé B, Ishii Y, **Dietrich MO**, Komatsu M, Horvath TL, Bouret SG. Loss of Autophagy in Proopiomelanocortin Neurons Perturbs Axon Growth and Causes Metabolic Dysregulation. Cell Metabolism. 2012 Jan 24.

13. Thaler JP, Yi CX, Schur EA, Guyenet SJ, Hwang BH, **Dietrich MO**, Zhao X, Sarruf DA, Izgur V, Maravilla KR, Nguyen HT, Fischer JD, Matsen ME, Wisse BE, Morton GJ, Horvath TL, Baskin DG, Tschöp MH, Schwartz MW. Evidence that Obesity is Associated with Hypothalamic Injury in Rodent Models and Humans. Journal of Clinical Investigation. 2012 Jan 3;122(1):153-62. doi: 10.1172/JCI59660.

Lista de capítulos de livros publicados

1. **Dietrich MO**, Horvath TL. Wired for Hunger: The Brain and Obesity and Anorexia Nervosa: A Mortal Clash between Reward and Hunger. Cerebrum 2010. Dana Foundation.

Outras produções bibliográficas

1. **Dietrich MO**, Horvath TL. Neural regulation of food intake and energy balance. Nature Reviews Neuroscience. 2010 (Pôster).

ANEXO D: Formação e produção científica anterior ao período de doutoramento (2000-2008)

Prêmios

2006 1 Lugar - I Prêmio Cristália de Pesquisa, Brasil.

Lista de artigos científicos publicados

1. Coitinho AS, **Dietrich MO**, Hoffmann A, Dall'Igna OP, Souza DO, Martins VR, Brentani RR, Izquierdo I, Lara DR. Decreased hyperlocomotion induced by MK-801, but not amphetamine and caffeine in mice lacking cellular prion protein (PrP(C)). Brain Res Mol Brain Res. 2002 Nov 15;107(2):190-4.
2. Dall'Igna OP, **Dietrich MO**, Hoffmann A, Neto W, Vendite D, Souza DO, Lara DR. Catalepsy and hypolocomotion induced by a nitric oxide donor: attenuation by theophylline. Eur J Pharmacol. 2001 Nov 30;432(1):29-33.
3. Dall'Igna OP, Da Silva AL, **Dietrich MO**, Hoffmann A, de Oliveira RV, Souza DO, Lara DR. Chronic treatment with caffeine blunts the hyperlocomotor but not cognitive effects of the N-methyl-D-aspartate receptor antagonist MK-801 in mice. Psychopharmacology (Berl). 2003 Mar;166(3):258-63.
4. Lourenço Da Silva A, Hoffmann A, **Dietrich MO**, Dall'Igna OP, Souza DO, Lara DR. Effect of riluzole on MK-801 and amphetamine-induced hyperlocomotion. Neuropsychobiology. 2003;48(1):27-30.
5. Farina M, Frizzo ME, Soares FA, Schwalm FD, **Dietrich MO**, Zeni G, Rocha JB, Souza DO. Ebselen protects against methylmercury-induced inhibition of glutamate uptake by cortical slices from adult mice. Toxicol Lett. 2003 Oct 15;144(3):351-7.
6. Tort AB, **Dietrich MO**, Gonçalves CA, Souza DO, Portela LV. Influence of anticoagulants on the measurement of S100B protein in blood. Clin Biochem. 2003 Oct;36(7):519-22.
7. **Dietrich MO**, Souza DO, Portela LV. Serum S100B protein: what does it mean during exercise? Clin J Sport Med. 2004 Nov;14(6):368; author reply 368-9. Comment on: Clin J Sport Med. 2003 Sep;13(5):292-302.
8. **Dietrich MO**, Tort AB, Schaf DV, Farina M, Gonçalves CA, Souza DO, Portela LV. Increase in serum S100B protein level after a swimming race. Can J Appl Physiol. 2003 Oct;28(5):710-6.
9. Tort AB, Mantese CE, dos Anjos GM, **Dietrich MO**, Dall'Igna OP, Souza DO, Lara DR. Guanosine selectively inhibits locomotor stimulation induced by the NMDA antagonist dizocilpine. Behav Brain Res. 2004 Oct 5;154(2):417-22.
10. **Dietrich MO**, Mantese CE, Dos Anjos GM, Rotta LN, Perry ML, Souza DO, Lara DR. Increased locomotor response to amphetamine, but not other

psychostimulants, in adult mice submitted to a low-protein diet. Physiol Behav. 2004 Oct 30;83(1):129-33.

11. **Dietrich MO**, Mantese CE, Anjos G, Souza DO, Farina M. Motor impairment induced by oral exposure to methylmercury in adult mice. Environmental Toxicology and Pharmacology. 2005 Jan; 19(1):169-175.
12. **Dietrich MO**, Mantese CE, Porciuncula LO, Ghisleni G, Vinade L, Souza DO, Portela LV. Exercise affects glutamate receptors in postsynaptic densities from cortical mice brain. Brain Res. 2005 Dec 14;1065(1-2):20-5.
13. Machado-Vieira R, **Dietrich MO**, Leke R, Cereser VH, Zanatto V, Kapczinski F, Souza DO, Portela LV, Gentil V. Decreased plasma brain derived neurotrophic factor levels in unmedicated bipolar patients during manic episode. Biol Psychiatry. 2007 Jan 15;61(2):142-4.
14. Lopez-Lopez C, **Dietrich MO**, Metzger F, Loetscher H, Torres-Aleman I. Disturbed cross talk between insulin-like growth factor I and AMP-activated protein kinase as a possible cause of vascular dysfunction in the amyloid precursor protein/presenilin 2 mouse model of Alzheimer's disease. J Neurosci. 2007 Jan 24;27(4):824-31.
15. **Dietrich MO**, Muller A, Bolos M, Carro E, Perry ML, Portela LV, Souza DO, Torres-Aleman I. Western style diet impairs entrance of blood-borne insulin-like growth factor-1 into the brain. Neuromolecular Med. 2007;9(4):324-30.